Structured Ion-Containing Polyethylene-like Polymers

Dissertation

zur Erlangung des akademischen Grades eines

Doktors der Naturwissenschaften (Dr. rer. nat.)

vorgelegt von

Anne Saumer

aus Herrenzimmern

an der

Mathematisch-Naturwissenschaftliche Sektion

Fachbereich Chemie

Konstanz, 2023

Tag der mündlichen Prüfung: 19. Januar 2024

1. Referent: Prof. Dr. Stefan Mecking

2. Referentin: Prof. Dr. Karen I. Winey

Die vorliegende Dissertation entstand in der Zeit von Mai 2019 bis Januar 2023 unter der Leitung von Herrn Prof. Dr. Stefan Mecking am Fachbereich Chemie der Universität Konstanz.

Danksagung

Mein Dank gilt Prof. Dr. Stefan Mecking, der mir dieses vielseitige und spannende Thema in die Hände gelegt hat und mir eine Promotion im Fast-Track Verfahren in seiner Arbeitsgruppe ermöglichte. Ich hatte im Rahmen der Arbeit alle Freiheiten, die ich mir vorstellen konnte und gleichzeitig die Unterstützung, die ich gebraucht habe.

Bei Prof. Dr. Karen I. Winey möchte ich mich nicht nur für die Übernahme des Zweitgutachtens bedanken, sondern auch für die hervorragende und früchtetragende Zusammenarbeit während meiner gesamten Promotion.

Bei Prof. Dr. Alexander Wittemann bedanke ich mich für die Übernahme des Prüfungsvorsitzes.

Meinem thematischen Vorgänger, Laborpartner und langjährigen Freund Dr. Manuel Häußler gilt mein großer Dank. Nicht nur hat er mir leidenschaftlich das Thema der Polymerelektrolyte ans Herz gebracht, sondern durch unzählige Diskussionen und hilfreiche Gespräche dazu beigetragen, dass meine Arbeit Früchte trägt. Bei Dr. Christina Rank möchte ich mich für die Einarbeitung in die Welt der ionischen Polykondensate bedanken.

Den Doktoranden der Winey-Gruppe, mit denen ich eng zusammengearbeitet habe, möchte ich für die Kooperation danken. Insbesondere betone ich hier die Messung und Interpretation von temperaturabhängigen Röntgen- und Leitfähigkeitsmessungen, sowie die Erstellung der Phasendiagramme. Die gemeinsame Diskussion und Interpretation der Ergebnisse schätze ich sehr. Mein Dank gilt hier Dr. Benjamin Paren, Dr. Jinseok Park, Benjamin Ferko und Eli Fastow.

Meinen Mitarbeiterpraktikant*innen, Hiwis und Bachelor-Studentinnen möchte ich für eine tatkräftige Unterstützung im Labor danken. Dazu gehören Hannah Mehringer, Leah Kutschera, Lena Schittenhelm, Robin Zunker, Katharina Scherer und Laura Haßfeld. Insbesondere Katharina möchte ich in dieser Liste hervorheben, die nach ihrer Bachelor-Arbeit so viel Freude am Thema gefunden hatte, dass noch ein langer Hiwi angehängt wurde.

Ein großer Dank gilt außerdem meinen Labor-PartnerInnen, insbesondere Melissa Birkle, die fast seit Tag 1 in L707 mit mir alles durchstand, was L707 so zu bieten hatte. Außerdem gilt er natürlich Dr. Manuel Häußler und allen Master-Studierenden, die zeitweise Teil der L707-Gruppe waren, Viola Burlein, Dario Rothauer, Robin Zunker und Felix Schoder.

Viola Burlein möchte ich an dieser Stelle extra erwähnen, die auf dem spannenden Feld der Polymerelektrolyte weiterarbeiten wird. Die Zusammenarbeit in den letzten Monaten meiner Promotion hat mir sehr viel Spaß gemacht und war äußerst fruchtbar.

Trotz langer Corona-Phase hatte ich eine wunderbare Zeit in unserem schönen Büro mit Natalie Schunck, Stefanie de Roo und Nina Mast. Für die vielen gemeinsamen Diskussionen und Gespräche möchte ich mich ganz herzlich bedanken.

Lars Bolk gilt mein großer Dank für die geduldige Einführung in die Welt der DSC und GPC. Ich habe super viel lernen dürfen und möchte die Zusammenarbeit nicht missen. Außerdem bedanke ich mich für Computer-Administration und alles, was dazu gehört.

Bei Robin Kirsten bedanke ich mich für das unkomplizierte Labor-Management und bei Dr. Marina Krumova für unzählige Stunden und Versuche am Mikroskop, AFM und TEM. Gisela Berner gilt mein Dank für das Rücken-Freihalten bezüglich jeder Art von administrativen Dingen und Verwaltungsangelegenheiten, das weiß ich sehr zu schätzen.

Brigitte Bössenecker und Elana Harbalik danke ich für die vielen WAXS- und SAXS-Messungen. Ulrich Haunz und Anke Friemel sowie Dr. Inigo Göttker gen. Schnetmann danke ich für die Unterstützung bei NMR-Messungen. Bei Dr. Doreen Herzog, Dr. Adrian Donner und Florian Stumpf bedanke ich mich für ESI-MS Messungen. Dr. Dominik Gruber und Dr. Taylor Nelson gilt mein Dank für die Einführung in die Welt der Titrationen. Bei Franziskus Hauth möchte ich mich für viele Stunden Einführung in die Welt der Enzyme bedanken. Ich habe nicht nur grundlegende biochemische Skills von ihm lernen können, sondern auch eine Begeisterung für die Welt der Proteine und Enzyme mitgenommen.

Für eine ganz fantastische Zeit in der Arbeitsgruppe Mecking möchte ich mich bei allen daran Beteiligten bedanken. Insbesondere bei denjenigen, die mir die Welt der Polymere schmackhaft gemacht haben und mir nicht nur den Arbeitsalltag versüßt haben, sondern auch die Zeit nach der Arbeit. Dr. Manuel Schnitte, Dr. Manuel Häußler, Lukas Odenwald, Dr. Florian Wimmer, Dr. Annika Sickinger, Dr. Stefanie de Roo und Dr. Natalie Schunck möchte ich hier namentlich nennen. Es war mir ein inneres Blumenpflücken!

Für die Korrektur dieses Schriftstückes bedanke ich mich herzlich bei Viola Burlein, Dr. Manuel Häußler, Dr. Natalie Schunck und Melissa Birkle.

Bei meinen Freunden und Kommilitonen möchte ich mich für eine wunderbare Zeit im Studium und während der Promotion bedanken. Ein großer Dank geht außerdem an meine Familie, insbesondere meine Eltern, für die emotionale und finanzielle Unterstützung in dieser ganzen Zeit.

Abschließend möchte ich mich bei Philip bedanken, für den Support und Rückhalt, sowie die mentale Unterstützung zu jeder Zeit.

Vielen Dank.

PUBLICATIONS

Parts of this thesis have been published previously.

Journal Publications

Staiger, A.[†], Paren, B. A.[†], Zunker, R., Hoang, S., Häußler, M., Winey, K. I., Mecking, S. *Journal of the American Chemical Society* **2021**, *143*, 16725 – 16733.
'Anhydrous Proton Transport within Phosphonic Acid Layers in Monodisperse Telechelic Polyethylenes'

Saumer, A., Mecking, S. *ACS Sustainable Chemistry & Engineering* **2023**, *11*, 33, 12414 – 12422.
'Recyclable and Degradable Ionic-Substituted Long-Chain Polyesters'

Park, J.[†], Staiger, A.[†], Mecking, S., Winey, K. I. *Macromolecules* **2021**, *54*, 4269 – 4279.
'Structure-Property Relationships in Single-Ion Conducting Multiblock Copolymers: A Phase Diagram and Ionic Conductivities.'

Poster Presentations

Staiger, A., Mecking, S., Winey, K. I.
At the *Forschungstag 2022* of the Baden-Württemberg Stiftung, Stuttgart, June 2022.
'Precise Polymer Ion Conductors'

Publications Related to this Work

Park, J., Staiger, A., Mecking, S., Winey, K. I. *ACS Nano* **2021**, *15*, 16738 – 16747.
'Sub-3-Nanometer Domain Spacings of Ultrahigh-χ Multiblock Copolymers with Pendant Ionic Groups'

Park, J., Staiger, A., Mecking, S., Winey, K. I. *ACS Cent. Sci.* **2022**, *8*, 388-393
'Ordered Nanostructures in Thin Films of Precise Ion-Containing Multiblock Copolymers'

[†] Both authors contributed equally to this work.

Park, J., Staiger, A., Mecking, S., Winey, K. I. *ACS Macro Lett.* **2022**, *11*, 1008-1013.
'Enhanced Li-Ion Transport through Selectively Solvated Ionic Layers of Single-Ion Conducting Multiblock Copolymers'

Parts of this thesis have been reproduced and reprinted with permission.

Chapter 3:

Staiger, A.[†], Paren, B. A.[†], Zunker, R., Hoang, S., Häußler, M., Winey, K. I., Mecking, S. *Journal of the American Chemical Society* **2021**, *143*, 16725 – 16733. 'Anhydrous Proton Transport within Phosphonic Acid Layers in Monodisperse Telechelic Polyethylenes' (DOI: 10.1021/jacs.1c08031)

Chapter 4:

Park, J.[†], Staiger, A.[†], Mecking, S., Winey, K. I. *Macromolecules* **2021**, *54*, 4269 – 4279. 'Structure-Property Relationships in Single-Ion Conducting Multiblock Copolymers: A Phase Diagram and Ionic Conductivities.' (DOI: 10.1021/acs.macromol.1c00493)

Park, J., Staiger, A., Mecking, S., Winey, K. I. *ACS Nano* **2021**, *15*, 16738 – 16747.
'Sub-3-Nanometer Domain Spacings of Ultrahigh-χ Multiblock Copolymers with Pendant Ionic Groups'

Chapter 5:

Saumer, A., Mecking, S. *ACS Sustainable Chemistry & Engineering* **2023**, *11*, 33, 12414 – 12422.
'Recyclable and Degradable Ionic-Substituted Long-Chain Polyesters'

ZUSAMMENFASSUNG - ABSTRACT

Eine Vielzahl an Faktoren beeinflussen die Materialeigenschaften eines Werkstoffes und bestimmen mögliche Anwendungsfelder. Es ist unumstritten, dass die Mikrostruktur von Polymeren ausschlaggebend ist für die Kristallinität, die Kristallstruktur, sowie andere Effekte, die materialabhängig auftreten können. Im Falle von Polymeren mit ionischen Gruppen sind solche zusätzlichen Einflüsse insbesondere das Auftreten und die Struktur der ionischen Aggregate. Polymere mit einer genauen Kettenlänge oder einem exakten Abstand zwischen funktionellen Gruppen ermöglichen eine vorhersehbare und feine Abstimmung der Struktur-Eigenschafts-Beziehungen. Bislang gibt es nur wenige solcher genau definierten Polymere, die in der Regel eine langwierige mehrstufige Synthese im Labormaßstab erfordern, was sie für industrielle Anwendungen unbrauchbar macht. Im Gegensatz dazu lassen sich Polymere mit ionischen Gruppen und unkontrollierter Morphologie wie Nafion oder Surlyn als statistische Copolymere leicht und kostengünstig in großem Maßstab herstellen, doch fehlt es an einem tieferen Verständnis ihrer Struktur-Eigenschafts-Beziehung, und eine Kontrolle derselben ist schwer zu erreichen. Im Rahmen der vorliegenden Arbeit wurde diese Problematik in verschiedenen Ansätzen angegangen, sowohl in Polymerelektrolyten mit Fokus auf den Ionentransport als auch durch Einführung sehr niedriger ionischer Anteile, wodurch die Materialeigenschaften der zugrundeliegenden Polymere positiv beeinflusst wurden.

Polymere, die Phosphonsäuregruppen tragen, wurden als wasserfreie, protonenleitende Membranen bei erhöhten Betriebstemperaturen für Anwendungen in Brennstoffzellen entwickelt. Die Synthese von phosphonierten Polymeren und die Kontrolle über die Nanostruktur solcher Polymere ist jedoch eine Herausforderung. In dieser Arbeit wurde eine einfache Synthese von langkettigen aliphatischen Materialien mit genau 26 oder 48 Kohlenstoffatomen und Phosphonsäure-Endgruppen ($C_{26}PA_2$ und $C_{48}PA_2$) aus erneuerbaren Ressourcen entwickelt. Diese Materialien kombinieren die Strukturierungsfähigkeit von monodispersen Polyethylenen mit der Fähigkeit von Phosphonsäuregruppen, starke Wasserstoffbrückenbindungen zu bilden. Eine Anhydridbildung wurde nicht beobachtet bei erhöhten Temperaturen, sodass ein Ladungsträgerverlust durch eine Kondensationsreaktion auch bei höheren Temperaturen vermieden wird. Unterhalb der Schmelztemperatur weisen beide Materialien ein kristallines Polyethylengerüst und eine geschichtete Morphologie mit planaren Phosphonsäureaggregaten auf, die bei $C_{26}PA_2$ und $C_{48}PA_2$ durch 29 bzw. 55 Å voneinander getrennt sind (Abbildung 1).

Oberhalb der Schmelztemperatur koexistieren die amorphen Polyethylensegmente mit den geschichteten Aggregaten. Dieses Phänomen ist bei $C_{26}PA_2$ besonders ausgeprägt und wurde als thermotrope smektische flüssigkristalline Phase identifiziert. Unter diesen Bedingungen wird eine außerordentlich hohe Korrelationslänge (940 Å) entlang der Schichtnormalen beobachtet, was die Stärke des von den Phosphonsäuregruppen gebildeten Wasserstoffbrückenbindungs-netzwerks belegt. Die Protonenleitfähigkeit in beiden Materialien erreicht in Abwesenheit von Wasser 10^{-4} S/cm bei 150 °C. Diese neuen präzisen Materialien auf Phosphonsäurebasis verdeutlichen die Relevanz, die molekulare Struktur zu kontrollieren, um selbstorganisierte nanoskalige Aggregate zu bilden und dadurch eine hohe Protonenleitfähigkeit zu ermöglichen.

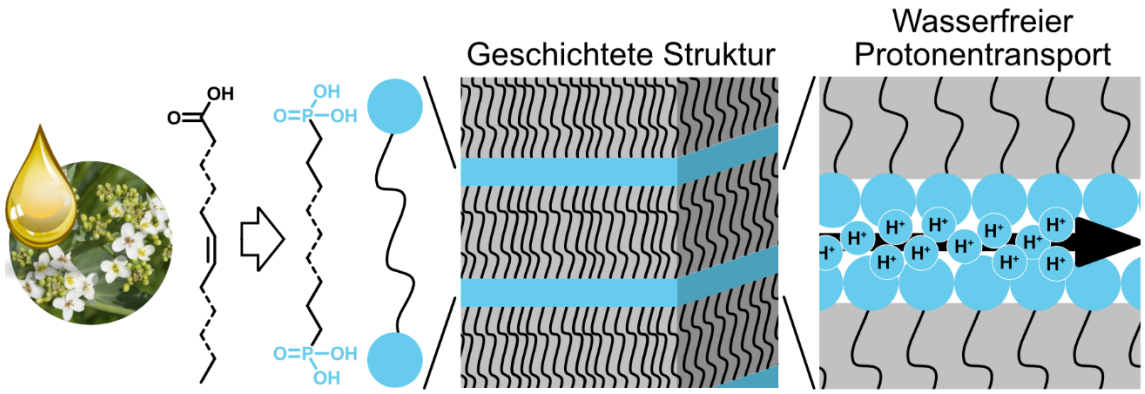

Abbildung 1 Schematische Darstellung der Synthese von Phosphonsäure-terminierten präzisen Polyethylen-artigen Materialien aus Pflanzenölen, ihrer geschichteten Struktur im Festkörper und in der Schmelze, und des wasserfreien Protonentransports innerhalb der geschichteten Aggregate.

Die Transporteigenschaften in präzise funktionalisierten, ionenhaltigen Materialien sind von großem Interesse für die Entwicklung von ionenleitenden Polymerelektrolyten, zum Beispiel für Anwendungen in Lithium- oder Natriumionenbatterien. Die kontrollierte Positionierung der ionischen Gruppen bewirkt eine Abhängigkeit der Leitfähigkeit von der nanoskaligen Morphologie. Dies wurde am Beispiel von präzise sulfonierten Polyestermaterialien angestrebt, die durch schrittweise Polykondensation aus einem kurzkettigen, ionischen, sulfonierten Block (Dimethylsulfosuccinat) und einem langkettigen, hydrophoben Polyethylen-Abstandshalter mit genau 10, 12 oder 18 Methyleneinheiten hergestellt wurden. Eine Untersuchung der Morphologie und Leitfähigkeit erfolgte im Rahmen einer Kooperation in der Gruppe von Prof. Dr. K. I. Winey. Bei Raumtemperatur weisen diese Polymere schichtförmige Ionenaggregate auf, die beim Erhitzen in hexagonale oder gyroide Morphologien übergehen. Die Polyethylensegmente schmelzen gleichzeitig mit dem Übergang der ionischen Aggregate von geschichteten zu

gyroiden Strukturen. Gemeinsam mit früher beschriebenen sulfonierten Polyestern mit einer größeren Länge des Polyethylen-Abstandshalters wurde ein Phasendiagramm entwickelt, das die Abhängigkeit der Morphologie der ionischen Aggregate vom polaren Volumenanteil (f_{polar}) und der Temperatur zeigt (Abbildung 2). Die gewünschte gyroide Morphologie wurde bei $0{,}27 < f_{polar} < 0{,}41$ gefunden, was ein breiter Bereich im Gegensatz zu früher beschriebenen Diblock-Copolymeren ist. Eine Untersuchung des Ionentransports in Abhängigkeit von der Morphologie der Ionenaggregate zeigt eine klare Bevorzugung der bikontinuierlichen Gyroidstruktur gegenüber der eindimensionalen hexagonalen oder der zweidimensionalen geschichteten Morphologie. Auf Grundlage dieser Ergebnisse wurden Leitlinien für die Entwicklung von ionischen Polymeren mit bikontinuierlichen Morphologien aufgestellt, die zur Entwicklung von Materialien mit effektivem Ionentransport führen oder Anwendung in der Nanolithografie finden.

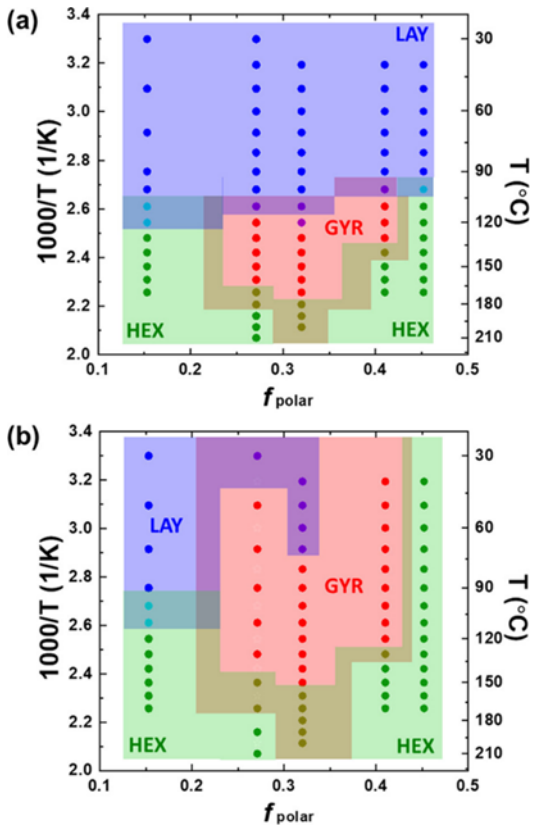

Abbildung 2 Morphologiekarten von Natrium-Polyestersulfonaten beim Erhitzen (a) und Abkühlen (b). Die Morphologie der ionischen Aggregate wird als LAY (geschichtet), GYR (gyroid) und HEX (hexagonal) abgekürzt.

Da sich die Gyroidstruktur nur dann bildet, wenn das Polyethylengerüst geschmolzen ist, könnte eine Expansion des Temperaturbereichs der Gyroidstruktur durch Unterbrechung der kristallinen Ordnung im Polyethylengerüst erreicht werden. Um die präzise Positionierung der

Sulfonatgruppen und folglich deren genauen Abstand beizubehalten, wurde Pripol als dimere Fettsäure gewählt, ein langkettiges aliphatisches Diol mit genauer Länge der Methylenkette. Da dieses Monomer f_{polar} beeinflusst, wurde dieser Wert in Abhängigkeit von der molaren Menge an Pripol und der Länge des linearen Diols berechnet (Abbildung 3). Es wurden verschiedene Kombinationen von Pripol und Längen des Diols experimentell getestet, und ein starker Einfluss des verzweigten Pripols auf die Morphologie wurde festgestellt. Beispielsweise wurde die Kristallinität des Polyethylen-Rückgrats sowohl mit 20 % Pripol in Kombination mit C_{12}-Diol als auch mit C_{18}-Diol erfolgreich gehemmt, wobei bei Raumtemperatur für Polymere mit C_{18}-Diol eine hexagonale Morphologie und für C_{12}-haltige Polymere unausgeprägte Schichten gefunden wurden. Dies zeigt den starken Einfluss von Pripol nicht nur auf f_{polar}, sondern auch auf die Gesamtordnung der Materialien.

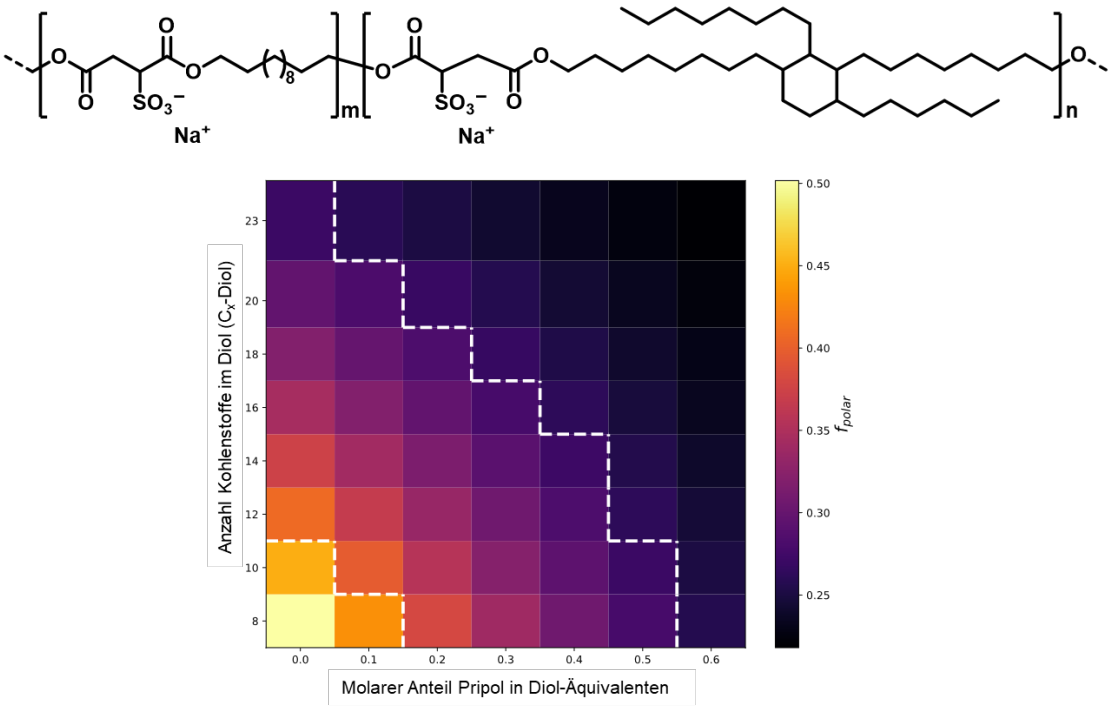

Abbildung 3 Oben: Struktur von Pripol enthaltenden Polyestersulfonaten mit Natrium als Gegenion. Unten: Berechnetes f_{polar} in Abhängigkeit von der Menge an Pripol und der Länge des Diols. Gestrichelte Linien zeigen die verschiedenen vorhergesagten Morphologien, wobei $f_{polar} > 0{,}41$ zu hexagonalen Morphologien führt, $f_{polar} < 0{,}27$ zu geschichteten Aggregaten und $0{,}27 < f_{polar} < 0{,}41$ die erwartete gyroide Region darstellt.

Durch Einführung von solch hohen molaren Anteilen an ionischen Gruppen in Polymere werden leitfähige Polymerelektrolyte zugänglich. Werden geringere Gehalte an ionischen Gruppen in Polyethylen eingeführt, können die guten mechanischen und thermischen Eigenschaften von Polyethylen erhalten bleiben. Gleichzeitig können sie durch den Grad der

Funktionalisierung und das zur Neutralisierung der ionischen Gruppen verwendete Kation beeinflusst werden. Solche Ionomere mit polyethylenähnlichen Eigenschaften basieren in der Regel auf Poly(ethylen-*co*-methacrylsäure)-Polymeren. Während diese durch einen variierenden Methacrylsäuregehalt oder eine teilweise Neutralisierung mit verschiedenen Kationen eine breite Palette von Einstellmöglichkeiten bieten, fehlt ihnen jegliche Abbaubarkeit oder chemische Recyclingmöglichkeit. In dieser Arbeit wurde eine neue Polyesterreihe mit niedrigen Anteilen an ionischen Gruppen entwickelt, die aus Pflanzenölen synthetisiert werden kann und in ihren strukturellen und mechanischen Eigenschaften Polyethylen-ähnliche Eigenschaften aufweist. Es wurden sowohl sulfonsäure- als auch neutralisierte sulfonathaltige Polyester untersucht und eine Untersuchung der Eigenschaftsabstimmung bei Neutralisation mit verschiedenen zweiwertigen Kationen (Mg^{2+}, Ca^{2+}, Zn^{2+}) durchgeführt. Ihre langkettigen aliphatischen Rückgrate bieten kristallisierbare Hartsegmente, und geringe Mengen an eingebauten Sulfonatgruppen bieten die Möglichkeit, die Polyesterketten ionisch zu vernetzen, was zu besseren rheologischen Eigenschaften führt. Säurehaltige Polyester weisen eine hohe Wasseraufnahmefähigkeit auf und zeigen einen schnellen Kettenabbau sowie eine vollständige chemische Rückführung zum Monomer. Die Oberflächeneigenschaften der neutralisierten sulfonathaltigen Polyester sind verbessert und zeigen eine höhere Adsorptionsfähigkeit. Diese Ergebnisse ermöglichen eine Feinabstimmung der Eigenschaften von rezyklierbaren polyethylenähnlichen Polymeren und erweitern den Anwendungsbereich dieser vielversprechenden Polyethylen-Alternativen.

Zusammenfassend lässt sich sagen, dass diese Arbeit Leitlinien für die Herstellung und Untersuchung präziser ionenhaltiger Polymere für Anwendungen wie Protonenaustausch-membranen in Brennstoffzellen oder feste Polymerelektrolyte liefert. Zu den Vorteilen gehört die kontrollierte Morphologie sowohl innerhalb der nicht-ionischen Abstandshalter als auch der ionischen Aggregate. Eine zufällige Gruppierung der ionischen Aggregate, die ein Hauptproblem und ein Nachteil der klassischen Polymerelektrolyte darstellt, kann durch diesen Ansatz verhindert werden. Hier wurden Grenzen für die Generierung von bikontinuierlichen Strukturen, insbesondere Gyroidstrukturen, in solchen ionenhaltigen Polymeren gesetzt. Durch diese Untersuchungen wird ein tieferes Verständnis für das Auftreten dieser höchst wünschenswerten Morphologien in Polymerelektrolyten gewonnen. In dieser Arbeit wurde der Schwerpunkt auf polyethylenähnliche Polymere gelegt, aber der Anwendungsbereich kann auf andere Polymere ausgedehnt werden und ist nicht darauf beschränkt.

Der einfache synthetische Ansatz wurde auf ionenhaltige Materialien mit sehr geringen Mengen an ionischen Gruppen ausgedehnt, was zu recycelbaren und abbaubaren Polymeren mit HDPE-ähnlichen Eigenschaften führt. Parameter, die angepasst werden müssen, sind der Ionengehalt und die ionische Gruppe selbst, der Polyethylen-Abstandshalter zwischen den funktionellen Gruppen oder die Art der funktionellen Gruppe. Diese Studien bilden die Grundlage für die Entwicklung HDPE-ähnlicher Polymere, die sich in ihrer Starrheit, Härte, Festigkeit oder Dehnbarkeit unterscheiden, aber insgesamt rezyklierbar und abbaubar bleiben.

TABLE OF CONTENTS

ANNOTATIONS

LIST OF ABBREVIATIONS

ADMET	acyclic diene metathesis
DBTO	dibutyltin oxide
DP_n	degree of polymerization
DSC	differential scanning calorimetry
dmso	dimethyl sulfoxide
dtbpx	1,2-bis{(ditertbutylphosphino)methyl}benzene
δ	chemical shift
ε_{tb}	elongation at break
EIS	electrochemical impedance spectroscopy
ESI	electrospray ionization
E_t	Young's modulus
EVE	ethyl vinyl ether
f_{polar}	polar volume fraction
G'	storage modulus
G''	loss modulus
GPC	gel permeation chromatography
HDPE	high-density polyethylene
ΔH_m	enthalpy of fusion
HMSS	dimethylsulfosuccinic acid
HRMS	high-resolution mass spectrometry
LAH	lithium aluminium hydride
LC	liquid crystalline
LDPE	low-density polyethylene
mol-%	mol fraction
M_n	number-averaged molecular weight
M_w	weight-averaged molecular weight
m/z	mass-to-charge ratio

η_0	zero-shear viscosity
n.d.	not determined
NMR	nuclear magnetic resonance
OOT	order-to-order transition
OTf	trifluoromethanesulfonyl group
PBAT	poly(1,4-butylene adipate-*co*-terephthalate)
PBS	poly(1,4-butylene succinate)
PE	polyethylene
PEM	proton exchange membrane
PEMFC	proton exchange membrane fuel cell
PEMA	poly(ethylene-*co*-methacrylic acid)
PEO	poly(ethylene oxide)
PES	polyestersulfonate
PLM	polarized light microscopy
ppm	parts per million
PS	Polystyrene
PTFE	poly(1,1,2,2-tetrafluoroethylene)
rt	room temperature
σ_y	stress at yield
SAXS	small-angle X-ray scattering
SMSS	sodium dimethylsulfosuccinate
SIPE	Single ion-conducting polymer electrolyte
θ	angle
TBT	titanium tetra-*n*-butoxide
THF	tetrahydrofurane
T_c	crystallization temperature
T_m	melting temperature
TMSBr	trimethylsilyl bromide
TOCSY	total correlation spectroscopy
U_T	toughness
vs.	*versus*
WAXS	wide-angle X-ray scattering
wt.-%	percentage by weight

XRD	X-ray diffraction
χ	crystallinity
χ_{eff}	effective Flory-Huggins interaction parameter

LABELING OF COMPOUNDS

All telechelic compounds used in this work, which consist of a hydrocarbon backbone and are of precise chain length, are labeled as

$$C_x(E)_2$$

where *x* is the number of carbon atoms within the hydrocarbon chain separating the two end groups, and E is the functional group in α and ω position of the chain. End groups are, amongst others, alcohols (OH), bromides (Br), or phosphonic acids ($PO(OH)_2$). The latter is additionally abbreviated as C_xPA_2 (C_x-di**p**hosphonic **a**cid). In case of the diols used for polycondensation reactions, the term C_x-diol is also used.

The polymer electrolyte materials based on polyestersulfonates are denoted as

PES*x*M

where PES abbreviates **p**oly**e**ster**s**ulfonate, *x* accounts for the number of methylene units in the alcohol spacer (C_x-diol), and M is the counterion at the sulfonate group (M = Na, Li or NBu_4). Polyestersulfonate materials containing 80 mol-% C_x-diol and 20 mol-% Pripol are denoted as

PES*x*M-Pripol

with the same definitions of *x* and M as for PESxM.

Non-ionic reference polyesters used in this work are accessed from long-chain aliphatic diols and diesters and are referred to as

PE*x.x*

where PE abbreviates **p**oly**e**ster and *x* accounts for the number of carbon atoms separating the alcohol and carboxylate, and is restricted to either 12 or 18 within this work.

Sulfonate-containing polyesters with low amounts of sulfonate are denoted as

PE*x.x*-SO3C-*n*

with PE and *x.x* having the same definition as in PE*x.x*, C being the counterion to the sulfonate group (C = H: sulfonic acid, C = Mg, Ca, Zn) and *n* being the molar amount of sulfosuccinate used in the reaction with respect to the aliphatic diol segment.

To abbreviate the series PE*x.x*-SO3Mg, PE*x.x*-SO3Ca and PE*x.x*-SO3Zn, which are usually compared with each other, the term **PE*x.x*-SO3M** is used (M = Mg, Ca, Zn).

The reference polyester series without sulfosuccinate units but with metal stearate (M = Mg, Ca, Zn; comparable to PE12.12-SO3C) is denoted as

$$PE12.12\text{-}M_{stearate}$$

Note that this polymer does not contain in-chain sulfonate groups as it is generated from C12-diol, C12-diacid, 1.0 mol% dimethylsuccinate and metal stearate.

1 General Introduction

Polymers represent one of the most important and versatile material classes to date. The monomers for the most widely used polymers such as polyethylene and polypropylene are typically accessed from fossil resources, e.g. ethylene and propylene. Although these resources are limited, their economic value was and is undefeated. Built from different monomers, the properties and material characteristics of polymers derive from the microstructure and, hence, the interactions between the chains. For example, polyethylene, as the most widely produced polymer, is simple in terms of composition, since it only consists of carbon and hydrogen. Its versatile use derives from its degree of branching and is solely dependent on van der Waals interactions.[1] Introducing other forces into polymers significantly alters their properties and gives rise to an enlarged field of applications. New classes of materials are obtained when ionic interactions play a role in polymers, which are often inspired by nature. If low amounts of ionic groups are introduced, the physical properties can be influenced significantly, leading to materials with similar chemical compositions yet strongly changed physical properties.[2] These materials were defined as ionomers and are currently used for example as thermoplastic elastomers, in packaging applications or as blend compatibilizers.[3] Introducing high amounts of ionic groups results in polymers which are interesting regarding their transport properties and are so-called polymer electrolytes. Since the invention of lithium ion batteries by J. B. Goodenough, M. S. Whittingham, and A. Yoshino, awarded with a Nobel Prize in 2019, the development of advanced electrolyte membranes is of great interest.[4] Solid polymer electrolytes are promising candidates to replace the currently used liquid electrolytes, which are disadvantageous due to their flammability and low ion density in the dissolved state.

Depending on the required application, not only the material properties need to be adaptable but also the persistency of polymers. For example, pipes made from high-density polyethylene (HDPE) need a high persistence to environmental influences, whereas packaging material that is unintentionally exposed to nature is demanded to be degradable and should be metabolized by microorganisms on a short time scale.[5] Varying the properties of polyethylene

and materials with polyethylene-like properties, for example by introducing ionic groups, opens the door towards a large variability in mechanical properties as well as different degrees of persistency and recyclability. This field has been of interest to researchers for decades, and new materials have been developed that broaden the spectrum of accessible property combinations.

1.1 Ion-containing Polyethylenes and Polyesters

Polymers consisting of both, ionic and non-ionic monomers, can be copolymerized to form a variety of ion-containing polymers. For example, ionic polyethylenes are accessible from copolymerization of methacrylic acid and ethylene, or ionic polyesters can be generated *via* polycondensation of different monomers. In this way, elastomers, thermoplastic elastomers, or thermoplastics can be ionically functionalized, and such products are commercially available. The most commonly used ionic groups are sulfonate or carboxylate groups either in their acidic form or partially neutralized, but other functional groups also being studied.[6] In addition, the properties are influenced by the placement of the functional or ionic groups, which can be either randomly attached to the polymer backbone or be regularly placed, e.g. alternating in the case of polyesters. They can also be placed along the main chain, at the ends of the polymer chain (so-called telechelics), or along the side chains (see Figure 1.1).[7] The introduction of the ionic groups can occur directly during the polymerization or pre-polymers with reactive sites can be functionalized after the polymerization.

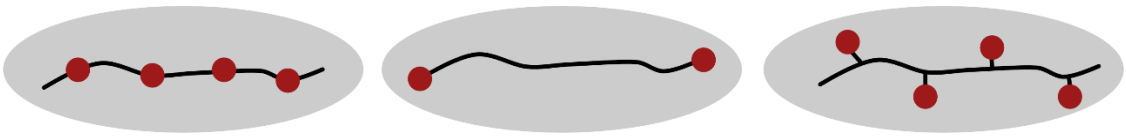

Figure 1.1 Different placements of functional or ionic groups within the polymer backbones: Within the main chain (left), at the ends of the chain (center) or at the side chains (right).

1.1.1 Ion-containing Polymers

Ionomers are defined as ion-containing polymers, where the ionic groups are covalently attached to the polymer chains. The degrees of functionalization are lower compared to polymer electrolytes and are in the range of < 10 mol% with respect to the repeating unit.[6] The first ionomer presented was Surlyn by DuPont in 1964, which is the trade name for a random copolymer of ethylene and methacrylic acid, poly(ethylene-*co*-methacrylic acid) (PEMA).[8] The acidic groups are partially neutralized with sodium or zinc cations, giving rise to a great variety of

different polymers. Applications are found in electronic or medical packaging and are versatile due to its high puncture strength, toughness, and hot tack.[9] Surlyn is commercially produced as a thermoplastic ionomer, and many other ionomers have been presented and are produced on an industrial scale since its first introduction 60 years ago.[2]

Due to the strong ionic interactions, ionomers can be described as nano-structured materials. The ionic blocks, surrounded by the polymer backbone with a low dielectric constant, phase separate and form nanodomains. According to the Eisenberg-Hird-Moore (EHM) model, the ionic interactions overlap to form multiplets, which are regions of reduced polymer chain mobility induced by the ionic cross-linking.[10] The strength of these associations and, consequently, the size and rigidity of the multiplets, depend on steric effects of the polymer chains, the strength of the ionic interactions as well as the degree of functionalization. With an increasing ionic fraction, the multiplets overlap and form so-called clusters (see Figure 1.2).

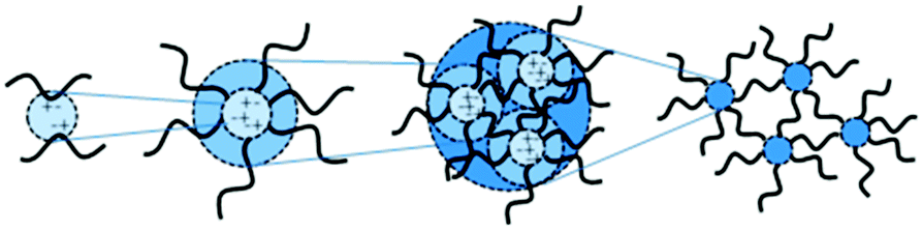

Figure 1.2 Schematic depiction of the hierarchical structure of ion clusters. From left to right: ion pair formation, multiplet formation from overlapping ion pairs, cluster formation from the multiplets and the phase separated polymer network. Reprinted with permission from [11]. Copyright 2015 Royal Society of Chemistry.

The amorphous phases in semicrystalline ionomers contain the ionic groups either as single ion pairs or multiplets, clusters are regarded as separate phase and, if present, introduce a second glass transition. Thus, three phases exist: a crystalline domain, consisting of lamellae in polyethylene-based ionomers where the polymer backbone is chain folded, the amorphous domains with a low dielectric constant, and the ionic domains dispersed within the amorphous domains.[12]

The uncontrolled aggregate formation in ionomers can be ascribed to the uncontrolled incorporation of the ionic groups in the polymer backbone. PEMA is synthesized by free radical polymerization of ethylene and methacrylic or acrylic acid in a process that is typical for low-density polyethylene (LDPE).[7] Other factors such as the polymer chain architecture (linear or branched) or the copolymer composition hinder a deeper understanding of the structure-property relationship in acid- and ion-containing polymers. Gaining control over the placement

of the ionic groups on a molecular level allows for a more fundamental investigation of the aggregates and the consequences on the material properties not only by experimental techniques but also by computational methods.[13-14] Significant effort has been made to introduce the ionic groups in a precise rather than a random way to control the microstructure of the polymers. For example, in precise PE-based ionomers, the crystallization of the unfunctionalized segments leads to a phase exclusion of the ionic groups and layered aggregates form.[14-17] Combined with atomistic molecular dynamics simulations, it was found that in precise PE-based ionomers with carboxylic acid groups, a hairpin turn occurs close to the functionality, forming layered aggregates separated by the crystalline domains (see Figure 1.3).[18]

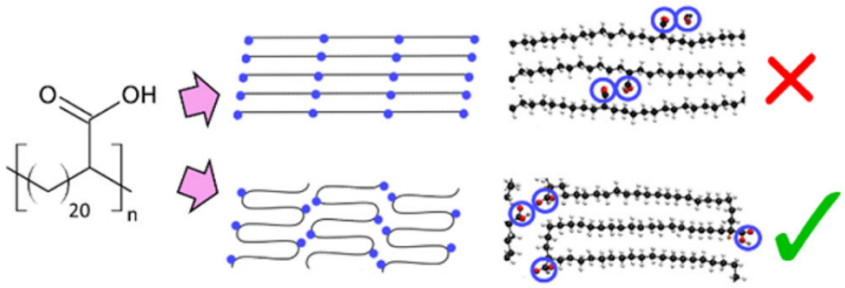

Figure 1.3 Structure of PE-based ionomers containing carboxylic acid groups in a precise positioning along the polymer backbone. The top row shows a possible structure with layered aggregates and stretched chains which is not adapted; the bottom row shows the hair-pin turns observed. Reprinted with permission from [18]. Copyright 2017 American Chemical Society.

The ionic aggregates and their near-aggregate regions of reduced chain mobility according to the EHM model alter the mechanical properties to a significant degree, i.e. enhanced yield stress is obtained due to a hindered chain relaxation in the amorphous phases.[19] A formation of layered aggregates upon stress in carboxylic acid containing ionomers was shown to be the reason for a substantial degree of strain hardening.[15] Control over the microstructure in ionomers facilitates a correlation of the material properties to the ionic aggregate morphology and enables a fine-tuning and adaptation of the material properties to meet the demands in sophisticated applications.

As described above, ionomers are not limited to PE-based polymers but can be based on any other polymers. One important class of ionomers previously investigated are polyesters, in particular polybutylene succinate (PBS) and polybutylene adipate terephthalate (PBAT), which are labeled as biodegradable polyesters, making them valuable materials to investigate the influence of ionic groups on their biodegradation. The material properties of PBS are of poor quality, since it is a brittle material. Introducing ionic groups is used as a method to improve the

material properties and to tune the biodegradation at the same time.[20-24] In case of PBAT, its LDPE-like properties can be tuned by introducing ionic groups, and, comparable to PBS, its biodegradation rate and water dispersibility was shown to be adjustable.[24-25] Lee et al. showed that phosphate containing PBAT materials, neutralized with different bivalent cations, were highly flexible materials on par with PBAT and they found a significantly increased biodegradability compared to the non-ionic reference polyester.[24] However, the general material properties of PBS and PBAT limit their application field even when they are improved by ionic interactions.

1.1.2 Telechelics

A subclass of ionomers are telechelics, where the ionic groups are placed at the ends of the polymer chains. Telechelic ionomers of low or medium molecular weight are desired precursors for example to access segmented ionomers *via* chain extension or for the generation of ionic polyurethanes.[7] They can also be used as cross-linkers or to generate dendritic polymers.[26] A large number of strategies is available to access telechelic polymers, amongst which are atom transfer radical polymerization, living anionic or cationic polymerization, ring opening metathesis polymerization or selective insertion polymerization, to name a few.[26-27]

The nature of the telechelic end groups is crucial for the properties of the polymers. For example, alcohol end groups can be used with difunctional isocyanates for polyurethane generation or, for instance, can be further reacted with dicarboxylic acids to obtain block-copolyesters. Rank et al. presented polyethylene telechelics with carboxylate end groups with a defined chain length and showed a layered structuring of the ionic aggregates. Selective ion transport along these layers was found.[28] Paren and Häußler et al. introduced sulfonate end groups on these polyethylene telechelics and showed a higher dissociation of the counterions from the ionic groups, leading to a higher ionic conductivity within the layers.[29]

Accessing telechelic molecules with a uniform chain length is possible from fatty acids, which naturally bear an oligomethylene unit of a defined chain length with a specific number of double bonds that can be used for further functionalization. For example, oleic acid with its C_{18} unit or erucic acid with a C_{22} unit both contain one double bond in the chain that can be used, for example, in olefin metathesis to obtain telechelic diacids (or diesters). Witt et al. presented a 'chain doubling approach', in which a selective isomerization of the double bond in the metathesis

product to the chain end and a subsequent second metathesis step allow for an effective chain doubling of the original fatty acid chain (Figure 1.4).[30]

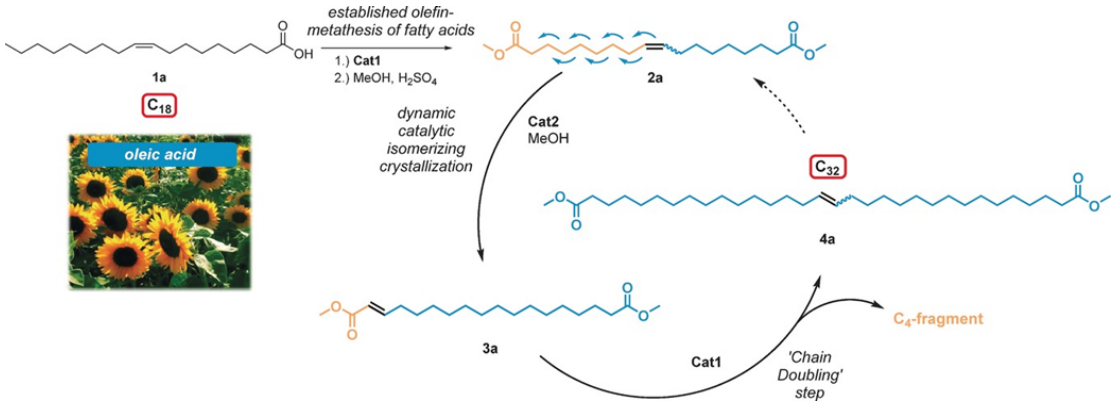

Figure 1.4 Conversion of mono-unsaturated fatty acids to ultra-long chain aliphatic telechelics with a precise chain length. Reprinted with permission from [30]. Copyright 2017 John Wiley and Sons.

Telechelics with precisely 32 carbon units can be access this way when oleic acid is used, and a chain length of 48 was shown to be accessible using erucic acid as starting material. A different method to access precise telechelic materials with a polyethylene backbone from fatty acids is isomerizing alkoxycarbonylation, where a carboxylic acid or ester group is selectively introduced at the ω-chain end (Figure 1.5).[31-32]

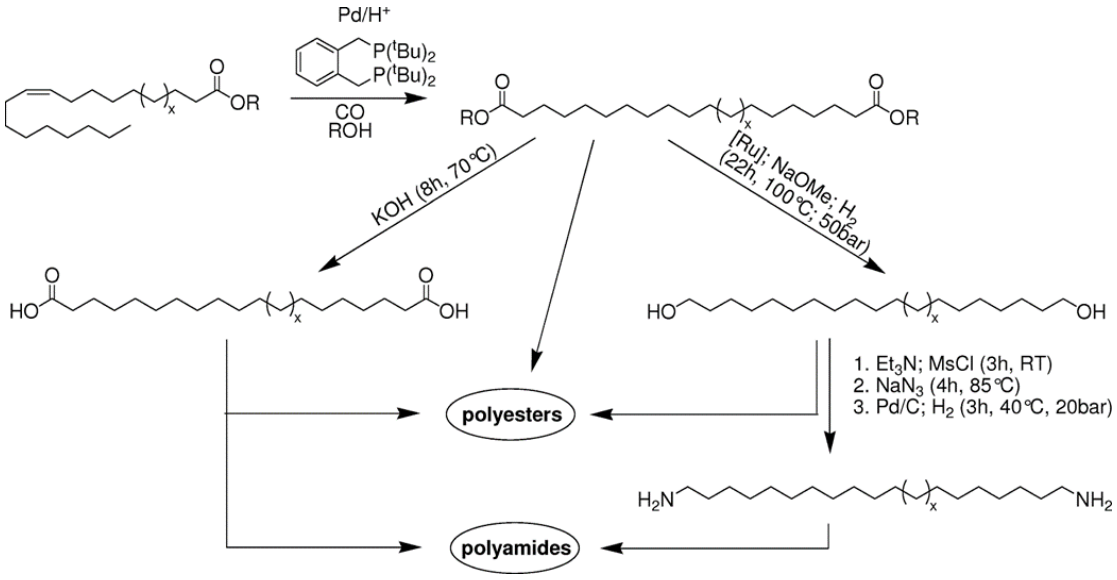

Figure 1.5 Catalytic conversion of oleic acid (x = 1) or erucic acid (x = 5) by isomerizing alkoxycarbonylation to obtain telechelic compounds with a precise chain length. Further possible transformations of the telechelic end groups are depicted as well as possible syntheses of polymers from the telechelic materials. Reprinted with permission from [33]. Copyright 2011 American Chemical Society.

The end groups of these precise telechelics can be further converted to alcohol or amine groups by standard organic reactions. For example, a reduction of the ester groups with lithium aluminum hydride yields the respective diol, and a further conversion of the alcohol end groups gives access to different functional groups, such as amine or bromide groups. One application of long-chain aliphatic telechelics is the synthesis of polymers to obtain polyethylene-like polymers with in-chain functional groups.[33-35]

1.1.3 Polyethylene-like Polymers

The highly linear chains in HDPE allow for a high crystallinity in the polymers, originating from non-covalent interactions (Figure 1.6). This property enables the high mechanical strength of HDPE and is the reason for its versatile applications. However, its hydrophobic nature can impede wettability with water as well as adhesion of other polar substances on the polymer surface. Also, the lack of functional groups or other accessible sites is the reason for the high persistency of PE in nature, hindering a biodegradation process. Introducing functional groups is consequently of interest since they present breaking points for example for hydrolytic or enzymatic cleavage.[36]

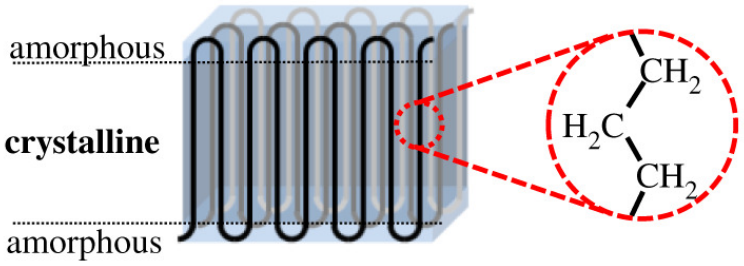

Figure 1.6 Crystallization of linear polyethylene-chains in lamellae. Reprinted with permission from [37]. Copyright 2020 Royal Society of Chemistry.

Using telechelic monomers of precise chain length in a step-growth polymerization rather than ethylene in a chain-growth polymerization leads to polymers with crystallinity comparable to HDPE, and the respective polymers accessible from these compounds can be considered polyethylene-like. They include polyesters, polycarbonates or polyamides, to name a few.[37] The functional groups also enable the chemical recycling of these polymers by hydrolysis or solvolysis to re-gain the valuable monomers, which can subsequently be repolymerized. This allows for fully recyclable polyesters and polycarbonates with a C_{18} repeating unit (polyester-18.18 and polycarbonate-18), on-par with HDPE in all major material properties.[38]

A tuning of the properties of polymers can be achieved for example by varying the nature of the functional group or the functional group density. Thus, polyacetals and polycarbonates show significantly faster hydrolytic chain cleavage than polyesters.[39] Poly(H-phosphonate)s with long-chain aliphatic spacers hydrolytically degrade on a time scale of a few days, which could be slowed down by transforming the functional groups into phenylphosphonates.[40] Since the functional groups disturb the PE crystallinity, the chain length of the telechelic monomers is crucial for the thermal properties of the resulting polymer. Stempfle et al. observed a significant decrease in the melting temperature with decreasing monomer chain length of polyesters made from fatty acid derived long-chain diols.[41]

To summarize, telechelic monomers can be accessed from renewable resources such as fatty acids and can be further converted into polymers which represent valuable alternatives to benchmark polymers. A precise positioning of functional groups within the polymer chains allows for comparable crystallinities as PE while breaking points are present for possible degradation mechanisms or recycling processes.

1.2 Ion Transport related to Energy Storage

There is no doubt that energy storage is one of the main challenges the world faces today and in the future. An increasing portion of renewable energy also increases the demand for storage of energy in order to be available at all times. Electrochemical energy storage is one of the key methods, where energy is stored by charge transfer reactions within the electrodes.[42] The most prominent representative is the lithium ion battery, where lithium transports the charge through a liquid electrolyte, and is intercalated in the graphite anode upon charging or in a cobalt oxide structure upon discharging.[43] The electrolyte, which separates the anode from the cathode, is an organic liquid to date, and calls for a strong improvement, as it is flammable and one of the main reasons for the safety issues with lithium ion batteries. Solid polymer electrolytes represent a possible solution due to their inflammable nature and the possibility to dissolve ions when polar polymers are chosen.[44]

Another method for energy storage of increasing relevance are of fuel cells, where hydrogen and oxygen are reacted under controlled conditions to form water, which generates electric energy as well as heat. Here, the proton exchange membrane separating anode and cathode is again a key component of the overall fuel cell design.[45]

1.2.1 Solid Polymer Electrolytes

The disadvantages of liquid electrolytes such as insufficient electrochemical and thermal stability, low ion selectivity and the major issue of flammability drive the intense search for alternative electrolyte materials.[46] Solid polymer electrolytes (SPEs) are one class of promising alternatives amongst others such as ceramics, oxides or sulfides.[47] In the 1970s, poly(ethylene oxide) was found to be a suitable polymer solvent for alkali metal salts, which opened the field of polymer electrolyte research.[48] However, other issues arise from SPEs with dissolved salt in a polymer matrix. Anions and cations typically show different mobilities and lead to cation transference numbers (defined as the charge fraction carried by the different ions) lower than 0.5 [49] Another disadvantage is the formation of ion pairs since the polymer matrix exhibits low permittivity. This leads to a significant loss of charge carriers and reduces the overall conductivity. Also, problematic dendrite formation is not suppressed by polyether electrolytes, and further development of this approach is required.[49] By covalently attaching either the anions or the cations on a polymer backbone, single-ion conducting polymer electrolytes are formed. Only one ionic species is mobile in this case, typically the cation, hindering electrode polarization and enabling high transference numbers of ~ 1.[50] Placing the ionic groups in precise positions rather than in a random fashion along the polymer backbone allows for hairpin-fold turns at the ionic group position and enables the formation of structured ionic aggregates such as layers (Figure 1.7).

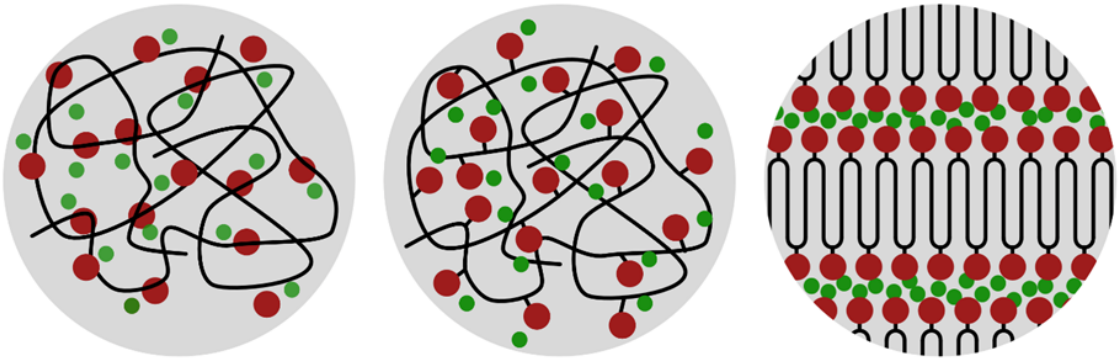

Figure 1.7 Schematics of different forms of solid polymer electrolytes: salt dissolved in a polymer matrix (left), single-ion conducting polymers where the anion is covalently attached to the polymer backbone (center) and precise single-ion conducting polymers with a regular placement of the anions along the polymer chains (right).

This was shown by Winey and coworkers for many different materials such as polyethylene bearing sulfonic acid or carboxylic acid groups on every 21st carbon atom, or in case of copolyesters with a precise polyethylene spacer of 48 methylene units separating the ionic functionality.[51-53] Layered structures were also found in polyethylene oxide-based polymers with tethered sulfonate groups by Abbott et al.[54] Controlling the morphology *via* the placement of the ionic groups allows for a simultaneous control over the ion clustering behavior, which is difficult to achieve in random copolymers.

Ionic aggregate structures are not limited to two-dimensional layered morphologies, other possible morphologies are hexagonal (one-dimensional) or double gyroid (three-dimensional), for instance. Especially the latter is of interest regarding ion conductivity due to the interconnected channels, allowing for a transport in all dimensions.[55] Yan and Rank et al. developed polyestersulfonates as multiblock copolymers with a long-chain polyethylene segment as hydrophobic spacer and a short-chain unit bearing a sulfonate group, which phase separate and form self-assembled layers at room temperature. Upon heating, these layers were shown to transition into double gyroid morphologies and, upon further heating, hexagonal structures evolve (Figure 1.8).[56]

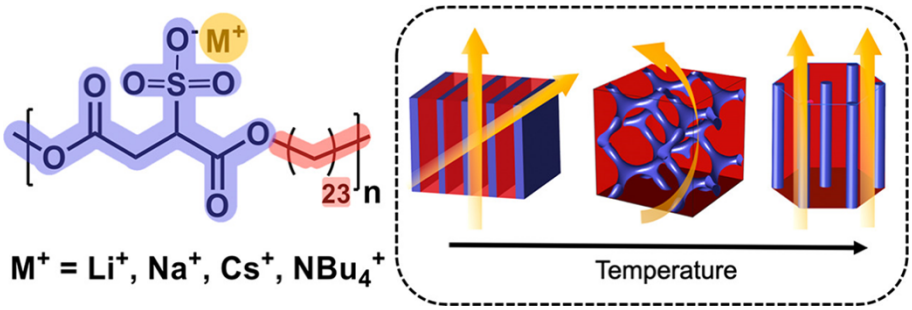

Figure 1.8 Left: Repeating unit of precise sulfonate-containing polyesters with a polyethylene spacer of uniform length. Right: Scheme of different ionic aggregate morphologies accessible with increasing temperature (layered, gyroid and hexagonal). Reprinted with permission from [56]. Copyright 2020 American Chemical Society.

A strong dependence of the ionic conductivity on the aggregate morphology was found, and a beneficial impact of the gyroid structure on the ion transport was concluded. As a prerequisite for the gyroid morphology, amorphous polymer backbones and a well-defined polymer microstructure was identified. These results encourage the development of single-ion conducting solid polymer electrolytes with close control over the ionic aggregate morphology with the aim of three-dimensionally interconnected structures to enhance ion transport.

1.2.1 Fuel Cells and Proton Exchange Membranes

For on-site production of energy where the supply needs to be uninterrupted and based on demand, fuel cells are a valuable and sustainable alternative to the generation of energy from fossil fuels. Proton exchange membrane fuel cells (PEMFCs) are among the five main types of fuel cells, which are characterized by the electrolyte type. Others are alkaline fuel cells, phosphoric acid fuel cells,, molten carbonate fuel cells and solid oxide fuel cells.[42]

In PEMFCs, the polymer membrane acting as an electrolyte is the core of the cell, to which the electrodes are attached. To date, the most used polymer electrolyte is Nafion, a perfluorinated polymer with pendant sulfonic acid groups developed by DuPont.[57-59] Nafion is synthesized by copolymerization of tetrafluoroethylene and a perfluorinated vinyl ether bearing a sulfonic acid group (see Figure 1.9).

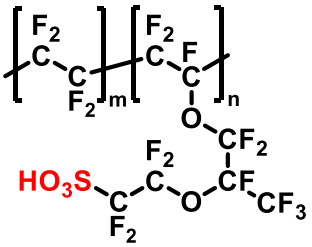

Figure 1.9 Chemical structure of Nafion, a random copolymer of tetrafluoroethylene and perfluorinated vinyl ether with a pendant sulfonic acid group (marked in red).

The exact structure of the random copolymer Nafion was subject to extensive studies yet remains a subject of discussion to date.[57,60] The water channels are assumed to be cylindrical, allowing for a one-dimensional proton transport along the hydrophilic domains, separated by the hydrophobic polytetrafluoroethylene-like phase.[61] Placing the ionic groups in polymer electrolytes in precise positions along the polymer backbone rather than in a random fashion allows for a control over the microstructure. Self-assembled layers were shown in many examples to have a beneficial impact on proton transport, making a control over the ionic aggregate morphology a main aim in polymer electrolyte research.[62] Trigg et al. showed that precise sulfonic acid containing polyethylenes order into well-defined layered structures, which remain present upon hydration and lead to a proton conductivity comparable to Nafion (Figure 1.10).[53] This is remarkable due to the lower acidity of alkylsulfonic acids compared to the perfluorinated vinyl ether derivative in Nafion and highlights the beneficial impact of crystalline structure on proton transport. For a long time it was assumed that crystallinity impedes proton conductivity due to the reduced polymer segmental motion as well as the crystallites themselves acting as

barriers. Systematic studies by Li and coworkers on solution grown PEO single crystals have shown that these effects cannot be generalized and that the conductivity is not influenced by crystallization at moderate ion contents.[63] Not only the proton conductivity can be enhanced by the presence of crystalline phases, but also the mechanical properties of the matrix material are improved, making this approach of interest to access proton exchange membranes of the next generation.

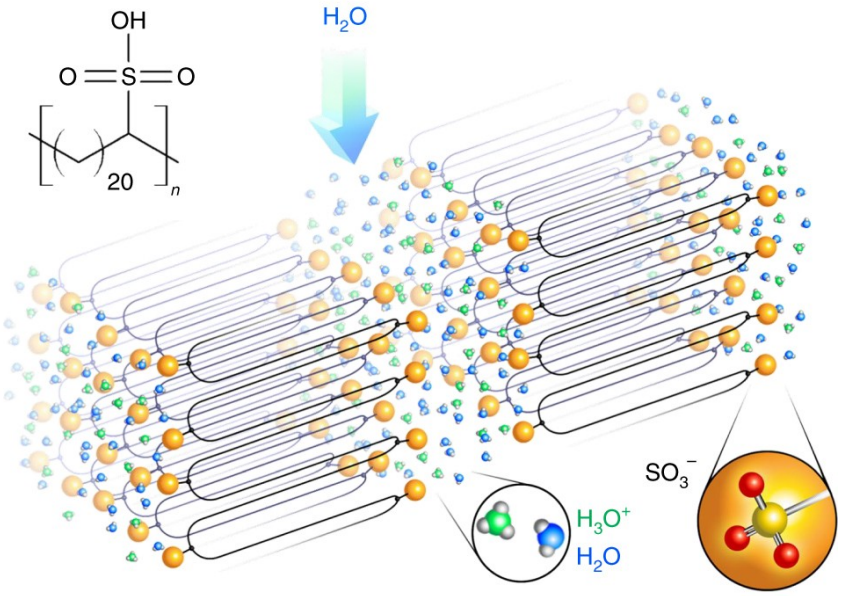

Figure 1.10 Schematic representation of precisely sulfonated polyethylene with hydrated sulfonic acid channels in the form of layers allowing for high proton conduction on par with Nafion. Reprinted with permission from [53]. Copyright 2018 Springer Nature.

One major challenge of Nafion is that high proton conductivities are only reached under hydration, which is a prerequisite for the formation of water channels within the cluster-network.[57] Possible water concentration gradients would lead to back-diffusion, which is why a constant hydration and equilibrium must be held. It was shown that a water content of 30 – 60 % is necessary for operations at high currents.[42] However, the requirement of hydration limits its application to temperature and pressure combinations where the boiling point of water is not reached. Operating temperatures above 80 °C are desirable since the electrode reactions are significantly faster at higher temperatures, and the large problem of carbon monoxide poisoning the catalyst is reduced at temperatures where CO does not adsorb to the materials.[64-65] However, under low humidities and at higher temperatures, the proton conductivity of Nafion is significantly reduced, and the thermal stability of the membrane reaches its limit.[66] These

disadvantages and limitations promote the search for alternatives which are thermally stable at elevated temperatures and exhibit a high proton conductivity in the anhydrous state.

2 Objectives

Polymers containing ionic groups are relevant in different fields, for example for energy storage in form of electrolytes, for nanolithographic methods to transfer structures to inorganic materials, or for tuning specific properties of a parent polymer with respect to their potential application. For these purposes, aliphatic polymers with polyethylene-like properties are of interest, since they can posess well-defined morphologies due to their linear hydrocarbon backbones. Accessing ion-containing polymers with such defined morphologies is challenging due to the propensity of the ionic groups to from poorly controllable clusters. The synthesis of ionic polymers with precise positioning of the ionic groups along the backbone allows for an elucidation of the properties' correlation with respect to the ionic groups position and, hence, the design of polymer morphology.

This work reports on the synthesis of polyethylene-like telechelic phosphonic acids with precise chain lengths of 26 and 48 carbons. A catalytic approach is chosen to obtain such precise telechelics, and the interplay of structure and proton transport ability is investigated (*Chapter 3*). The development of new ion-conducting polymer electrolytes with a precise positioning along the polymer backbone motivates the synthesis of single-ion conducting polymer electrolytes exhibiting double gyroid structures, which are further investigated regarding their structure-property relationships. A special focus is set on identifying the temperature regime in which the ionic aggregates exhibit gyroid structures, as well as the expansion of this regime to lower temperatures (*Chapter 4*). The effect of low amounts of ionic groups incorporated in polyethylene-like polyesters is investigated with regard to the material properties. The stability of these ion-containing polymers in aqueous environments as well as their recyclability in order to regenerate valuable monomers is elucidated (*Chapter 5*).

3 Phosphonic Acid Functionalized Polyethylene-like Telechelics

3.1 Introduction

The storage and on-site production of green energy is a major challenge facing the future of energy infrastructure. Fuel cells are amongst the most promising candidates to meet this increasing demand for energy supply. Much effort is being invested into the search for better proton exchange membranes (PEMs) for the use in fuel cells. State-of-the-art PEMs consist of single-ion conducting polymers, which typically have perfluorinated backbones and sulfonic acid groups covalently attached to the polymer backbone, with one of the industry standards being Nafion™.[57-59] Rapid proton transport in polymers containing sulfonic acid groups is enhanced by the presence of water, which leads to the formation of charge carriers in nanoscale hydrophilic domains.[67] However, the dependence of proton transport on water restricts the use of such polymer membranes to temperatures below 100 °C at atmospheric pressure. Higher operating temperatures are desirable for many reasons, for example to prevent catalyst poisoning by the adsorption of fuel impurities or regarding the simultaneous generation of electric and thermal energy.[64-65] Thus, polymers with a high thermal stability and a high proton conductivity in the absence of water are desirable. Recent studies have demonstrated the potential of phosphoric acid-doped polybenzimidazoles as high temperature anhydrous PEMs, though while proton conductivity is high, these PEMs are vulnerable to acid leaching.[65,68-69]

To overcome this challenge, polymers bearing covalently bound phosphonic acid groups are promising candidates, as they are resistant to acid leaching and exhibit higher thermal and chemical stability than their sulfonated analogues, as well as transport protons effectively under both humid and dry conditions.[70-71] The lower acidity of phosphonic acid compared to sulfonic

acid typically leads to lower overall conductivities in phosphonated polymers.[72] However, the self-dissociable, amphoteric nature of phosphonic acid gives rise to well-connected hydrogen-bonded networks in phosphonated polymers and these aggregated phosphonic acid groups are essential for achieving high proton conductivities.[73-75] A sophisticated design of phosphonated polymers with a high degree of functionalization may capitalize on this hydrogen-bonded network formation and lead to enhanced proton transport. A complementary approach to accessing highly proton-conducting PEMs is to utilize polymers with ionic functional groups precisely spaced, and covalently attached to the polymer backbone.[76] Designing precisely spaced polymers can lead to control over both the ionic aggregate nanostructure and the polymer crystallinity.[18,28,51,56,77-79] Trigg et. al. reported a polyethylene-like material with precisely placed sulfonic acid groups along the backbone, which exhibits a nanoscale layered morphology when hydrated that results in excellent proton conductivity.[53] However, introducing phosphonic acid groups to the polymer backbone in a precise way is hampered by several synthetic difficulties, such as the high tendency of the phosphonic acid groups to aggregate and, in the case of polymerization with esterified phosphonic acid derivatives, the harsh conditions necessary to cleave the ester bonds in the polymer.[80-82] These issues and the tedious multi-step procedures required have hindered studies of precisely phosphonated polymers synthesized via acyclic diene metathesis (ADMET).[16,83-84]

Ionic polymers can form thermotropic liquid crystalline (LC) phases in a temperature range above the crystalline solid and below the isotropic liquid.[85] The intermolecular interactions of the ionic groups and the polymer backbones can lead to the formation of LC nanostructures formed by nanosegregation of the polar and unpolar segments.[86] In proton conductors, the formation of hydrogen-bonded networks by self-induced ordering of the functional groups is favourable with regard to long-range and fast proton transport.[87] Liang et al. reported on phosphonic acid end-functionalized compounds that exhibit thermotropic LC phases at elevated temperatures, forming bilayered assemblies.[88] The beneficial impact of the liquid crystalline phases on the anhydrous proton conductivity was clearly demonstrated.

Polyethylene (PE) based materials are attractive as PEMs due to their ability to crystallize and self-assemble into ordered aggregate morphologies, as well as their chemical stability.[89-92] These features can be combined with covalently-attached ionic groups in PE telechelics, which contain functional groups as end groups. Telechelic polyethylenes generated by ethylene insertion chain growth have a distribution of chain lengths, even from living catalytic chain transfer

protocols.[27,93-94] Witt *et al.* recently reported an alternative route to polyethylene telechelics, giving access to end group functionalized and low molecular weight PE with precise chain lengths, e.g. 48 carbon atoms. This scalable approach is based on entirely catalytic reactions starting from common plant based fatty acids as a feedstock.[28,30,95] The precisely monodisperse backbones crystallize in a polyethylene-like orthorhombic motif, resulting in layers of functional groups alternating with highly-crystalline extended-chain polymer segments as demonstrated for carboxylate- and sulfonate-terminated telechelics with alkaline metal counterions.[28,95] For these monovalent end groups, the hydrocarbon segments are still able to exhibit order even though the end groups may reduce ordering. For bivalent end groups such as phosphonates the interplay of charge vs. order has yet to be investigated.

This chapter reports on monodisperse polyethylene chains with two phosphonic acid end groups that form extended-chain layered aggregates that facilitate the anhydrous transport of protons. These polymers achieve a maximum conductivity in the thermotropic liquid crystalline phase at favorable temperatures around 140 °C.

3.2 Results and Discussion

The long chain aliphatic C_{48} telechelics were previously investigated with regard to their ion conductivity in dicarboxylates and disulfonates.[28-29] They show very instructive structure-property relationships due to the strong tendency of the aliphatic hydrocarbon segments to crystallize and the strong ionic interactions of the metal carboxylate and sulfonate end groups. To investigate the influence on the structure-conductivity interplay, phosphonic acid groups as bivalent end groups were introduced to these precise telechelics, with polyethylene spacer lengths of C_{26} and C_{48}.

3.2.1 Synthesis of Phosphonic Acid Functionalized Telechelics

The saturated C_{26} and C_{48} telechelic starting materials were obtained by reported procedures.[30] Starting from erucic acid, a self-metathesis reaction directly yields the C_{26} building block precursor.[96] A further dynamic catalytic crystallizing double bond isomerization step followed by an effective olefin self-metathesis resulted in 'chain doubling' to the C_{48} precursor. Subsequent hydrogenation of the double bond and reduction of the acid ester end groups yields the respective C_{26} and C_{48} diols, $C_{26}(OH)_2$ and $C_{48}(OH)_2$. Reaction conditions were established for increased batch sizes and the work-up was simplified compared to the original procedure (cf. Supporting Information for details). Note that this synthetic approach is transferable to other fatty acid substrates, giving access to multiple chain lengths of the polyethylene. The end group modification of the polyethylene-like telechelics is challenging due to their limited solubility and the difficulty to separate starting materials from the products in case of non-quantitative conversions. Therefore, reaction conditions were implemented for all reaction steps that meet the following demands: sufficient solubility of the starting materials, quantitative conversions, simple work-up conditions and applicability to increased batch sizes. The conversion to $C_{26}Br_2$ and $C_{48}Br_2$, which was originally performed by an Appel reaction of $C_{48}(OH)_2$ with CBr_4 and PPh_3,[95] was replaced by a more atom-efficient bromination with phosphorus tribromide in toluene (Scheme 3.1). This reaction was implemented in collaboration with Dr. Manuel Häußler and is described in detail in his thesis.[97] The purification of the product included the hot filtration over a short plug of silica and recrystallization from the solution. This yielded the pure $C_{26}Br_2$ and $C_{48}Br_2$. The conversion of the end groups was monitored by ^1H nuclear magnetic resonance

(NMR) spectroscopy via the indicative high-field shift of the *α*-methylene resonance from 3.7 to 3.4 ppm (in tetrachloroethane-d_2 at 110 °C). Phosphonate ester groups were introduced by a Michaelis-Arbuzov reaction with triethyl phosphite to quantitatively yield $C_{26}(PO(OEt)_2)_2$ and $C_{48}(PO(OEt)_2)_2$. Excess triethyl phosphite was distilled off after the reaction was completed.

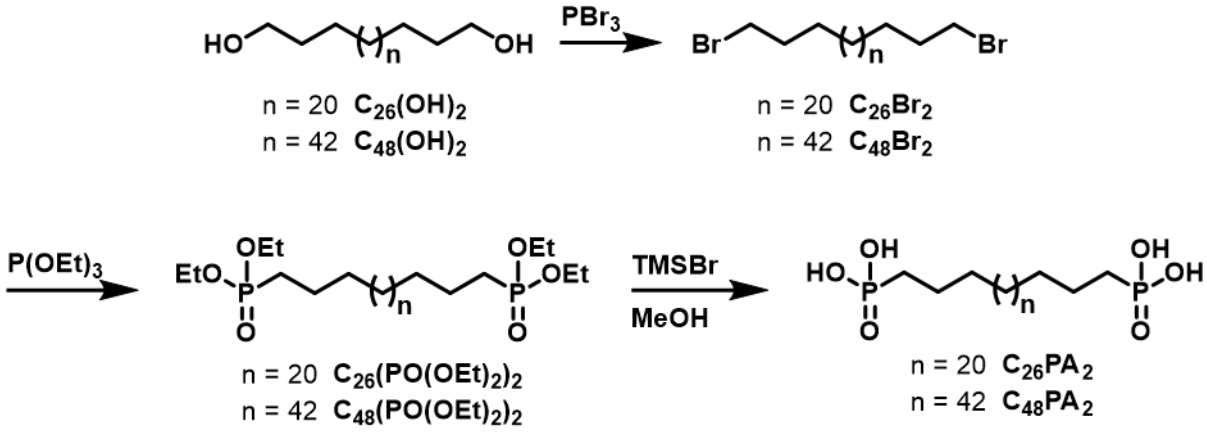

Scheme 3.1. Synthesis of telechelic phosphonic acids starting from the respective telechelic diols.

The endgroups' ^{31}P NMR resonance (31.4 ppm and 30.8 ppm for $C_{26}(PO(OEt)_2)_2$ and $C_{48}(PO(OEt)_2)_2$, respectively, in dmso-d_6 at 110 °C) agrees with reported values for other alkyl diethylphosphonates (typically measured in chloroform-d_1, 32.4 ppm).[98] The crude materials were used in the following McKenna deprotection without further purification. The desired $C_{26}(PO(OH)_2)_2$ and $C_{48}(PO(OH)_2)_2$ (abbreviated as $C_{26}PA_2$ and $C_{48}PA_2$) were obtained by phosphonate ester cleavage by McKenna reactions with trimethylsilyl bromide under mild conditions and subsequent protonation in a water/methanol mixture.[99] The hydrolysis reaction was monitored by ^{31}P NMR at 110 °C in dmso-d_6. ^{31}P NMR shifts of the products agree with an *n*-tetradecylphosphonic acid reference (Figure 3.1). In further purification by recrystallization from methanol, the limited solubility of the products was overcome by working at temperatures above the solvent boiling point in a microwave reactor with an operating pressure of up to 30 bar. This yielded the target products in high purity. No additional, high field shifted ^{31}P NMR signals were detected, unlike reported for poly(vinylphosphonic acid).[100] Therefore, a formation of anhydrides by condensation of the phosphonic acid groups during the synthesis and purification steps can be excluded.

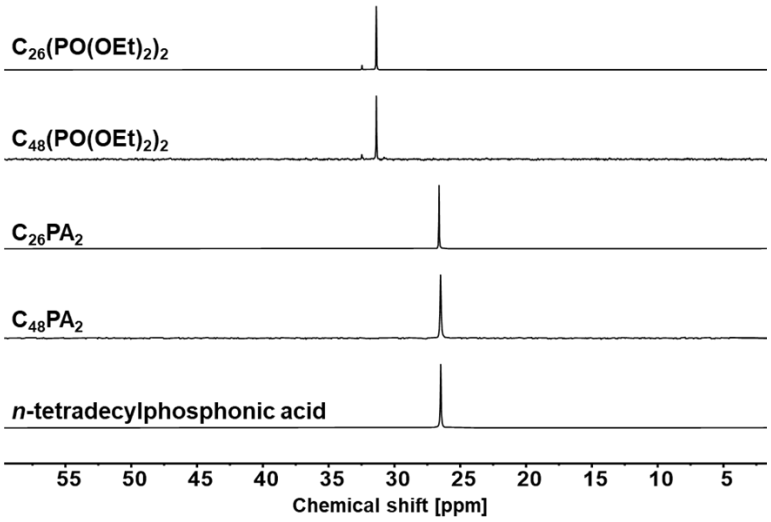

Figure 3.1 ^{31}P NMR at 110 °C in dmso-d_6 of the synthesized telechelic phosphonate esters and telechelic phosphonic acids. As a reference, *n*-tetradecylphosphonic acid is shown.

3.2.2 Thermal Properties

Thermogravimetric analysis (TGA) under nitrogen atmosphere and air provided insights on the thermal stability of the telechelic phosphonic acid materials $C_{26}PA_2$ and $C_{48}PA_2$ (Figure 3.2). For both materials, only trace weight loss is observed up to 200 °C, which may be due to traces of residual solvent. The telechelics do not undergo significant condensation reactions below 200 °C. Decomposition under nitrogen atmosphere occurs at onset temperatures of 467 °C and 454 °C ($C_{26}PA_2$ and $C_{48}PA_2$, respectively) with low residual mass, presumably originating from non-volatile inorganic phosphorus oxides. The decomposition under air exhibits comparable onset temperatures to those under nitrogen, and was previously reported for 1-heptylphosphonic acid to be a result of the polyethylene chain oxidation.[101]

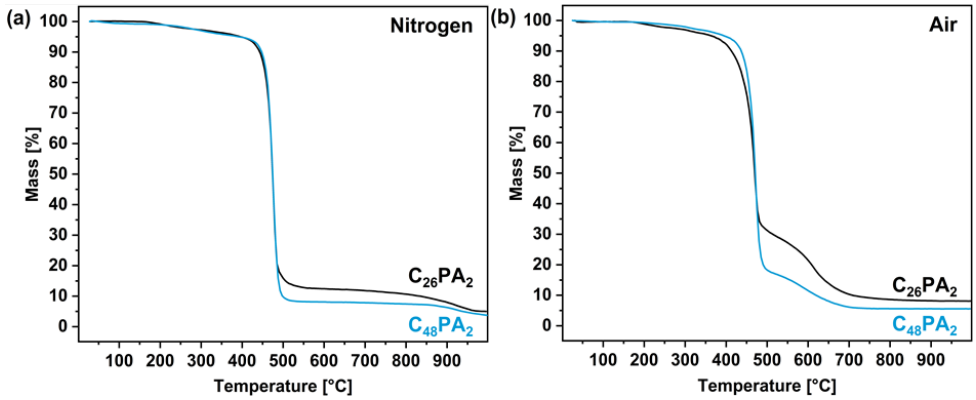

Figure 3.2. TGA thermal graphs of $C_{26}PA_2$ (black) and $C_{48}PA_2$ (blue) at a heating rate of 10 °C/min from 30 to 1000 °C under a constant stream of (a) nitrogen and (b) air.

Between 200 °C and 450 °C, a material weight loss of approximately 5 % is observed for both $C_{26}PA_2$ and $C_{48}PA_2$. Complete condensation reaction of the phosphonic acid functional groups would account for a material weight loss of 6.8 % and 4.3 % ($C_{26}PA_2$ and $C_{48}PA_2$, respectively). The observed weight loss in this temperature region being in this range suggests it likely arises from condensation reactions. A final decomposition step is observed under both nitrogen (~880 °C) and air (~580 °C). The thermal stability of the materials towards the formation of anhydrides was further investigated by ^{31}P NMR spectroscopy. Both phosphonic acid materials were held in closed vials for 4, 24, 72 and 96 h at 140 °C and subsequently dissolved in dmso-d_6 for NMR analysis at 110 °C. A high-field shifted additional phosphorus resonance would be expected for the phosphonic acid anhydride formed by condensation reactions.[100] Both $C_{26}PA_2$ and $C_{48}PA_2$ feature only the unaltered sharp resonance of the starting material at 26.6 ppm ($C_{26}PA_2$) and 27.2 ppm ($C_{48}PA_2$) (*cf.* experimental section 3.4.1, Figure 3.7), confirming that the phosphonic acid functionalized polyethylene chains do not undergo condensation reactions below 200 °C. The phase transitions of $C_{26}PA_2$ and $C_{48}PA_2$, respectively, as observed in DSC thermograms differ significantly (Figure 3.3 and summarized in Figure 3.3 and Table 3.1.

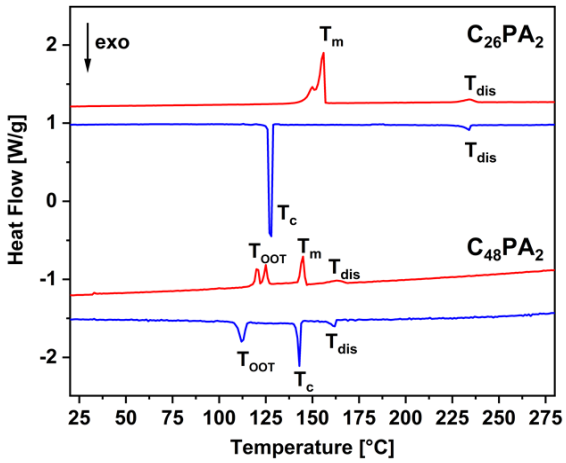

		T_{OOT} (°C)	T_m or T_c (°C)	$T_{dis.}$ (°C)
$C_{26}PA_2$	Heating		150.0, 155.7	234.1
	Cooling		127.6	234.0
$C_{48}PA_2$	Heating	120.5, 124.9	145.0	163.0
	Cooling	112.0	142.8	161.5

Figure 3.3 and Table 3.1 DSC traces of $C_{26}PA_2$ (top) and $C_{48}PA_2$ (bottom) from 0 to 280 °C (second heating/cooling cycle, heating/cooling rate of 1 °C/min). Red curves represent heating, blue curves represent cooling process. Data were shifted vertically for clarity. Thermal properties are reported, transition temperatures are from the 2nd heating and 2nd cooling cycles in DSC.

Distinct and reversible transitions are observed between 110 and 160 °C for both $C_{26}PA_2$ and $C_{48}PA_2$, associated with changes in the polyethylene backbones, as corroborated by X-ray scattering results presented below. $C_{26}PA_2$ exhibits a double melting peak (T_m) at 150.0 - 155.7 °C, and a crystallization temperature (T_c) at 127.6 °C. $C_{48}PA_2$ has a similar T_m at 145 °C, but the

T_c (143 °C) is nearly the same as the melting point. We attribute both the higher T_m and lower T_c in $C_{26}PA_2$ to the higher concentration of phosphonic acid groups, which will impede the melting and crystallization processes of the polyethylene backbone. Much higher melting points between 200 and 220 °C have been reported for the small molecules C_4PA_2 to $C_{12}PA_2$, likely due to the even higher concentration of phosphonic acid groups, whose aggregates similarly impede the melting process.[75] There are also order-to-order transitions (T_{OOT}) in $C_{48}PA_2$ below the melting point, which results from transitions between crystal structures in the polyethylene backbone. Though we are able to identify the peaks corresponding to melting and crystallization of the polyethylene backbone, the melting enthalpy is challenging to assign due to overlapping transitions, as well as intermediate transitions between crystal structures.

For both materials, an additional endothermic process is visible at temperatures above the melting temperatures of the PE backbones, T_{dis} (234 °C and 162 °C for $C_{26}PA_2$ and $C_{48}PA_2$ during cooling, respectively). At these temperatures, the hydrogen bond network formed by the phosphonic acid groups transitions into a disordered state and occurs at the same temperature on heating and cooling. This behaviour was studied in detail by X-ray Scattering and by polarized light microscopy, as discussed in the following section (3.2.3).

To gain insight into the structural changes upon temperature variations as well as to investigate the anhydrous proton conductivity of these materials, temperature dependent X-ray scattering, polarized light microscopy and electrochemical impedance spectroscopy (EIS) was performed. X-ray and EIS measurements were conducted by Dr. B. A. Paren within a cooperation with the group of Prof. Dr. K. I. Winey at the University of Pennsylvania. The discussion and interpretation of the data was performed cooperatively with Dr. B. A. Paren and can be found in a joint publication.[102]

3.2.3 Morphology and Proton Conductivity

The hierarchical morphologies of the two precise telechelic phosphonate polyethylenes are a result of the interplay between the van-der-Waals forces between the nonpolar polyethylene segments and the polar interactions of the phosphonic acid groups. By combining temperature dependent X-ray scattering studies with polarized light microscopy (PLM) we gained insight into the nanoscale structures and morphological transitions present in these materials. Figure 3.4 shows the X-ray scattering profiles of $C_{26}PA_2$ and $C_{48}PA_2$ at selected temperatures during cooling from above T_{dis}. At high temperatures, both $C_{26}PA_2$ and $C_{48}PA_2$ exhibit only a broad amorphous

halo centred at q ~ 1.3 $Å^{-1}$, indicating melted polyethylene segments. Additionally, both polymers exhibit a broad, asymmetric peak at q ~ 0.2-0.3 $Å^{-1}$, which corresponds to the disordered packing of the phosphonic acid groups. Upon cooling, transitions in the polymers are consistent with the DSC results. We also note that the morphologies in both polymers are fully reversible with some hysteresis in $C_{26}PA_2$ upon heating to 170 °C (*cf.* experimental section 3.4.2, Figure 3.11) and this is discussed with regard to proton conductivity in the below. When the polyethylene backbone is still in the melt state in both $C_{26}PA_2$ and $C_{48}PA_2$, sharp equidistant peaks appear upon cooling below T_{dis}, in the low q-range with ratios of 1:2:3:4:5, relative to q*, which indicates the presence of layered aggregate morphologies. This derives from a nanophase separation of the acidic end-groups from the PE chains into layered aggregates as reported before for phosphonated polymers[84] and for the carboxylic acid analogues $C_{21}(COOH)_2$ and $C_{46}(COOH)_2$.[28] Upon further cooling, the layered aggregate morphologies persist as the polymers crystallize and experience additional order-to-order transitions.

The alkyl chain packing behaviour of $C_{26}PA_2$ becomes semicrystalline with a hexagonal crystal structure upon cooling below 130 °C, followed by an order-to-order transition to a monoclinic phase crystal structure at lower temperatures. This hexagonal to monoclinic transition does not appear in the DSC trace, which may be because the transition is occurring over a wide range of temperatures. In the case of $C_{48}PA_2$, an unidentified semicrystalline structure (indicated as X on Figure 3.4) forms first upon cooling from the melt state and the PE chains transition into co-existing monoclinic and orthorhombic phases (detailed positions of all observed reflections at the selected temperatures can be found in the experimental section 3.4.2, Table 3.2 and Table 3.3).

The previously reported carboxylic acid analogues C_{21}-$(COOH)_2$ and C_{46}-$(COOH)_2$ both show an orthorhombic PE crystallinity at all temperatures below the melting transition, while a monoclinic structure of the PE backbones was also observed in the zinc carboxylate analogue, $C_{46}(COO)_2Zn$.[28] The larger bivalent functional groups require a larger head group separation that induces monoclinic packing of the PE chains.[103] Similarly, relative to the carboxylic acid groups the large phosphonic acid groups in $C_{26}PA_2$ and $C_{48}PA_2$ produce monoclinic crystals.

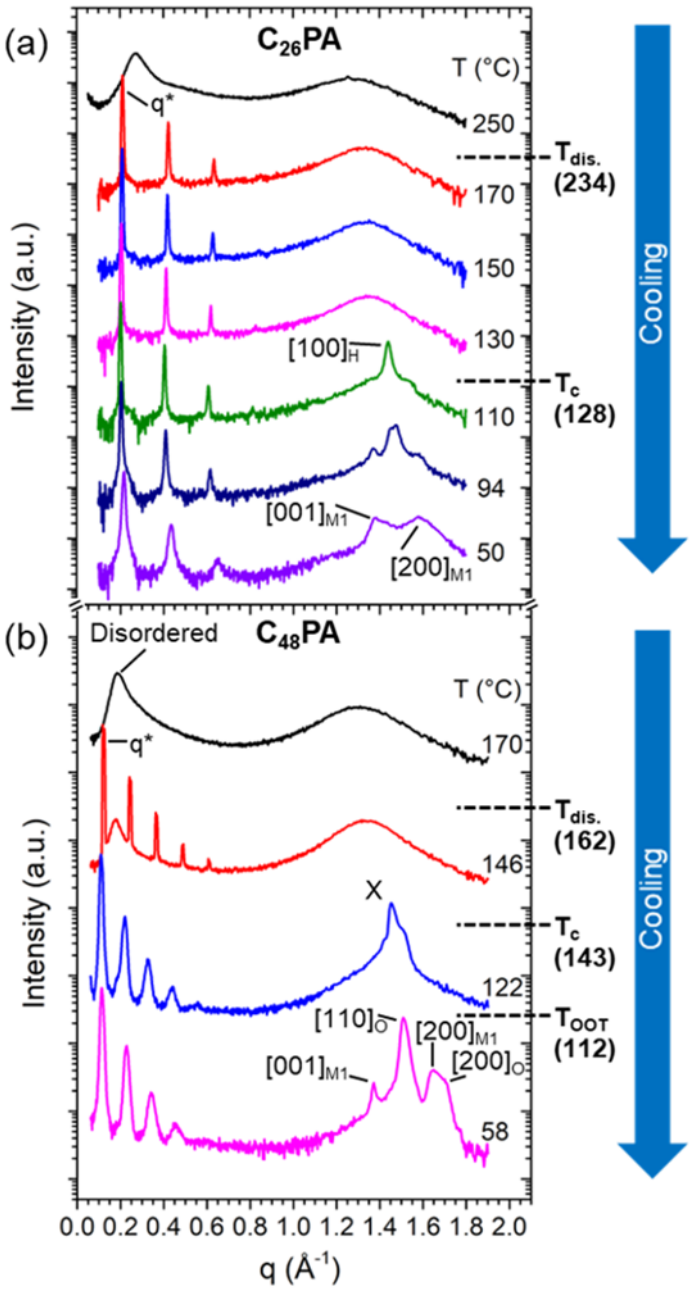

Figure 3.4 X-ray scattering profiles of (a) $C_{26}PA_2$ and (b) $C_{48}PA_2$ at selected temperatures upon cooling. Reflections at $q > 1.0$ Å^{-1} indicate chain packing as Hex, M1, O and X, representing hexagonal, monoclinic, orthorhombic and an unknown phase, respectively. Data was shifted vertically for clarity. Transition temperatures from DSC measurements (on cooling) are noted. Measurements were conducted and data was interpreted by Dr. Benjamin A. Paren at the University of Pennsylvania.

The center-to-center distances (d*) between the aggregate layers can be calculated from the peak positions ($d^* = 2\pi/q^*$, as detailed in the Supporting Information) and are 29 Å ($C_{26}PA_2$) and 55 Å ($C_{48}PA_2$) at 30 °C. A higher value in $C_{48}PA_2$ for d* compared to the short chain analogue is expected because the interlayer spacing strongly depends on the polymer length. The layer

spacings remain relatively constant throughout the complete cooling process (± 2 Å). The domain sizes along the layer normal can be calculated with the Scherrer equation ($\xi_L = 2\pi/\Delta q$, Δq being the full width at half-maximum of q*). For $C_{26}PA_2$, the domain size is 900 Å when the backbone is melted and decreases to 500 Å when the backbone is crystalline. For $C_{48}PA_2$, the domain size along the layer normal is as large as 2800 Å when the backbone is melted, but we note that the layers coexist with some acid groups in the disordered state. The domain size then similarly decreases to 500 Å upon the crystallization of the PE backbone. This much higher extent of order in the layered aggregates when the PE backbone is amorphous is likely a result of the greater polymer backbone mobility, that produces better uniformity across the samples. We also note that the domain sizes of ~500 Å at room temperature are significantly larger than the domain sizes of 170 Å and 350 Å in the carboxylate telechelic analogues, $C_{21}(COOH)_2$ and $C_{46}(COOH)_2$, respectively.[28] Tilt angle θ between the polyethylene chains and the layer normal are calculated from d* and the length of the all-*trans* chain conformation added to the approximate length of the head groups (for definition of the tilt angle, see experimental section 3.4.2, Figure 3.8).[95] This yields tilt angles of 45° ($C_{26}PA_2$) and 36° ($C_{48}PA_2$), assuming chain lengths of 40.8 and 68.5 Å, respectively. A larger tilt for the shorter $C_{26}PA_2$ is attributed to a greater amount of steric hindrance in the system resulting from the higher volume fraction of head groups. These tilt angles are comparable to the carboxylate analogues $C_{21}(COOH)_2$ and $C_{46}(COOH)_2$, which tilt at 42° and 35°, respectively.[28]

As previously described, the PE segments of $C_{26}PA_2$ and $C_{48}PA_2$ are amorphous and exist with layered acid aggregates between T_m and $T_{dis.}$, above which the layered aggregates break apart. A similar phenomenon has been reported in phosphonic acid functionalized materials by Liang et al. wherein the layered morphology was described as a thermotropic liquid crystalline (LC) phase.[88] To explore this phase behaviour further, C26PA2 was investigated by PLM in the isotropic melt above $T_{dis.}$ and in the liquid crystalline state between $T_{dis.}$ and T_m. Under crossed polarizers, the smectic liquid crystalline phase displays characteristic cross-like interference patterns consistent with periodic layers emanating from a central position (Figure 3.5).[104] In traditional semicrystalline polymers, the contrast originates from the alternating layers of crystalline and amorphous phases, in this liquid crystalline phase the contrast arises from the index of refraction differences between the phosphonate and hydrocarbon portions of the telechelic polymers. Interestingly, upon cooling below T_m, the cross-like interference patterns in $C_{26}PA_2$ persist indicating that as the PE backbone crystallizes there is little rearrangement of the

layered morphology, which is consistent with the X-ray scattering. The presence of LC phases has been reported previously for different phosphonic acid functionalized materials.[88,105] In case of $C_{26}PA_2$ and $C_{48}PA_2$, the liquid crystalline phases are stable over which the LC phases are stable is consistent with the high strength of the hydrogen bonded network in these polymers and could be advantageous in various applications involving electroactive polymers, e.g. ionic polymeric transducers.

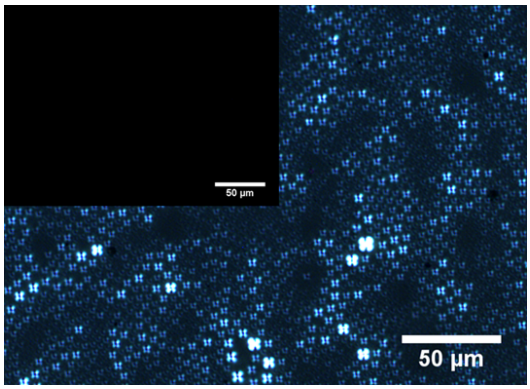

Figure 3.5. PLM images with crossed polarizers of $C_{26}PA_2$. (inset) The isotropic melt at 240 °C; (main image) Liquid crystalline phase after cooling from 240 °C to 233 °C at 10 K/min and holding for 20 min. The diameters of these cross-like interference patterns are ~ 3 µm.

The ionic conductivity of $C_{26}PA_2$ and $C_{48}PA_2$ was determined from 30 °C to 170 °C under dry conditions using electrochemical impedance spectroscopy (EIS) measurements (Figure 3.6). The bulk morphologies are also indicated. Previously, the telechelic carboxylate salts demonstrated Arrhenius-like behaviour ($\sigma_{DC} = \sigma_0 e^{-E_a/(RT)}$, with σ_0 defined as the conductivity at indefinitely high temperature and E_a as the activation energy for the ion conduction). This behaviour originates from the decoupling of the ion movement from the polymer backbone segmental dynamics.[28] Upon cooling, the conductivity of $C_{26}PA_2$ in the liquid crystalline phase shows Arrhenius-like behaviour above ~120 °C, the crystallization temperature of the PE backbone. While this occurs when the backbone is melted and there may be some chain mobility, this linear relationship suggests that proton motion is dominated by the dynamics within the phosphonate, rather than the segmental dynamics. The non-Arrhenius behaviour of the conductivity below the melting/crystallizing indicates the role of segmental dynamics and other structural changes in the bulk. The hysteresis in the structural changes and the conductivity upon cooling and heating in $C_{26}PA_2$ are reproducible and thus are not attributable to material decomposition. Note that $C_{48}PA_2$ exhibits an abrupt increase in conductivity at ~ 155 °C, which corresponds to the transition

upon cooling from disordered aggregates to a liquid crystalline structure of layered aggregates and amorphous PE backbones (see Figure 3.6).

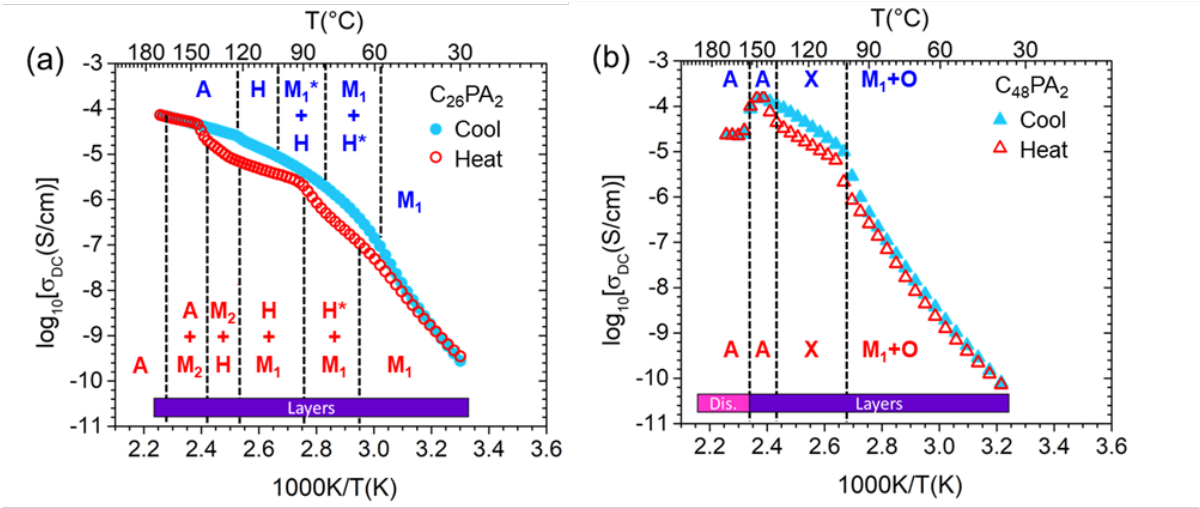

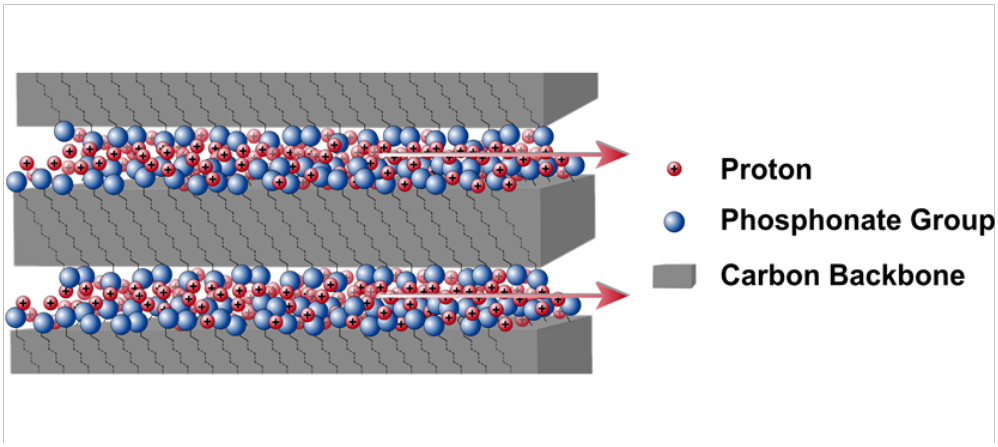

Figure 3.6. (Top) Temperature dependence of ionic conductivity obtained from EIS measurements under dry conditions upon cooling (blue) and heating (red) in (a) $C_{26}PA_2$ and (b) $C_{48}PA_2$. The packing of the PE segments as identified from X-ray scattering measurements are labeled and the transition temperatures represented by vertical dashed lines: A: amorphous, X: unknown phase, M1 and M2: two monoclinic phases, O: Orthorhombic phase, H: hexagonal phase. Phases marked with * are the minority phase. The colored bars indicate phosphonate aggregate morphologies, which are either disordered (Dis.) or layered aggregates. (Bottom) Schematic representation of proton transport within the layered aggregates. Dashed lines are representative for C_{26} and C_{48} segments.

This change in conductivity is reversible and comparable in magnitude upon heating and cooling, and highlights the advantage of self-assembled phosphonic acid aggregates (as compared to disordered morphologies) with respect to transport properties, which is consistent with Steininger et al.[75] In the case of $C_{26}PA_2$, the layered aggregate morphology is present at all temperatures tested in the EIS, and thus a significant jump in conductivity could not be observed between the disordered and liquid crystalline morphologies. In the thermotropic LC regime,

when the aggregates are layered and the backbone is melted, both $C_{26}PA_2$ and $C_{48}PA_2$ exhibit proton conductivities of ~10^{-4} S/cm, specifically 5.1×10^{-5} S/cm and 1.5×10^{-4} S/cm at 150 °C, respectively. $C_{48}PA_2$ unexpectedly has a higher conductivity than $C_{26}PA_2$ in this LC regime, even though $C_{48}PA_2$ has a lower charge concentration. The ion-exchange capacity, IEC, of $C_{48}PA_2$ is 4.8 mmol/g, compared to an IEC of 7.0 mmol/g in $C_{26}PA_2$. A possible reason for this faster proton transport is a more advantageous hierarchical structure for ion conduction in $C_{48}PA_2$. The domain size of 2800 Å in $C_{48}PA_2$, as previously discussed, may lead to more uniformity and longer pathways for the protons to travel as compared to the domain size of 500 Å in $C_{26}PA_2$. Previous studies of proton conducting polymers aligned by mechanical shearing demonstrated that the improved long-range order increased the anhydrous proton conductivity in the LC state.[106-108] We note that while the maximum conductivity reached in the LC regime by $C_{48}PA_2$ is 1.5×10^{-4} S/cm at 150 °C, the conductivity of $C_{26}PA_2$ reaches 7.3×10^{-5} S/cm at 180 °C, the maximum temperature measured, and may continue to increase with temperature until T_{dis} at ~234 °C.

Considering the absence of both water and additives in the phosphonic acid functionalized materials reported here, the conductivity is high and on par with or exceeds that of other recently studied phosphonic acid functionalized polymers. Atanasov et al. reported a poly(2,3,5,6-tetraflurostyrene-4-phosphonic acid), PWN70 (IEC = 6.6 mmol/g), with anhydrous proton conductivity of 7.3×10^{-6} S/cm at 150 °C, significantly lower than both $C_{26}PA_2$ and $C_{48}PA_2$ at that temperature.[100] However, we note that the conductivity of PWN70 reaches 1.6×10^{-4} S/cm at 220 °C, the maximum temperature measured. The phosphonic acid functionalized materials presented by Liang et al. exhibit thermotropic LC phases, and the system with the highest concentration (IEC = 3.5 mmol/g) shows the highest proton conductivity, 5.5×10^{-5} S/cm at 150 °C[88] and increases further to 2.3×10^{-4} S/cm at 200 °C in the LC regime. Therefore, in addition to charge concentration, both the mobility of the polymer backbone and the nanoscale structure of the ionic aggregates impact proton transport, and these attributes merit further investigation in future work. To further increase the transport abilities of these materials, a macroscopic alignment of the materials in the LC phase could be advantageous to decrease the presence of grain boundaries. The promising conductivities of $C_{26}PA_2$ and $C_{48}PA_2$ compared to other phosphonated polymers in addition to the pronounced ordering of the phosphonic acid aggregates presents opportunities to further develop these telechelic polymers. For example, intermediate length between 26 and 48 carbons will increase charge concentration over $C_{48}PA_2$,

while having improved long-range order relative to $C_{26}PA_2$. Moreover, precise positioning of functional groups is likely key to designing self-assembled and liquid crystalline morphologies for highly conductive, advanced proton exchange membranes.

3.3 Summary and Conclusion

Phosphonic acid-terminated polyethylene telechelics with precise chain lengths can be accessed by straightforward synthetic protocols. Simple reaction conditions with readily available substrates were implemented that yield quantitative conversions of the starting materials and are applicable to increased batch sizes, which makes this approach valuable for industrial applications. The thermal properties suggest these materials are suitable as proton conductors at intermediate operating temperatures (~ 150 °C) in fuel cells without undesired condensation reactions occurring. Layered aggregates of the phosphonic acid groups prevail below and above the melting transition of the PE backbones and transition to a disordered state at ~80 °C above T_m for $C_{26}PA_2$ and ~20 °C for $C_{48}PA_2$. At 150 °C, when the backbone is melted, the proton conductivities through the layered aggregates in $C_{26}PA_2$ and $C_{48}PA_2$ reach 5.1×10^{-5} S/cm and 1.5×10^{-4} S/cm, respectively, though the maximum conductivity of $C_{26}PA_2$ may be higher at yet-unexplored temperatures greater than 180 °C. The beneficial impact of the layered aggregate morphology on the proton conductivity is evident in $C_{48}PA_2$ by the significant loss in conductivity at higher temperature corresponding to a disordered state. The wide temperature ranges of these liquid crystalline states make these materials interesting for the use as electro-active polymers in high-performance actuators and sensors. These applications merit further exploration. Additionally, alignment strategies via mechanical shearing or templating could be applied to these telechelic polymers to further increase their proton conductivity. The presented systematic approach towards the understanding of proton transport in structured phosphonic acid functionalized materials suggests that the development of next-generation proton exchange membranes will benefit from highly-ordered self-assembled nanoscale morphologies.

3.4 Experimental Section

3.4.1 Thermal Stability

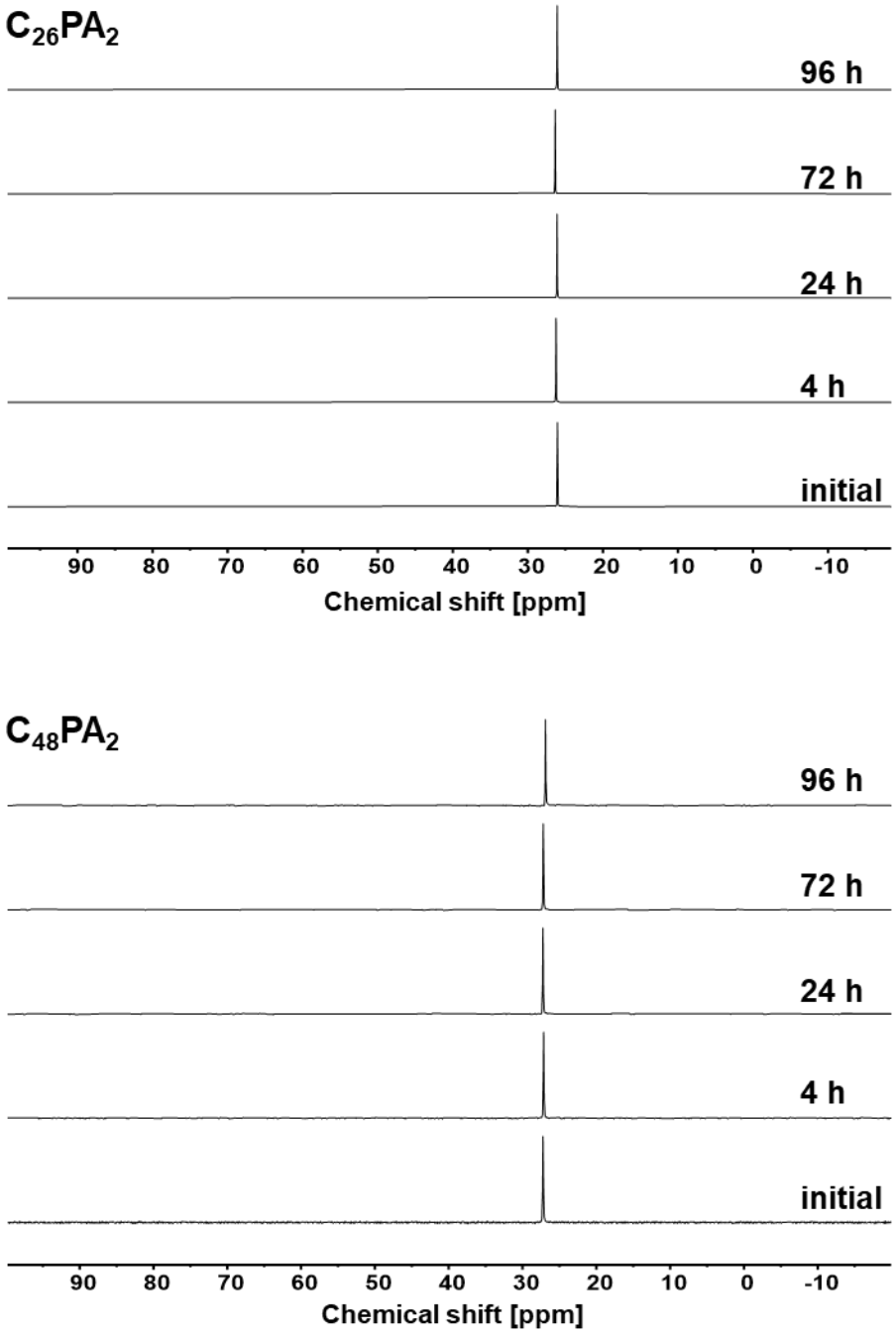

Figure 3.7 Evolution of ^{31}P NMR spectra of C_{26} (top) and $C_{48}PA_2$ (bottom) after exposure to 140 °C for 4, 24, 72 and 96 h, respectively. Shown are $^{31}P\{^1H\}$ NMR spectra (dmso-d_6, 161 MHz, 110 °C).

3.4.2 Structural Characterization

Table 3.2 $C_{26}PA_2$: List of assigned peak positions at selected temperatures during cooling and heating. The crystal structures are abbreviated with M (monoclinic), H (hexagonal) and O (orthorhombic). From the positions of the first, second, and third reflexes in the small-q area (q*, 2q*, and 3q*) the centre-to-centre distance d* between the aggregate layers was calculated from $d^* = n2\pi/q$, where *n* is the peak number. *d* was determined for the peaks at q*, 2q*, and 3q* and the reported d* is the mean of these values. The average domain sizes along the layer normal ξ_L was calculated from the full width at half-maximum (Δq) of the first peak at q*, with the Scherrer equation ($\xi_L = 2\pi/\Delta q$). During heating, a second set of equidistant peaks in the small q-range with ratios of 1:2:3:4 is present, differentiated by indices q^*_1 and q^*_2 with the corresponding d* and ξ_L, respectively.

COOLING	50 °C	94 °C	110 °C	130 °C	150 °C	170 °C	250 °C
$[001]_M$ [Å-1]	1.390						
$[200]_M$ [Å-1]	1.594						
$[100]_H$ [Å-1]			1.443				
q* [Å-1]	0.218	0.206	0.203	0.207	0.210	0.212	-
d* [Å]	28.8	30.5	30.9	30.4	29.9	29.7	-
ξ_L [Å]	532	833	907	915	913	887	-

HEATING	50 °C	94 °C	110 °C	130 °C	150 °C	170 °C	250 °C
$[001]_M$ [$Å^{-1}$]	1.391		1.373	1.372	1.370		
$[200]_M$ [$Å^{-1}$]	1.600		1.594	1.615	1.619		
$[-201]_M$ [$Å^{-1}$]				1.734	1.746		
$[100]_H$ [$Å^{-1}$]			1.426	1.416			
q^*_1 [$Å^{-1}$]	0.219	0.217	0.216	0.219	0.209	0.214	-
q^*_2 [$Å^{-1}$]					0.240		-
d^*_1 [Å]	28.7	29.0	29.1	28.7	30.0	29.4	-
d^*_2 [Å]					26.2		-
ξ_{L1} [Å]	538	562	514	246	650	936	-
ξ_{L2} [Å]					284		

Table 3.3 $C_{48}PA_2$: List of assigned peak positions at selected temperatures during cooling. No hysteresis during heating and cooling in the X-ray scattering data was observed. Thus, list of heating reflexes is redundant. The crystal structures are abbreviated with M (monoclinic), H (hexagonal) and O (orthorhombic). From the positions of the first, second, and third reflexes in the small-q area (q*, 2q*, and 3q*) the centre-to-centre distance *d** between the aggregate layers was calculated from $d^* = n2\pi/q$, where *n* is the peak number. *d* was determined for the peaks at q*, 2q*, and 3q* and the reported d* is the mean of these values. The average domain sizes along the layer normal ξ_L was calculated from the full width at half-maximum (Δq) of the first peak at q*, with the Scherrer equation ($\xi_L = 2\pi/\Delta q$).

$C_{48}PA_2$	58 °C	122 °C	146 °C	170 °C
$[001]_{M1}$ [Å^{-1}]	1.372			
$[200]_{M1}$ [Å^{-1}]	1.645			
$[110]_O$ [Å^{-1}]	1.512			
$[200]_O$ [Å^{-1}]	1.691			
q* [Å^{-1}]	0.114	0.111	0.118	-
d* [Å]	55.3	56.8	53.1	-
ξ_L [Å]	442	473	2870	-

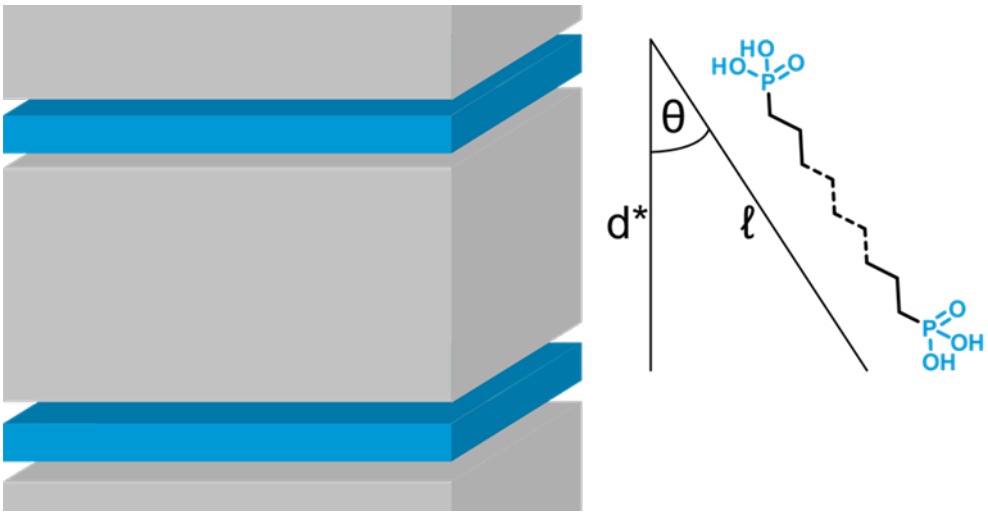

Figure 3.8 Schematic representation of the layered aggregates and the definition of the chain tilt to the layer normal. The blue regions represent the phosphonic acid layers and the grey regions represent the PE segments.

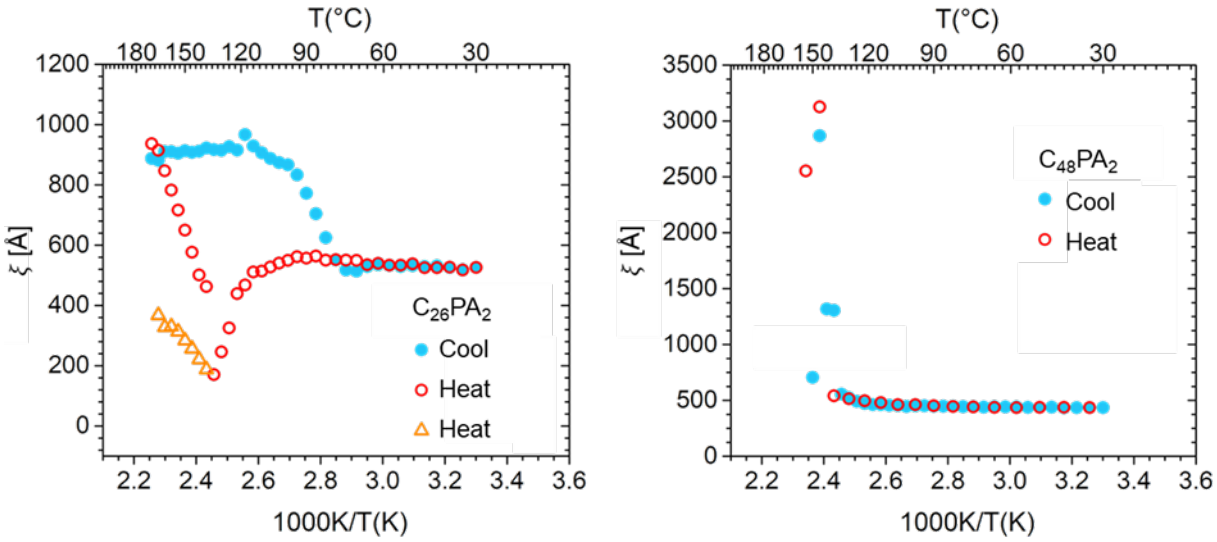

Figure 3.9 Domain size ξ_L for all measured temperatures during cooling and heating for $C_{26}PA_2$ (left) and $C_{48}PA_2$ (right). In case of $C_{26}PA_2$ during heating, the second domain size derives from the second set of equidistant reflexes observed in the small-q range at temperatures between 138 and 166 °C.

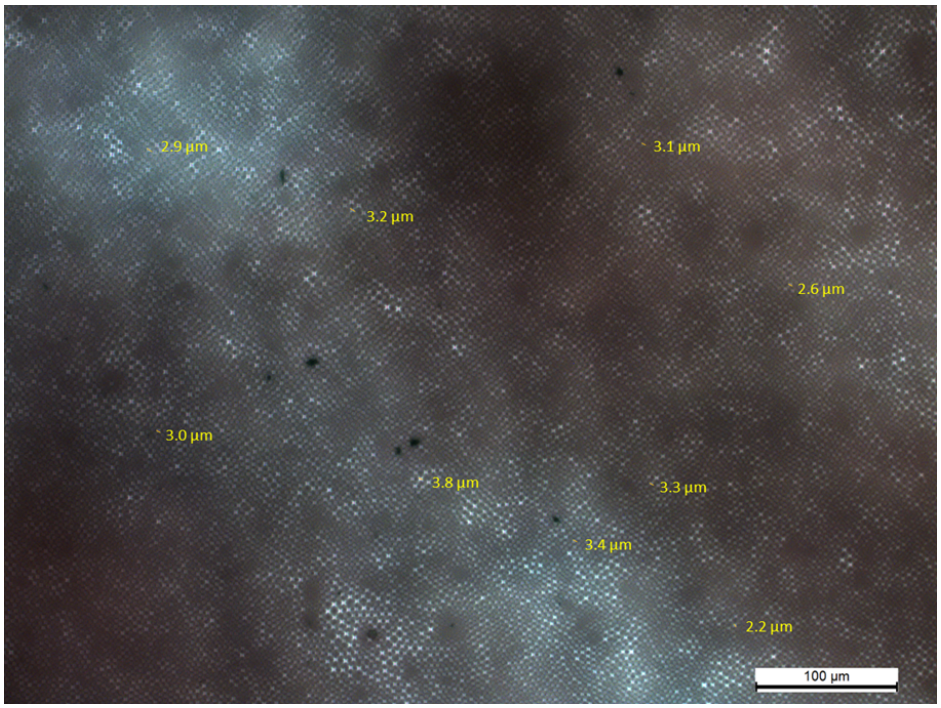

Figure 3.10 PLM image with crossed polarizer of $C_{26}PA_2$ at 233 °C by cooling from the isotropic melt and subsequent isothermal crystallization at 233 °C for 20 min. Representative measurements of Maltese crosses are labelled and account for 3.1 ± 0.4 µm.

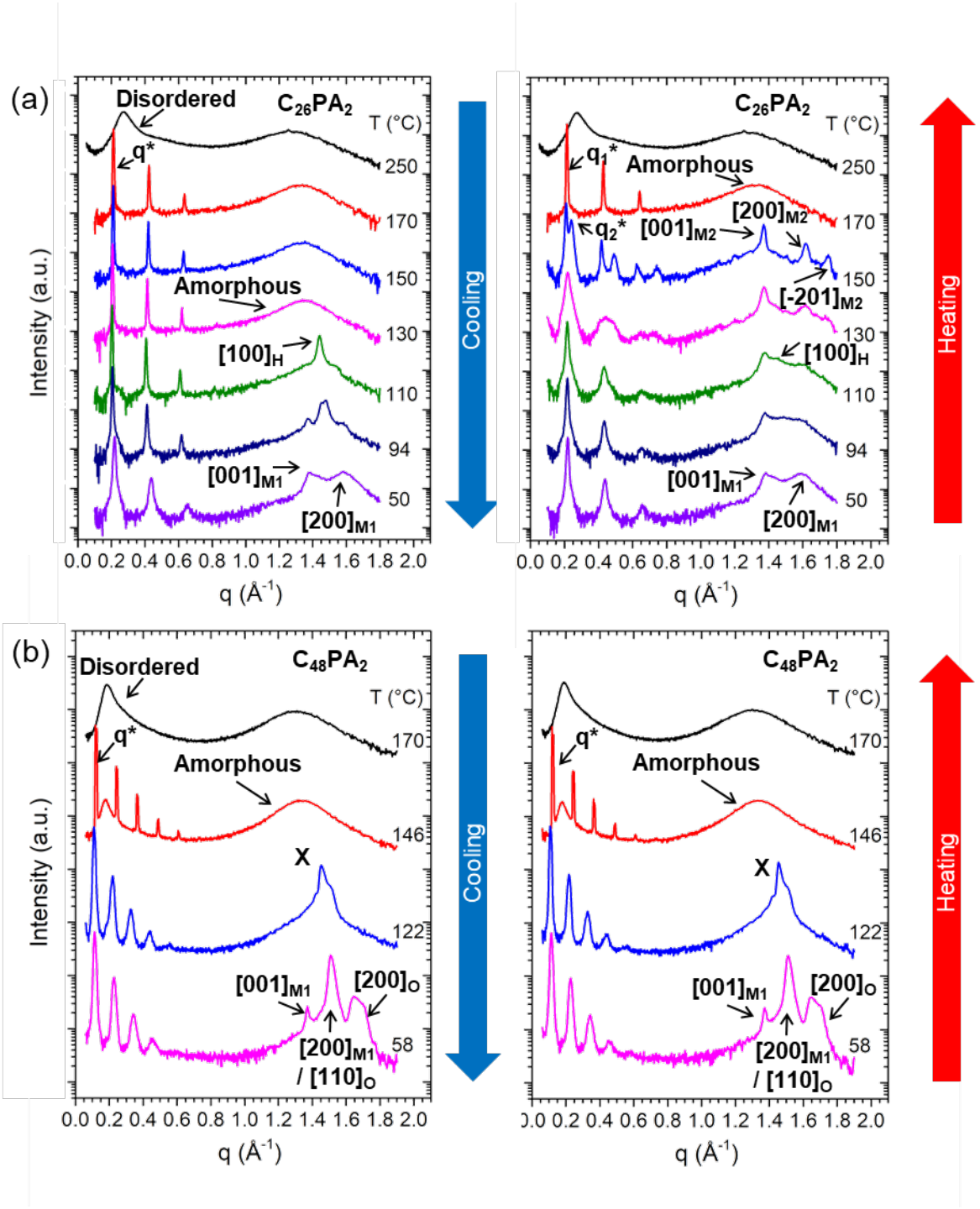

Figure 3.11 In-situ X-ray scattering profiles during the first cooling and second heating processes at selected temperatures of $C_{26}PA_2$ (a) and $C_{48}PA_2$ (b). The identified reflections in the wide-angle area are assigned to the different phases abbreviated with O: orthorhombic; M1 and M2: different monoclinic phases; X: unidentified; H: Hexagonal, respectively.

3.4.3 Synthesis of α,ω-difunctionalized C_{26} and C_{48} backbones

The C_{48} starting material was obtained by a reported procedure (Scheme S1).[30] The batch scales were increased and at the same time the catalysts loadings were reduced. For the workup of the products, simplified protocols were elaborated.

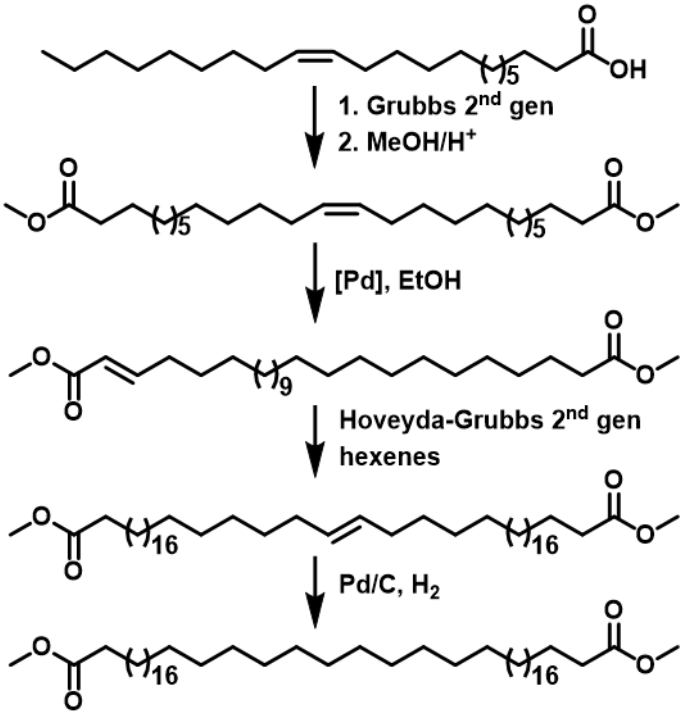

Scheme 3.2 Synthesis of $C_{48}(COOMe)_2$. A self-metathesis of erucic acid ((*Z*)-Docos-13-enoic acid), followed by a dynamic crystallizing isomerization prior to the two-step one-pot 'chain doubling reaction' to access the C_{48} building block. A hydrogenation of the double bond yields the polyethylene telechelic.

Synthesis of symmetric unsaturated $C_{24}(COOMe)_2$

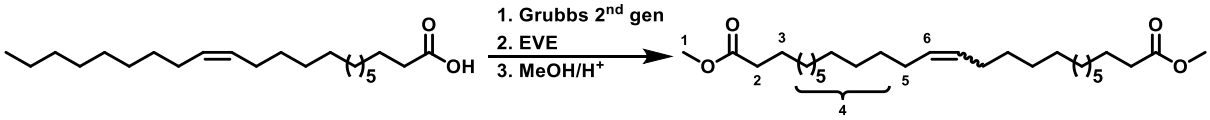

Erucic acid (1 L, 860 g, 2.54 mol) was melted at 45 °C and transferred to a 1 L glass reactor. The melt was degassed under reduced pressure three times at 45 °C under stirring until no further gas evolution was visible. The catalyst (Grubbs 2nd generation, 647 mg, 0.76 mmol, 300 ppm) was dissolved in dry dichloromethane (5 mL) and added to the reactor. The reaction mixture was stirred at 45 °C. Precipitation of the forming diacid from the reaction mixture started 10 minutes

after injection of the catalyst solution. After full solidification of the mixture (typically within 60 min) the reaction was quenched with ethyl vinyl ether (50 mL). Ethyl acetate (500 mL) was added, and the mixture was heated to 60 °C until all solids were dissolved. The diacid was crystallized at 6 °C, filtered off and washed with ethyl acetate. Methanol (3 L) and concentrated sulfuric acid (98 %, 3 mL) were added, and the mixture was refluxed for 3 h. The diester was crystallized from the solution at 6 °C and filtered off. Two recrystallization steps in methanol and subsequent filtration in heptane over a short plug of silica yielded the pure symmetric unsaturated $C_{24}(COOMe)_2$ in 57 % yield.

^{1}H NMR (400 MHz, $CDCl_3$, 25 °C): δ[ppm] = 5.38 (td, $^3J_{HH}$ = 3.7, 1.8 Hz, 2H, H-6), 3.66 (s, 3H, H-1), 2.30 (t, $^3J_{HH}$ = 7.5 Hz, 4H, H-2), 1.99 – 1.92 (m, 4H, H-5), 1.66 – 1.57 (m, 4H, H-3), 1.38 – 1.21 (m, 32H, H-4).

Synthesis of unsaturated α,β-$C_{24}(COOMe)_2$

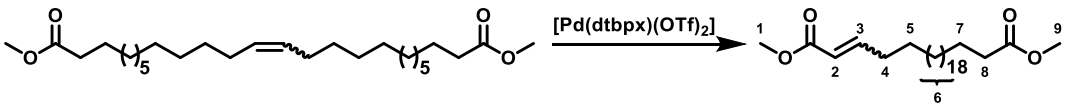

A 1 L glass reactor equipped with a heating/cooling mantle was charged with the symmetric unsaturated $C_{24}(COOMe)_2$ (200 g, 441.8 mmol), and the solid was dissolved in THF (0.5 L) and ethanol (0.6 L). The solution was heated mildly until all solids were dissolved (35 – 40 °C) and subsequently degassed to remove oxygen. The catalyst $[Pd(dtbpx)(OTf)_2]$ (442 µmol, 350 mg, 0.1 mol%) was dissolved in 5 mL of the reaction mixture and added to the stirred solution. The system was cooled to 15 °C over 2 h by means of a cryostat to determine the exact temperature where initial crystallites form (typically 15 – 25 °C). The mixture was heated to 5 °C above the crystallization temperature and a temperature program controlled by the cryostat was initiated: 1. cooling to the crystallization temperature with 0.01 °C/min, 2. cooling to -20 °C with 0.05 °C/min. The reaction was quenched by addition of trimethylamine (20 mL) at -20 °C. The precipitate was filtered off in the cold and washed with cold methanol (-30 °C). The solids were recrystallized from methanol (2 – 3 times) and heptane (1 – 2 times) until only the desired α,β-unsaturated isomer was present. The recrystallization progress was monitored by ^{1}H NMR spectroscopy. All filtrates were combined, and the solvent was removed in vacuum to obtain a mixture of isomers, which could be used in the same reaction again to achieve effectively full conversion of the starting material.

^{1}H NMR (400 MHz, $C_2D_2Cl_4$, 25 °C): δ [ppm] = 6.97 (dt, $^3J_{HH}$ = 15.6, 7.0 Hz, 2H, H-3), 5.82 (dt, $^3J_{HH}$ = 15.6, $^4J_{HH}$ = 1.6 Hz, 2H, H-2), 3.72 (s, 3H, H-1), 3.66 (s, 3H, H-9), 2.30 (t, $^3J_{HH}$ = 7.6 Hz, 4H, H-8), 2.20 (dtt, $^3J_{HH}$ = 7.0, 1.6 Hz, 2H, H-4), 1.64 – 1.54 (m, 2H, H-7), 1.50 – 1.38 (m, 2H, H-5), 1.37 – 1.20 (m, 36H, H-6).

Synthesis of unsaturated $C_{46}(COOMe)_2$: 'Chain Doubling'

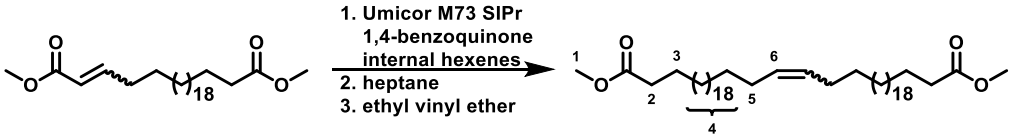

A 700 mL Schlenk tube was charged with α,β-$C_{24}(COOMe)_2$ (50 g, 110 mmol, 1 equiv) and degassed. Dichloromethane (60 mL) was added and the Schlenk tube was placed in a 40 °C water bath. 140 mL of a 2- and 3-hexene mixture was cannula transferred to the reaction mixture. The catalyst (Umicor 73 S^{i}Pr, 456 mg, 0.5 mol%) and 1,4-benzoquinone was dissolved in 6 mL dichloromethane and added to the reaction mixture dropwise over 20 minutes. A strong gas evolution was observed (butene formation). The reaction was allowed to stir at 40 °C for 30 minutes. Heptane (dry, 100 mL) was added and the excess hexene was removed under reduced pressure within 2 h. This initiated the formation of the C_{48} product as indicated by precipitation. The reaction was quenched with ethyl vinyl ether and the residual solvent was removed. The green slurry was suspended in *iso*-propanol (100 mL) and centrifuged. The solids were washed with *iso*-propanol (2 x 100 mL) and recrystallized from toluene. The desired product was obtained as a crystalline white solid in 80 % yield and was used in the next step without further purification.

^{1}H NMR (400 MHz, $C_2D_2Cl_4$, 110 °C): δ [ppm] = 5.47 (td, $^3J_{HH}$ = 3.6 Hz, $^4J_{HH}$ = 1.8 Hz, 2H, H-6), 3.71 (s, 6H, H-1), 2.35 (t, $^3J_{HH}$ = 7.0 Hz, 4H, H-2), 2.08 – 1.99 (m, 4H, H-5), 1.75 – 1.63 (m, 4H, H-3), 1.48 – 1.28 (m, 76H, H-4).

Synthesis of saturated $C_{24}(COOMe)_2$ and $C_{46}(COOMe)_2$

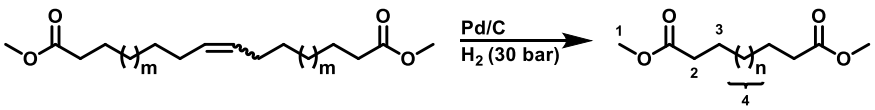

m = 7 **unsaturated $C_{24}(COOMe)_2$**
m = 18 **unsaturated $C_{46}(COOMe)_2$**

n = 20 **$C_{24}(COOMe)_2$**
n = 42 **$C_{46}(COOMe)_2$**

A stainless-steel pressure reactor equipped with a mechanical stirrer was charged with 20 g unsaturated C_{24}/$C_{46}(COOMe)_2$ ($C_{24}(COOMe)_2$: 44.2 mmol; $C_{46}(COOMe)_2$: 26.3 mmol) and Pd/C

(5 % metal content, 2 g, 10 wt.%). THF (100 mL) and methanol (20 mL) were added and the reactor was pressurized with 30 bar hydrogen and heated to 100 °C. After 24 h, the reaction mixture was cooled to room temperature and the reactor was vented. The solvent was removed under reduced pressure and the solids were isolated by Soxhlet extraction with toluene. This afforded the pure saturated C_{24}/$C_{46}(COOMe)_2$ in quantitative yield. The isolated Pd/C could be reused several times without activity loss.

$C_{24}(COOMe)_2$: ^{1}H NMR (400 MHz, $CDCl_3$, 300 K) δ [ppm] = 3.66 (s, 6H, H-1), 2.29 (t, $^3J_{HH}$ = 7.56 Hz, 4H, H-2), 1.66-1.55 (m, 4H, H-3), 1.35-1.18 (m, 40H, H-4).

$C_{46}(COOMe)_2$: ^{1}H NMR (400 MHz, $C_2D_2Cl_4$, 110 °C): δ [ppm] = 3.71 (s, 6H, H-1), 2.35 (t, $^3J_{HH}$ = 7.4 Hz, 4H, H-2), 1.73 – 1.64 (m, 4H, H-3), 1.44 – 1.29 (m, 84H, H-4).

3.4.4 Synthesis of C_{26} and C_{48} α,ω-diphosphonic acids

The end group modification of C_{26} and C_{48} telechelics is challenging due to the limited solubility of many of the intermediate products in common organic solvents, especially at room temperature. A synthesis route *via* $C_{26/48}Br_2$ was elaborated to enable further reactions at the resulting electrophilic methylene unit (Scheme 3.3).

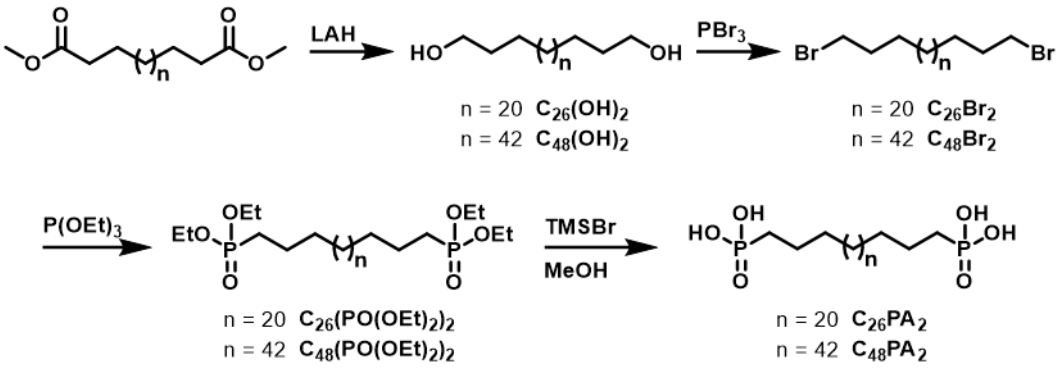

Scheme 3.3 Synthesis scheme of the synthesis route starting from $C_{24/46}(COOMe)_2$ with a reduction of the ester groups with lithium aluminum hydride (LAH) and a subsequent bromination of the alcohol end groups with phosphorus tribromide to afford the $C_{26/48}$-Br_2. A Michaelis-Arbuzov reaction with triethylphosphite reaction affords $C_{26/48}(PO(OEt)_2)_2$. The phosphonate esters are cleaved by a McKenna reaction with trimethylsilyl bromide (TMSBr) and subsequent methanol addition to obtain the free phosphonic acids C_{26} and $C_{48}PA_2$.

Synthesis of saturated $C_{24}(COOMe)_2$ and $C_{48}(COOMe)_2$

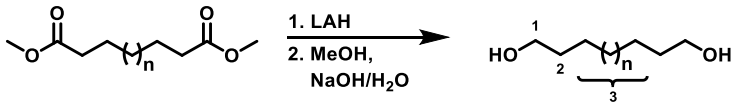

n = 20 $C_{24}(COOMe)_2$
n = 42 $C_{46}(COOMe)_2$

n = 20 $C_{26}(OH)_2$
n = 42 $C_{48}(OH)_2$

A 1 L three-necked flask equipped with a reflux condenser was charged with $C_{24}/C_{46}(COOMe)_2$ ($C_{24}(COOMe)_2$: 12 g, 15.7 mmol, 1.0 equiv.; $C_{46}(COOMe)_2$: 30 g, 66.0 mmol, 1.0 equiv.). THF was added (600 mL) and the reaction mixture was degassed and cooled to 0 °C with an ice bath. Lithium aluminum hydride (3.4 equiv) was added slowly under vigorous stirring. The ice bath was removed and the reaction was slowly heated and kept under reflux for 6 h. After cooling to room temperature, the excess reagent was deactivated by slow addition of methanol (50 mL) and a 0.1 M solution of NaOH in water (3 mL). The solvent was removed and the residual solids were solvent extracted with toluene in a Soxhlet apparatus. The product crystallized from the toluene solution and was filtered off, recrystallized from toluene again and washed with *iso*-propanol (100 mL). The $C_{26}(OH)_2/C_{48}(OH)_2$ was obtained as white crystalline solid ($C_{26}(OH)_2$: 79 % yield, 20.8 g, 52.17 mmol; $C_{48}(OH)_2$: 82 % yield, 9.1 g, 12.9 mmol).

$C_{26}(OH)_2$: ^{1}H NMR ($C_2D_2Cl_4$, 400 MHz, 110 °C) δ[ppm] = 3.67 (t, $^3J_{HH}$ = 6.60 Hz, 4H, H-1), 1.67-1.57 (m, 4H, H-2), 1.47-1.31 (m, 44H, H-3).

$C_{48}(OH)_2$: ^{1}H NMR ($C_2D_2Cl_4$, 400 MHz, 110 °C): δ[ppm] = 3.67 (t, $^3J_{HH}$ = 6.6 Hz, 4 H, CH_2OH), 1.62 (m, 4H, CH_2CH$_2$OH), 1.55 – 1.25 (m, 88 H, CH_2).

Synthesis of $C_{26}Br_2$ and $C_{48}Br_2$

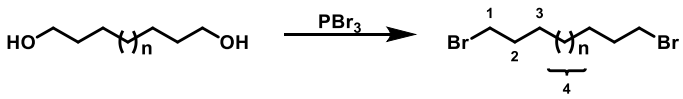

n = 20 $C_{26}(OH)_2$
n = 42 $C_{48}(OH)_2$

n = 20 $C_{26}Br_2$
n = 42 $C_{48}Br_2$

A Schlenk flask was charged with $C_{26}/C_{48}(OH)_2$ ($C_{26}(OH)_2$: 10.0 g, 25.1 mmol, 1.0 equiv.; $C_{48}(OH)_2$: 5.0 g, 7.1 mmol, 1.0 eq.). Toluene ($C_{26}(OH)_2$: 150 mL; $C_{48}(OH)_2$: 500 mL) was added and the suspension was stirred at room temperature. Phosphorus tribromide (5 equiv) was added to the suspension. The suspension was heated from room temperature to 90 °C linearly within 16 h on a computer-controlled heating plate. The clear solution was kept at 90 °C for 3 days. After cooling the reaction mixture to room temperature, ethanol (100 mL) was added and the solvents

were evaporated. Toluene (400 mL) was added and heated to 80 °C to form a suspension. The hot mixture was filtered over a short plug of silica to remove the phosphorus salts. The product was crystallized from the solution, filtered off and obtained as a white solid ($C_{26}Br_2$: 80 % yield, 10.5 g, 20.1 mmol; $C_{48}Br_2$: 88 % yield, 5.2 g, 6.2 mmol).

$C_{26}Br_2$: ^{1}H NMR ($C_2D_2Cl_4$, 400 MHz, 110 °C): δ[ppm] = 3.35 (t, $^3J_{HH}$ = 7.56 Hz, 4H, H-1), 1.91 – 1.80 (m, 4H, H-2), 1.49 – 1.36 (m, 4H, H-3), 1.36 – 1.18 (m, 40H, H-4).

$C_{48}Br_2$:^{1}H NMR ($C_2D_2Cl_4$, 400 MHz, 110 °C): δ[ppm] = 3.46 (t, $^3J_{HH}$ = 6.9 Hz, 4H, H-1), 1.96 – 1.86 (m, 4H, H-2), 1.58 – 1.13 (m, 88 H, H-3 and H-4).

Synthesis of $C_{26}(PO(OEt)_2)_2$ and $C_{48}(PO(OEt)_2)_2$

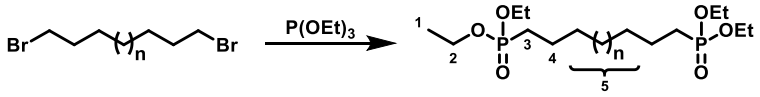

n = 20 **$C_{26}Br_2$** n = 20 **$C_{26}(PO(OEt)_2)_2$**
n = 42 **$C_{48}Br_2$** n = 42 **$C_{48}(PO(OEt)_2)_2$**

A 50 mL two-necked Schlenk tube equipped with a distillation bridge and a collecting flask was charged with C_{26}/$C_{48}Br_2$ ($C_{26}Br_2$: 4.0 g, 7.6 mmol; $C_{48}Br_2$: 1.0 g, 1.2 mmol). Triethyl phosphite ($C_{26}Br_2$: 60 mL; $C_{48}Br_2$: 20 mL) was added. The reaction mixture was heated to 150 °C for 3 days, whereby the by-product bromoethane was distilled off. The reaction mixture was heated to 200 °C to distill off the residual triethyl phosphite and the product (abbreviated as $C_{26}(PO(OEt)_2)_2$/$C_{48}(PO(OEt)_2)_2$, respectively) was obtained in quantitative yield and used in the next step without further purification.

$C_{26}(PO(OEt)_2)_2$:

^{1}H NMR (dmso-d_6, 400 MHz, 110 °C): δ[ppm] = 4.09 – 3.93 (m, 8H, H-2), 1.74 -1.60 (m, 4H, H-3), 1.58 – 1.45 (m, 4H, H-4), 1.43 – 1.19 (m, 56H, H-1 & H-5).

^{31}P{^{1}H} NMR (dmso-d_6, 161 MHz, 110 °C): δ[ppm] = 31.4 (s).

^{13}C{^{1}H} NMR (dmso-d_6, 100 MHz, 110 °C): δ[ppm] = 60.1 (4C, C-2), 29.1 – 27.4 (22C, C-5), 24.4 (2C, C-3), 21.4 (2C, C-4), 15.5 (4C, C-1).

ESI-MS (m/z): 639.487 [M + H$^+$], 661.4696 [M + Na$^+$]

$C_{48}(PO(OEt)_2)_2$:

^{1}H NMR (dmso-d_6, 400 MHz, 110 °C): δ[ppm] = 4.09 - 3.92 (m, 8H, H-2), 1.67 (t, $^3J_{HH}$ = 7.7 Hz, 4H, H-3), 1.56 – 1.46 (m, 4H, H-4), 1.45 – 1.10 (m, 100 H, H-1 & H-5).

^{31}P{^{1}H} NMR (dmso-d_6, 161 MHz, 110 °C): δ[ppm] = 30.8 (s).

ESI-MS (m/z): 969.8128 [M + Na^+], calc. 969.8150 [$C_{56}H_{116}P_2O_6Na^+$].

Synthesis of $C_{26}PA_2$ and $C_{48}PA_2$

n = 20 $C_{26}(PO(OEt)_2)_2$ n = 20 $C_{26}PA_2$

n = 42 $C_{48}(PO(OEt)_2)_2$ n = 42 $C_{48}PA_2$

A Schlenk tube was charged with C_{26}/$C_{48}(PO(OEt)_2)$ ($C_{26}(PO(OEt)_2)_2$: 1.5 g, 2.3 mmol, 1.0 equiv.; $C_{48}(PO(OEt)_2)_2$: 1.1 g, 1.2 mmol, 1.0 equiv.) and chloroform (15 mL) was added. Trimethylsilyl bromide (10 equiv.) was added. The reaction mixture was stirred at 40 °C for 24 h. After cooling to room temperature, the mixture was poured into methanol (100 mL) to precipitate the product. The product was washed with methanol (3 x 30 mL). Recrystallization from methanol (25 mL, 20 min at 120 °C) in a microwave reactor was performed. The precipitate was filtered and washed with methanol (30 mL) and *n*-pentane (30 mL). The product, abbreviated as $C_{26}PA_2$/$C_{48}PA_2$, respectively, was dried under reduced pressure and obtained as a white powder ($C_{26}PA_2$: 83 % yield, 1.03 g, 1.95 mmol; $C_{48}PA_2$: 83 % yield, 827 mg, 1.0 mmol).

$C_{26}PA_2$:

^{1}H NMR (dmso-d_6, 400 MHz, 110 °C): δ [ppm] = 7.55 (s, *broad*, 4H, R-PO(O*H*)$_2$), 1.59 – 1.45 (m, 8H, H-1 & H-2), 1.42 – 1.21 (m, 44H, H-3).

^{31}P{^{1}H} NMR (dmso-d_6, 161 MHz, 110 °C): δ [ppm] = 26.6 (s).

^{13}C{^{1}H} NMR (dmso-d_6, 100 MHz, 110 °C): δ [ppm] = 29.6 – 27.9 (22C, C-3), 27.0 (2C, C-1), 22.0 (2C, C-2).

Elemental analysis (%): calc. 59.29 (C), 10.72 (H); found: 59.49 (C), 10.73 (H).

$C_{48}PA_2$:

^{1}H NMR (dmso-d_6, 400 MHz, 110 °C): δ [ppm] = 7.03 (s, *broad*, 4H, R-PO(O*H*)$_2$), 1.62 – 1.45 (m, 8H, H-1 & H-2), 1.45 – 1.17 (m, 88H, H-3).

^{31}P{^{1}H} NMR (dmso-d_6, 161 MHz, 110 °C): δ [ppm] = 27.2 (s).

^{13}C{^{1}H} NMR (dmso-d_6, 100 MHz, 110 °C): δ [ppm] = 29.8 – 27.9 (44C, C-3), 26.9 (2C, C-1), 22.0 (2C, C-2).

Elemental analysis (%): calc. 69.02 (C), 12.07 (H), 7.42 (P); found: 68.40 (C), 11.84 (H), 7.12 (P).

3.5 Materials and Methods

All reactions were performed under inert gas atmosphere using standard glovebox and Schlenk techniques. The self-metathesis of erucic acid and the following isomerizing crystallization were conducted in an Orb jacketed 1 L glass reactor supplied by syrris equipped with a mechanical Teflon-coated stirrer and an internal temperature control. The setup was connected to a Huber CC-505 cryostat with a Pilot ONE controller. The microwave assisted recrystallization steps were performed in an Anton Paar Monowave 300 Microwave reactor. As reactor vessels, 30 mL borosilicate glass vials with PEEK snap-caps and PTFE coated silicone rubber seals were used. The temperature inside the reactor was monitored non-invasively by an IR sensor.

Erucic acid was obtained from Merck (technical grade, 90 %) and recrystallized from *iso*-propanol twice prior to use. Grubbs 2nd generation catalyst, obtained from abcr, was stored in a glove box under inert gas atmosphere. Ethyl vinyl ether was supplied by Merck. The catalyst used in the isomerization reaction ([Pd(dtbpx)(OTf)$_2$], dtbpx: 1,2-bis[(di-*tert*-butylphosphino)methyl]benzene) was obtained by a reported procedure.[33] 1-hexene, supplied by Merck, was isomerized with [Pd(dtbpx)(OTf)$_2$] to a mixture of 2- and 3-hexene as described elsewhere.[30] THF and toluene were dried over sodium prior to use. Ethanol (p.A.), n-heptane (99 % purity) and sulfuric acid (98 %) were purchased from Carl Roth. All solvents used in recrystallization steps were used in technical grade. The catalyst used in the 'chain doubling' step (Umicor M73 SIPr) was supplied by Umicor. Lithium aluminum hydride (LAH), triethyl phosphite (98 % purity), phosphorus tribromide, trimethylsilylbromide (TMSBr, 97 %) and Aliquat 336 were supplied by Sigma-Aldrich. The reference n-tetradecylphosphonic acid was purchased from abcr. All deuterated solvents used for NMR spectroscopy were supplied by Eurisotop.

The characterization of the soluble intermediate products by NMR spectroscopy was performed in chloroform-d_1, 1,1,2,2-tetrachloroethane-d_2 or dimethylsulfoxide-d_6 as solvent at 25 °C or 110 °C, respectively. A Bruker Avance 400 spectrometer was used. ^{1}H chemical shifts were referenced to the residual solvent signal, ^{31}P shifts were referenced externally to phosphoric acid (85%).

For differential scanning calorimetry, a Netsch DSC 204 F1 with a heating rate of 10 K/min was used. All data reported are from the second heating cycles. Thermogravimetric analysis was performed on a Netzsch STA 429 F3 Jupiter. All measurements were performed with 80 mL/min flowrate and a heating rate of 10 K/min. For measurements under air, a synthetic 80:20 mixture

of N_2:O_2 was used. Samples were dried in a vacuum drying oven for at least 48 h (5 mbar, 50 °C) prior to measurements.

Electrospray ionization high-resolution mass spectrum (ESI-HRMS) of $C_{48}(P(OEt_2)_2)$ was aquired on a Bruker microTOF focus II mass spectrometer *via* direct inject of the sample dissolved in a 1:1 mixture of acetonitrile and chloroform. For $C_{26}(P(OEt)_2)_2$, ESI-HRMS was measured on an Agilent 6546 QTOF system with MassHunter (version 10.1.62).

Elemental analysis of $C_{48}PA_2$ was carried out by MIKROLAB Kolbe. All other elemental analyses were performed in-house on an Elementar vario MICRO cube elemental analyzer.

Polarized light microscopy (PLM) was performed with a Leica DM4000M and with a Linkam THMS600 hot stage.

Methods performed at the University of Pennsylvania (in the group of Prof. Dr. K. I. Winey)

X-ray scattering measurements were performed as a function of temperature on $C_{26}PA_2$ and $C_{48}PA_2$. $C_{26}PA_2$ and $C_{48}PA_2$ powder was placed in a glass capillary and dried at 170 °C under vacuum for 1-2 days, after which the capillary was removed from vacuum at room temperature, and immediately sealed. The Dual Source and Environmental X-ray scattering (DEXS) facility operated by the Laboratory for Research on the Structure of Matter at the University of Pennsylvania, with a Xeuss 2.0 system (Xenocs) using GeniX3D Cu source (λ = 1.54 Å) was used for X-ray scattering measurement. Sample-to-detector distances are 35 cm for SAXS and 16 cm for WAXS, covering a total q range of ~ 0.4 – 2.9 $Å^{-1}$. Samples were heated to 170 °C using a Linkam HFSX350-GI stage. X-ray measurements were taken every 4°C on cooling (C_{26} and C_{48}), from 170 °C to 30 °C, measuring at each temperature for at least 15 minutes. X-ray measurements were then taken every 4 °C (C_{26}) 8 °C (C_{48}) from 30 °C to 170 °C measuring at each temperature for at least 15 minutes. C_{26} was additionally heated to 250 °C in order to access the final transition temperature. For both $C_{26}PA_2$ and $C_{48}PA_2$, temperature steps were selected to optimize the number of measurements that could be taken, while being sure to use the smallest temperature steps over the temperature ranges which demonstrated thermal transitions in the DSC and EIS results. The 2D X-ray scattering profiles were azimuthally integrated to 1D data using Foxtrot software after subtracting the glass capillary window background. X-ray scattering peak positions were determined using the simultaneous fitting of scattering peaks with pseudo-Voigt functions.

Proton conductivity was determined using electrochemical impedance spectroscopy (EIS) under vacuum, as a function of temperature. As-received $C_{26}PA_2$ or $C_{48}PA_2$ powder was sandwiched between two stainless steel electrodes, with 100 µm silica spacers, to ensure constant separation between electrodes. The sandwich of polymer between electrodes was placed onto a hot plate at 170 °C (above the melting temperature of both polymers), and the top electrode was gently pressed down until contacting the spacers. This electrode-electrolyte assembly was placed into a cryostat and heated to 170 °C, before fully tightening the electrodes for maximum contact with the polymer. The sample was equilibrated under vacuum at 170 °C ($C_{26}PA_2$) or 150 °C ($C_{48}PA_2$) for at least 12 hours to ensure the sample was dry. The measurements were performed using Solartron Modulab XM materials test system in the frequency window 10^{-1} - 10^{6} Hz under an applied 0.5 V. For The $C_{26}PA_2$ or $C_{48}PA_2$ impedance spectra sample was measured every 2°C ($C_{26}PA_2$) or 4°C ($C_{48}PA_2$) upon cooling, from 170 °C to 30 °C, dwelling for 15 minutes at each temperature before measurement to let the polymer equilibrate. The sample was then heated back to 170°C and measured under these same conditions. Impedance spectra were fit with an equivalent circuit model (a parallel combination of a resistor and a constant phase element in series with the high-frequency resistance) to determine the through-plane high-frequency resistance R, which is used to calculate the through-plane conductivity, $\sigma_{DC} = L/(A*R)$, where L is film thickness and A is the cross-sectional area.

3.6 Appendix

3.6.1 NMR Spectra

NMR spectra of $C_{26}PA_2$ and $C_{48}PA_2$ and their diester analogues ($C_{26/48}(PO(OEt)_2)_2$) are shown. NMR spectra of intermediates can be found in the respective publication.[102]

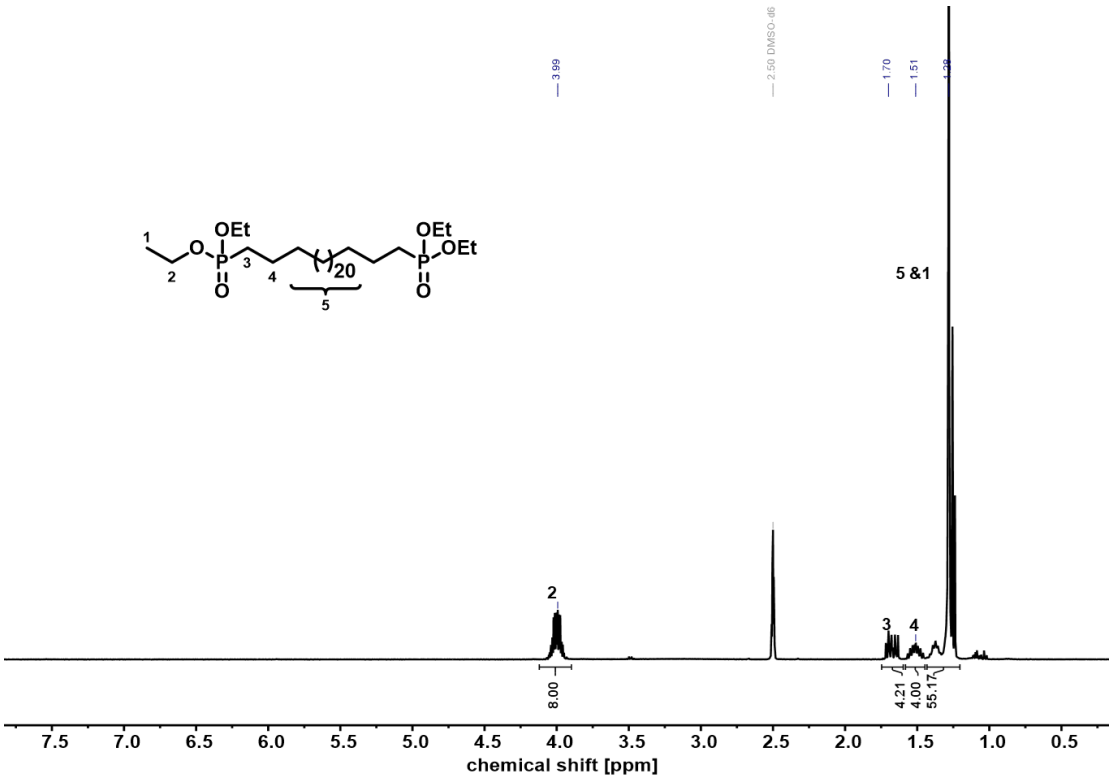

Figure 3.12 ^{1}H NMR spectrum (400 MHz, dmso-d_6, 110 °C) of $C_{26}(PO(OEt)_2)_2$.

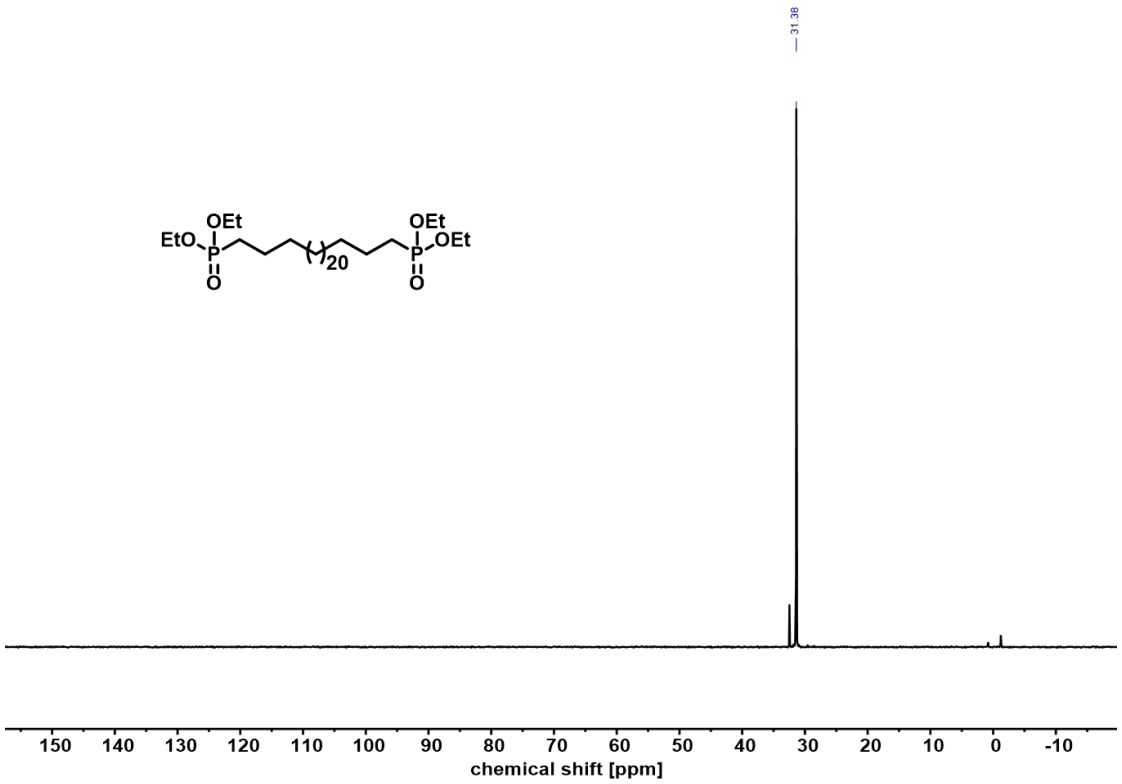

Figure 3.13 $^{31}P\{^{1}H\}$ NMR spectrum (161 MHz, dmso-d_6, 110 °C) of $C_{26}(PO(OEt)_2)_2$.

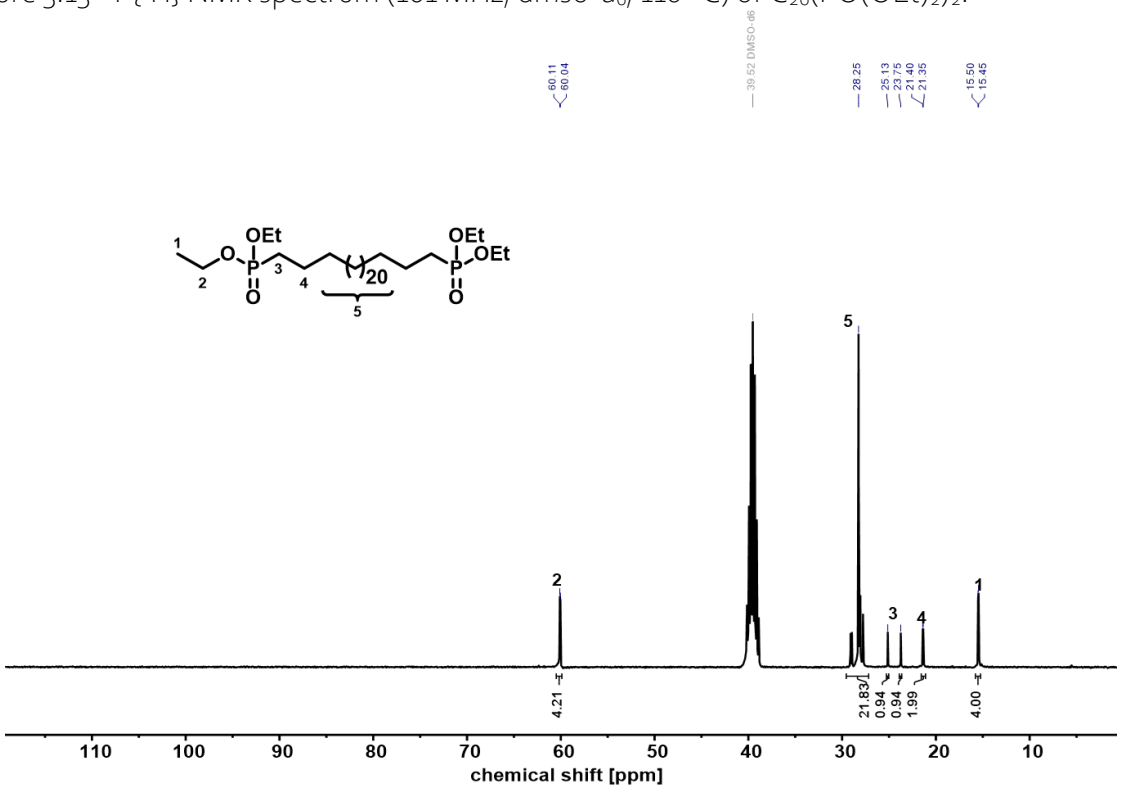

Figure 3.14 $^{13}C\{^{1}H\}$ NMR spectrum (100 MHz, dmso-d_6, 110 °C) of $C_{26}(PO(OEt)_2)_2$.

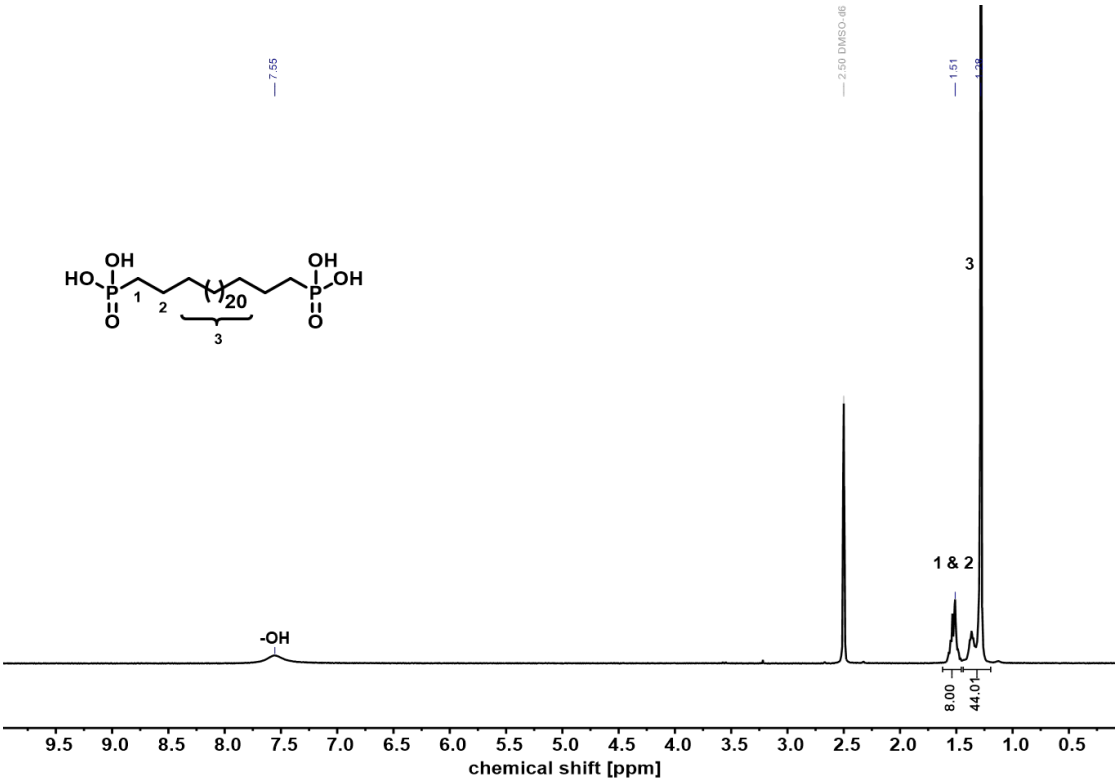

Figure 3.15 ^{1}H NMR (400 MHz, dmso-d_6, 110 °C) of $C_{26}PA_2$.

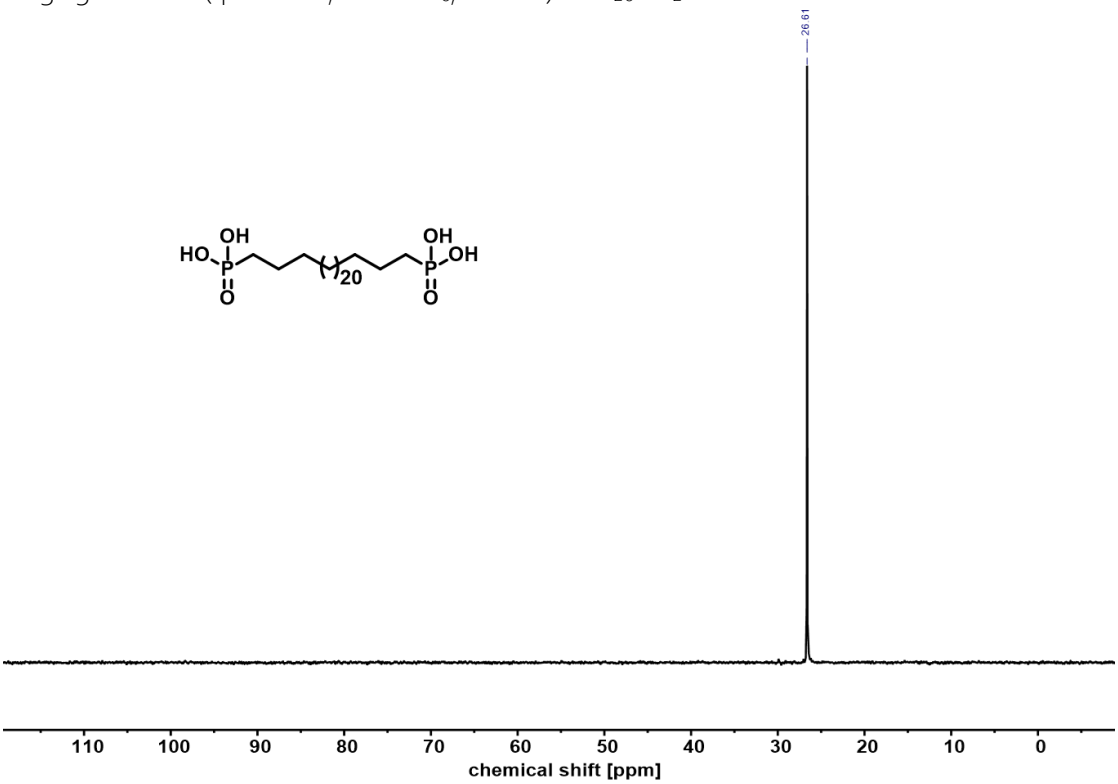

Figure 3.16 ^{31}P{^{1}H} NMR (161 MHz, dmso-d_6, 110 °C) of $C_{26}PA_2$.

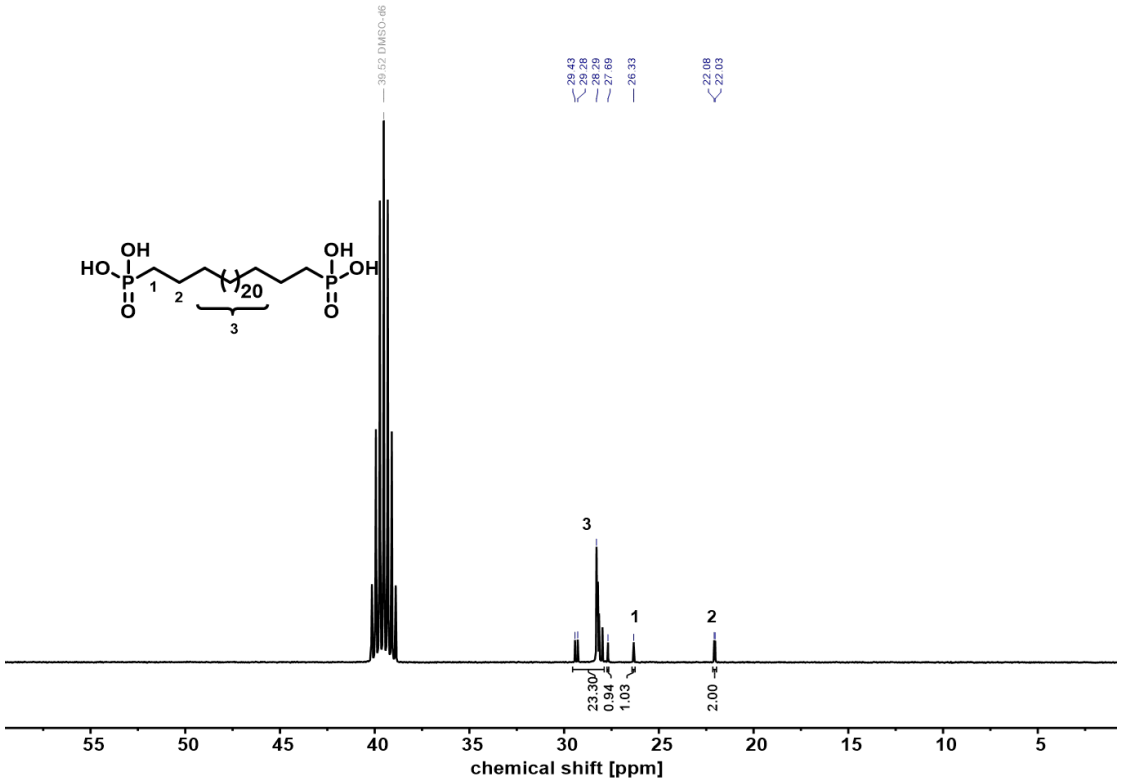

Figure 3.17 $^{13}C\{^{1}H\}$ NMR (100 MHz, dmso-d_6, 110 °C) of $C_{26}PA_2$.

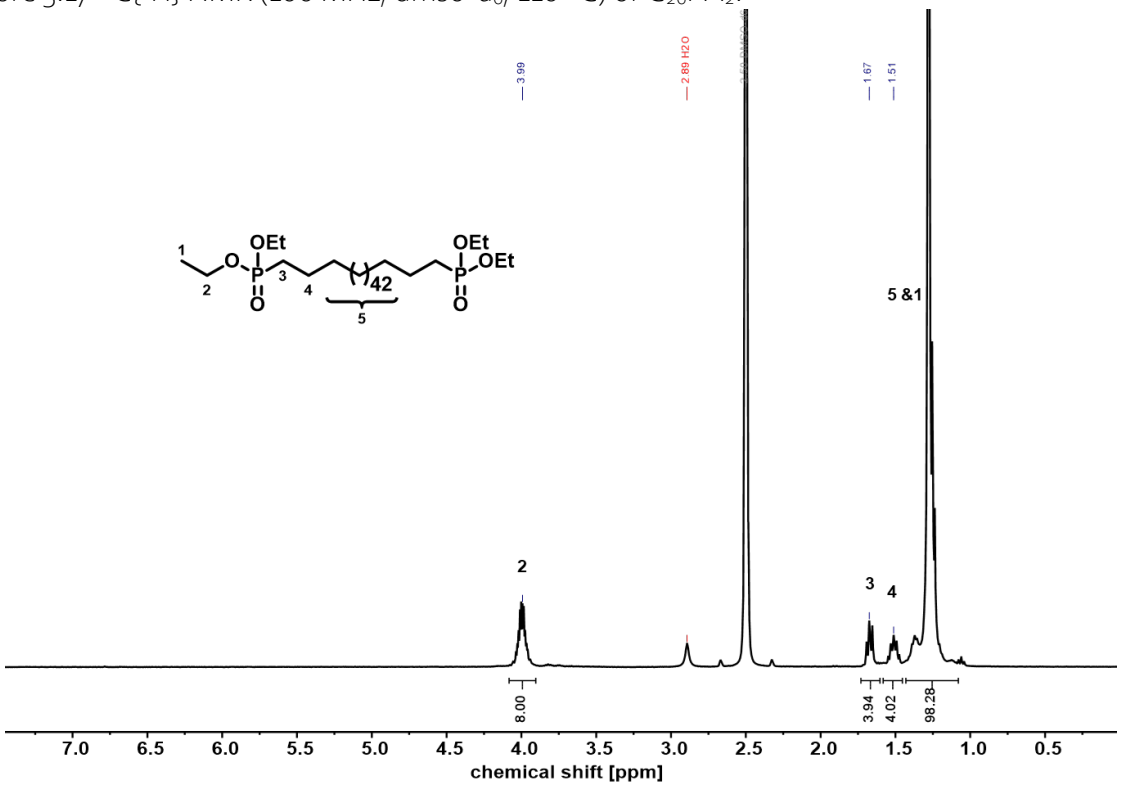

Figure 3.18 $^{1}H\{^{31}P\}$ NMR spectrum (400 MHz, dmso-d_6, 110 °C) of $C_{48}(PO(OEt)_2)_2$.

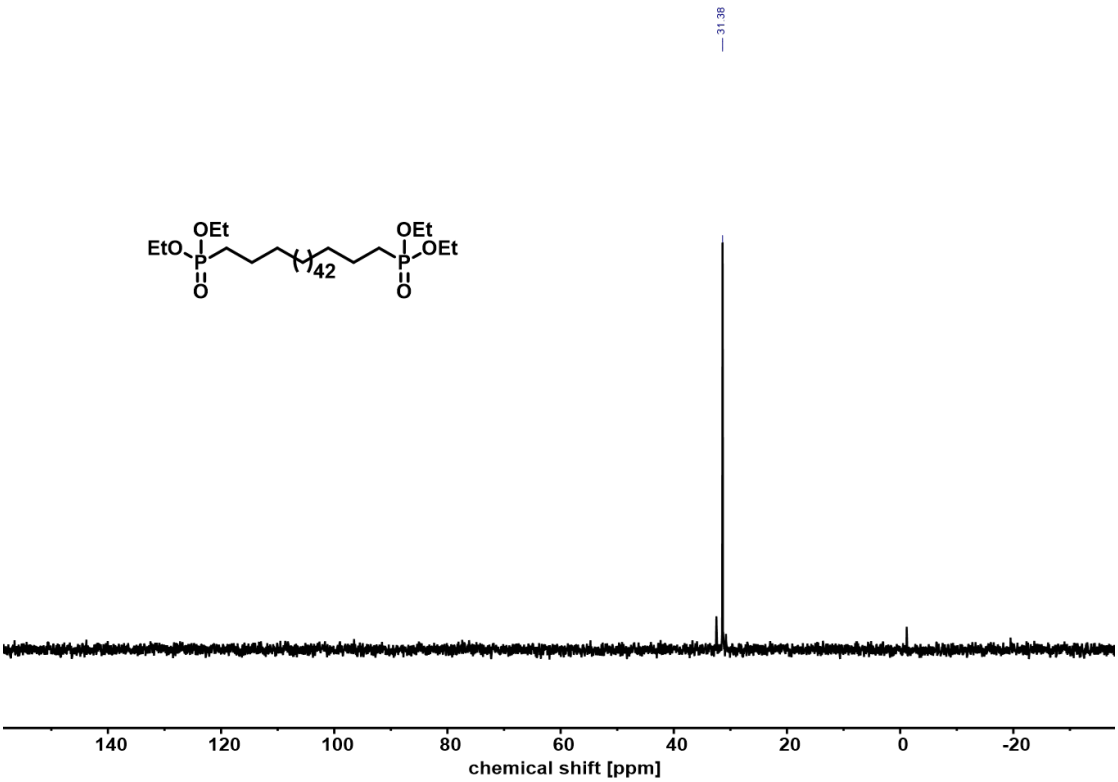

Figure 3.19 $^{31}P\{^{1}H\}$ NMR spectrum (161 MHz, dmso-d_6, 110 °C) of $C_{48}(PO(OEt)_2)_2$.

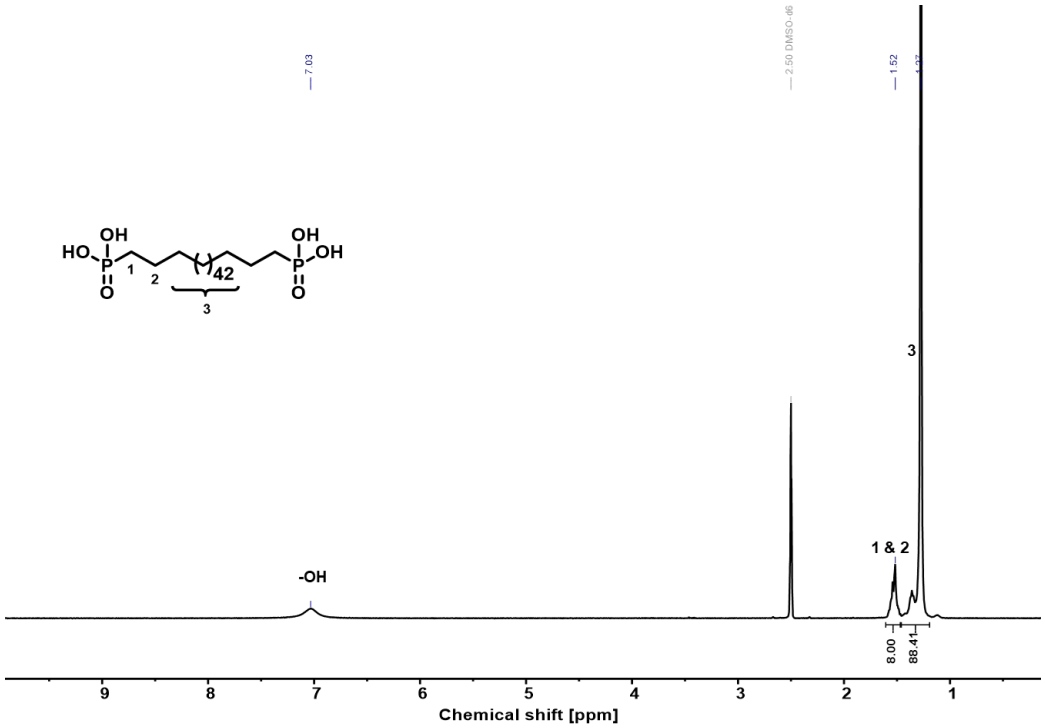

Figure 3.20 ^{1}H NMR (400 MHz, dmso-d_6, 110 °C) of $C_{48}PA_2$.

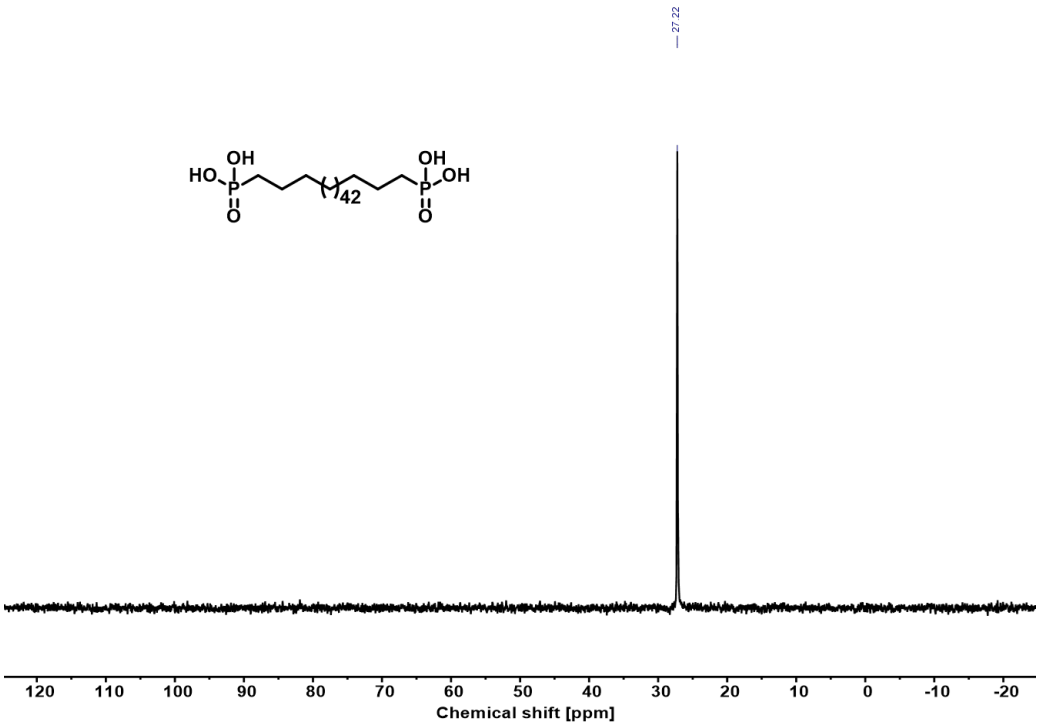

Figure 3.21 $^{31}P\{^{1}H\}$ NMR (161 MHz, dmso-d_6, 110 °C) of $C_{48}PA_2$.

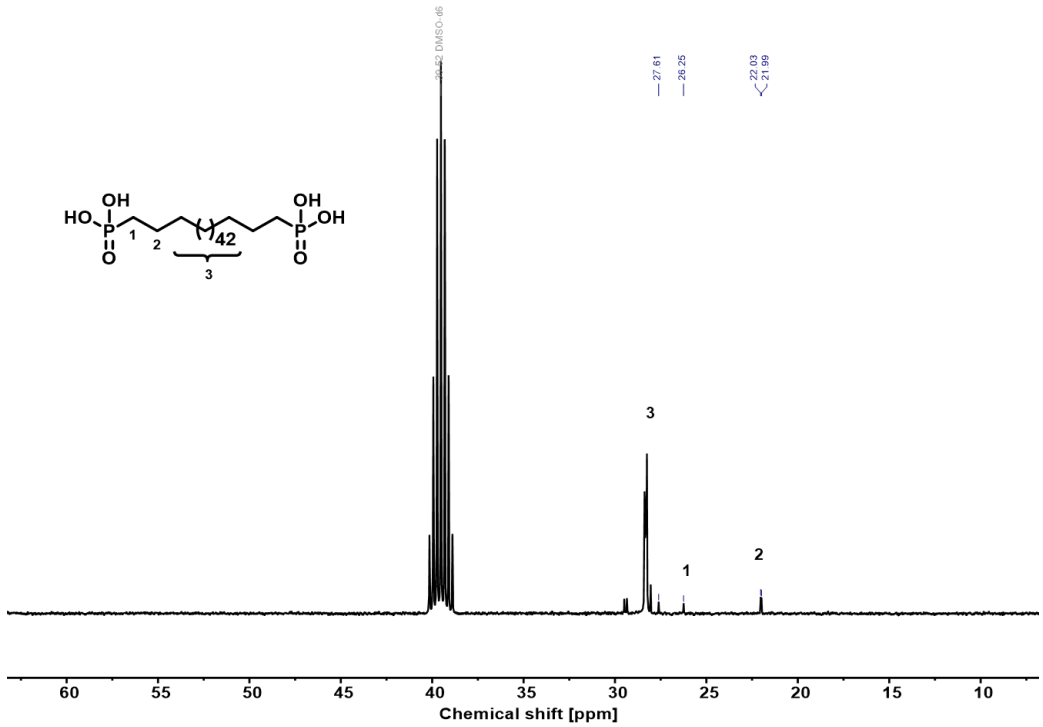

Figure 3.22 $^{13}C\{^{1}H\}$ NMR (100 MHz, dmso-d_6, 110 °C) of $C_{48}PA_2$.

3.6.2 ESI-MS

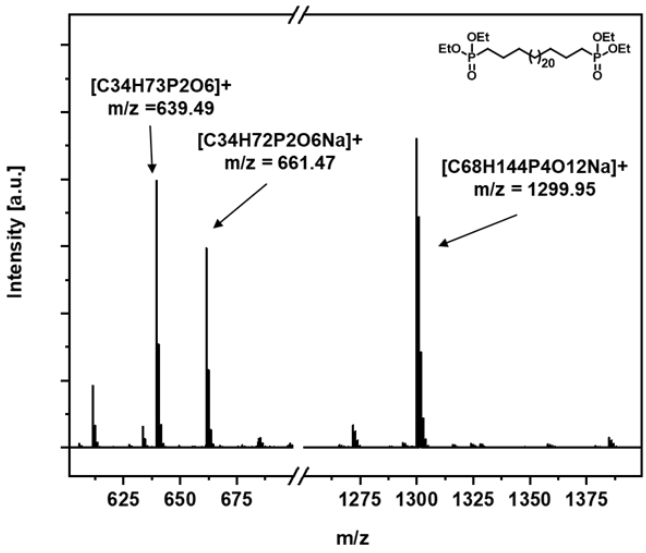

Figure 3.23 ESI-HR mass spectrum of $C_{26}(PO(OEt)_2)_2$ in chloroform/acetonitrile.

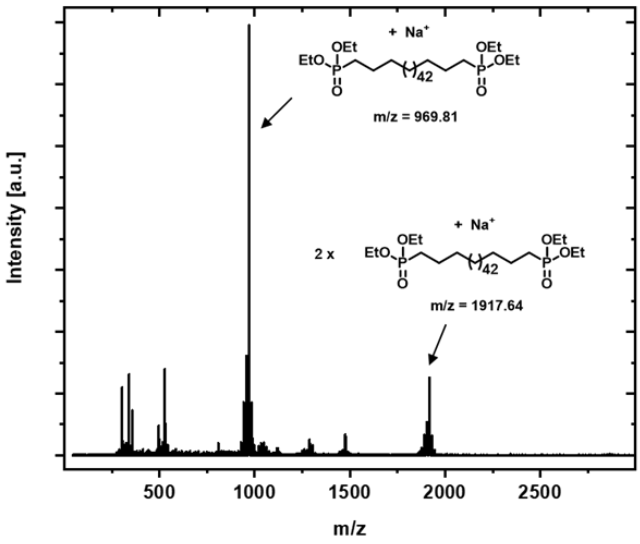

Figure 3.24 ESI-HR mass spectrum of $C_{48}(PO(OEt)_2)_2$ in chloroform/acetonitrile.

4 Gyroid Structures in Precisely Functionalized Polymer Electrolytes

4.1 Introduction

To date, battery systems mostly rely on liquid electrolyte systems. Developing solid polymer electrolytes is crucial to enable better all-solid-state batteries.[47] The most common solid polymer electrolyte system studied is based on poly(ethylene oxide) (PEO), where salt is dissolved in the polymer.[109] Single-ion conducting polymer electrolytes (SIPEs) can be a next level, as the anions are covalently bound to the polymer backbones, thereby hindering electrode polarization and leading to higher transference numbers.[49-50] This approach is promising yet needs further development due to the so far poor ionic conductivities and a lack of understanding of the structure-property relationships.

Several studies show the importance of the ionic aggregate morphology on the ion transport behavior in SIPEs.[51,56,110-113] The polymer chemistry largely dictates the ionic aggregate morphology, which highlights the importance of further developing SIPEs. It was shown that by a precise positioning of the immobilized anions along the polymer backbone rather than a random distribution, the ionic groups can microphase separate to form well-ordered ionic aggregate morphologies.[14,16,18,53,114] In contrast to the widely reported polymer electrolytes containing randomly placed anions and, consequently, ill-defined ion clustering, these precise ion-containing materials allow a conclusive study of the morphology-property relationships, where the ion-transport behavior can be directly correlated with the ion morphology. One approach to access such precise ionic polymers is polycondensation, in which ionic and non-ionic blocks alternate through the choice of monomers. The choice of linear aliphatic, non-ionic monomers with a defined length between the telechelic end groups as apolar segments,

alternating with polar short-chain monomers containing sulfonate groups, leads to defined ionic aggregate morphologies such as layers, hexagonally packed cylinders or double gyroids.[51,56] Of these structures, the latter is the most interesting to further investigate, since ionic conductivities are improved compared to the one- and two-dimensionally connected layered or hexagonal structures.[56,115-116] Moreover, the bicontinuous domains in double gyroids can improve the mechanical properties compared to other morphologies, *e.g.* higher modulus and toughness can be reached.[117-118]

The difficulty to access the gyroid phase was shown by self-consistent field theory calculations, which revealed that it can only be the thermodynamically stable phase within a narrow range of the parameters that define the phase behavior. Amongst these parameters are the effective Flory-Huggins interaction parameter (χ_{eff}), which varies with the ionic composition of the SIPE, the volume fractions of the polar block (f_{polar}) and the degree of polymerization (DP_n). In previously reported precise polyestersulfonates where the ionic groups were spaced by a polyethylene segment with precisely 23 methylene groups, different temperature regimes in which the gyroid structure appeared were observed for different cations (lithium and sodium), which can be correlated to the difference in χ_{eff}.[56] The exploration of a longer apolar polyethylene block (precisely 48 methylene groups) as a spacer between the sulfonate groups showed no appearing gyroid morphology over the entire temperature window investigated (20 - 180 °C), showing the importance of f_{polar} to access this structure.

Starting from this prior knowledge, the synthesis of different precise polymers containing pendant sulfonate groups was aimed at to explore the phase behavior of these materials as a function of f_{polar} and temperature. The structure-property relationship with regard to ion conductivity was focused on. Additionally, the borders of this straight-forward approach were elaborated, by varying the chain lengths and by reducing the crystallinity within the apolar blocks.

Please note, that the results presented in the following chapter originate from a close collaboration with the group of Prof. Dr. K. I. Winey at the University of Pennsylvania. In-situ X-ray scattering as well as DSC measurements and the data acquisition and processing were performed by Dr. Jinseok Park and Benjamin Ferko. Detailed information on the parameters and measurement protocols can be found in the corresponding publications as well as in the thesis of Dr. Jinseok Park.[119-123]

4.2 Results and Discussion

4.2.1 Gyroid Structures in Polyestersulfonates

Previously, a series of polyethylene-based ionic multiblock copolymers containing polar blocks, each with one sulfonated ionic group, were synthesized *via* step-growth polymerization.[51,95] They exhibit various order-to-order transitions as a function of temperature. These precisely segmented polyethylene-based sulfonates (PES*x*M) have exactly *x* methylene units in the polyethylene block and were synthesized with different counterions M through ion exchange (Li^+, Na^+ and Cs^+). Notably, the shorter analogue PES23Na with a volume fraction of the polar domain (f_{polar}) of ~ 0.28 exhibits gyroid morphologies.[56] The similar multiblock copolymer PES48Na with a 48 carbon polyethylene block with f_{polar} ~ 0.16 does not exhibit the gyroid morphology.[51]

To elucidate the phase behavior of these multiblock copolymers as a function of f_{polar} and temperature, a new series of PES*x*Na and PES*x*Li multiblock copolymer electrolytes were synthesized. These materials comprise nonpolar polyethylene blocks (*x* = 10, 12 and 18) and short polar blocks with one sulfonate ionic group. They complement the previously presented PES23M and PES48M materials and widen the portfolio of precise ionic polyesters exhibiting gyroid structures.

The step-growth polymerization to PES18 materials was performed according to the previously reported procedure, using a mechanical stirrer equipped with a helical agitator. However, the degrees of polymerization reached by this method were limited. Therefore, a different stirring technique was used for the polyesters PES12 and PES10, where no mechanical stirrer was attached to the flask but an elliptical (PTFE)-coated stir bar with a lanthanide magnetic core was used. This method still enabled sufficient stirring until a high melt viscosity was reached, while at the same time a higher vacuum could be reached due to the better sealing of the Schlenk flask. This led to DP_n values of 70 and higher, whereas the DP_n reached for PES18, PES23 and PES48 did not exceed values of 35.[51,56]

For the previously synthesized PES23 and PES48 polymers, the counterion exchange from tetra-*n*-butylammonium to lithium or sodium was conducted by treating the pre-polymer PES*x*NBu_4 with an aqueous solution of LiCl or NaCl, respectively, from which the polymers PES*x*Li and PES*x*Na precipitated as a white solid.[51] Washing with water and methanol yielded the pure polymers. This procedure was applied to PES18 materials as well, but was not possible to use for

the shorter chain analogues PES12 and PES10. In these cases, a treatment with aqueous solutions lead to dissolution of the polymer, which was attributed to the increased ion density in the polymer, hence the higher solubility in water. This hampers the established washing procedure to remove the residual tetra-*n*-butylammonium and excess salt. Therefore, a new workup procedure had to be implemented. The materials were dissolved in the salt solutions and subsequently dialyzed in distilled water to remove the excess salt. However, only partial salt exchange could be achieved this way. Repeating this procedure, dissolving in salt solution and subsequent dialyzing, lead to a full conversion to the lithium and sodium materials. To ensure the absence of tetra-*n*-butylammonium in the final polymers, and to estimate the degree of polymerization and molecular weights of the polymers, ^{1}H NMR spectroscopy and end-group analysis was performed (the method of calculation for DP_n and M_n can be found in the Experimental section 4.5.1, spectra are depicted in the appendix, section 4.6,). Note that in contrast to traditional diblock copolymers, the molecular weight dispersity does not impact f_{polar} because the monomeric repeat units are precise. The basic properties of the synthesized PES*x*Na and PES*x*Li polymers are listed in Table 4.1.

Table 4.1 Basic Properties of PES*x*Na and PES*x*Li.

	DP_n [a]	M_n [a] [kg/mol]	f_{polar} [b]
PES10Na	71	12.7	0.45
PES12Na	75	14.5	0.41
PES18Na	35	8.2	0.32
PES12Li	110	20.4	0.41
PES18Li	32	7.3	0.31

[a] The degree of polymerization and the molecular weight were determined by end-group analysis of ^{1}H NMR spectra. [b] The volume fraction of sulfosuccinate blocks.

To gain insight into the temperature-dependent structural behavior and ionic conductivities of the precise polyestersulfonates, DSC, X-ray scattering and electrochemical impedance spectroscopy was performed on these materials. The measurements presented in this section were conducted and interpreted by Dr. Jinseok Park within a research collaboration of our group and the group of Prof. Dr. Karen I. Winey at the University of Pennsylvania. The results are summarized here, further details are given in the thesis of Dr. Jinseok Park and in the respective publications.[119-121]

The PES*x*Na polymers are semicrystalline at room temperature, exhibiting melting temperatures of 92, 101 and 126 °C for PES10Na, PES12Na and PES18Na, respectively (see Figure 4.1). The increasing melting temperatures with increasing length of the polyethylene spacer can be explained by the better ability of the chains to fold in a hairpin-like fashion during the crystallization procedure.[53] However, none of the materials show a crystallization peak in the first or second cycle, showing that the recrystallization of the polyethylene segments is significantly hindered by the polar ionic interactions. Glass transition temperatures are observed at increasing temperatures with a shorter length of the polyethylene spacer, thus higher f_{polar}, as expected. No order-to-order (OOT) transitions are visible in PES10Na and PES18Na, whereas reversible peaks can be seen in PES18Na at 190.5 °C upon the first heating and 170.6 °C upon the first cooling cycle. Their nature was examined in more detail *via* small-angle X-ray scattering.

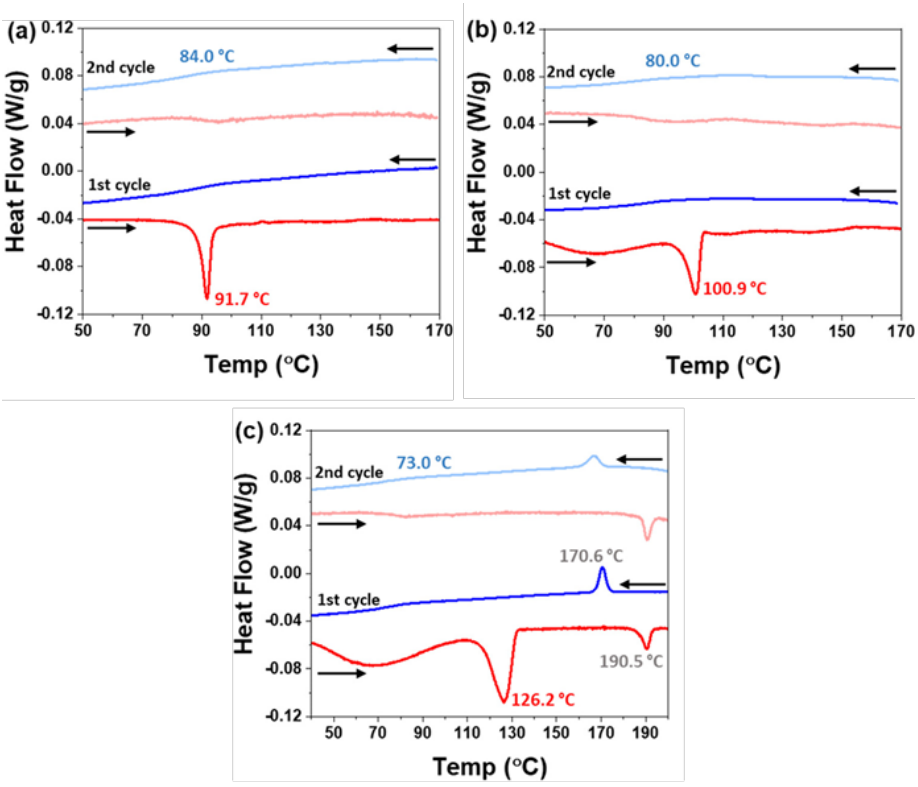

Figure 4.1 DSC traces of (a) PES10Na, (b) PES12Na, and (c) PES18Na measured at 1 °C/min ramp rate, including heating (red) and cooling (blue) of first and second cycles. DSC traces of first and second cycles were arbitrarily shifted for clarity. Melting transition, order-to-order transition and glass transition temperatures are shown in red, grey and blue, respectively. Measurements and data interpretation were conducted by Dr. J. Park (Winey group).

The X-ray scattering profiles of PES10Na, PES12Na and PES18Na were recorded upon heating and cooling and are displayed at specific temperatures in Figure 4.2. The scattering data at all recorded temperatures can be found in the respective publication.[120]

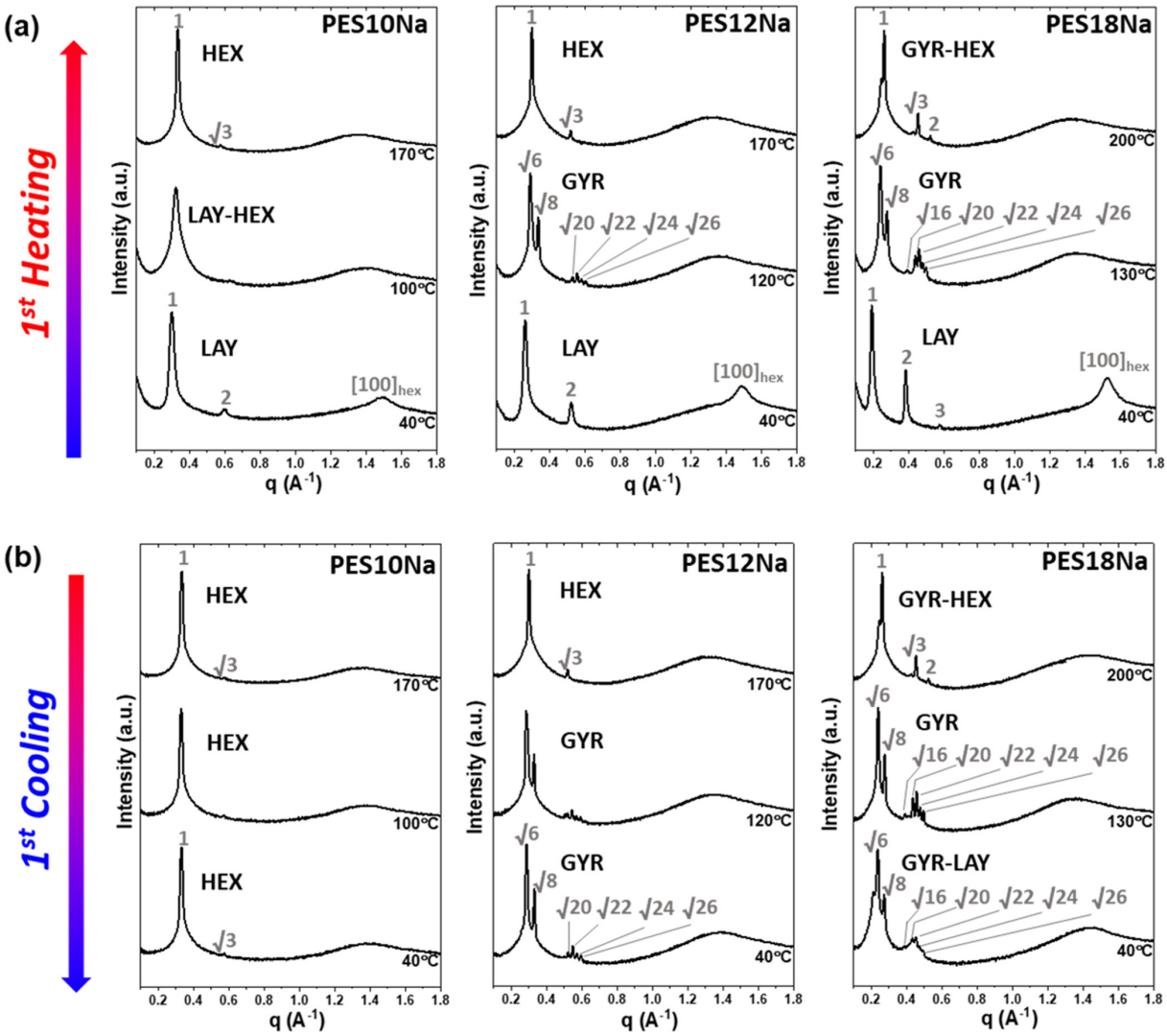

Figure 4.2 In-situ X-ray scattering profiles at selected temperatures upon (a) heating and (b) cooling of PES10Na, PES12Na and PES18Na. Identified ionic aggregate morphologies are indicated as LAY (layered), HEX (hexagonal) and GYR (gyroid).

Before the first heating, all polymers show a distinct peak at $q \sim 1.5$ Å^{-1}, which can be assigned to the [100] hexagonal lattice within the polyethylene segments.[124] *Via* deconvolution and integration of the hexagonal reflex and the amorphous halo, crystallinities of 33, 42 and 62 % are calculated. The increasing crystallinity with increasing length of the polyethylene spaces is conclusive with the higher capability to crystallize in a hairpin-like fashion, as described above. Additionally, all polymers exhibit layered aggregates before the first heating, as indicated by the equidistant peaks at $q < 0.7$ Å^{-1}. The d-spacing of the layers increases in the order PES10, PES12 and PES18Na ($d = 2\pi/q = 21.0$, 24.1, 32.9 Å, respectively), since the length of the polyethylene spacer increases. During the first heating cycle, the aggregates transition to a gyroid morphology upon the melting process of the polyethylene chains, in case of PES12Na and PES18Na. This is indicated by the formation of a broad peak at $q \sim 1.5$ Å. In case of PES10Na, the melting of the

polyethylene segments is accompanied by an OOT to form hexagonal ionic aggregate morphologies. The fact that only two methylene segments less than PES12Na leads to hexagonal rather than gyroid morphologies shows the sensitivity of the nanoscale aggregate morphology to the polymer composition. Upon further heating, the hexagonal morphology in PES10Na remains, whereas both PES12Na and PES18Na exhibit a gyroid-hexagonal transition. The slow dynamics observed in DSC measurements are also visible in X-ray scattering experiments, where no crystallization of the polyethylene segments is observed on the time scale of the experiment. Instead, the hexagonal morphology in PES10Na remains over the entire temperature range investigated, and the PES12Na and PES18Na polymers transition back into the gyroid morphology, which then persists at room temperature. After 7 days, the chains have recrystallized and transitioned into layered structures again, as was previously reported for PES23Na and PES48Na.[51,56]

From the results discussed herein and the temperature-dependent morphologies observed for the previously investigated PES23Na and PES48Na, morphology maps upon heating and cooling as a function of f_{polar} were constructed (see Figure 4.3). The transition of the layered aggregates into either hexagonal (f_{polar} ~ 0.16 and 0.45) or gyroid (f_{polar} ~ 0.26, 0.32 and 0.41) morphologies upon heating is accompanied by the melting of the polyethylene segments, as seen in the first heating trace of the DSC measurements. With a further increase in temperature, polymers with f_{polar} ~ 0.16 and 0.45 show a direct transition from layered to hexagonal morphologies, whereas polymers with f_{polar} of 0.27, 0.32 and 0.41 form a gyroid morphology and subsequently transition into hexagonal morphology. This shows that the gyroid morphology is present at intermediate temperatures and $0.27 < f_{polar} < 0.41$. This wide range of f_{polar} is unusual, since the experimental composition window is typically only ~ 4 vol.-%.[125] The morphology map upon cooling features a large area of gyroid morphologies, which can be attributed to the slow crystallization kinetics. Consequently, the morphologies present in the melt state persist below T_m for $f_{polar} > 0.27$. The slow kinetics also cause a wide range of GYR-HEX coexistence, hindering the OOT.

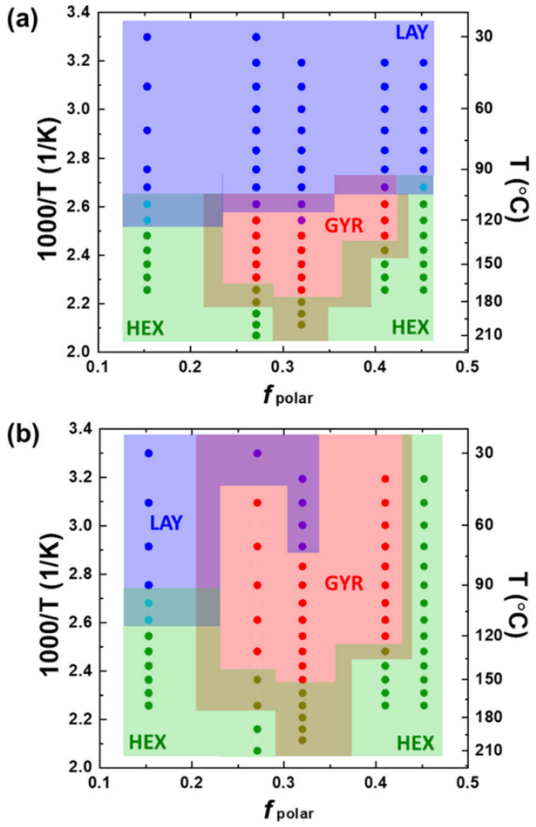

Figure 4.3 Morphology maps upon heating (a) and cooling (b) as a function of f_{polar} *vs.* temperature. Ionic aggregate morphologies are indicated as LAY (layered, blue), HEX (hexagonal, green) and GYR (gyroid, red). Mixed phases are indicated as light blue (LAX/HEX), purple (LAX/GYR) and olive (GYR/HEX). f_{polar} corresponds to PES10Na (0.45), PES12Na (0.41), PES18Na (0.32). Data of PES23Na (f_{polar} = 0.27) and PES48Na (f_{polar} = 0.16) are reported elsewhere.[51,56]

The ionic conductivity of the synthesized polyestersulfonates was determined *via* electrochemical impedance spectroscopy and was investigated with regard to its temperature dependence upon cooling as well as the morphology dependence (see Figure 4.4). In all cases, Vogel-Fulcher-Tammann (VFT) relationships are observed, indicating that the ion transport is coupled to the polymer segmental dynamics. If this were not the case, an Arrhenius-like dependence of the conductivity on temperature should be observed. The VFT fitting of the data can be found in the publication.[120] In case of PES18Na, a plateau is observed above 130 °C when the gyroid transitions into hexagonal morphologies. This indicates higher ionic conductivity in gyroid morphologies compared to hexagonal morphologies and can be concluded from the faster ion transport in the three-dimensionally interconnected ionic aggregate channels in the gyroid structure compared to one-dimensional hexagonal structures. This morphology change was also visible in DSC measurements, showing that it involves a high enthalpic change. However, in case of PES12Na, the HEX-GYR transition is not reflected in the ionic conductivity

measurement and was also not visible in DSC traces, showing the lower enthalpic change and therefore the lack of different conductivity regimes. Both phases follow the same VFT behavior and consequently have comparable fragility strength coefficients. In general, a reduced conductivity is observed with decreasing length of the polyethylene spacer, even though the density of charge carriers increases. This is closely related to the increasing glass transition temperatures with decreasing length of the spacer. This finding again shows that the ion transport is not fully decoupled from polymer segmental dynamics.

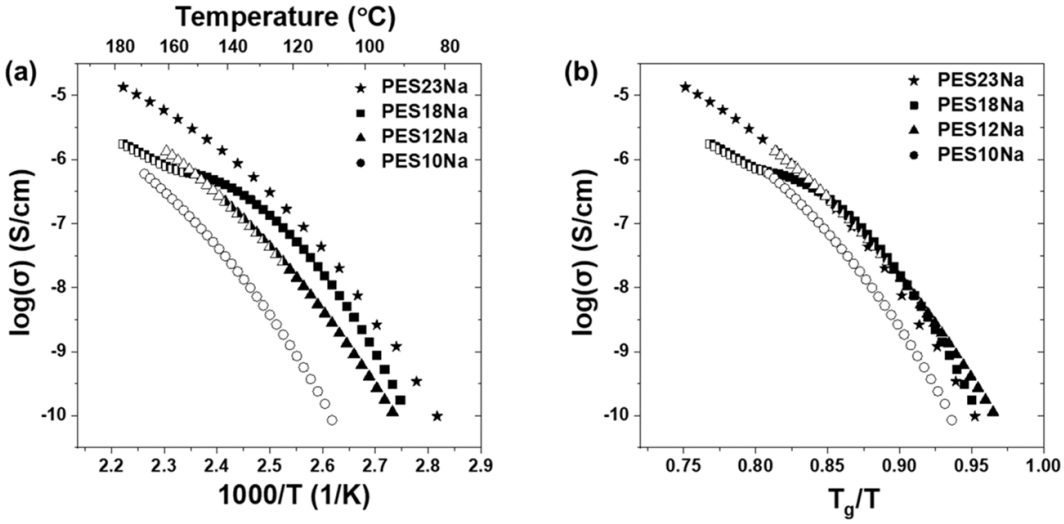

Figure 4.4 (a) Temperature dependent ionic conductivities upon cooling and (b) normalized by the T_g of PES10Na, PES12Na and PES18Na. Data for PES23Na was previously reported.[56] Filled symbols represent gyroid, open symbols represent hexagonal morphologies, half-filled indicate GYR-HEX coexistences.

When looking at the conductivity in a T_g-normalized way, the conductivities of PES12Na, PES18Na and PES23Na are very similar in the range of $0.85 < T_g/T < 0.95$, which is the range where the gyroid morphology is present. The ionic conductivities exceed those of PES10Na, exhibiting hexagonal morphologies, by one order of magnitude at $T_g \sim 0.90$, which again highlights the beneficial impact of the gyroid compared to the hexagonal structure in these polymers.

To summarize, the results presented here show the strong correlation between the nanoscale morphology of the ionic aggregates and phase behavior, with the ion transport properties in precise single-ion conducting multiblock copolymers.

4.2.2 Amorphous Polyestersulfonates

The previously shown beneficial impact of the bicontinuous double gyroid (DG) morphology on ion conductivity suggests the design of materials, where the gyroid morphology is persistent at room temperature. The investigated polyestersulfonates show broad temperature windows in which the DG morphology is present and, simultaneously, the polyethylene spacers are amorphous. In order for the DG phase to persist, chain stretching and crystallization of the polyethylene segments need to be hindered, which would favour the formation of layered domains. By suppressing this driving force, the interfacial area can be minimized, leading to constant mean curvature interfaces, as present in the DG phase.

One possible way of reducing crystallinity is the introduction of double bonds in the polyethylene segments. Since 1,18-octadecanediol is synthesized from oleic acid *via* self-metathesis and subsequent hydrogenation of the double bond, this synthesis route can be used to access 1,18-octadec-9-ene diol with an internal double bond. This compound was successfully synthesized in a 3-step reaction (self-metathesis, esterification and reduction of ester groups with LAH). The step-growth polymerization of the unsaturated diol with NBu_4DSS catalyzed by $[Ti(O^nBu)_4]$ was achieved by reducing the reaction temperature to 140 °C compared to the typical conditions used for PES*x*NBu_4 polycondensations (160 °C). This ensured that the double bonds remained intact and no cross-linking occurred during the reaction. *Via* this method, uPES18Na could be obtained with a DP_n of 38. Several approaches were made to cross-link uPES18Na at elevated temperatures when it exhibits the desired gyroid morphology within the ionic aggregates. They were performed by Dr. J. Park in group of Prof. Dr. K. I. Winey. The results and a detailed discussion can be found in his thesis.[119]

To hinder crystallization of the polyethylene segments in PES12Na, a commercially available dimer fatty acid derived from oleic acid (called *Pripol*) was used to partially replace the linear C_{12} spacer. This spacer is a branched C_{36} diol segment, which strongly influences the f_{polar} value of the new polyestersulfonates. Therefore, the f_{polar} values were calculated by Benjamin Ferko by weighing the van der Waals volumes of the sulfonate contribution against the hydrocarbon backbone. This was performed for different chain lengths of the polyethylene spacers, as well as for different molar Pripol contents (see Figure 4.5).

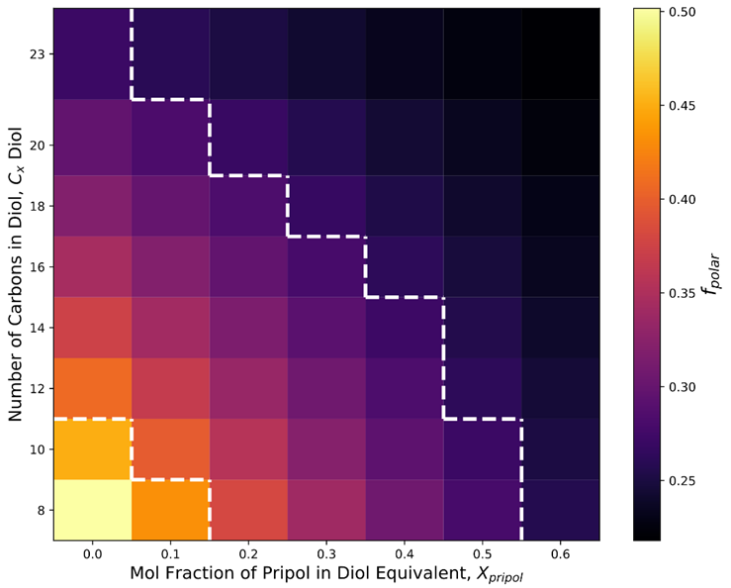

Figure 4.5 Calculation of the polar volume fraction f_{polar} in Pripol-modified PES*x*Na depending on the molar amount of Pripol and the number of carbon atoms in the aliphatic polyethylene segment. Region within dashed lines represents where an appearance of the gyroid structure is expected according to f_{polar} ($0.27 \leq f_{polar} \leq 0.41$).

The synthesis of PES12Na with 20 mol% of Pripol (PES12Na-Pripol) was targeted to investigate the borders of this approach. The standard polycondensation procedure that was implemented for the polyestersulfonates (*cf.* section 4.4) was followed, using the tetra-*n*-butylammonium salt of dimethyl sulfosuccinate and titanium (IV) butoxide as a catalyst. The salt exchange to obtain PES12Na-Pripol™ was conducted by dissolving the polymer in methanol and subsequently adding brine, which precipitates the polymer. The solid residue was dissolved in brine and dialyzed in deionized water to remove residual salt. This process only yielded 96% conversion to sodium, which is why it was repeated by dissolving the polymer in brine and subsequent dialysis. *Via* ^{1}H NMR spectroscopy, a degree of polymerization of 25 was calculated, corresponding to a molecular weight of M_n = 6.5 kg/mol. The ratio of Pripol to C_{12} was determined from the amount of aliphatic -CH_3 groups observed in the ^{1}H NMR spectrum (multiplet at 0.86 ppm), which correspond to the two side chains in the Pripol segment (Figure 4.6). This reveals a total Pripol content of 28%. The slightly increased value of Pripol™ compared to the ratio of monomers introduced to the original polymerization mixture can be explained by the volatility of C_{12}-diol at the reaction conditions employed (160 °C, 3 x 10^{-2} mbar). Full conversion of tetra-*n*-butylammonium counterions to sodium was achieved after the second dialysis step.

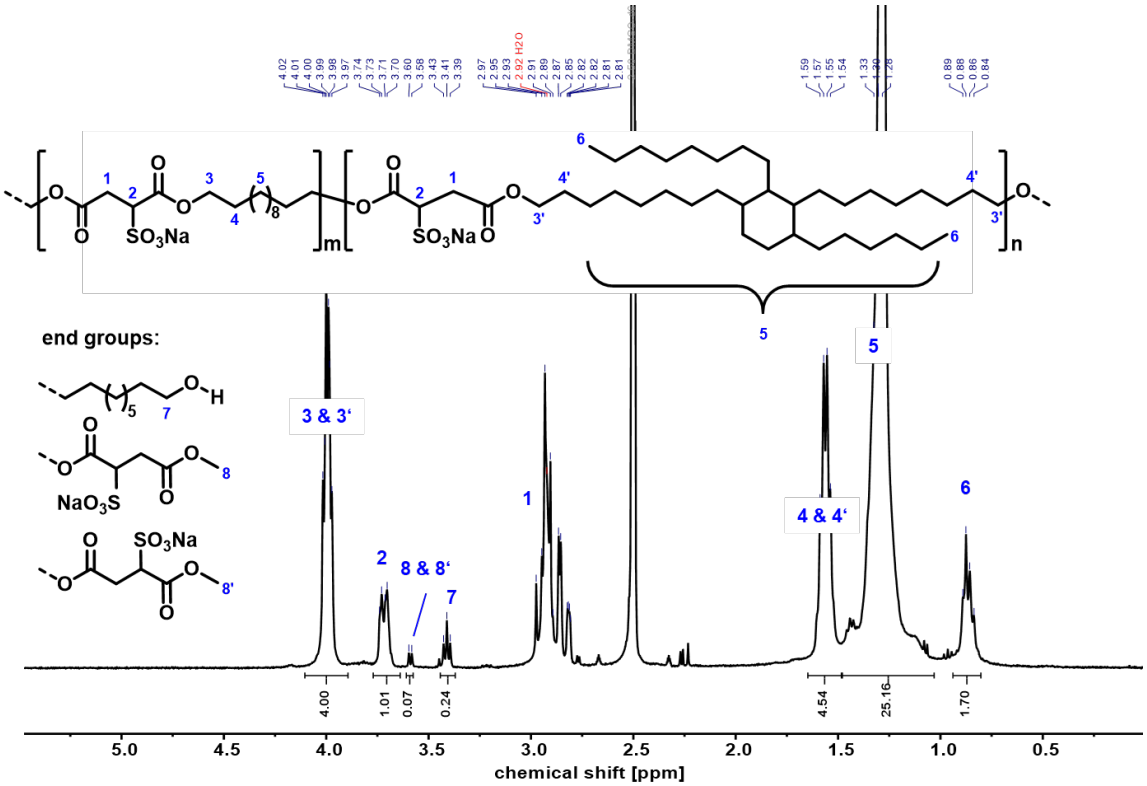

Figure 4.6 ^{1}H NMR (400 MHz, dmso-d_6, 383 K) spectrum of synthesized PES12Na-Pripol. Note that diastereotopic protons **1** overlap with the broad signal at 2.9 ppm, which corresponds to residual water in the dmso-d_6 solvent.

In-situ X-ray scattering at temperatures between 30 °C and 210 °C showed, that the targeted gyroid structure was not present in PES12Na-Pripol (Figure 4.7). Instead, layered structures were found in the low-angle regime, transitioning to disordered aggregates above 90 °C. However, the wide-angle range only featured an amorphous halo, showing that crystallization of the polyethylene segments was successfully hindered. DSC measurements confirm the absence of crystallinity, a melting or crystallization transition is observed in neither the first nor the second heating/cooling trace. However, broad transitions can be found at ~50 °C, which might arise from layered-disordered transitions in the ionic aggregates. The appearance at a different temperature is explained by the different heating/cooling rates between the methods.

Since the Pripol monomer and 1,18-octadecanediol have a more similar distance between the hydroxy end groups compared to 1,12-dodecanediol, PES18Na-Pripol was synthesized. A DP_n of 35 was reached with a Pripol content of 23% (as determined by ^{1}H NMR spectroscopy). The salt exchange was carried out successfully, and the conversion of NBu_4^+ to Na^+ reached 100 % after three exchange steps (see Figure 4.8). After the cation exchange, a DP_n of 37 was determined, showing that the workup procedure is suited and does not cleave the polyester chains.

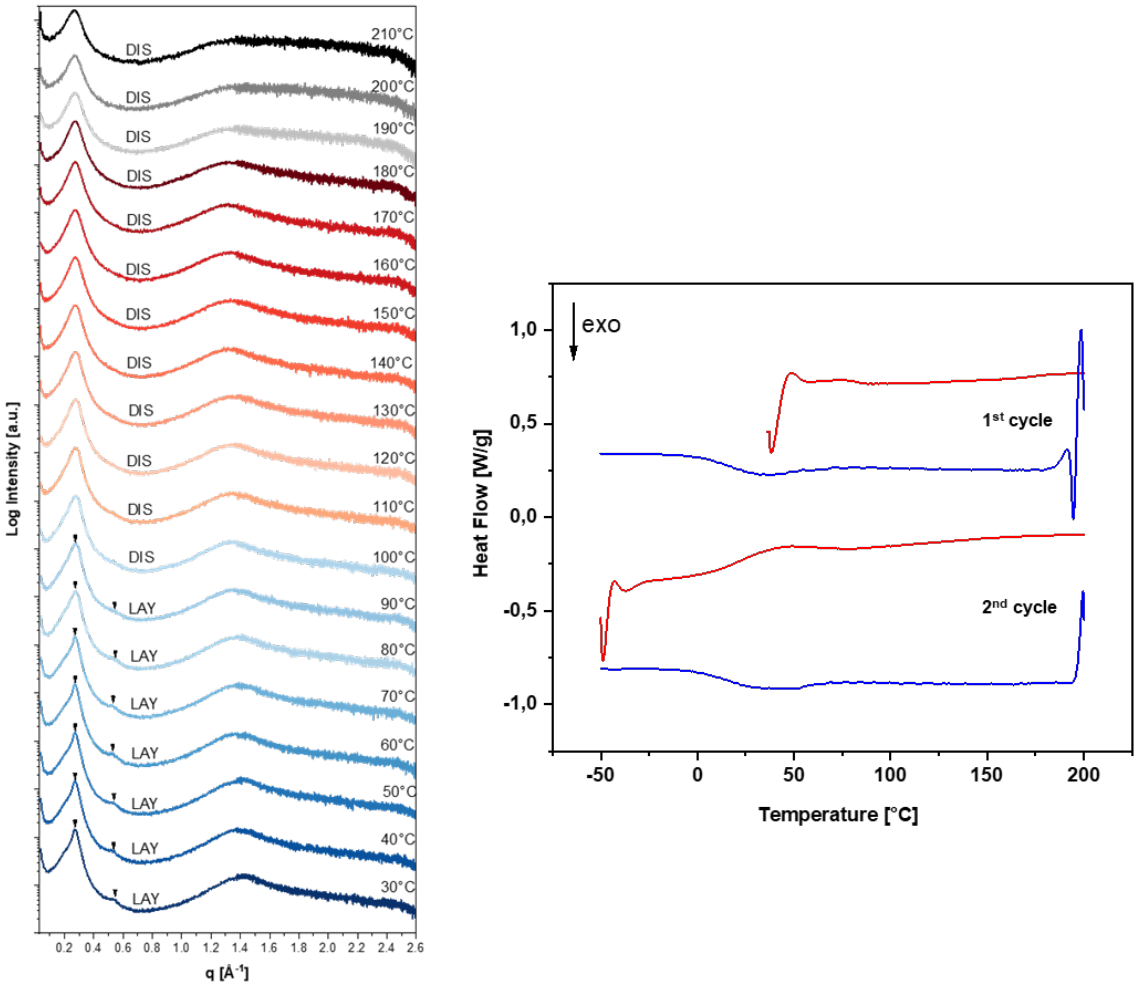

Figure 4.7 Left: In-situ X-ray scattering profiles of PES12Na-Pripol upon heating. Ionic aggregate morphologies in the low-q area are marked as LAY (layered) and DIS (disordered). Right: DSC traces of PES12Na-Pripol (10 K/min heating/cooling rate, red displays heating, blue displays cooling trace). Data were shifted vertically for clarity.
X-ray scattering measurements and data evaluation were carried out by Benjamin Ferko (Winey group).

From the same batch, PES18Li-Pripol was synthesized. However, the ion exchange from NBu_4^+ to Li^+ was challenging since only slow conversion to Li^+ during the dialysis process was achieved (see Figure 4.8). After four salt exchange steps, a conversion of 98 % was achieved, which was sufficient to investigate the structures of the ionic aggregates since such low amounts of the bulky NBu_4^+ are expected to not disturb the aggregate formation significantly. The DP_n of PES18Li-Pripol accounts to 27, showing that the extensive work-up process lowers the molecular weight in case of lithium, which is not observed in PES18Na-Pripol. However, this reduced DP_n is still sufficient to investigate the ionic aggregate morphologies.

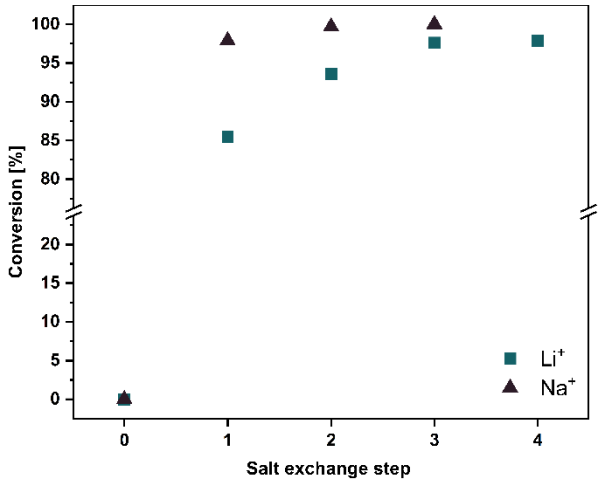

Figure 4.8 Conversion of PES18NBu4-Pripol to PES18Na-Pripol and PES18Li-Pripol.

The investigation of the ionic aggregate structure of these materials was again carried out by Benjamin Ferko (Winey group). X-ray scattering profiles were taken at specific temperatures upon heating and cooling (Figure 4.9). In case of sodium counterions, crystallinity in the polyethylene segments can be observed neither during heating nor during the cooling process, only a clear amorphous halo is visible in the range of 1.0 - 1.8 $Å^{-1}$. This shows that the 20% incorporated Pripol successfully hindered the crystallization also in case of the longer-chain aliphatic C_{18} segments. However, in case of PES18Li-Pripol, a crystalline peak is visible at ~ 1.5 $Å^{-1}$. This peak disappears above 80 °C, which corresponds to the melting transition of the polyethylene segments. The ionic aggregates show different structures for the lithium and sodium derivatives: while PES18Na-Pripol shows hexagonal morphologies over the entire temperature range investigated, PES18Li-Pripol exhibits layered morphologies at room temperatures which transition to hexagonal aggregates above 80 °C. In both materials, the hexagonal structures are very pronounced and exhibit narrow reflexes, correlating to large domain sizes and a high degree of order within the crystallites.

The fact that PES12Na-Pripol exhibits very weakly pronounced layered structures at room temperature, and PES18Na-Pripol well defined hexagonal structures, shows the importance to choose chain-lengths of the diol close to the chain length of the Pripol in order to obtain defined ionic aggregates. However, neither polymer adapts a gyroid morphology throughout the entire temperature range. In case of PES18Na-Pripol, this can be attributed to the lowered f_{polar} compared to PES18Na, thus favouring the hexagonal morphology.

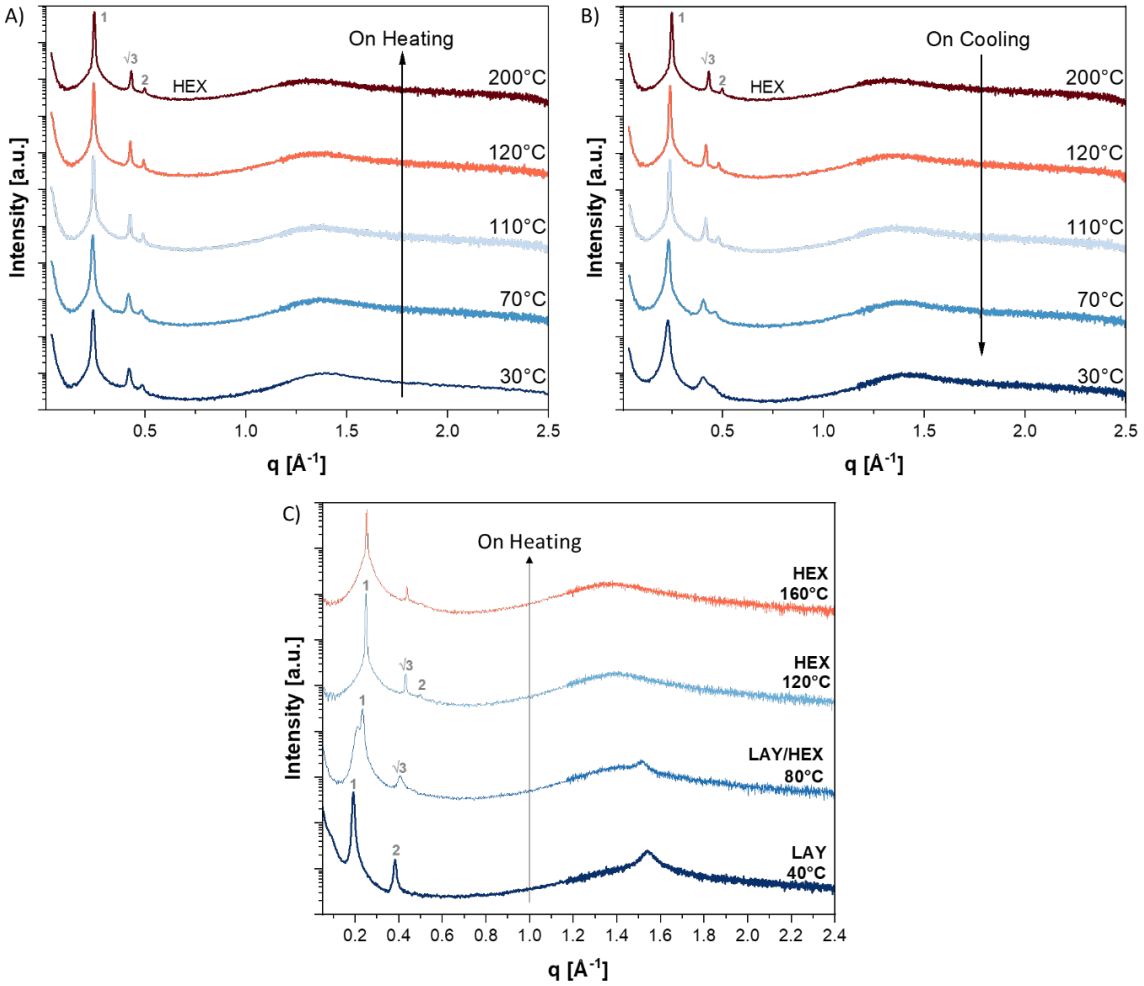

Figure 4.9 In-situ X-ray scattering profiles of PES18Na-Pripol upon heating. Ionic aggregate morphologies in the low-*q* area are marked as HEX (hexagonal). Measurements and data evaluation were carried out by Benjamin Ferko (Winey group).

Even though the synthesized Pripol containing materials do not exhibit double gyroid morphologies, they are highly interesting to further investigate regarding their ion-transport properties and to gain insight into the thin-film behaviour of these precise yet fully amorphous materials.

4.3 Summary and Conclusion

Highly ordered materials provide a tool for rational advances in various applications. Materials which self-assemble into the double gyroid morphology (DG) are of particular interest since the three-dimensional networks in DGs provide beneficial properties with regard to selective ion transport. Additionally, such ordered morphologies with sub-3 nm domain spacings are of interest as nanopatterning templates. In this chapter, alternating multiblock copolymers were synthesized *via* step-growth polycondensation and characterized regarding their ionic aggregate morphologies. Different counterions for the ionic blocks were introduced and investigated as well as different hydrophobic block chain lengths to define adaption of the DG morphology.

For the synthesis of precisely sulfonated polyesters containing short polyethylene segments as hydrophobic blocks, a previously used step-growth polymerization approach was further developed to facilitate the polycondensation and to reach higher degrees of polymerization. So far, the synthesis was limited to semicrystalline polyestersulfonates, which are insoluble in water and precipitate upon the cation exchange. This process was modified to enable the introduction of different cations in polyestersulfonates containing amorphous backbones. Since the DG morphology in the previously studied materials containing linear backbones only appears at temperatures above the melting temperature of the polyethylene segments, the suppression of crystallinity was aimed for. For this purpose, the linear diols employed for polycondensations were partially substituted by long-chain aliphatic diols bearing side chains. Specifically, the dimer fatty acid derived from oleic acid (Pripol) with alcohol groups was studied. The synthesis was achieved in a straight-forward fashion, similar to the previously produced linear polyestersulfonates. The ion exchange to sodium and lithium was performed successively and the ionic aggregate morphologies were investigated in collaboration with the Winey group at the university of Pennsylvania. The collected X-ray scattering profiles show that the crystallization of the polyethylene segments is indeed suppressed upon incorporation of 20 % Pripol in PES12 and PES18Na. However, the PES12Na-Pripol shows undefined layered aggregates and the PES18Na-Pripol shows well-ordered hexagonal aggregates.

In summary, a synthetic approach to access different polyestersulfonates with varying chain lengths and crystallinities was elaborated and the resulting materials provided further insights into structure-property relationships. This approach provides a deeper understanding of the aggregate morphology in precise multiblock copolymers bearing functional groups. From the

insights obtained, criteria to design future materials exhibiting the double gyroid morphology can be established.

4.4 Experimental Section

PES*x*Na and PES*x*Li multiblock copolymer electrolytes were synthesized by step-growth polymerization of tetra-*n*-butylammonium dimethyl sulfosuccinate (NBu_4DSS) and diols with *x* methylene units.

4.4.1 Synthesis of PES*x*NBu4, PES*x*Na and PES*x*Li

Synthesis of PES10Na and PES12Na

A 100 mL two-necked Schlenk tube was charged with the starting materials of NBu_4DS (4.623 g, 9.88 mmol, 1.0 eq.) and 1,10-decanediol (1.722 g, 9.88 mmol, 1.0 eq.) or 1,12-dodecanediol (2.000 g, 9.88 mmol, 1.0 eq.), respectively, and an elliptical PTFE coated stir bar with a lanthanide magnetic core. The Schlenk tube was equipped with a distillation bridge with one collecting flask and connected to a membrane pump. The reaction mixture was heated to 100 °C until a homogeneous melt was obtained. The catalyst [$Ti(O^nBu)_4$] was added as a solution in dry toluene (0.01 M, 0.5 mL, 0.05 mol-%). The reaction mixture was heated to 120 °C and the pressure was slowly reduced to 100 mbar over 5 h. The pressure was then reduced to oil pump vacuum (10^{-2} mbar) and the temperature was increased to 160 °C and held for 16 h. To obtain the sodium salt, brine (100 mL) and deionized water (20 mL) were added and the flask was ultrasonicated for 10 minutes until the polymer was dissolved. The solution was dialyzed for three days (5 L deionized water bath, water exchange 3x/day). The solvent was removed by lyophilization and NMR analysis ensured the absence of tetra-*n*-butylammonium counterions. In the case of remaining tetra-*n*-butylammonium, the process was repeated. The polymers were obtained in 80 % yield.

Assignment of ^{1}H NMR signals according to Figure 4.10 (PES10NBu4) and Figure 4.12 (PES12NBu4), *cf.* Appendix (section 4.6).

PES10NBu4 ^{1}H NMR (400 MHz, dmso-d_6, 300 K): δ [ppm] = 3.96 (m, 4H, H-3 and H-3'), 3.63 (vd, $^3J_{HH}$ = 11.2 Hz, 1H, H-2), 3.57 (s, 0.07H, *end group* H-7 or H-7'), 3.56 (s, 0.07H, *end group* H-7 or H-7'), 3.23 – 3.13 (m, 8H, H-8), 2.96 – 2.71 (m, 2H, H-1), 1.68 – 1.45 (m, 12H, H-4, H-4' and H-9), 1.39 – 1.19 (m, 20H, H-5 and H-10), 0.94 (t, $^3J_{HH}$ = 7.3 Hz, 12H, H-11).

PES12NBu4 ^{1}H NMR (400 MHz, dmso-d_6, 300 K): δ [ppm] = 3.96 (t, $^3J_{HH}$ = 6.5 Hz, 4H, H-3 and H-3'), 3.63 (vd, $^3J_{HH}$ = 11.4 Hz, 1H, H-2), 3.57 (s, 0.08H, *end group* H-7 or H-7'), 3.56 (s, 0.08H, *end*

group H-7 or H-7'), 3.24 – 3.12 (m, 8 H, H-8), 2.97 – 2.71 (m, 2H, H-1), 1.67 – 1.46 (m, 12H, H-4, H-4' and H-9), 1.41 – 1.16 (m, 24H, H-5 and H-10), 0.94 (t, $^{3}J_{HH}$ = 7.3 Hz, 12H, H-11).

Synthesis of PES12Li

The polymer PES12NBu4 (2 g) was dissolved in an aqueous LiCl solution (2 M, 50 mL) and methanol (50 mL). The solution was dialyzed for 3 days (5 L of deionized water bath, exchange of water 3×/day). The solvent was removed by lyophilization, and ^{1}H NMR spectra showed the absence of tetra-*n*-butylammonium counterions. The process was repeated until no tetra-*n*-butylammonium remained. PES12Li was obtained in 80% yield (0.98 g).

Assignment of ^{1}H NMR signals according to Figure 4.13, *cf.* Appendix (section 4.6).

PES12Li ^{1}H NMR (400 MHz, dmso-d_6, 300 K): δ[ppm] = 3.95 (m, 4H, H-3 and H-3'), 3.61 (vd, $^{3}J_{HH}$ = 11.3 Hz, 1H, H-2), 3.57 (s, 0.11H, *end group* H-7 and H-7'), 2.96 – 2.71 (m, 2H, H-1), 1.56 – 1.45 (m, 4H, H-4, H-4'), 1.39 – 1.19 (m, 16H, H-5).

Synthesis of PES18Na

For the synthesis of PES18Na, the published procedure by Rank *et al.* was followed.[47] A 100 mL two-necked Schlenk tube was charged with the starting materials NBu_4DSS (3.50 g, 7.5 mmol, 1.0 eq.) and 1,18-octadecanediol (2.15 g, 7.5 mmol, 1.0 eq.) and a mechanical stirrer with a helical agitator was placed into the tube. The mixture was degassed and flushed with nitrogen three times and heated to 130 °C to obtain a homogeneous melt. The catalyst [$Ti(O^{n}Bu)_4$] was added as a 0.01 M solution in toluene (375 µL, 3.75 µmol, 0.05 mol-%) *via* syringe to the stirred solution. The reaction mixture was heated slowly to 160 °C within 4 hours. Vacuum was applied and the reaction mixture was stirred for 20 h. The viscous melt was cooled to room temperature and an NMR sample was taken. To obtain the sodium salt of the polymer, brine (100 mL) and deionized water (20 mL) were added to 1.9 g of the polymer. Upon heating to 60 °C, the polymer started to precipitate from the aqueous solution as a white solid. The precipitate was filtered off and washed with deionized water. It was dried in a vacuum drying oven at 3 mbar for 3 days. The polymer PES18Na was obtained in 84 % yield (1.08 g).

Assignment of ^{1}H NMR signals according to Figure 4.15, *cf.* Appendix (section 4.6).

PES18NBu4 ^{1}H NMR (400 MHz, dmso-d_6, 383 K): δ[ppm] = 3.94 (t, $^{3}J_{HH}$ = 6.6 Hz, 4H, H-3 and H-3'), 3.61 (vd, $^{3}J_{HH}$ = 11.5 Hz, 1H, H-2), 3.56 (s, 0.03H, *end group* H-7 or H-7'), 3.55 (s, 0.1H, *end group* H-7 or H-7'), 3.36 (dt, $^{3}J_{HH}$ = 6.6 Hz, 5.1 Hz, 0.2H, *end group* H-6), 3.24 – 3.09 (m, 8H, H-8),

2.94 – 2.71 (m, 2H, H-1), 1.65 – 1.44 (m, 12H, H-4, H-4' and H-9), 1.42 – 1.14 (m, 36H, H-10 and H-5), 0.93 (t, $^{3}J_{HH}$ = 7.3 Hz, 12H, H-11).

Synthesis of PES18Li

The polymer PES18NBu4 (3.1 g) was dissolved in an aqueous LiCl solution (2 M, 100 mL). The polymer started to precipitate as a white solid upon vigorous stirring. The precipitate was filtered off and washed with deionized water until no precipitate formed from the filtrate upon addition of $AgNO_3$ in water (0.01 M). The polymer was washed with acetone to facilitate the drying process. The polymer was dried in a vacuum drying oven at 3 mbar for 3 days, and was obtained in 65% yield (1.36 g).

Assignment of ^{1}H NMR signals according to Figure 4.16, *cf.* Appendix (section 4.6).

PES18Li ^{1}H NMR (400 MHz, dmso-d_6, 300 K): δ[ppm] = 3.99 (t, 4H, H-3 and H-3'), 3.68z (vd, $^{3}J_{HH}$ = 10.7 Hz, 1H, H-2), 3.58 (s, 0.07H, *end group* H-7 and H-7'), 3.42 (dt, $^{3}J_{HH}$ = 6.2 Hz, 6.2 Hz, 0.21H, *end group* H-6), 2.96 – 2.80 (m, 2H, H-1), 1.59 – 1.54 (m, 4H, H-4 and H-4'), 1.39 – 1.19 (m, 28H, H-5).

4.4.2 Synthesis of unsaturated PES18Na

Synthesis of uPES18Na

9-Octadecenediol was synthesized in a 3-step procedure starting from oleic acid.

A self-metathesis with the Grubbs 2nd generation catalyst yielded 9-octadecenedioic acid, which was subsequently esterified with methanol.[30]

A reduction of 9-octadecenedimethyl dioate (15 g, 1.0 eq.) with lithium aluminum hydride (4.0 eq.) in THF and subsequent Soxhlet extraction yielded the desired 9-octadecenediol.[41]

For the step-growth polymerization of NBu4DSS and 9-octadecene diol, both monomers were placed into a 25 mL Schlenk tube equipped with an elliptical poly(tetrafluoroethylene) (PTFE)-coated stir bar and a distillation bridge with a collecting flask. The reaction mixture was heated to 140 °C, and the catalyst [Ti(O^{n}Bu)$_4$] was added as a 0.01 M solution in toluene (1 mol-%). A membrane pump was attached and the pressure was reduced to 800 mbar. After 2 hours, the pressure was slowly reduced to 25 mbar over 6 hours. Subsequently, an oil pump was attached and the pressure was further reduced to 10^{-2} mbar and held for 48 hours. The polymer was cooled to room temperature and dispersed in brine (4 mL). The dispersion was dialyzed for

5 days (5 L deionized water, exchanged 2x/day). The solvent was removed by lyophilization. The complete removal of tetra-*n*-butylammonium counterions was monitored by ^{1}H NMR spectroscopy in dmso-d_6, and the absence of NaCl was confirmed by X-ray scattering.

Assignment of ^{1}H NMR signals according to Figure 4.18 (uPES18NBu4) and Figure 4.19 (uPES18Na), *cf.* Appendix (section 4.6).

uPES18NBu4 ^{1}H NMR (400 MHz, 300 K, dmso-d_6): δ [ppm] = 5.36 (m, 2H, H-7), 3.95 (t, $^{3}J_{HH}$ = 6.7 Hz, 4H, H-3 and H-3'), 3.60 (vd, $^{3}J_{HH}$ = 11.4 Hz, 1H, H-2), 3.56 (s, 0.03H, *end group* H-9 or H-9'), 3.55 (s, 0.08 H, *end group* H-9 or H-9'), 3.36 (dt, $^{3}J_{HH}$ = 6.6 Hz, 5.1 Hz, 0.14H, *end group* H-8), 3.17 (m, 8H, H-10), 2.83 (m, 2H, H-1), 1.93 (m, 4H, H-6), 1.62 – 1.46 (m, 12H, H-4, H-4' and H-11), 1.37 – 1.18 (m, 28H, H-5 and H-12), 0.93 (t, 12H, H-13).

uPES18Na ^{1}H NMR (400 MHz, 300 K, dmso-d_6): δ [ppm] = 5.36 (m, 2H, H-7), 3.95 (t, $^{3}J_{HH}$ = 6.7 Hz, 4H, H-3 and H-3'), 3.60 (vd, $^{3}J_{HH}$ = 11.4 Hz, 1H, H-2), 3.55 (s, 0.13H, *end group* H-9 and H-9'), 3.36 (m, 0.13H, *end group* H-8), 2.83 (m, 2H, H-1), 1.93 (m, 4H, H-6), 1.51 (m, 4H, H-4 and H-4'), 1.34 – 1.18 (m, 20H, H-5).

4.4.3 Synthesis of Pripol containing PES*x*NBu4, PES*x*Na and PES*x*Li

<u>Synthesis of PES12Na-Pripol</u>

A 100 mL two-necked Schlenk tube was charged with the starting materials, NBu_4DSS (4.000 g, 8.552 mmol, 1.0 eq.), 1,12-octadecanediol (1.500 g, 5.236 mmol, 0.8 eq.), Pripol 2033 (710 mg, 1.309 mmol, 0.2 eq.) and the catalyst [Ti(O^{n}Bu)$_4$] (8 mg, 33 µmol, 0.5 mol%). The tube was equipped with an elliptical PTFE coated stir bar with a lanthanide magnetic core. The Schlenk tube was equipped with a distillation bridge with one collecting flask and connected to a membrane pump. The reaction mixture was set under nitrogen atmosphere and heated to 180 °C. After two hours, the pressure was gradually reduced to 50 mbar over 2 hours and held at 50 mbar for 30 min. The temperature was reduced to 160 °C and oil pump vacuum (10^{-2} mbar) was applied. These reaction conditions were held for 3 days.

For PES12Na-Pripol, the polymer was dissolved in methanol and a 2 M aqueous solution of NaCl (10 mL) was added, upon which the solution turned turbid. The mixture was dialyzed for 3 days (5 L deionized water, exchanged 2x/day) and the solvent was removed by lyophilization. This process only yielded 96% conversion to sodium, and it was repeated by dissolving the

polymer in brine and subsequent dialysis. ^{1}H NMR spectroscopy showed a full cation exchange exchange and a DP_n of 25.

Assignment of ^{1}H NMR signals according to Figure 4.20, *cf.* Appendix (section 4.6).

PES12Na-Pripol ^{1}H NMR (400 MHz, 383 K, dmso-d_6): 4.09 – 3.91 (m, 4H, H-3 and H-3'), 3.73 (vd, $^{3}J_{HH}$ = 10.9 Hz, 1H, H-2), 3.60 & 3.59 (s, 0.03H, *end group* H-8 and H-8'), 3.42 (t, $^{3}J_{HH}$ = 10.9 Hz, 6.50 Hz, 0.24H, *end group* H-7), 3.00 – 2.79 (m, 2H, H-1), 1. 63 – 1.50 (m, 4H, H-4 and H-4'), 1.49 – 1.17 (m, 32H, H-5), 0.93 – 0.81 (m, 1.38 H, H-6).

Synthesis of PES18NBu4-Pripol, PES18Na-Pripol and PES18Li-Pripol

A 100 mL two-necked Schlenk tube was charged with the starting materials of NBu_4DSS (3.061 g, 6.545 mmol, 1.0 eq.), 1,18-octadecanediol (1.500 g, 5.236 mmol, 0.8 eq.), Pripol 2033 (710 mg, 1.309 mmol, 0.2 eq.) and the catalyst DBTO (8 mg, 33 µmol, 0.5 mol%). The tube was equipped with an elliptical PTFE coated stir bar with a lanthanide magnetic core. The Schlenk tube was equipped with a distillation bridge with one collecting flask and connected to a membrane pump. The reaction mixture was set under nitrogen atmosphere and heated to 180 °C. After two hours, the pressure was gradually reduced to 50 mbar within two hours and held at 50 mbar for 30 min. The temperature was reduced to 160 °C and oil pump vacuum (10^{-2} mbar) was applied. These reaction conditions were held for 3 days.

For PES18Na-Pripol, 1.091 g of the polymer was used to exchange the cations. The polymer was dissolved in methanol and precipitated in a 2 M aqueous solution from NaCl (35 mL). The polymer was filtered off and washed with water until the filtrate was free from chloride (tested by addition of silver nitrate). ^{1}H NMR spectroscopy showed a cation exchange of 97%. The polymer was dispersed in an aqueous solution of NaCl (2 M), filtered off and washed with water. After drying, the polymer was obtained as a white powder in 54 % yield (429 mg).

For PES18Li-Pripol, 4.188 g of the polymer was dissolved in methanol and precipitated in a 2M aqueous solution of LiCl (35 mL). The suspension was centrifuged and the polymer was washed with water (2 x 10 mL). Due to the gel-like nature of the polymer, it was diluted with water and dialyzed (2 days, 5 L distilled water, exchanged 3x/day). ^{1}H NMR spectroscopy showed a cation exchange of 86%. The polymer was dispersed in aqueous LiCl solution (2 M), dialyzed and lyophilized again. It was obtained as a white solid as the pure sodium salt without remaining tetra-*n*-butylammonium.

Assignment of ^{1}H NMR signals according to Figure 4.22, *cf.* Appendix (section 4.6).

PES18Na-Pripol ^{1}H NMR (400 MHz, 383 K, dmso-d_6): 4.09 – 3.87 (m, 4H, H-3 and H-3'), 3.69 (vd, $^3J_{HH}$ = 10.9 Hz, 1H, H-2), 3.58 (s, 0.03H, *end group* H-8 or H-8'), 3.57 (s, 0.03H, *end group* H-8 or H-8'), 3.40 (t, 0.16H, *end group* H-7), 2.98 – 2.77 (m, 2H, H-1), 1. 61 – 1.48 (m, 4H, H-4 and H-4'), 1.45 – 1.14 (m, 32H, H-5), 0.91 – 0.78 (m, 1.38 H, H-6).

PES18Li-Pripol ^{1}H NMR (400 MHz, dmso-d_6, 383 K): δ [ppm] = 4.20 – 3.90 (m, 4H, H-3 and H-3'), 3.69 (vd, $^3J_{HH}$ = 10.9 Hz, 1H, H-2), 3.59 (s, 0.03H, *end group* H-8 or H-8'), 3.58 (s, 0.06H, *end group* H-8 or H-8'), 3.41 (t, 0.25H, *end group* H-7), 3.24 – 3.17 (m, 0.20H, *residual* $N(C\mathbf{H_2}(CH_2)_2CH_3)_4^+$), 2.99 – 2.78 (m, 2H, H-1), 1.62 – 1.49 (m, 4H, H-4 and H-4'), 1.47 – 1.05 (m, 35H, H-5), 0.91 – 0.80 (m, 1.45H, H-6).

4.5 Materials and Methods

All reactions described were performed under an inert gas atmosphere using standard glovebox and Schlenk techniques.

Sodium dimethyl sulfosuccinate was synthesized according to the procedure published by Srilakshmi et al.[126] 1,18-Octadecanediol was synthesized from 1,18-dimethyl octadecanedioate by reduction with lithium aluminum hydride according to a reported procedure.[39] 1,12-dodecanediol and 1,10-decanediol were purchased from Merck in ≥98% purity. NaCl was supplied by Carl Roth, LiCl was supplied by Merck. Pripol 2033 was obtained from CRODA. Dialysis tubes by SpectraPor were supplied by Carl Roth and used for purification of the polymers (3.5 kDa pore size, 54 mm broadness; for polymers containing Pripol: 1.0 kDa pore size, 38 mm broadness). To obtain the PES*x*Li materials, the corresponding PES*x*NBu4 polymers with tetra-*n*-butylammonium counterions (NBu4) were synthesized according to a previously reported procedure.[51]

The characterization of the soluble intermediate products by NMR spectroscopy was performed in dimethylsulfoxide-d_6 as solvent at 110 °C. A Bruker Avance III HD 400 spectrometer with a TBO probe with Z-gradient was used. 1H chemical shifts were referenced to the solvent signal (residual proton signal). Multiplicities are reported as follows: s (singlet), d (doublet), t (triplet), m (multiplet), v (virtual), and combinations thereof. MestreNova software by Mestrelab Research S.L. was used for the evaluation of NMR data. Deuterated solvents used for NMR spectroscopy were supplied by Eurisotop.

For differential scanning calorimetry conducted in-house, a Netsch DSC 204 F1 with a heating rate of 10 K/min was used. All data reported are from the second heating cycles, unless stated otherwise. Data were evaluated using NETZSCH Proteus Thermal Analysis software (version 6.1.0).

4.5.1 Calculation of the DP_n

The degree of polymerization (DP_n) and the number weighted molecular weight (M_n) of the PES*x*NBu_4 materials were determined by integration of the signals in the ^{1}H NMR, as reported before.[51] As shown before, the DP_n does not change during the cation exchange of the polymers.[51] Exemplary, the ^{1}H NMR spectrum of PES12Na is shown in Figure S4. The signal of the backbone of the oligoethylene segment (*B*, triplet at 3.96 ppm) was integrated and referenced to

100H. The end group signals for the methyl ester (E_1, 3H, singlets at 3.55 and 3.56 ppm) and for the hydroxymethyl group (E_2, 2H, doublet of triplet at 3.36 ppm) were integrated and the DP_n was calculated according to

$$DP_n = \frac{\int B}{\frac{\int E_1}{3} + \frac{\int E_2}{2}} + 1 = \frac{100}{\frac{\int E_1}{3} + \frac{\int E_2}{2}} + 1$$

and is defined as the number-average amounts of monomers in a polymer chain.

The number weighted molecular weights (M_n) were calculated with the DP_n and the molecular weight of the repeating unit (M_{rep}) according to

$$M_n = M_{rep} \times \frac{DP_n}{2}$$

4.5.2 Methods performed at the University of Pennsylvania

by Dr. Jinseok Park and Benjamin Ferko in the group of Prof. Dr. K. I. Winey

X-ray scattering experiments were performed at the Dual Source and Environmental X-ray Scattering (DEXS) facility at the Laboratory for Research on the Structure of Matter, University of Pennsylvania. The DEXS facility is equipped with a Xeuss 2.0 from Xenocs, which includes a PILATUS 1M detector for small-angle scattering, a PILATUS 100K detector for wide-angle scattering, and a GeniX3D beam source (8 keV, Cu Kα, λ = 1.54 Å). The sample-to-detector distance of ~370 and ~158 mm is used for the small- and wide-angle detectors, respectively. Powder samples kept in a vacuum desiccator were sealed in 1.0 mm diameter glass capillaries before measurements. The two-dimensional scattering data were collected isothermally every 10 °C for 10 min, after 15 min equilibration. The heating and cooling rates were 10 °C/min. The scattering data was isotropic and integrated into $I(q)$ plots. Small- and wide-angle $I(q)$ plots were arbitrarily shifted to display the scattering data at 0.1 $Å^{-1} < q < 1.8$ $Å^{-1}$.

Differential scanning calorimetry (DSC) experiments were performed using a TA Instruments DSC2500 for all polymers. The powder polymer samples were kept in a vacuum desiccator and dried at 50 °C under vacuum overnight prior to performing DSC measurements. Due to the slow crystallization kinetics, the samples were measured at a 1 K/min ramping rate under a nitrogen atmosphere. The measured temperature range varies due to the degradation temperatures, which were in the range of ~ 180 to 210 °C with increasing polyethylene block lengths.

For electrochemical impedance spectroscopy (EIS), a Solartron Analytical Modulab XM MTS spectrometer with a Janis VPF-100 cryostat was used to measure the electrochemical impedance of samples at frequencies of 0.1–1 MHz and an amplitude of 100 mV. Hot-pressed polymer films (1 cm diameter) were sandwiched between two electrodes and equilibrated at ~170 °C under vacuum in the cryostat. Isothermal frequency-sweep measurements were performed while cooling, every 2 °C with 5 min equilibration. The bulk resistance (R) at each temperature was obtained from the Nyquist plot, and DC ionic conductivity (σ) was calculated from the polymer thickness (h) and area (A), $\sigma = \frac{h}{A \times R}$.

4.6 Appendix

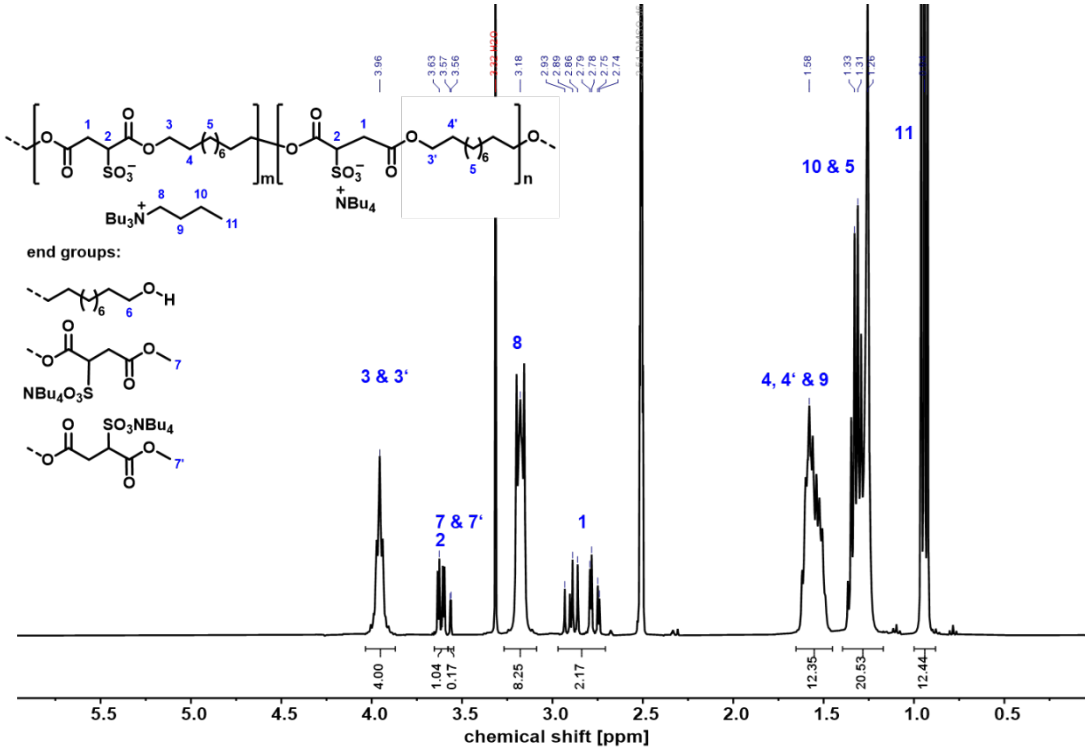

Figure 4.10 ^{1}H NMR (400 MHz, dmso-d_6, 300 K) spectrum of PES10NBu4. Note that protons **1** are diastereotopic. The degree of polymerization is defined as $DP_n / 2 = m + n$.

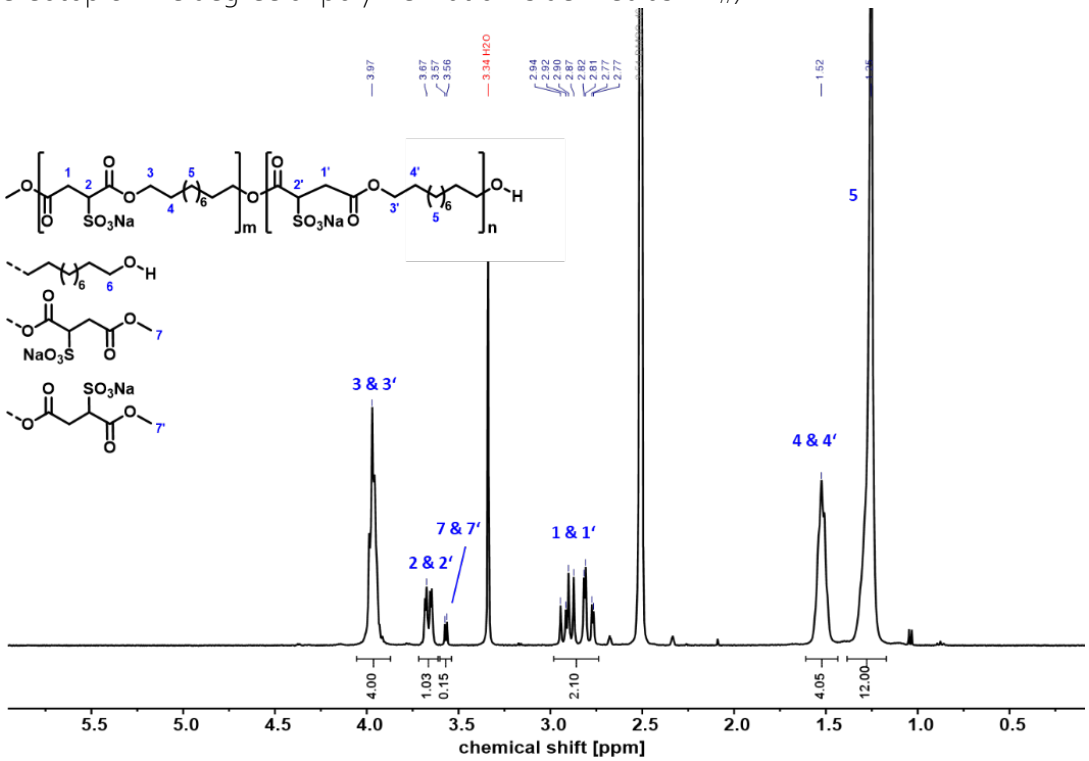

Figure 4.11 ^{1}H NMR (400 MHz, dmso-d_6, 300 K) spectrum of PES10Na. Note that protons **1** are diastereotopic, and that end-group **6** is not detected.

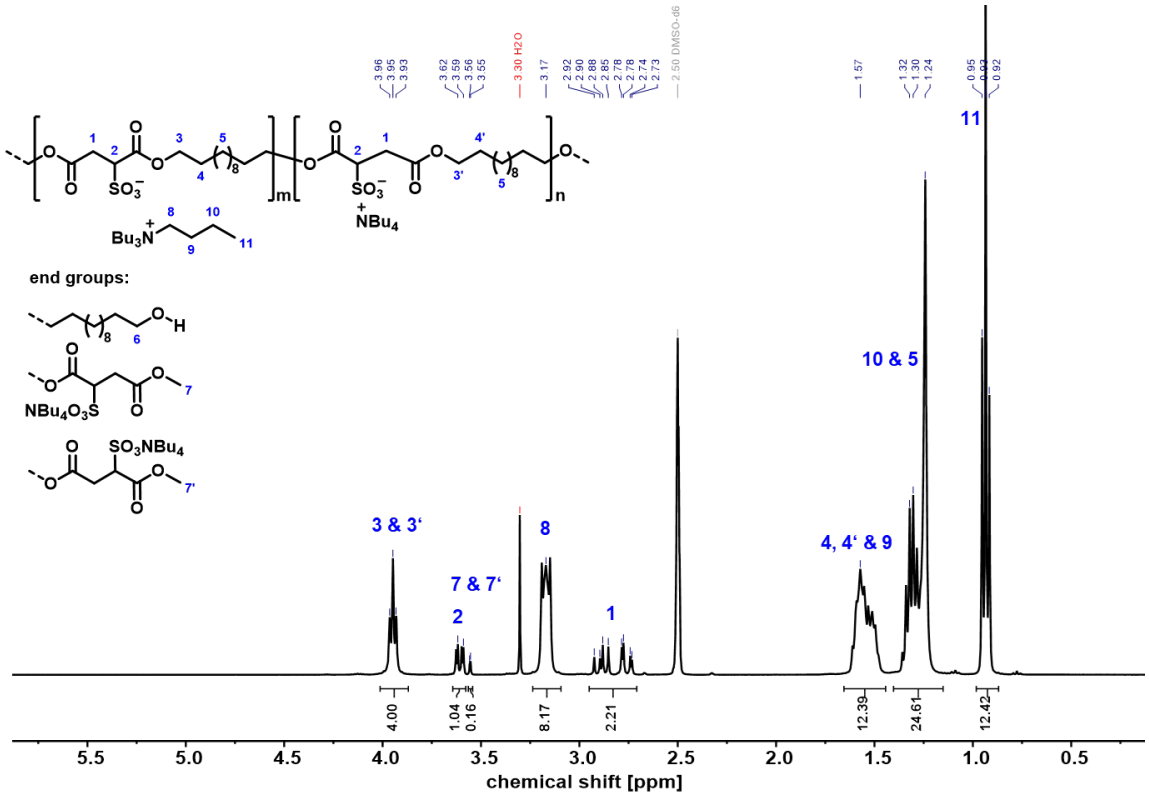

Figure 4.12 ^{1}H NMR (400 MHz, dmso-d_6, 300 K) spectrum of PES12NBu4. Note that protons **1** are diastereotopic, and that end-group 6 is not detected.

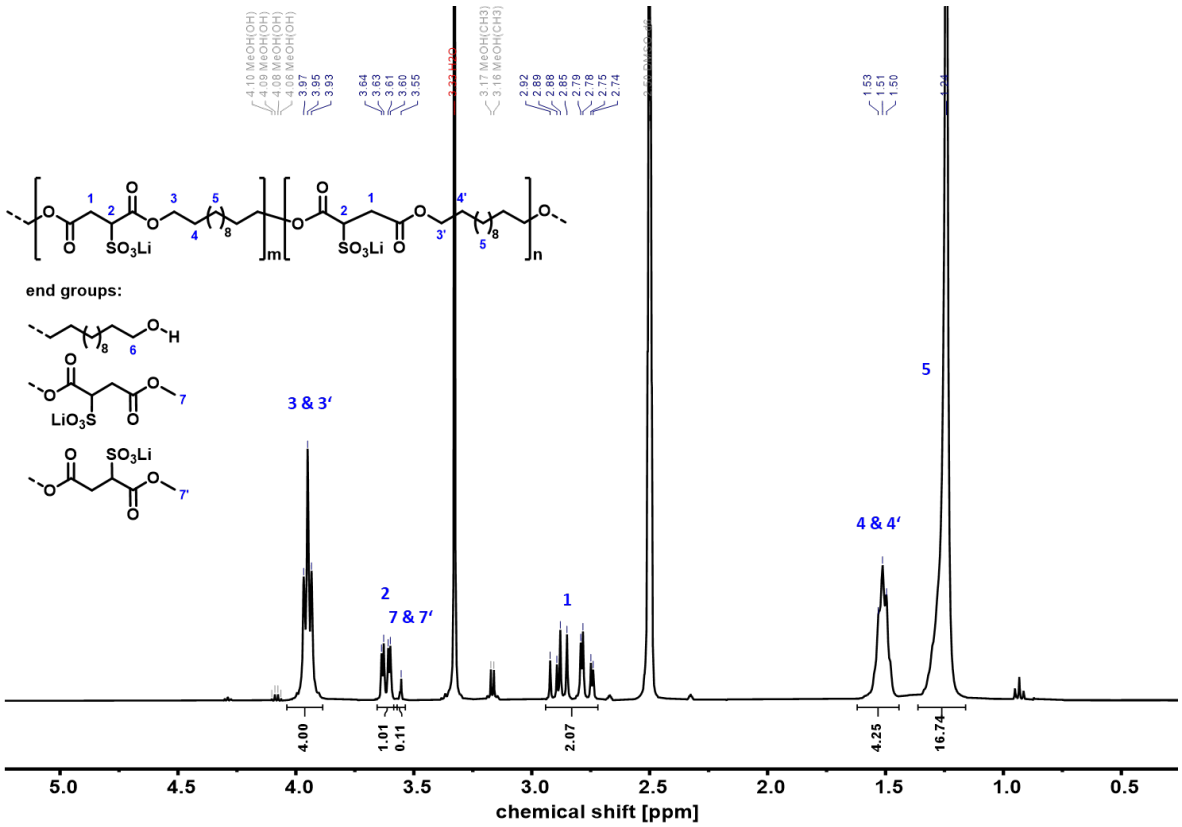

Figure 4.13 ^{1}H NMR spectrum of PES12Li. Note that protons **1** are diastereotopic.

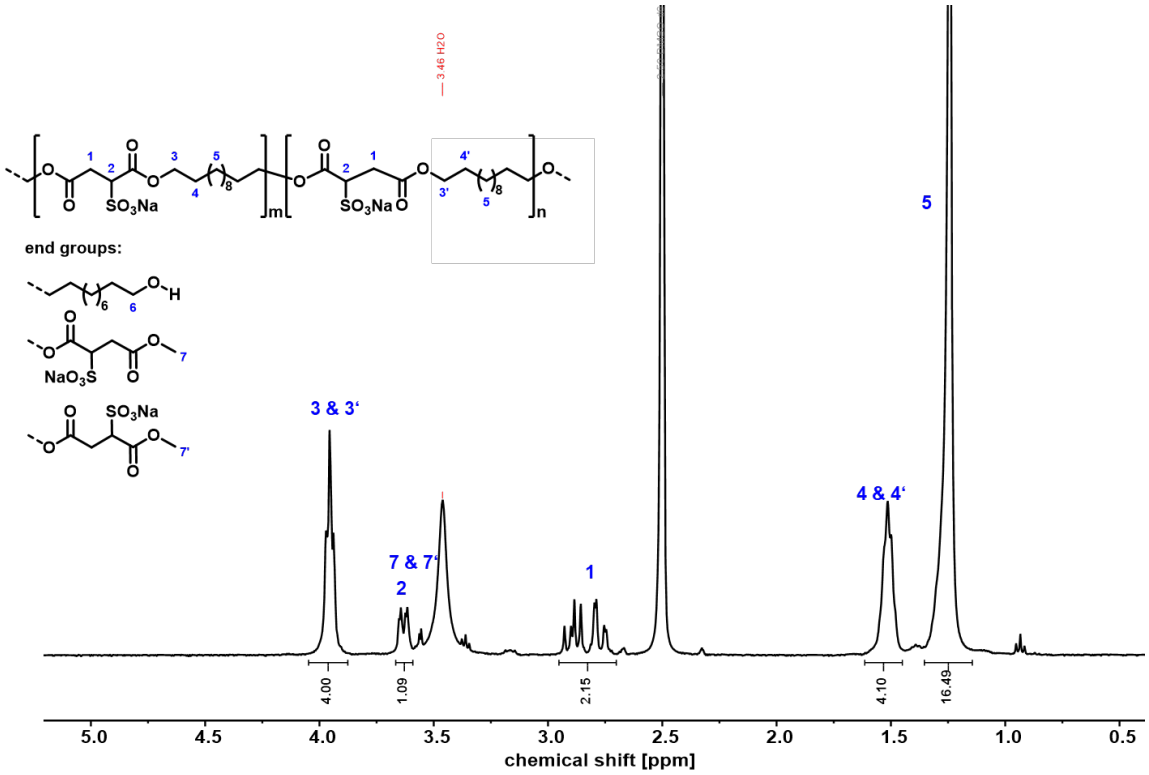

Figure 4.14 ^{1}H NMR spectrum of PES12Na (400 MHz, dmso-d_6, 300 K). The broad signal at 3.46 ppm corresponds to residual water in the dmso-d_6 solvent. Note that protons **1** are diastereotopic.

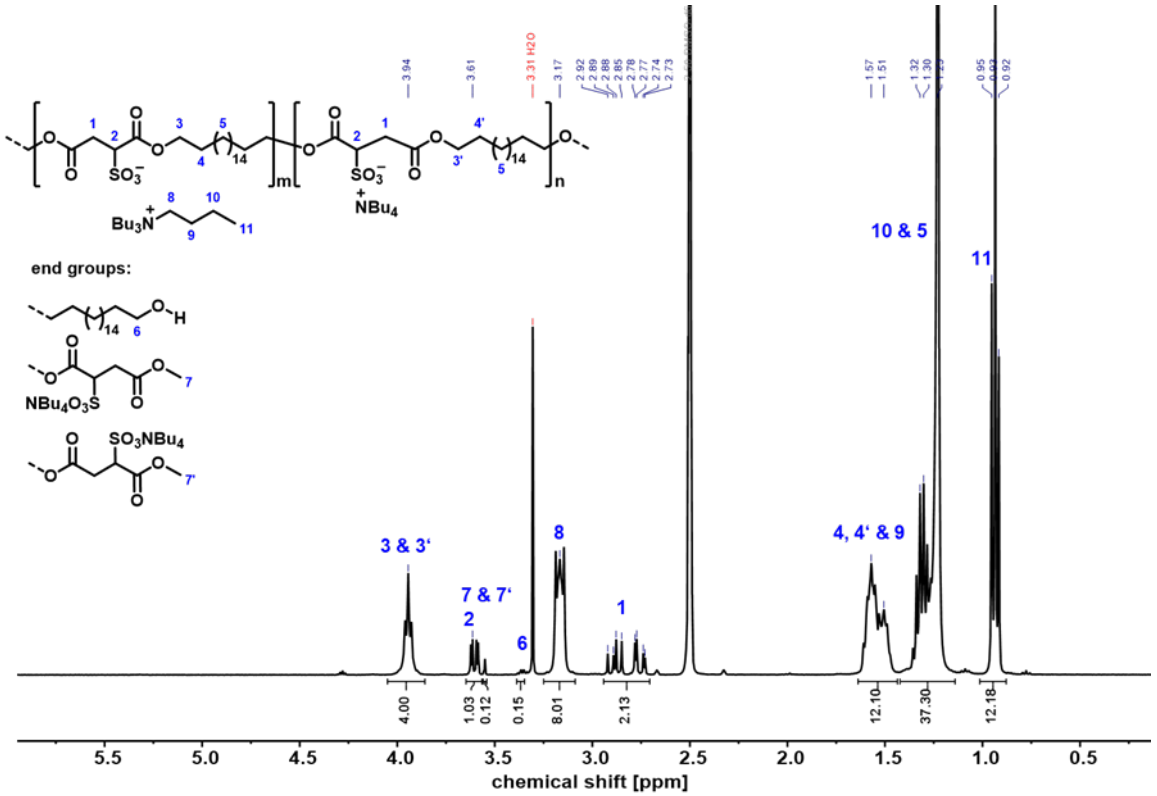

Figure 4.15 ^{1}H NMR (400 MHz, dmso-d_6, 383 K) spectrum of PES18NBu4. Note that protons **1** are diastereotopic.

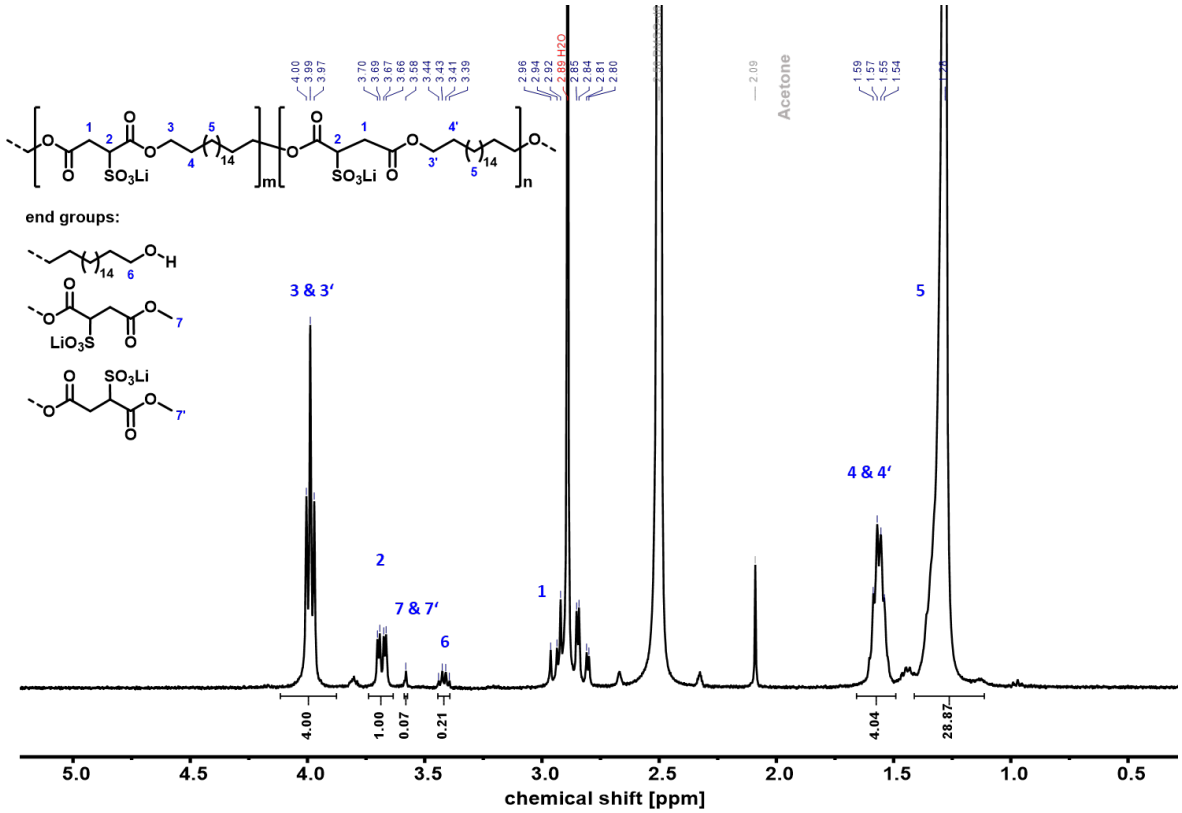

Figure 4.16 ^{1}H NMR (400 MHz, dmso-d_6, 383 K) spectrum of PES18Li. Note that protons **1** are diastereotopic.

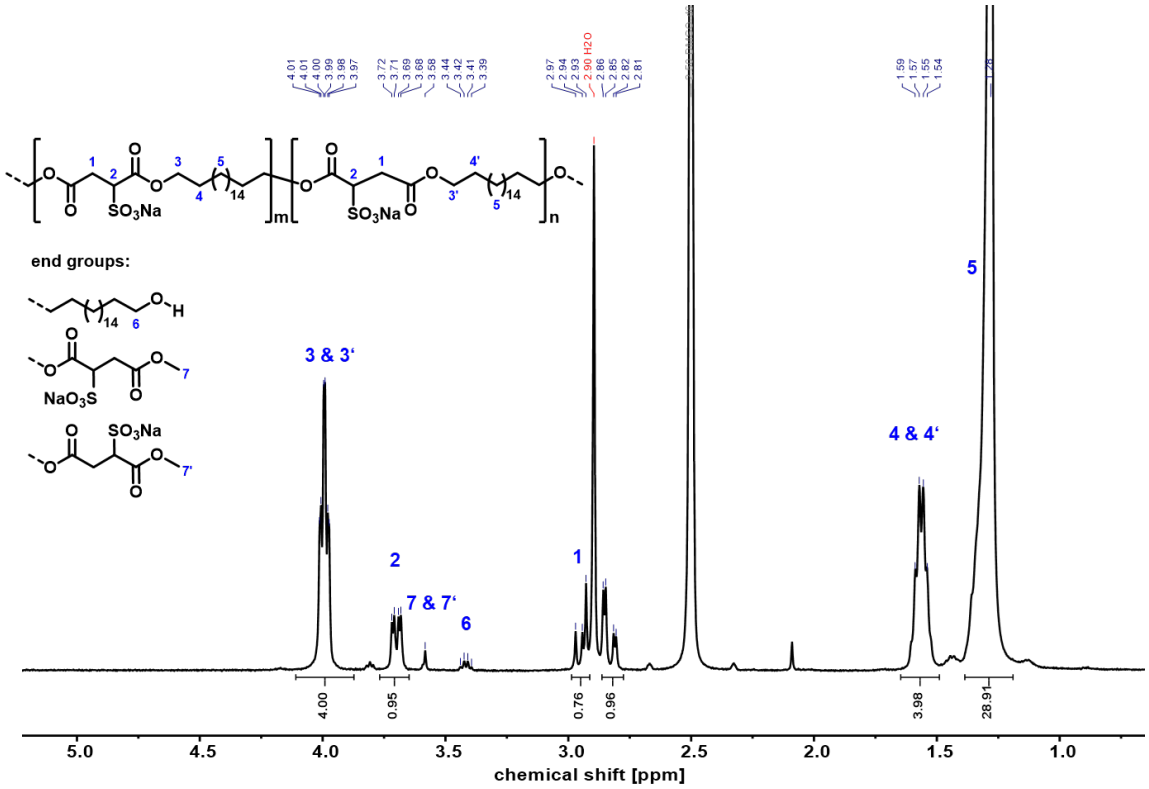

Figure 4.17 ^{1}H NMR (400 MHz, dmso-d_6, 383 K) spectrum of PES18Na. Note that protons **1** are diastereotopic.

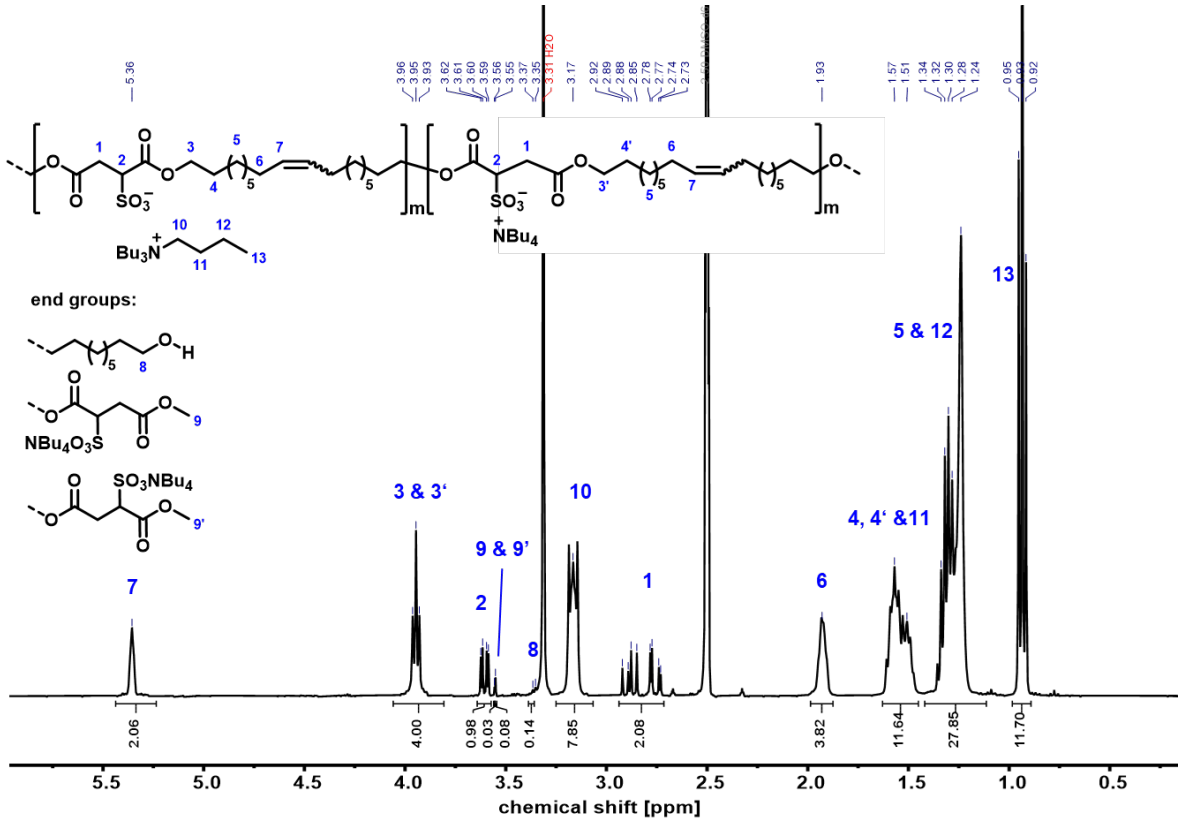

Figure 4.18 ^{1}H NMR (400 MHz, dmso-d_6, 300 K) spectrum of uPES18NBu4. Note that protons **1** are diastereotopic.

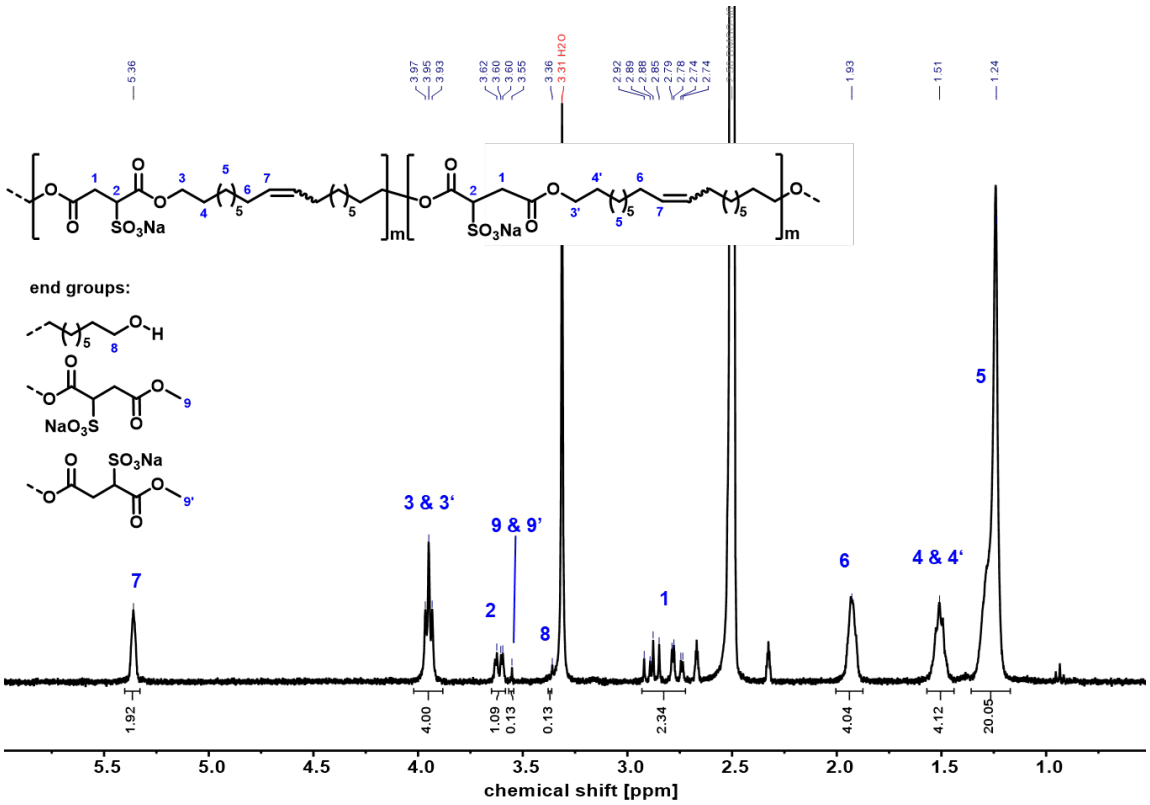

Figure 4.19 ^{1}H NMR (400 MHz, dmso-d_6, 300 K) spectrum of uPES18Na. Note that protons **1** are diastereotopic.

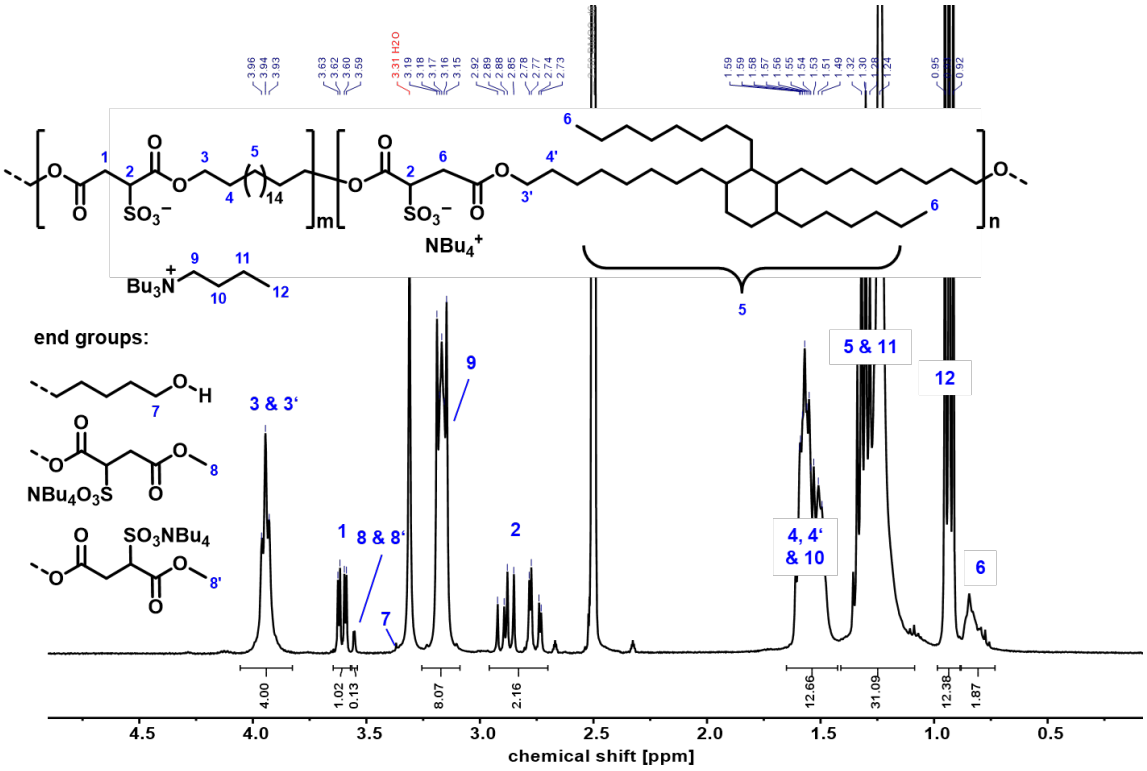

Figure 4.20 ^{1}H NMR spectrum (400 MHz, 300 K, dmso-d_6) of PES12NBu4-Pripol. Note that protons **1** are diastereotopic. End-group **7** is indicated at its theoretical position, however not detected.

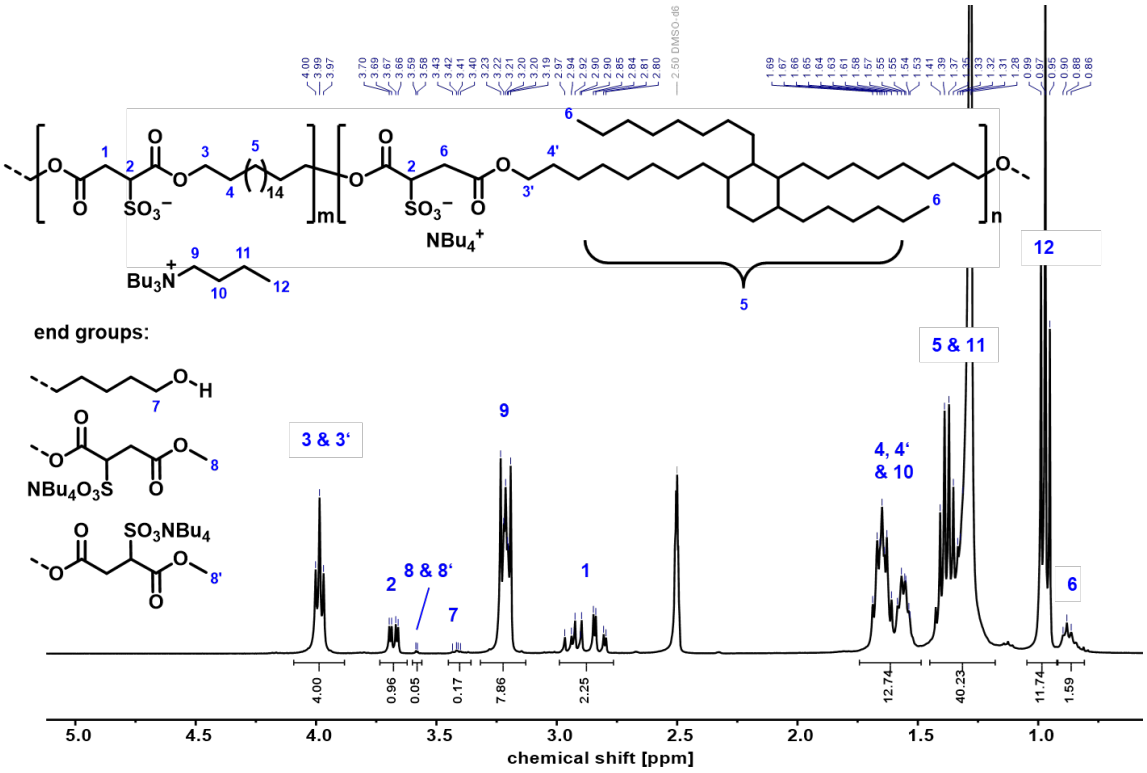

Figure 4.21 ^{1}H NMR spectrum (400 MHz, 300 K, dmso-d_6) of PES18NBu4-Pripol. Note that protons **1** are diastereotopic.

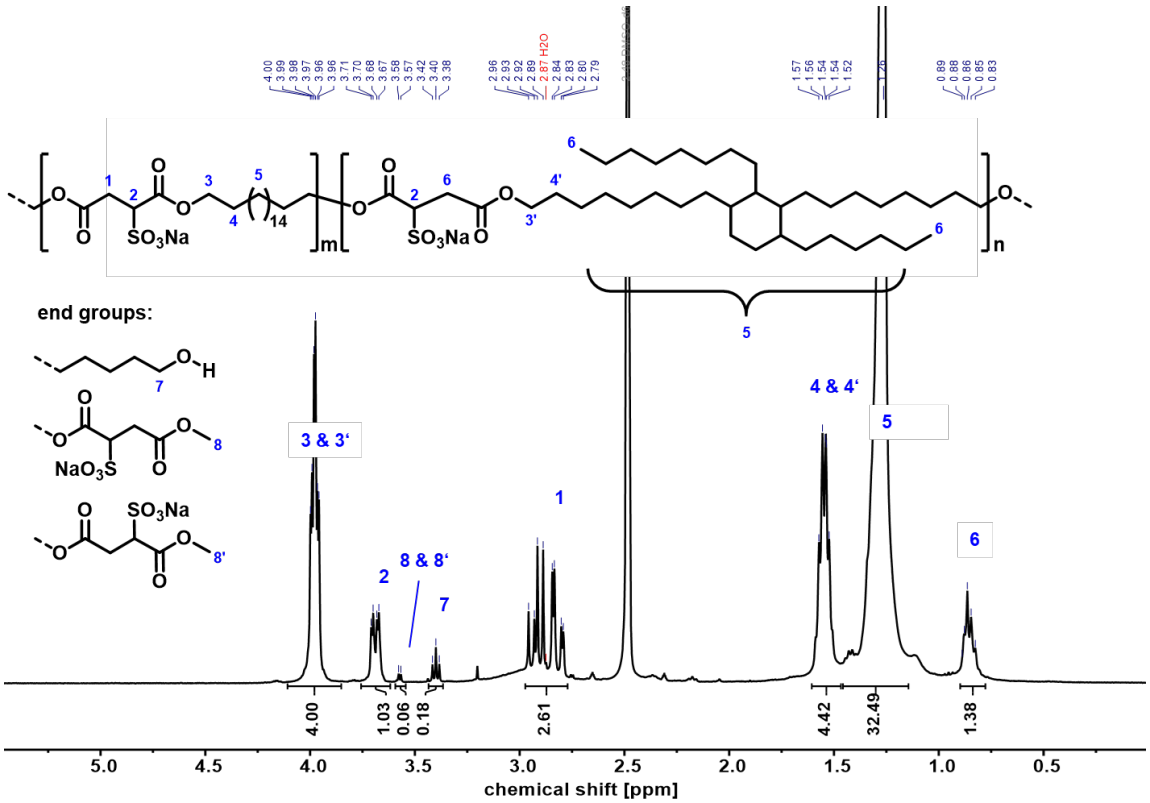

Figure 4.22 ^{1}H NMR spectrum (400 MHz, 383 K, dmso-d_6) of PES18Na-Pripol. Note that protons **1** are diastereotopic.

5 Ionic Substituted Polyethylene-like Materials

5.1 Introduction

Polyethylene (PE) as the polymer with the highest annual production is used for a wide range of applications. Its microstructure formed in its synthesis form ethylene can be varied *via* incorporation of comonomers, reflecting also the material's properties. PE-like polymers bearing ionic groups are accessible by various post-polymerization methods (e.g. sulfonation), which alter the material properties to a great extent due to the newly occurring coulombic interactions between the ionic moieties.[6,127-128] In case of acid-containing PEs, hydrogen-bond networks emerge and introduce intra- and intermolecular interactions complementing the van-der-Waals forces, which are typically decisive for the material properties.[13] The neutralization of the acid groups with different cations leads to ion-containing polymers, which present an important class of materials with physical cross-links that enhance tensile strength or impact the melt viscosity.[6] One major beneficial property gained is the enhanced surface adhesion compared to PE having a low surface free energy.[6] Ionic PEs are accessed by radical copolymerization under high pressure of ethylene and acidic comonomers, leading to random copolymers with poor control over the microstructure.

The amount of ionic groups within the polymer can be varied to a great extent, from very high amounts, which are interesting regarding their proton or ion conductivity as polymer electrolytes, to low amounts of up to 10 mol %, which find applications in orthotics, prosthetics, as coatings of golf balls or as adhesives, to name a few.[2,129-130] One industrially relevant example is Surlyn, a copolymer of ethylene and methacrylic acid developed by DuPont.[7] Both, the amount of polar comonomer and the percentage of acid group neutralization allows for a fine-tuning of the polymer properties.

There is an increasing need for sustainable materials derived from renewable feedstocks and for these materials to be (bio)degradable. An important factor to add to this is the recyclability of synthetic polymers, which is defined by both the ability to perform mechanical recycling, and the ability to undergo a closed-loop recycling, in particular to deconstruct and fully recover the monomers.[131] Degradable ion-containing polymers reported to date are restricted to short-chain polyesters, mainly based on polybutylene succinate (PBS) or polybutylene adipate terephthalate (PBAT).[20,132] Sulfonated PBS polymers were intensely studied by Han et al., and a significantly increased hydrolytic degradation rate was found with increasing ionic content.[20] Wu et al. presented sulfonated PBAT copolyesters and found reduced thermal stability as well as impaired mechanical properties.[25] However, the shown higher hydrophilicity and water dispersibility are valuable properties to tune the biodegradation rate of PBAT. Other degradable ionomers are based on polycarbonates,[133-135] polyurethanes[136-138] or polyphosphoesters.[139] However, the mechanical properties of these materials are either not reported or significantly limit their applications due to low toughness. Even though ionically functionalized PBS and PBAT are degradable, their mechanical properties limit their range of applications: while PBS is a brittle material, PBAT is rather soft and similar to LDPE.[140-141] The large group of poly(ethylene-*co*-methacrylic acid) (PEMA) polymers, including Surlyn, does not exhibit degradability or chemical recyclability. The physical recyclability was shown in zinc neutralized PEMA by Zhan et al.,[142] yet any form of chemical recycling or indication of (bio)degradability is lacking to date.

In this chapter, ion-containing polymers with HDPE-like properties are presented, based on long-chain aliphatic polyesters derived from fatty acids as renewable resources by introducing low amounts (< 0.5 mol% with respect to the total monomer feed) of ionic groups with different cations into PE18.18, a polyester composed of C_{18}-diacid and C_{18}-diol. Thereby, the mechanical and rheological properties of PE18.18 can be tuned and ion-containing polymers with HDPE-like properties are obtained. It was previously shown that PE18.18 with properties on par with HDPE is chemically recyclable in a closed-loop approach.[38] The obtained ion-containing polymers are not only interesting regarding biodegradation due to their in-chain functional groups and their increased hydrophilicity but can also be fully recycled to their valuable monomers.

5.2 Results and Discussion

5.2.1 Incorporation of Low Amounts of Sulfosuccinates in Long-chain Aliphatic Polyesters

Introducing sulfonate groups into polyesters is typically achieved by copolymerization of non-ionic monomers with 5-sulfo-isophthalate. The aim of accessing ion-containing polymers with HDPE-like properties makes such aromatic monomers unfeasible due to the strong interactions of the aromatic units and their negative influence on the chain structure of the aliphatic hydrocarbon segments. Aliphatic monomers with covalently bound sulfonate units have a significantly decreased thermal stability compared to sodium 5-sulfo-isophthalate, which needs to be considered in the synthesis of polyesters at high temperatures and under low pressures as well as in the presence of Lewis acidic catalysts.

To introduce ionic sulfonate groups in long-chain all-aliphatic polyesters, dimethyl sulfosuccinic acid (HMSS) was chosen for incorporation into PE12.12 and PE18.18. Since HMSS is a Brønstedt acid and can function not only as a monomer but also as a catalyst for polycondensation reactions, no additional catalyst was added to the reaction. The synthesis of PE18.18 with incorporated sulfonate units (PE18.18-SO_3H) was achieved starting from C_{18}-diacid and C_{18}-diol monomers as well as dimethyl sulfosuccinic acid (HMSS, see Scheme 5.1), which was used in low amounts (0.5, 0.8 and 1.0 mol% with respect to total diol). As a reference system, PE12.12-SO_3H was synthesized from C_{12}-diacid, C_{12}-diol and sulfosuccinic acid (1.0 mol%).

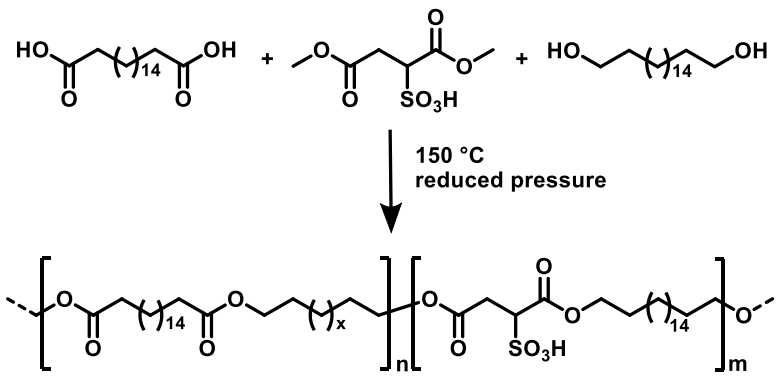

Scheme 5.1 Synthesis of PE18.18-SO_3H from C_{18}-diacid, HMSS and C_{18}-diol.

The polycondensations were performed at 150 °C as opposed to 180 °C typically used for PE18.18, to prevent thermal decomposition reactions. When a high melt viscosity was reached, where no more flow of the melt could be observed (typically after 4 – 6 hours), the reaction was

terminated and the polymer melt was mechanically removed from the flask. A series of PE18.18-SO3H-x (x = 0.5, 0.8 and 1.0 mol%) as well as their reference polymer PE18.18 without ionic groups were synthesized and investigated regarding their thermal, structural and mechanical properties.

The degree of polymerization (DP_n) and number-averaged molecular weight were estimated from ^{1}H NMR spectra, and the amount of sulfosuccinate present in the final polymer was determined (spectra can be found in the appendix, Figure 5.43 - Figure 5.52). The amount of sulfonic acid within the polymer was calculated (*cf.* section 5.5.2) and accounts for ~ 65 % of the input amount that was used in the reaction. This effect is likely to originate from the hygroscopic nature of HMSS: the monomer contains variable amounts of water which leads to a lower amount of HMSS included in the reaction. Notwithstanding, a series of polymers with varying sulfonate content was obtained. The molecular weight was determined *via* end group analysis from ^{1}H NMR spectra (*cf.* appendix, section 5.5.1).* Number average molecular weights from 20 to 25 kg/mol were determined by this method. These are in a similar range and consequently well comparable for all polymers including the parent non-ionic PE18.18, and the molecular weights are above the entanglement molecular weights of PE18.18 (4.2 kg/mol as determined from rheology *via* small amplitude oscillatory shear measurements).[143]

The incorporation of the sulfosuccinic acid in the polyester chains was investigated in closer detail. From ^{1}H NMR spectra, a successful incorporation is indicated by a newly appearing signal at 3.45 ppm corresponding to the α-methylene unit of a diol reacted with a sulfosuccinate unit (H7, see Figure 5.1). End-group analysis shows that carboxylic acid and alcohol end groups are found as in the parent non-ionic polyester, as well as methyl ester end groups placed at the mid- or long-chain diacid due to a significant degree of transesterification. To further investigate this, ^{1}H TOCSY experiments were performed on PE18.18-SO3H to elucidate whether the ^{1}H signals originating from the sulfosuccinate unit correlate with the ester end group at 3.67 ppm or not (see Figure 5.1). This experiment shows a correlation of the methylene group (H-5) next to the sulfonic acid containing carbon with the methylene groups in the backbone of the C_{18}-diol (H-3). Also, a clear response from the methylene group of the reacted ester is obtained (H-7). This indicates that the chosen measurement conditions are sufficient to capture correlations over the ester groups. Regarding the end groups, no response from E3 or E3' is observed.

* Note that GPC analysis was not possible with sulfonic acid containing polymers due to the incompatibility with the column material, which could possibly be harmed by acidic compounds.

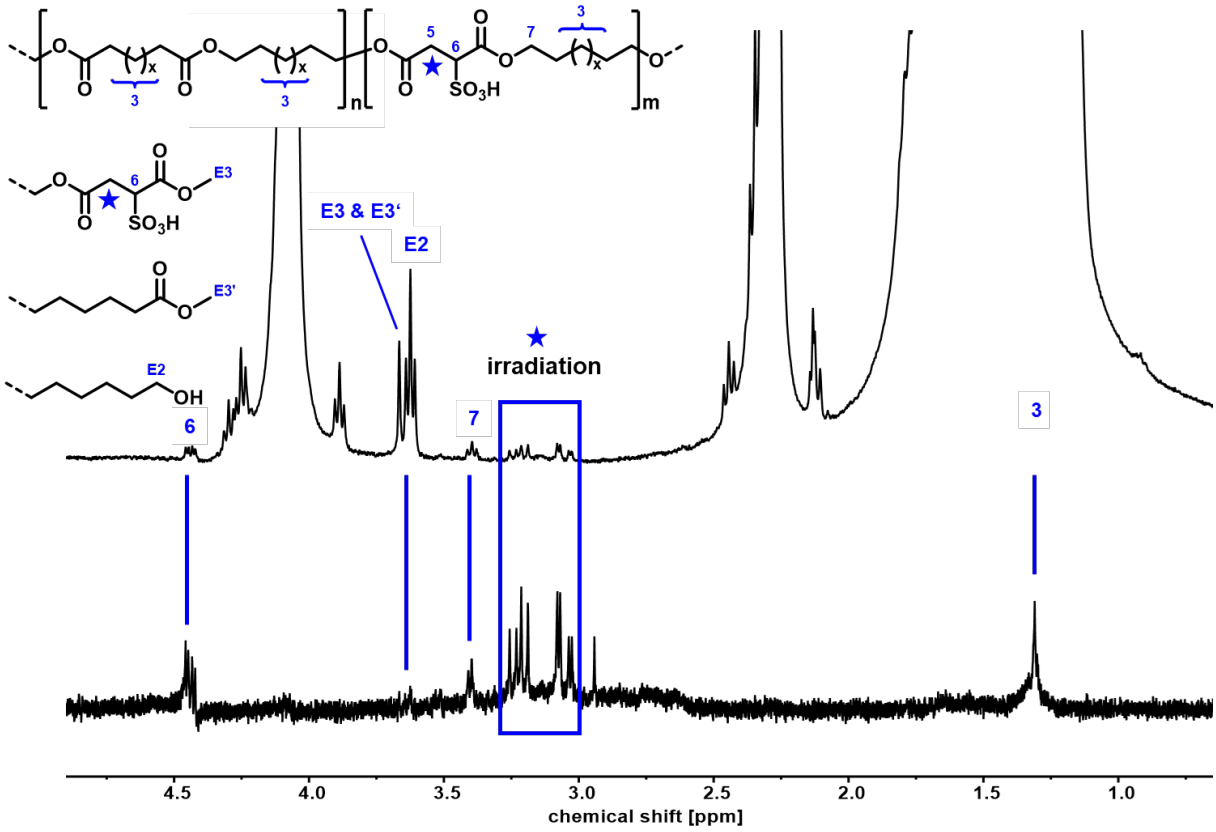

Figure 5.1 1D Selective gradient TOCSY NMR spectrum (bottom) and ^{1}H NMR spectrum (top, 400 MHz, 383 K, $C_2D_2Cl_4$) of PE18.18-SO3H-1.0. Irradiation at 3.00 - 3.27 ppm with a mixing time of 250 ms results in a response of H-6, H-7, H-3 and to a very low extent E2.

This result supports the assumption that transesterification has occurred to a major extent and that the methyl ester end group is mainly attached to the C_{18}-diacid, which is present to a much larger extent than sulfosuccinic acid. This finding underlines the successful synthesis of sulfonic acid containing all-aliphatic polyesters with long-chain repeat units and in-chain ionic groups.

In order to prevent any hydrolysis of the polyester groups during the workup and processing of the material, the synthesized polyesters were immediately processed in a micro-compounder after the removal from the flask. All polymers containing sulfonic acid units could be melted, extruded and injection moulded to produce tensile testing specimens. This is notable due to the strong hydrogen bonding system and the resulting high melt viscosity of the polymers (vide infra).

Ion exchange in sulfonic acid containing polyesters

The presence of free acid groups in polyesters can be used for the introduction of other cations *via* neutralization reactions. This was previously established by Lee *et al.* for PBS and

PBAT containing phosphorus acid moieties. The free acids were neutralized using Zn(2-ethylhexanoate)$_2$ as well as other bivalent metal cation salts of 2-ethylhexanoate. In this work, metal stearates were chosen as neutralizing agents. Excess metal stearate present in the final polymer is not expected to adversely affect polymer properties, as it is used in commercially produced polymers as lubricants. For example, they are used to facilitate the removal from the mould shape or to enhance the antistatic properties.[144] Additionally, the forming stearic acid can be removed in the workup process, when the dissolved polymer in xylene is precipitated in ^{i}PrOH. As counterions, the bivalent cations, magnesium, calcium, and zinc stearate were chosen. All compounds are commercially available in the form of metal stearates and are known to influence the material properties differently depending on their coordination strength to sulfonate groups.[145] In case of PE18.18-SO3H, 0.8 mol% of sulfosuccinic acid was used since this pre-polymer has a reasonably high sulfonate content and still shows significant ductility. For the PE12.12 derivative, 1.0 mol% was used. The synthesis of the pre-polymers was performed as described above. When a sufficient viscosity of the polymer melt was reached, as indicated by no more flow of the polymer melt, it was dissolved in xylene to perform the neutralization reaction. Parallelly, the metal stearates were dissolved in small amounts of xylene. The polymer batch was divided into three equally sized fractions and the stearates were added each. The mixtures were stirred for 10 minutes upon which the viscosity of the polymer solutions significantly increased. Subsequently, the solutions were precipitated in cold ^{i}PrOH, filtered off, stored in acetone over night to remove all residual xylene, washed with acetone and dried in a vacuum drying oven until no residual solvent was observed.

^{1}H NMR spectra remain unchanged regarding the pre-polymer PE18.18-SO3H-0.8 (or PE12.12-SO3H-1.0, respectively). One additionally occurring signal at 0.8 ppm corresponds to the ω-methyl group of excess stearate present in the final polymer. From the integral, a molar amount of ~ 4 mol% is determined for PE18.18-SO3M. For the PE12.12-SO3M derivatives, a value of ~ 2 mol% is calculated, which agrees with the molar input amount of stearate (1.5 mol% of metal stearate, accounting for 3 mol% stearate). However, the amount of stearate in PE18.18-SO3M exceeds the input by far (0.8 mol% in case of PE18.18-SO3M, accounting for 1.6 mol% stearate). This is likely due to the miscibility of the stearate in the PE18.18-SO3M matrix, which presumably incorporates the stearate upon the rapid precipitation in cold ^{i}PrOH during the workup procedure and consequently does not allow to remove excess stearate by washing of the polymers. However, the relative weight percent of stearate present in PE18.18-SO3M is low due

to the high molecular weight of the PE18.18 repeating unit (2 wt.-%, in case of PE12.12-SO_3M: 1.4 wt.-%). To compare any effects of excess stearate on the material properties of non-ion containing polymers, PE12.12 polymer without sulfonic acid was synthesized, yet the same amount of metal stearate was incorporated. These polymers are denoted as PE12.12-$M_{stearate}$ (M = Mg, Ca, Zn, respectively; ^{1}H NMR spectra can be found in the appendix, section 5.6.11, Figure 5.65 - Figure 5.70). All polymers contain ~7 mol% stearate in the final polymer (4 wt.-%). Consequently, the stearate amounts present in the reference polymers are higher than in PE12.12-SO_3M and PE18.18-SO_3M, and it can be assumed that the excess stearate does not impact the material properties to a larger extent than in the reference polymers PE12.12-$M_{stearate}$. Since the results obtained from tensile testing in case of PE12.12-$M_{stearate}$ clearly show no influence of the stearate on the mechanical properties (further discussed in section 5.2.2), this study was not repeated with PE18.18, where the C_{18}-diol is not commercially available.

Exemplary, the ^{1}H NMR spectrum of PE18.18-SO_3Zn is depicted in Figure 5.2 (all ^{1}H NMR spectra of PE12.12-SO_3M and PE18.18-SO_3M can be found in the appendix, section 5.6.10, Figure 5.53 - Figure 5.64). All protons located at the succinate unit can be identified (H-5 and H-6). Additionally, the protons H-7 of the esterified succinate unit with the C_{18}-diol are visible as triplet.

Since stearate was used in excess and is present in the final polymer, a calculation of the DP_n and M_n from ^{1}H NMR spectra is impeded. The signal of the α-methylene group in the stearate appears at 3.27 ppm and consequently overlaps with the end-group deriving from the C_{18}-diacid (or C_{12}-diacid, respectively). Instead, molecular weight and polydispersity determination was performed by GPC-SEC analysis with linear calibration against polystyrene (*cf.* appendix, Figure 5.19 and Table 5.9). The number-averaged molecular weights of the sulfonate containing polymers are all similar (48 – 52 kg/mol for PE12.12-SO_3M, ~61 kg/mol for PE18.18-SO_3M) and are well comparable to their non-ionic parent polyesters (PE12.12: 53 kg/mol; PE18.18: 68 kg/mol). The reference polymer series PE12.12-$M_{stearate}$ exhibits molecular weights of ~60 kg/mol, well comparable to the synthesized ion-containing polyesters. All polydispersity indexes are in the range expected for polyesters obtained *via* polycondensation and account for M_w/M_n = 2.0 – 2.2. The narrow polydispersity of the ion-containing polyesters is unexpected, since rheological data and mechanical testing suggest significant physical cross-linking of the chains, as discussed in section 5.2.2 (below). A corresponding aggregation is not observed in the chloroform solution, presumably due to the excess stearate coordinating to the polymer-bound metal cations (-SO_3-M-O_2C-), present in the solution in relatively high dilutions.

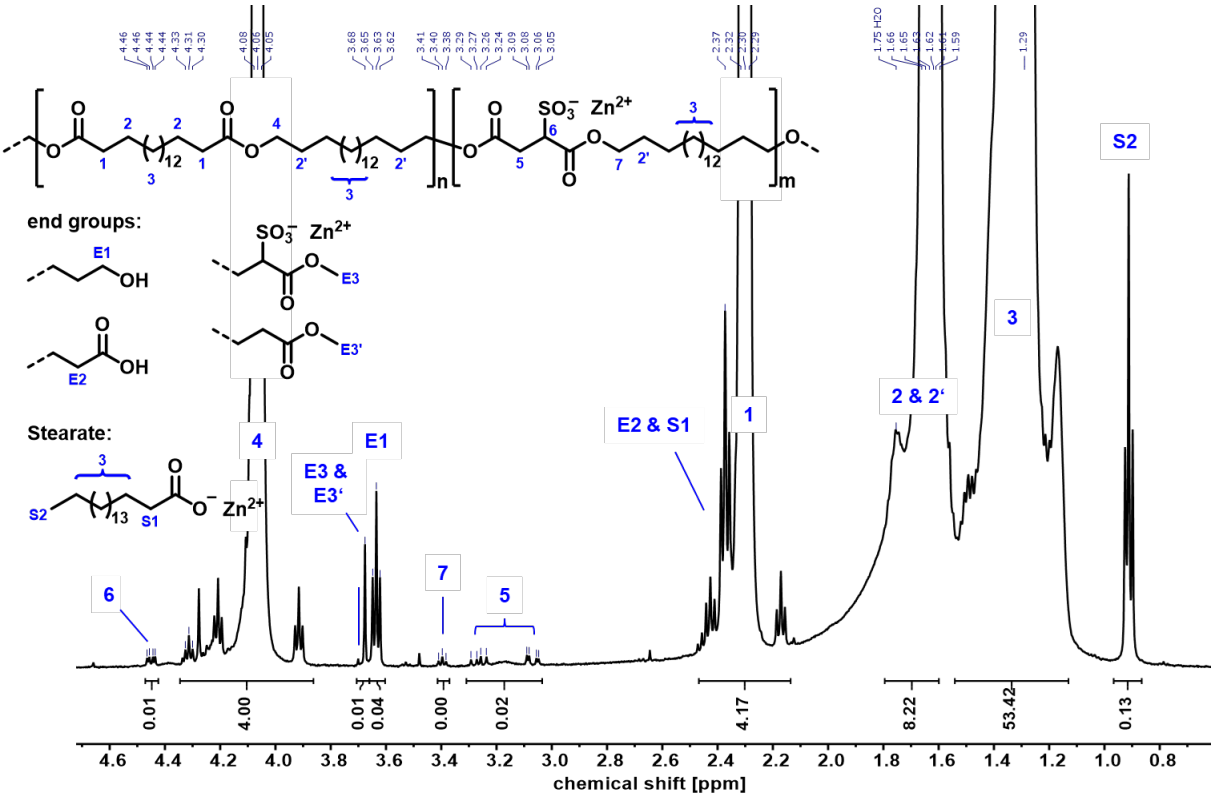

Figure 5.2 ^{1}H NMR (500 MHz, 323 K, $C_2D_2Cl_4$) of PE18.18-SO_3Zn. Note that protons H-5 are diastereotopic and that the sulfonate unit can be found on either position 6 or position 5.

The excess stearate present in the polymer was also detected *via* infrared spectroscopy (IR), spectra can be found in the appendix (section 5.6.2). In the carbonyl region, the Mg, Ca and Zn carboxylate groups are detected, showing that the stearate present is not stearic acid but the metal stearate. Due to shifts of the carbonyl band as opposed to the reference materials (pure magnesium, calcium, and zinc stearate), it is likely that the coordination of the stearate is not only one of M(stearate)$_2$, but also a -SO_3-M-O_2C-, where a metal sulfonate group in the polymer backbone and a stearate unit coordinate to one bivalent metal center.

To determine the amount of metal cation in the polymers, elemental analysis was performed (Table 5.1). The amount increases in the order Mg-Ca-Zn and is conclusive with the increasing molecular weight of the metal cations in this order. They are on par with the input amounts of metal stearate in the reaction input and underline that the excess metal is present in the final polymer, rather than removed in the workup process. Thus, it can be stated that the same molar amount of M^{2+} is present in all polymers.

Table 5.1 Elemental analysis of Mg, Ca and Zn containing polyesters PE12.12-SO3M and PE18.18-SO3M. The theoretical amount of metal (M_{theo}) according to the rection input of metal stearate to the pre-polymer is listed.

	C	H	M	M_{theo}
PE12.12-SO3Mg	70.81	10.66	0.31	0.26
PE12.12-SO3Ca	71.51	9.92	0.32	0.44
PE12.12-SO3Zn	71.29	10.99	0.72	0.71
PE18.18-SO3Mg	75.26	11.82	0.10	0.10
PE18.18-SO3Ca	75.29	12.00	0.13	0.16
PE18.18-SO3Zn	75.33	11.89	0.28	0.27

A further insight into the ionic group distribution was gained by statistical simulations. Assuming a random distribution of the ionic groups along the polymer backbone, supported by the results from ^{1}H NMR and TOCSY analysis, the amount of ionic groups per polymer chain was calculated. The results for the series PE18.18-SO3H are displayed in Figure 5.3, a description of the calculation method can be found in section 5.5.3). The majority of the polymer chains remain unfunctionalized (up to 75 % in case of PE18.18-SO3H-0.5 and up to 50 % in case of PE18.18-SO3H-1.0). Only few chains (< 15 %) have more than one ionic group in the polymer backbone, which is why intermolecular interactions can be regarded as the main forces, and intramolecular interactions as subordinated.

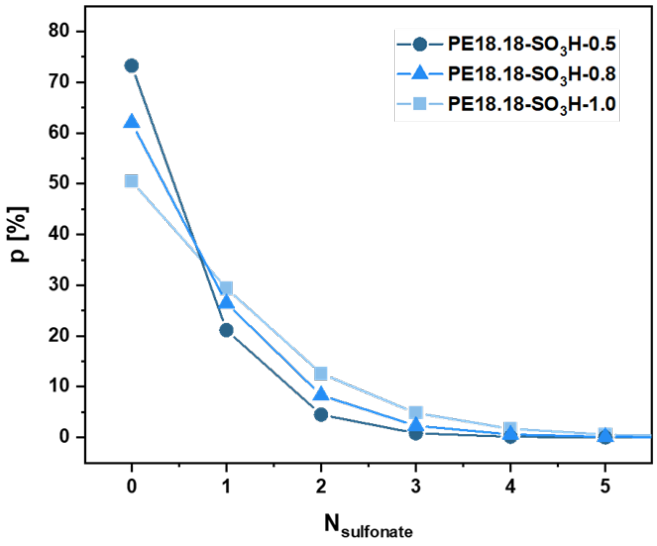

Figure 5.3 Statistical distribution of the amount of sulfonate groups per polymer chain ($N_{sulfonate}$) and the corresponding probability (p).

Special focus was set on polymer PE18.18-SO3H-0.8, as it is the pre-polymer for the series PE18.18-SO3M. For this case, an end group enrichment was determined by ^{1}H NMR (3.7 % of end groups being sulfosuccinate units). The distribution was also simulated considering the preference of sulfosuccinate to be located at a chain end. However, the results show no significant difference of the distribution (details on the calculation and results can be found in section 5.5.3). Thus, it can be assumed that ~60 % of the polymer chains in PE18.18-SO3M are unfunctionalized, making the large impact of the low amounts of functional groups on rheological and mechanical properties of special interest (as discussed below).

Again, all polymers synthesized, PE12.12-SO3M and PE18.18-SO3M were processed in a micro-compounder, extruded and injection moulded into tensile testing specimens. Additionally, melt-extruded films were drawn with a micro-cast film line (see Figure 5.4). The practical feasibility of these methods is beneficial since these methods are widely used in industry.

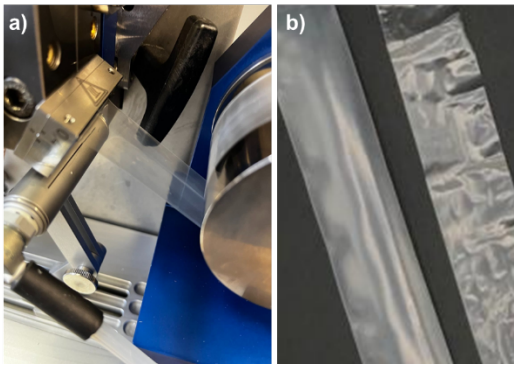

Figure 5.4 a) Film extrusion from a micro-compounder of PE18.18-SO3Zn. b) Films of different thicknesses of PE18.18-SO3Zn. Left film: ~ 60 µm thickness, right film: ~ 10 µm thickness.

The material properties depending on the nature of the cation introduced in PE18.18-SO3M (and PE12.12-SO3M, respectively) are further investigated, including thermal analysis, mechanical properties from tensile testing, rheological discussion, and a determination of the hydrophilicity of the polymers.

5.2.2 Counterion Influence on Material Properties

Thermal Properties

The thermal properties of the synthesized ion-containing polyesters were investigated *via* differential scanning calorimetry (DSC) and thermogravimetric analysis (TGA). The results obtained from DSC measurements are depicted in Figure 5.5 (thermograms and determined values can be found in the appendix, section 5.6.3).

All peak melting (T_m) and crystallization (T_c) temperatures as well as the enthalpies of fusion (ΔH_m) and crystallization (ΔH_c) are similar, and no clear trend is observed. The temperatures T_m and T_c vary within a range of 2-3 °C, all values for ion-containing polyesters are lowered compared to their non-ionic reference polymer PE12.12 and PE18.18, respectively. The slightly lowered melting temperature can be explained by the lower amount of chain regularity due to the ionic groups acting as defects.[146]

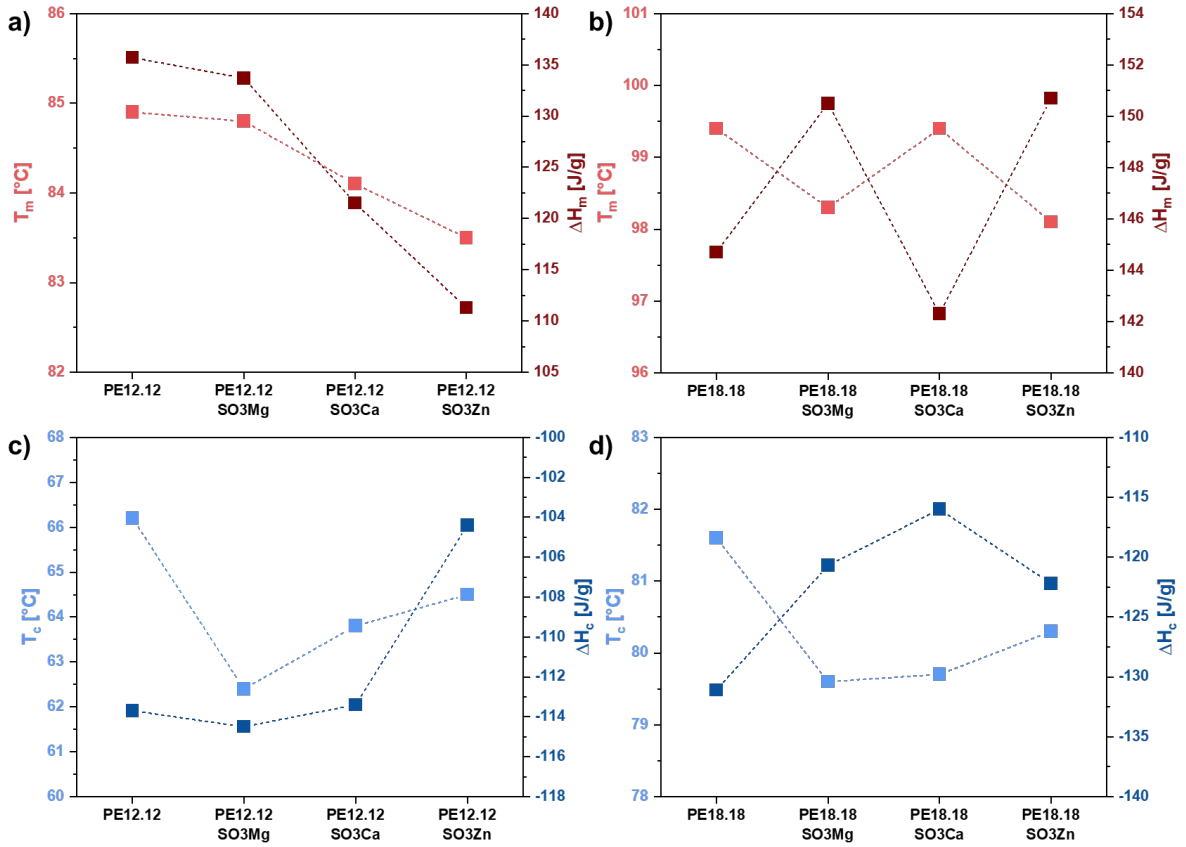

Figure 5.5 Thermal properties of PE12.12-SO3M and PE18.18-SO3M as obtained from DSC measurements (10 K/min, 2nd heating/cooling cycle). Peak melting temperatures and enthalpies of fusion of a) PE12.12-SO3M and b) PE18.18-SO3M. Peak crystallization temperatures and enthalpies of crystallization of c) PE12.12-SO3M and d) PE18.18-SO3M. Thermograms can be found in Figure 5.25 and Figure 5.26.

The decreased crystallite size with a lower degree of order also leads to lower crystallization temperatures. However, this effect is small, and the melting and crystallization temperatures remain comparable to the non-ion containing polyesters. All polymers show lower crystallization enthalpies compared to PE12.12 and PE18.18, respectively, which is conclusive with the lower degree of order. The enthalpies of fusion are clearly reduced by up to 25 J/g in case of

PE12.12-SO3Zn compared to PE12.12, whereas in case of PE18.18 all values are in the same range (variation of 8 J/g).

The same holds true for the acid containing derivatives PE12.12-SO3H and PE18.18-SO3H (*cf.* appendix, Table 5.11). Peak melting and crystallization temperatures remain similar to PE12.12 and PE18.18, respectively, and the enthalpies of fusion and crystallization are slightly lowered. These results show that the additional coulomb interactions in the polymers do not hinder the crystallizing ability of the hydrocarbon chains to a major extent, if they are present in such low concentrations as used herein. It can be summarized that the thermal properties of PE12.12 and PE18.18 are not significantly altered by the introduction of the ionic groups, which is beneficial for processing and applications.

Thermogravimetric analysis (TGA) under air was conducted to gain insight into the influence of the ionic groups on the thermal stability of the polymers. The temperatures at which 95 % remaining weight is observed (T_{95}) were determined for sulfonic acid containing polyesters (Table 5.2). The thermal stability is reduced to a minor extent by the introduction of sulfonic acid groups. However, processing conditions do not exceed 200 °C, meaning that the thermal stability of all polyesters synthesized remains sufficient for processing and applications, since all T_{95} values exceed 300 °C.

Table 5.2 Results from TGA analysis (30 – 1000 °C, 10 °C/min heating rate under air) of polyesters PE12.12-SO3H-1.0, PE18.18-SO3H-x and reference polyesters PE12.12 and PE18.18. Temperatures at which 5% weight loss is observed (T_{95}) are listed.

	x = 0.0	0.5	0.8	1.0
PE12.12-SO3H-x	374	-	-	358
PE18.18-SO3H-x	381	345	352	348

In case of the neutralized PE12.12-SO3M and PE18.18-SO3M derivatives, the temperatures T_{95} are again slightly reduced compared to the non-ion containing polyesters PE12.12 and PE18.18, respectively (see Table 5.3). However, they also remain above 300 °C and consequently are more than sufficiently high for possible melt processing conditions. After heating to 1000 °C under air, only small amounts of residual inorganic materials are indicated by TGA.

Table 5.3 Results from TGA (30 – 1000 °C, 10 °C/min) of polyesters PE12.12-SO3M and PE18.18-SO3M and their reference polyesters PE12.12 and PE18.18. For comparison, percentages by weight of cations as determined by elemental analysis are listed.

	T_{95} [°C] [a]	remaining weight [wt.-%] [b]	M^{2+} [wt.-%] [c]
PE12.12	374	0.46	-
PE12.12-SO3Mg	324	0.99	0.26
PE12.12-SO3Ca	322	1.03	0.44
PE12.12-SO3Zn	356	1.20	0.71
PE18.18	381	0.26	-
PE18.18-SO3Mg	347	0.51	0.10
PE18.18-SO3Ca	351	0.65	0.16
PE18.18-SO3Zn	374	1.19	0.27

a) Temperature at which a 5% weight loss was observed at 10 °C/min. b) Remaining weight at 1000 °C. c) wt.-% of Mg^{2+}, Ca^{2+} and Zn^{2+} as determined by elemental analysis.

Considering the remaining weight found in the TGA, it can be assumed that MgO, CaO and ZnO are formed upon combustion in case of PEx.x-SO_3M. With the increasing weight of the cation (Mg-Ca-Zn), the remaining weight increases concurrently, as expected. This also agrees with the elemental analysis results, which showed an increasing content by weight with increasing molar mass of the cation (in the order Mg-Ca-Zn), as discussed above. Note that while the sulfonic acid units are neutralized with the metal cations, an excess of metal stearate was used and is present in the final product, meaning that the present cations in the polymer are not necessarily all ionically bound to the polymers but are blended in the polymer matrix.

To summarize, the thermal stability of the synthesized ion-containing polyesters is not significantly reduced compared to the reference polyesters. Additionally, residual mass, observed in TGA, qualitatively confirms the composition of the polymers in terms of metal cation content.

Morphology

To probe the polyethylene-like character of the synthesized polymers, wide-angle X-ray scattering (WAXS) was conducted (see Figure 5.6, WAXS profiles of PE12.12-SO3H-1.0 and PE12.12-SO3M can be found in the appendix, section 5.6.4). Injection moulded specimens were

used, which were promptly cooled from the melt state to ~50 °C and immediately removed from the mould shape without applying additional controlled crystallization conditions.

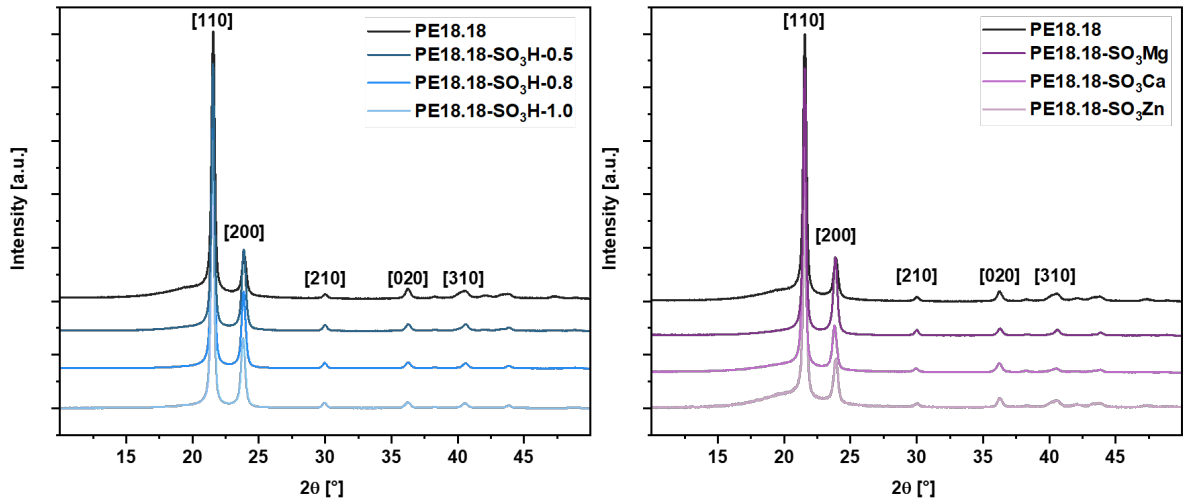

Figure 5.6 WAXS profiles of PE18.18 and PE18.18-SO3H (left) and PE18.18-SO3M (right). Reflexes corresponding to the orthorhombic unit cell of polyethylene are labeled. Data was shifted vertically for clarity.

All polymers investigated exhibit an orthorhombic crystal structure in the processed specimens. Several higher order reflexes are visible (> 30 °), underlining the high degree of order in these materials. A calculation of the crystallinity in case of the acid containing polymers is impeded since the age of the samples is crucial to be able to compare crystallinities. Even though the measurements were taken on the same day, the processing of the materials occurred over a period of two weeks, which impedes comparisons of the crystallinity from WAXS spectra. However, since all polymers exhibit orthorhombic semi-crystalline structures, a clear polyethylene-like character of the ion-containing polyesters investigated herein can be concluded.

Rheology

The melt rheology is key to the processing of ion-containing polymers, what may also reflect in the tensile properties of specimens prepared from the melt. Additionally, the strength of the physical cross-linking can be compared from rheological data, which is also indicative for their relevance in the solid state. For that purpose, dynamic frequency sweeps were conducted on PE18.18-SO3M as well as PE18.18 for comparison (Figure 5.7, data for PE12.12-SO3M can be found in the appendix, section 5.6.4).

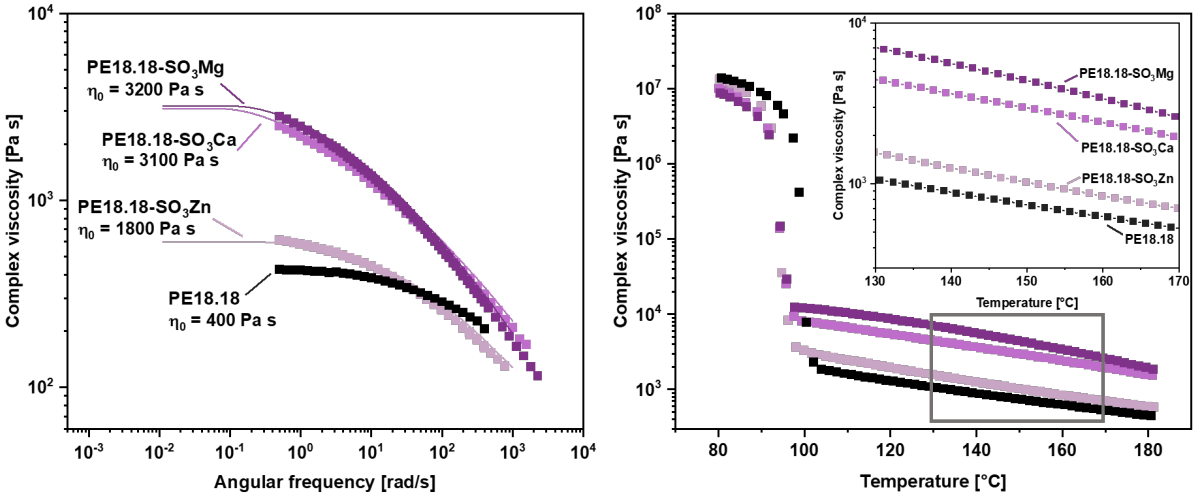

Figure 5.7 Left: Absolute complex viscosity as a function of the angular frequency of PE18.18 and PE18.18-SO3M at 180 °C. The solid lines represent the fit curve calculated with the multimode Maxwell model (10 modes). Zero-shear viscosities (η_0) are listed. Right: Temperature sweep rheology results of PE18.18 and PE18.18-SO3M, inset shows section marked in grey in closer detail (strain 0.1 %, angular frequency 6.28 rad/s, heating rate 10 °C/min).

In case of PE18.18-SO3M, the zero-shear viscosity (η_0) is significantly increased upon the introduction of ionic groups, with the Mg and Ca derivatives showing a 7-fold increase and Zn a 4-fold increase compared to PE18.18. This increase is remarkable regarding the very low amount of functionality in the polymer chains, and considering that only ~ 40 % of the polymer chains carry ionic groups. A clear trend is observed, with an increasing η_0 in the order Zn-Ca-Mg, with Zn having a significantly lower effect than Ca and Mg. The coordination of Mg and Ca to sulfonate is strong and a high degree of ionic cross-linking results. Makowski et al. also observed a significantly lower melt viscosity in Zn neutralized sulfonated EPDM, which was ascribed to two factors: on the one hand, the disulfonates -SO_3-Zn-O_3S- are broken up to form monosulfonates, -SO_3-Zn-O_2C-, with the excess stearate coordinating the zinc.[145] In case of Zn^{2+}, a coordination to carboxylate is preferred compared to Mg^{2+} and Ca^{2+} due to the more covalent character of Zn^{2+}. On the other hand, the excess zinc stearate present can act as plasticizer, which also leads to the observed phenomenon.

Temperature sweep rheology measurements revealed that the strong difference in the melt viscosity is present throughout the whole temperature range studied (80 – 180 °C). No sudden changes are observed upon heating in the melt state, showing that the ionic aggregates are present at all temperatures below 180 °C.

Mechanical Properties

To explore the versatility of this approach and to illuminate the influence of the different cations on the mechanical behavior, the tensile properties of the ion-containing polymers were investigated. For polymers PE18.18-SO3H, a significant effect on the ductility and toughness is visible (see Figure 5.8, values can be found in the appendix, section 5.6.6, Table 5.13).

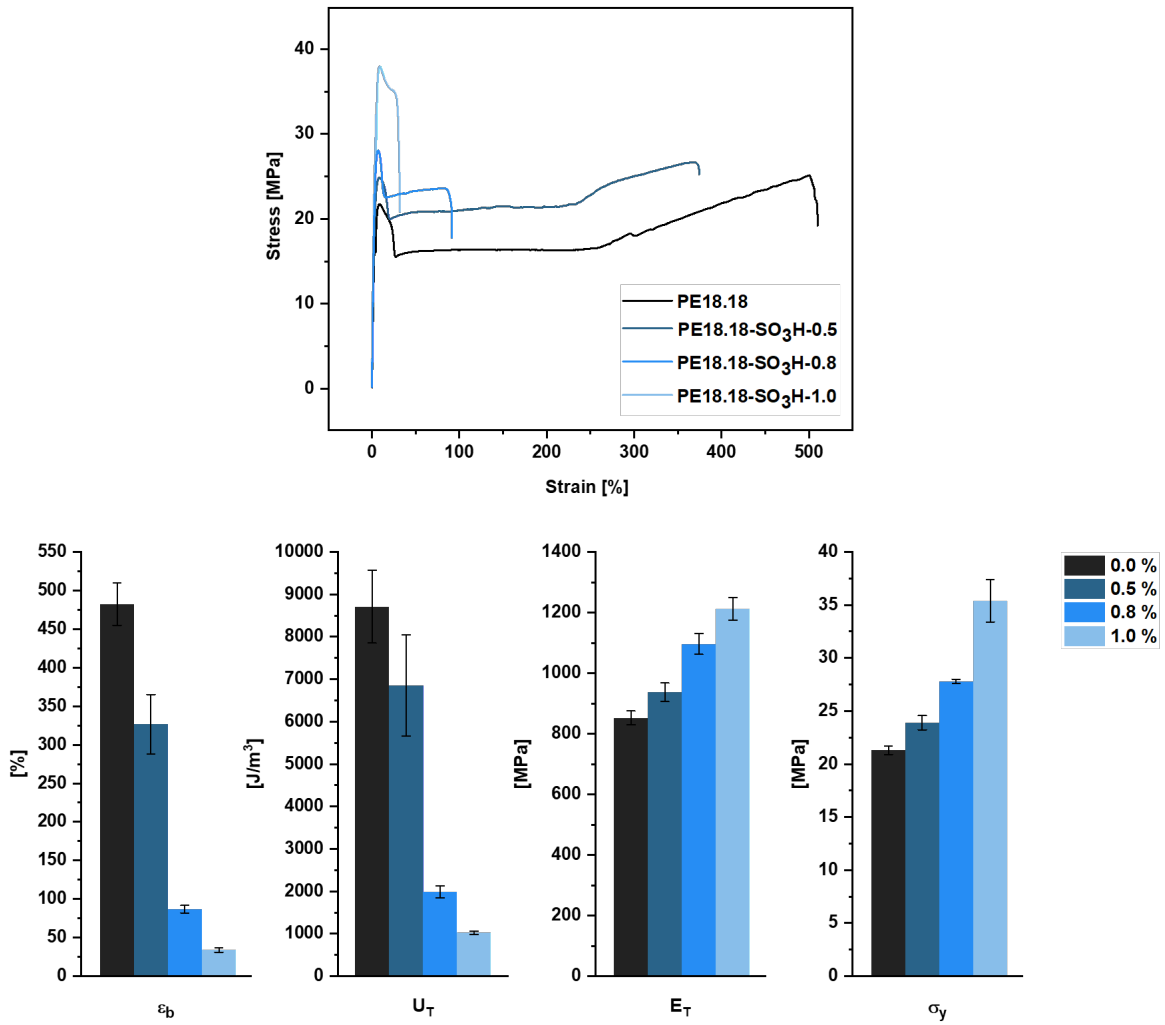

Figure 5.8 Top: Stress-strain curves of PE18.18-SO3H (right). Bottom: Comparison of tensile testing parameters of PE18.18-SO3H-x: Elongation at break (ε_b), toughness (U_T), Young's Modulus (E_T) and stress at yield (σ_y) are depicted. Error bars represent standard deviations calculated from three test specimens.

The sulfonic acid groups present in the materials significantly decrease the ductility (ε_b) from over 500 % in PE18.18 to less than 50 % in PE18.18-SO_3H-1.0. Consequently, the toughness (U_T) decreases concurrently from ~ 9000 J/m^3 to ~ 1000 J/m^3. The tensile strength increases with increasing sulfonic acid content, which can be clearly seen in the stress-strain curves. Going hand in hand with these effects, the Young's moduli (E_T) and the stress at yield (σ_y) also significantly

increase. This suggests that the sulfonic acid groups lead to a stiffening of the polymers, making higher strengths necessary for small deformations. For all these parameters, clear trends with increasing amounts of incorporated sulfonic acid are observed. The results obtained for the polymer PE12.12-SO3H-1.0 are on par with PE12.12. Respective tensile testing curves can be found in the appendix (*cf.* section 5.6.6). This might be assigned to the lower crystallinity of the materials and the higher compatibility of the polymer chains with the ionic aggregates. Note that the processing conditions were not optimized for the individual polymers or polymer series, but the best conditions for PE18.18 and PE12.12 were applied. However, the processing history is crucial and can change the mechanical testing results significantly. Consequently, it cannot be excluded that the applied conditions are well chosen for the PE12.12 derivatives but are not optimum conditions for the PE18.18 polymers.

When introducing bivalent cations to the sulfonate containing polymers, a strong dependence of the tensile properties on the nature of the cation is observed (see Figure 5.9). Both, magnesium- and calcium-containing polymers PE12.12-SO3M and PE18.18-SO3M show a significant reduction of the ductility and toughness. The highly ionic character of Mg^{2+} and Ca^{2+} leads to stronger ionic aggregates in the polymer matrix, reducing the chain mobility upon strain. This strongly associating effect is conclusive with the results obtained from rheological investigations and stresses the coordination of Mg^{2+} and Ca^{2+} to the incorporated sulfonate groups rather than the excess stearate. However, Zn^{2+} showed a much lower degree of cross-linking in rheology measurements, and a more ductile behavior in the solid state. This can be accounted for by the less ionic character of Zn^{2+} as discussed above. Hence, a coordination to sulfonate and stearate is likely for Zn^{2+} in the melt and crystallized state.

Even though the stiffness of the Mg, Ca and Zn containing materials is comparable, it is enhanced compared to PE18.18 and slightly reduced compared to the acid containing PE18.18-SO3H. The same trend is visible for PE12.12-SO3M. The hydrogen bonds stiffen the material the most, while the ionic aggregates have a less stiffening effect. This effect decreases in the order Mg-Ca-Zn, in line with the hardness of the cations according to the hard and soft acids and base concept (HSAB).[147]

Note that again no optimizations of the processing conditions were performed in this case, which would be necessary to conclude the observed effects from the cation nature with a higher certainty. However, the results found herein show that the mechanical properties can be altered

to a significant degree by using different cations, while maintaining the polyethylene-like nature of the polyesters.

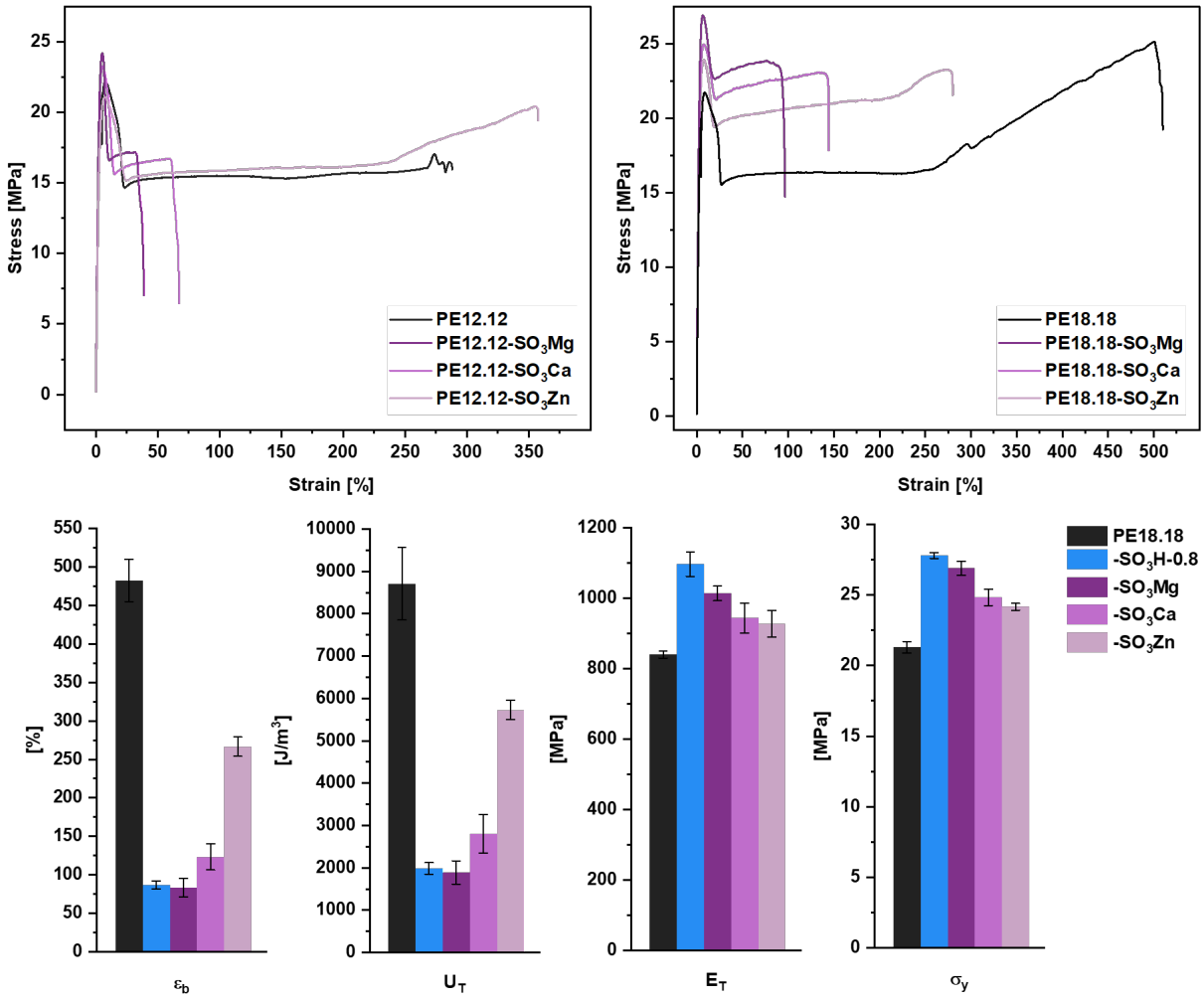

Figure 5.9 Top: Stress-strain curves of PE12.12-SO_3M-1.0 (left) and PE18.18-SO_3M-0.8 (right, M = Mg, Ca, Zn). Bottom: Comparison of tensile testing parameters of PE18.18, PE18.18-SO_3H-0.8 and PE18.18-SO3M-0.8 (M = Mg, Ca, Zn): Elongation at break (ε_b), toughness (U_T), Young's modulus (E_T) and stress at yield (σ_y) are depicted. Error bars represent standard deviations determined from three test specimens.

Hydrophilicity

To investigate the influence of the sulfonate groups on the surface properties of PE12.12 and PE18.18, water contact angle (WCA) measurements were performed on injection moulded specimens. The sulfonic acid containing materials show a clear trend in case of PE18.18-SO3H, where the increasing acid content leads to a decreasing WCA, showing the effect on the hydrophilicity of the surface (see Figure 5.10, WCA images can be found in the appendix,

section 5.6.7). The difference between the reference polyester PE18.18 and the polymer containing the highest amount of sulfonic acid (PE18.18-SO3H-1.0) is as high as ~15 °, which is a significant decrease. This is anticipated to be advantageous in terms of degradability, since the hydrolytically cleavable ester groups in the bulk polymer need to be accessible to water. A comparable effect was found by Han et al. in sulfonated PBS materials, where an incorporation of 5 mol% of sodium sulfonated diester unit also lead to a decrease of ~15 °.[148] In sulfonated PBAT, the incorporation of 12 mol% sulfonated unit decreased the WCA by ~20 °.[25] This underlines the significance of the WCA reduction observed in the materials presented herein, since the ionic content is much lower (≤ 1 mol% *vs.* 5 – 12 mol%), but the observed effect is comparable to those observed in literature (~15 °).

For the neutralized polyesters PE12.12-SO3M and PE18.18-SO3M, no trend is observed. In case of PE18.18, all ion-containing polymers show lower WCAs, however, the difference is smaller than in the acid-containing polymers (~8 °). For the series PE12.12-SO3M, no significant difference is observed. However, all polymers contain excess metal stearate, impeding to draw conclusions from the incorporated sulfonate groups on the WCA. Metal stearates are typically used as lubricants and, consequently, impact the surface properties of these materials significantly.

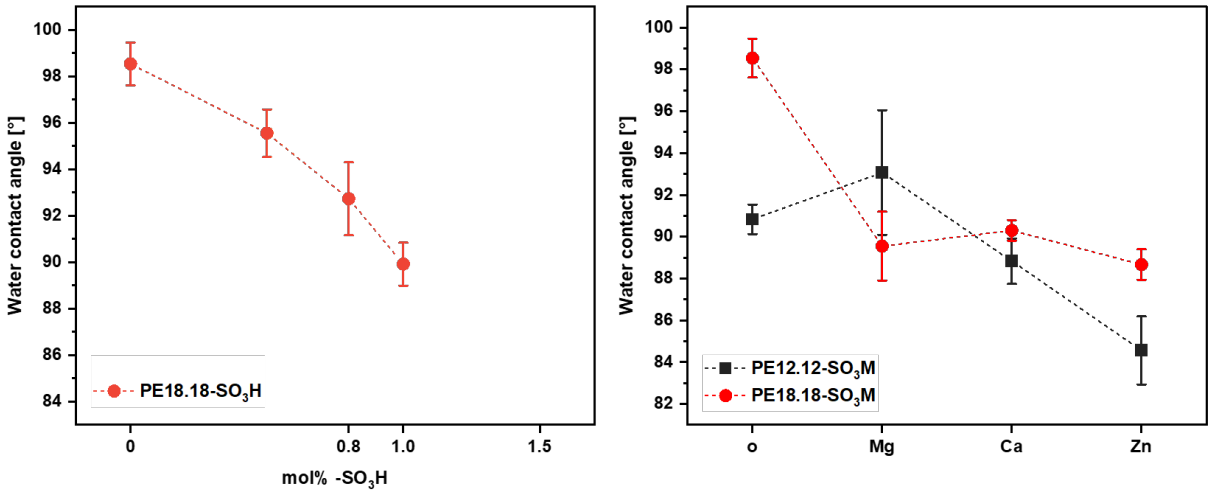

Figure 5.10 Water contact angle of PE18.18-SO3H (left) and PE12.12-SO3M and PE18.18-SO3M (right) as well as their non-ionic reference polyesters, PE12.12 and PE18.18. Error bars represent standard deviations calculated from three different droplets (six angles). Samples were surface cleaned with ^{i}PrOH and dried for 48 h prior to the measurements.

To study the ability of the sulfonic acid containing polymers to absorb water, samples were stored in water for several weeks. The samples used were injection moulded specimens

according to ASTM standard D5023-0 (rectangular rods) and cut into equally sized pieces (8 x 10 x 1 mm) to ensure the same surface area of all samples. Duplicates of each were immersed in water and the sample weight was measured several times along the experiment. For this purpose, the samples were taken from the solution, patted dry and weighed. This process was repeated until three independent measurements were obtained with deviations smaller than 10 µg. The results of the two studies (PE12.12-SO3H: 12 weeks, PE18.18-SO3H: 10 weeks) are depicted in Figure 5.11.

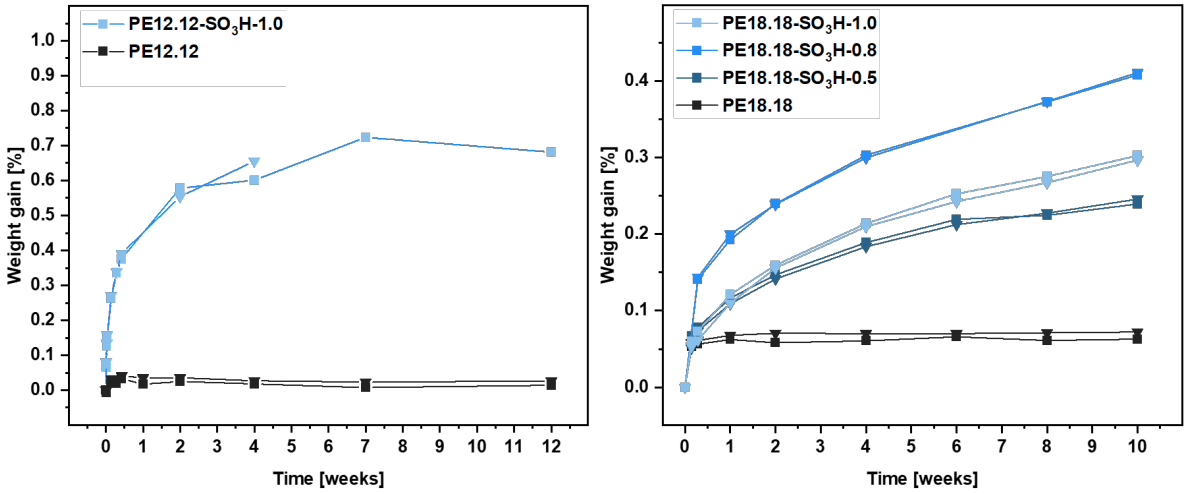

Figure 5.11 Water uptake of PE12.12-SO3H-1.0 (left) and PE18.18-SO3H (right) as well as of their non-ionic parent polymers (PE12.12 and PE18.18, respectively) after storage in water for 12 weeks. Samples were taken from the solution, patted dry and weighed. This was repeated until 3 values with a difference of < 10 µg was obtained.

In case of PE12.12-SO3H-1.0, a significant absorption of water is observed. After 12 weeks, ~0.7 wt.-% is gained. Note that no water is absorbed in PE12.12, showing that the incorporated acid is accountable for the water uptake. Also, a significant degree of embrittlement after 12 weeks was observed in acid containing polyesters, whereas the PE12.12 specimen remained unchanged by visual inspection. This is also true for PE18.18, where after a small initial water uptake of less than 0.05 wt.-%, no more weight gain is observed. The overall weight gain is lower compared to the PE12.12 derivative, which can be explained by the higher dilution of sulfonic acid groups in the polymer. Monitoring the degree of polymerization *via* ^{1}H NMR spectra, the same trend is visible (see Table 5.4): No major change is observed upon the exposure of PE12.12 and PE18.18 to water for 12 and 10 weeks, respectively, whereas a significant decrease in DP_n is observed for all sulfonic acid containing polymers. For PE12.12-SO3H-1.0 and PE18.18-SO3H, a ~50 – 60 % reduction of the DP_n and, hence, the number-average molecular weight was

determined. Consequently, the absorbed water detected as weight gain over time is not only absorbed by the polymer samples but is bound in the polymer due to chain cleavage of the ester bonds.

Table 5.4 Degrees of polymerization as calculated from ^{1}H NMR spectra of samples in water uptake study of PE12.12, PE12.12-SO3H and PE18.18, PE18.18-SO3H. Values before the study and after 10 and 12 weeks, respectively, of exposure to water are listed.

	DP_n 0 weeks	DP_n 12 weeks		DP_n 0 weeks	DP_n 10 weeks
PE12.12	98	101	PE18.18	68	64
			PE18.18-SO3H-0.5	84	39
			PE18.18-SO3H-0.8	90	33
PE12.12-SO3H-1.0	70	28	PE18.18-SO3H-1.0	82	38

The results from this water absorption study show the tendency of the investigated sulfonic acid containing polymers to take up water, which can then hydrolyze the ester groups, presumably catalyzed by the present sulfonic acids. The fact that all acid containing polymers exhibit a significant decrease in the DP_n from ^{1}H NMR spectra suggests that the water absorption is present throughout the bulk sample. Therefore, the functional groups within the bulk polymers are found to be accessible to water and can be cleaved upon exposure to nature. The formation of hydrophilic regions that take up water can be regarded as a prerequisite for enhanced degradability of polyesters. It is also reasonable to assume that the present acid groups catalyze ester cleavage within the bulk. A loss of forming monomers is unlikely under the conditions investigated herein due to the low solubility of the C_{18} monomers in water. If a virtually unlimited water reservoir such as a lake was present, a loss of monomers and oligomers could be expected (which can be mineralized by microorganisms).

To further investigate the influence of humidity on the polymer properties, injection moulded tensile testing specimen of PE18.18 and PE18.18-SO3H were stored in a humidity chamber at 25 °C and 60 % humidity for six weeks. The specimens were tested after the storage time (see Figure 5.12).

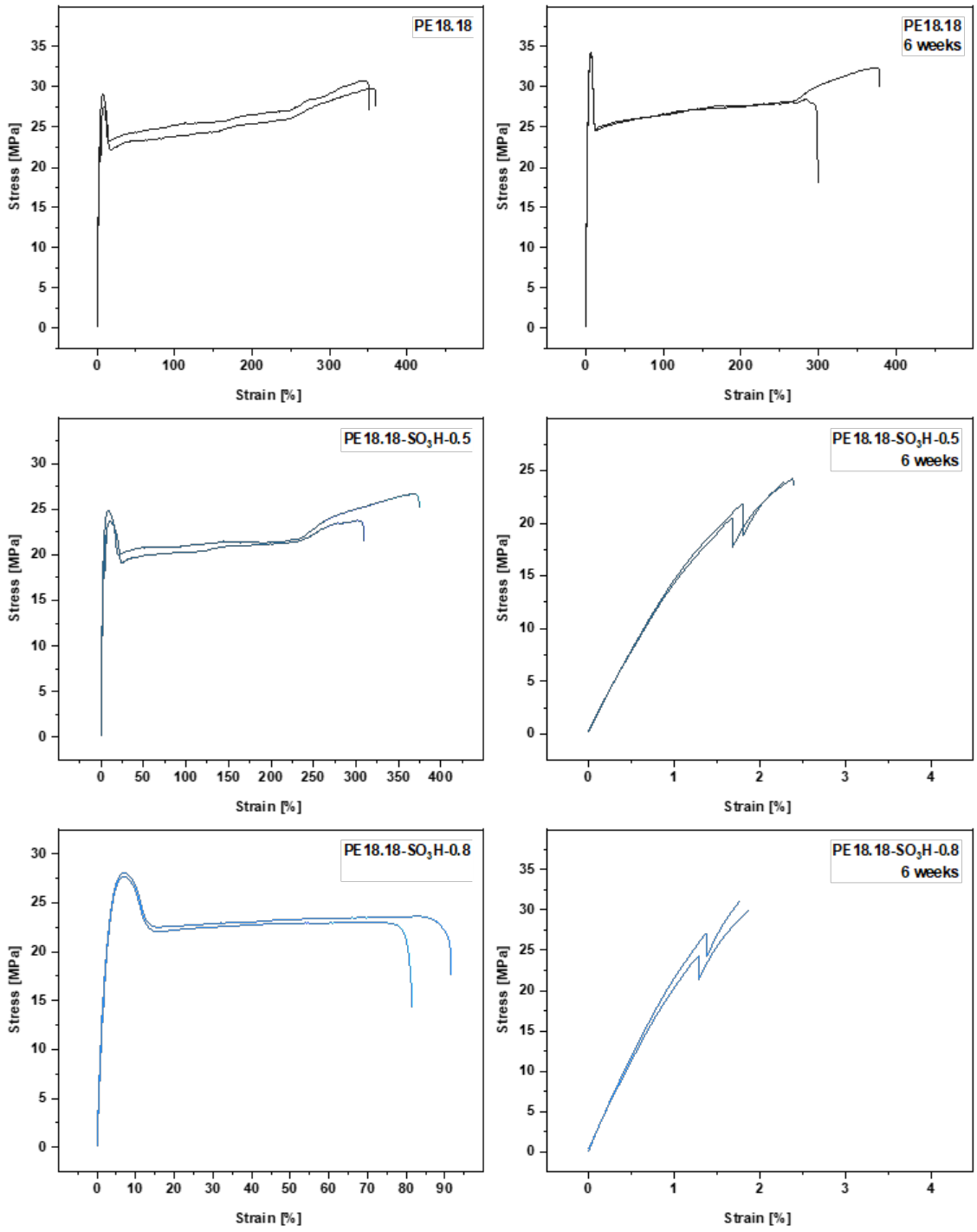

Figure 5.12 Stress-strain curves of PE18.18 and PE18.18-SO_3H-x (x = 0.5, 0.8). Left: specimens measured one day after processing. Right: specimens measured after storage at 25 °C and 60 % humidity for 6 weeks.

For the reference polymer PE18.18, tensile testing specimens were stored from a batch with medium molecular weight (DP_n = 99*), which had a medium ductility and toughness before the storage in the humidity chamber (ε_{tb} ~ 350 %). Additionally, a small amount of cross-linking was

* Calculated from end group analysis in ^{1}H NMR spectrum.

observed from GPC traces in this particular batch, which is not believed to change possible reactions of the polymer with water during the storage time. Note that this polymer shows an increased Young's modulus and yield point compared to non-cross-linked PE18.18. Upon storage, no significant change in the ductility was observed, whereas the Young's modulus increased (1000 MPa *vs.* 1400 MPa). This is likely due to a higher crystallinity since the chains rearrange over time and crystallinity increases. However, an analogous study was also carried out in another project within our group by M. Eck with a high-molecular weight batch without any cross-linking. It was possible to show that PE18.18 does not change its material properties over a time period of 4 weeks.[143] Ductility and toughness remain similar, as observed herein. The sulfonic acid containing polymers PE18.18-SO3H-0.5 and PE18.18-SO3H-0.8 show a significant decrease in ductility and are fully brittle materials after 6 weeks ($\varepsilon_{tb} < 3$ %). The Young's moduli increase from 970 MPa to 1500 MPa in case of PE18.18-SO3H-0.5, and from 1050 MPa to 2200 MPa for PE18.18-SO3H-0.8, showing the highly increased stiffness of the materials. The embrittlement can be explained by a decreased molecular weight, since ^{1}H NMR spectra show a significant decrease of the degrees of polymerization in PE18.18-SO3H (see Table 5.5). To be able to relate the effect on the DP_n with the exposure to humidity, reference samples were measured which were stored in a glovebox under nitrogen atmosphere for the same time. These samples exhibit no significant change of the DP_n, which shows that the decrease in molecular weight originates from the water present in the humidity chamber and that the chain cleavage is catalyzed by the incorporated sulfonic acid.

Table 5.5 Degrees of polymerizations of tensile testing specimens before and after storage at 25 °C and 60 % humidity for 6 weeks, as well as after storage under nitrogen atmosphere for 6 weeks. Values are determined *via* end-group analysis by ^{1}H NMR spectroscopy.

	DP_n (0 weeks)	DP_n (6 weeks, humidity)	DP_n (6 weeks, nitrogen atmosphere)
PE18.18	99	100	103
PE18.18-SO3H-0.5	74	31	77
PE18.18-SO3H-0.8	94	33	83

The sulfonic acid groups influence the polymers susceptibility to water to a large extent, exposing the incorporated ester groups to water even in injection moulded bulk samples where

the surface area is low. The non-ionic parent polymers PE12.12 and PE18.18 do not show chain break down if exposed to water or humidity on the time scales and under the conditions investigated herein. Thus, a significant impact of the sulfonic acid groups on the hydrolytic degradability of these polyesters is evident.

5.2.1 Recycling to Monomer

As previously reported by Häußler et al., the long-chain aliphatic polyester PE18.18 can be fully recycled to its monomers in a closed-loop fashion.[38] The full depolymerization of PE18.18 to its monomers was achieved *via* alcoholysis in methanol, establishing mild conditions (120 °C in methanol in a closed reaction vessel, or 170 °C in water), and obtaining highly crystalline monomer mixtures of C_{18}-diol and C_{18}-diacid (or diester, respectively) in 99 % yield. Additionally, repolymerization of the obtained mixture showed that the recycled polymer is on par with the original polymer regarding its thermal as well as mechanical properties. This approach is of particular interest for the materials studied in this work, since polyethylene-like ionomers are typically based on copolymers of ethylene and methacrylic acid, which do not exhibit in-chain functional groups that can be used as breaking points in depolymerizations. Consequently, a recycling to monomer approach in ion-containing polyethylene-like materials is lacking and makes the long-chain aliphatic polyesters studied here particularly attractive.

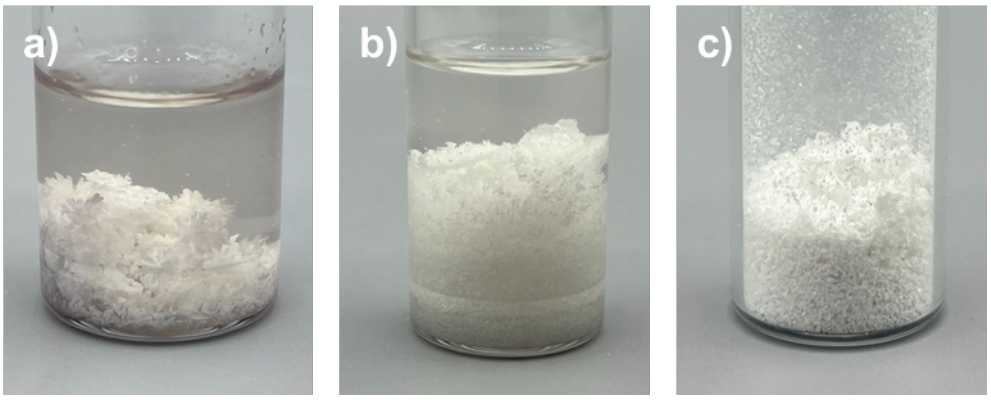

Figure 5.13 Images of recycling-to-monomer experiment of PE18.18-SO3H-1.0. a) crystallites as obtained from the solvolysis reaction; b) after recrystallization from methanol; c) dried powder after one recrystallization step.

Depolymerization experiments were conducted on PE18.18-SO3H-1.0 on a small scale (200 mg of injection moulded polymer sample). The polymer was immersed in methanol (8 mL) in a stainless-steel reactor vessel, sealed and heated to 150 °C for 6 days. Note that the reaction time was not optimized and a long time period was chosen to ensure full depolymerization.

Häußler et al. showed a complete depolymerization without additional catalyst in 12 hours.[38] After cooling to room temperature, crystallized solid was obtained. This mixture was filtered off, recrystallized from methanol, and dried. The resulting crystalline white powder was obtained in 80 % yield. Images of the crystalline materials can be found in Figure 5.13. Further optimization of the work-up procedure would presumably lead to higher yields if required (in case of PE18.18: 99 % according to literature[38]).

The obtained ratio C_{18}-diol:C_{18}-diester amounts to 1:0.99 according to the ^{1}H NMR spectrum (*cf.* appendix, section 5.6.12), meaning that the C_{18}-diol is obtained in slight excess. No remaining signals of ionic groups characteristic of the sulfosuccinic acid unit are detected, which shows that this minor fraction is soluble in the methanol fraction and completely separable from the aliphatic mixture. Thus, full flexibility for further repolymerizations is gained, where 1 mol% of diester can be added to the mixture and can be any diester, ionic substituted or not. These results show the possibility to completely depolymerize the ionic-substituted polyethylene-like polyesters presented here back to their valuable monomers.

5.2.2 Adsorption of Ink

The ability of polymers to adsorb ink is of interest not only to the packaging industry but also to the textile industry. Since hydrophobic polymers such as HDPE have low-energy surfaces (low surface free energies), the adhesion of inks on untreated polyethylene is limited. Consequently, these polymers require coatings or intensive surface treatments to enable adsorption of ink. This is true for both, water and solvent based inks on hydrophobic polymers but is especially relevant for water-based inks due to their environmental friendliness. Since the polymers investigated within this work show increased hydrophilic surface properties compared to polyethylene, their ability to adsorb ink is of interest.

For this purpose, melt extruded films produced with the micro-cast film line were printed on with an ink-jet printer. To simplify the investigations, only the blue color of the ink-jet printer was used, a water-based ink consisting of water, glycerol, glycol, 2-imidazolidinone and thiadiazole azo dye.[149] The pieces of films were adhered in the center of a DIN A4 paper with Sellotape before introduction into the printer. The logo of the University of Konstanz was printed on the film in blue color. After drying the films for 24 h at 50 °C to ensure sufficient drying of the color, the adhesion of the print on the film surface was tested by rigorously wiping over with a microfiber cloth applying a firm pressure. Representatively, the photographs of the imprinted films of HDPE,

PE18.18 and, PE18.18-SO3M before and after wiping are depicted in Figure 5.14. As reference materials, films made from PE18.18 and HDPE were investigated.

The delicate logo with its fine lines was successfully printed on all polymers. After rigorously wiping the surface, a clear difference can be observed for the different materials. In case of HDPE, no residue of the design remained, and on the PE18.18 film it was significantly blurred. The slightly better adsorption capability of PE18.18 compared to HDPE is expected, since the ester groups PE18.18 enhance the surface free energy, leading to a stronger adhesion. In case of PE18.18-SO3M, a much better adhesion of the color can be seen: the difference between the samples before and after wiping off the color is small. A slight blurring is observed in this case as well, but to a much lower extent than in PE18.18. The delicate lines of the logo can be identified after wiping in all ion-containing derivatives.

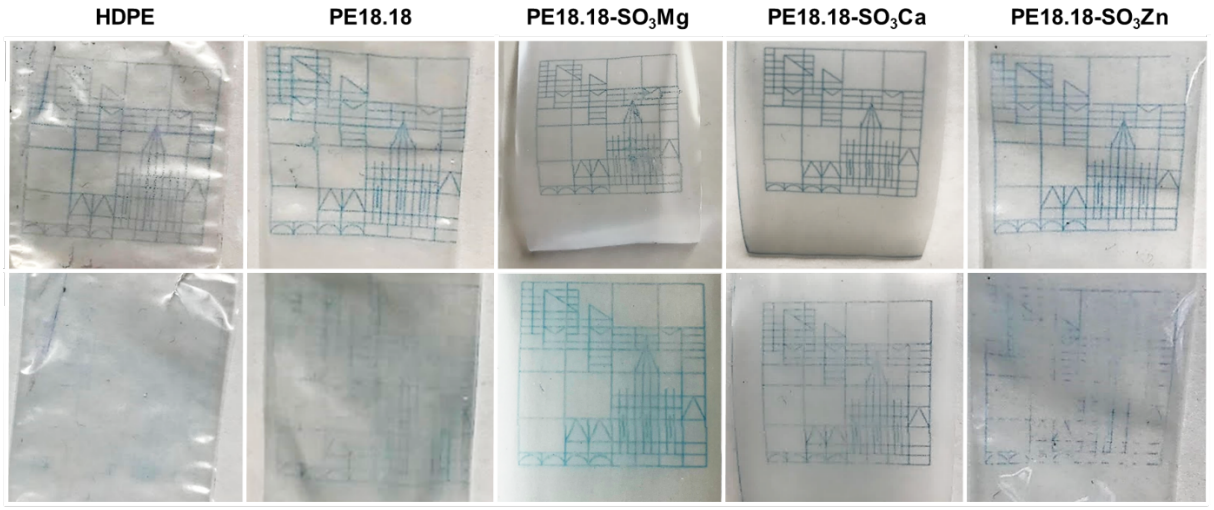

Figure 5.14 Photographs of imprinted films of HDPE, PE18.18, PE18.18-SO3Mg, PE18.18-SO3Ca and PE18.18-SO3Zn before (top row) and after (bottom row) wiping off the color.

To test whether the observed effect originates from the excess stearate or from the incorporated ionic groups, PE12.12, PE12.12-SO3Mg and PE12.12-$Mg_{stearate}$ were compared (Figure 5.15). Again, a significant blurring effect in case of PE12.12 is visible, yet the PE12.12-SO3Mg shows a high persistency of the ink. This effect is even more pronounced compared to the PE18.18 derivatives, which can be ascribed to the higher density of in-chain ester groups additionally increasing the surface energy. However, the reference polyester PE12.12-$Mg_{stearate}$, which also contains excess stearate but has no ionic groups incorporated in the polymer backbone, shows a significant blurring effect, comparable to that seen in PE12.12. The improved adhesion capability of the investigated polyesters appears not to originate from the incorporated stearate, but mainly derives from the incorporated ionic groups. This

observation makes these polymers interesting for packaging materials, where logos or information on the product can directly be printed on the packaging foil as opposed to HDPE, which requires a significant degree of surface modification prior to printing.[150] Also, the use as fibers in the textile industry is a possible application, since coloring and, consequently, good adsorption capability of the polymers is crucial for textiles. This way, recyclable fibers with good adhesion properties could be accessed.

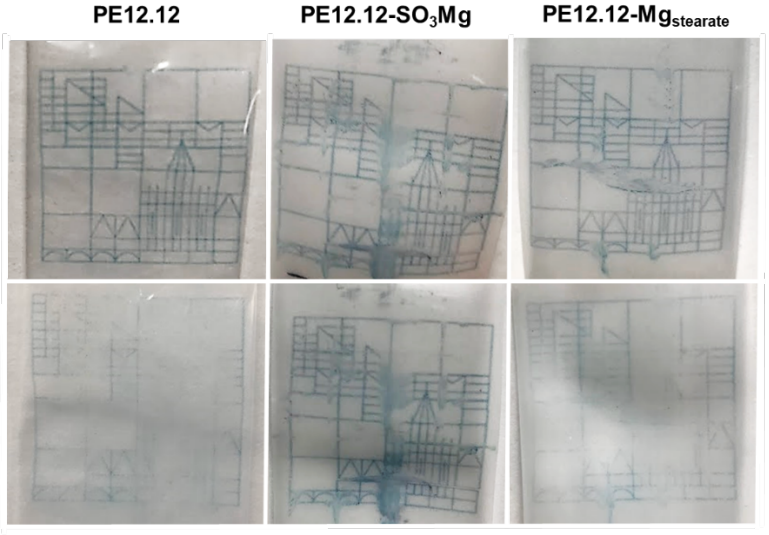

Figure 5.15 Photographs of imprinted films of PE12.12, PE12.12-SO3Mg and PE12.12-$Mg_{stearate}$ before (top row) and after (bottom row) wiping off the color. Note that ink adsorption on PE12.12-based polymers was generally more difficult, leading to more indistinct lines in the original image (top).

5.3 Summary and Conclusion

Ionic-substituted long-chain polyesters with molecular weights of M_n ~ 20 – 25 kg/mol are accessible by polycondensation of long-chain dicarboxylic acids and dimethyl sulfosuccinate with long-chain diols. Despite the anticipated lower reactivity of the sulfosuccinate due to the bulky ionic group, the ionic-substituted repeat units are primarily incorporated in the chains rather than as end groups. Appropriate polycondensation protocols, namely a limited temperature (160 °C) compared to protocols for the non-ionic polyester analogues, avoid any decomposition of the sulfonated monomer or reap units. The monomers sulfonic acid groups catalyze the polyesterification without the need for additional catalysts.

Despite the relatively low amounts of ionic repeat units (0.5 – 1.0 mol%), these can impact the processing and materials properties significantly. Sulfonic acid groups increase the stiffness and decrease the ductility of the materials, presumably due to hydrogen bonding networks. Particularly, they promote water uptake and hydrolytic degradation of the otherwise hydrophobic, stable non-ionic analogues. Bivalent counterions result in a significantly increased melt viscosity, which may be beneficial for processing methods requiring high melt stability like film blowing. An increased surface energy also reflects in a much better adhesion of inks and printability.

By virtue of the in-chain ester groups, the materials can be fully recycled to monomers. While the long-chain monomers are recovered as crystalline materials, the ionic-substituted monomer is separated completely. This is beneficial for reuse of the monomers, to generate desirable compositions of the recycled polymers.

In summary, a direct synthetic approach towards sulfonate containing polyethylene-like polyesters was elaborated. These materials are promising for packaging applications due to their capability to adsorb ink without further surface modifications. Additionally, applications in the textile industry are feasible, where ink adsorption is crucial to color fibers. Future studies could include a detailed view on the mechanical properties beyond those shown herein, for example the impact resistance or the abrasion resistance.

5.4 Experimental Section

Synthesis of Polyesters PE12.12-SO3H-x and PE18.18-SO3H-x

Different polymers were synthesized according to the same synthesis procedure, where the molar amount of dimethyl sulfosuccinic acid (HMSS) was varied (as listed in Table 5.6). The total amount of diester/diacid (HMSS and 1,18-dodecanediacid, abbreviated as C_{18}-diacid) accounts for one equivalent with respect to the used 1,18-dodecanediol (abbr. C_{18}-diol).

Table 5.6 Molar feed ratio in polycondensation reactions of PE12.12-SO3H-x and PE18.18-SO3H-x.

	diol	diacid	HMSS
PE12.12	1.00	1.00	0.00
PE12.12-SO3H-1.0	1.00	0.99	0.01
PE18.18	1.00	1.00	0.00
PE18.18-SO3H-0.5	1.00	0.995	0.005
PE18.18-SO3H-0.8	1.00	0.992	0.008
PE18.18-SO3H-1.0	1.00	0.99	0.01

For the synthesis of PE18.18-SO_3H_x, 1,18-octadecanediol (10.00 g, 34.90 mmol, 1.00 eq.), dimethyl sulfosuccinic acid and 1,18-octadecanedioic acid were weighed into a 250 mL round bottom flask equipped with a distillation bridge and a collecting flask. To stir the mixture, an elliptical PTFE coated stir bar with a lanthanide magnetic core was used. The reaction mixture was heated to 145 °C and stirred at 350 rpm in a 250 mL sandwich-type aluminum block, so that the flask was heated up to the top. The collecting flask was cooled with liquid nitrogen and connected to a membrane pump. Within 3 hours, the pressure was gradually reduced from 900 mbar to 50 mbar, upon which the viscosity increased significantly. The stirring speed was reduced at the same time, until the stir bar no longer moved. The membrane pump was replaced by an oil pump, and vacuum (5×10^{-3} mbar) was applied for another 2 h.

The obtained polymer was isolated by scratching from the flask in the melt state.

The same procedure was followed for polycondensation of PE12.12-SO_3H, with 1,12-dodecanediol (13 g, 64.26 mmol, 1.00 eq.), HMSS and 1,12-dodecanedioic acid.

All polymers containing sulfonic acid were stored in a glovebox under a nitrogen atmosphere.

PE12.12 ^{1}H NMR (400 MHz, $C_2D_2Cl_4$, 323 K) δ[ppm] = 4.11 (t, $^{3}J_{HH}$ = 6.7 Hz, H-4 and H-4‘), 3.74 and 3.71 (s, E3 and E3’), 3.67 (t, $^{3}J_{HH}$ = 6.5 Hz, E1), 2.66 (s, H-5), 2.39 (t, $^{3}J_{HH}$ = 7.4 Hz, E2), 2.33 (t, $^{3}J_{HH}$ = 7.4 Hz, H-1), 1.79 – 1.60 (m, H-2 and H-2‘), 1.56 – 1.31 (m, H-3).

PE12.12-SO3H-1.0 ^{1}H NMR (400 MHz, $C_2D_2Cl_4$, 323 K) δ[ppm] = 4.45 (dd, $^{3}J_{HH}$ = 10.5, 4.2 Hz, H-6), 4.31 (t, $^{3}J_{HH}$ = 6.7 Hz, H-7) 4.28 – 3.82 (m, H-4), 3.69 & 3.67 (s, E3 and E3‘), 3.63 (t, $^{3}J_{HH}$ = 6.6 Hz, E1), 3.39 (t, $^{3}J_{HH}$ = 6.7 Hz, S1), 3.26 (dd, $^{3}J_{HH}$ = 17.3, 10.5 Hz, H-5), 3.07 (dd, $^{3}J_{HH}$ = 17.3, 4.2 Hz, H-5), 2.36 (t, $^{3}J_{HH}$ = 7.4 Hz, E2), 2.30 (t, $^{3}J_{HH}$ = 7.5 Hz, H-1), 1.70 – 1.54 (m, H-2 and H-2‘), 1.42 – 1.20 (m, H-3).

PE18.18-SO3H-0.8 ^{1}H NMR (500 MHz, $C_2D_2Cl_4$, 323 K) δ[ppm] = 4.45 (dd, $^{3}J_{HH}$ = 10.6, 4.0 Hz, H-6), 4.31 (t, $^{3}J_{HH}$ = 6.8 Hz, H-7), 4.27 – 3.85 (m, H-4), 3.68 (s, E3 & E3‘), 3.63 (t, $^{3}J_{HH}$ = 6.6 Hz, E1), 3.40 (t, $^{3}J_{HH}$ = 6.6 Hz, S1), 3.26 (dd, J = 17.4, 10.6 Hz, H-5), 3.07 (dd, J = 17.4, 4.0 Hz, H-5), 2.38 (t, $^{3}J_{HH}$ = 7.4 Hz, E2), 2.46 – 2.14 (m, H-1), 1.71 – 1.53 (m, H-2 and H-2‘), 1.51 – 1.11 (m, H-3).

Synthesis of Polyesters PE12.12-SO3M (M = Mg^{2+}, Ca^{2+}, Zn^{2+})

For the synthesis of PE12.12-SO_3M, the same polycondensation procedure as for PE12.12-SO_3H was followed. A reaction scale of 50.00 g 1,12-dodecanediol (247 mmol, 1.00 eq.), 56.34 g 1,18-dodecanedioic acid (245 mmol, 0.99 eq.) and 0.56 g HMSS (2.5 mmol, 0.01 eq.) was used. When the melt viscosity reached a limit where no more melt flow was observed, the polymer was dissolved in xylene (250 mL) at 130 °C. After a homogeneous solution was obtained, the batch was divided into 3 parts (by weight). To each aliquot, a solution of zinc, calcium or magnesium stearate in xylene (50 mL) was added, respectively (3.71 mmol, 0.015 eq.). The mixtures were stirred for 10 min and precipitated in cold ^{i}PrOH (-30 °C). After filtration, the polymers were washed with acetone and dried in a vacuum drying oven for 3 days.

PE12.12-SO3Mg ^{1}H NMR (500 MHz, $C_2D_2Cl_4$, 323 K) δ[ppm] = 4.45 (dd, $^{3}J_{HH}$ = 10.5, 4.2 Hz, H-6), 4.34 – 3.87 (m, H-4), 3.67 (s, *end groups* E3 & E3’), 3.63 (t, $^{3}J_{HH}$ = 6.7 Hz, *end group* E1), 3.39 (t, $^{3}J_{HH}$ = 6.7 Hz, H-7), 3.26 (dd, $^{3}J_{HH}$ = 17.3, 10.5 Hz, H-5), 3.07 (dd, $^{3}J_{HH}$ = 17.3, 4.2 Hz, H-5), 2.32 (t, $^{3}J_{HH}$ = 5.4 Hz, *stearate* S1 and *end group* E2), 2.30 (t, $^{3}J_{HH}$ = 7.6 Hz, H-1), 1.68 – 1.58 (m, H2 & H2’), 1.40 – 1.25 (m, H-3), 0.91 (t, $^{3}J_{HH}$ = 6.8 Hz, *stearate* S2).

PE12.12-SO3Ca ^{1}H NMR (500 MHz, $C_2D_2Cl_4$, 323 K) δ[ppm] = 4.45 (dd, $^{3}J_{HH}$ = 10.5, 4.2 Hz, H-6), 4.35 – 3.87 (m, H-4), 3.67 (s, *end groups* E3 & E3’), 3.63 (t, $^{3}J_{HH}$ = 6.6 Hz, *end group* E1), 3.39 (t, $^{3}J_{HH}$ = 6.6 Hz, H-7), 3.26 (dd, $^{3}J_{HH}$ = 17.3, 10.5 Hz, H-5), 3.07 (dd, $^{3}J_{HH}$ = 17.3, 4.2 Hz, H-5), 2.37 (t,

$^{3}J_{HH}$ = 5.4 Hz, *stearate* S1 and *end group* E2), 2.30 (t, $^{3}J_{HH}$ = 7.5 Hz, H-1), 1.68 – 1.57 (m, H2 & H2'), 1.41 – 1.24 (m, H-3), 0.91 (t, $^{3}J_{HH}$ = 6.4 Hz, *stearate* S2).

PE12.12-SO3Zn ^{1}H NMR (500 MHz, $C_2D_2Cl_4$, 323 K) δ [ppm] = 4.44 (dd, $^{3}J_{HH}$ = 10.2, 4.3 Hz, H-6), 4.35 – 3.87 (m, H-4), 3.67 (s, end groups E3 & E3'), 3.63 (t, $^{3}J_{HH}$ = 6.7 Hz, end group E1), 3.39 (t, $^{3}J_{HH}$ = 6.7 Hz, H-7), 3.26 (dd, $^{3}J_{HH}$ = 16.8, 10.2 Hz, H-5), 3.06 (dd, $^{3}J_{HH}$ = 16.8, 4.3 Hz, H-5), 2.37 (t, $^{3}J_{HH}$ = 7.8 Hz, *stearate* S1 and *end group* E2), 2.35 – 2.23 (m, H-1), 1.70 – 1.55 (m, H2 & H2'), 1.41 – 1.23 (m, H-3), 0.91 (t, $^{3}J_{HH}$ = 6.8 Hz, *stearate* S2).

Synthesis of Polyesters PE18.18-SO3M (M = Mg^{2+}, Ca^{2+}, Zn^{2+})

For the synthesis of PE18.18-SO_3M, the same polycondensation procedure as for PE18.18-SO_3H was followed. A reaction scale of 45 g 1,18-octadecanediol (157 mmol, 1.00 eq.), 49.00 g 1,18-octadecanedioic acid (156 mmol, 0.992 eq.) and 0.28 g HMSS (1.3 mmol, 0.008 eq.) was used. When the viscosity reached a limit where no more melt flow was observed, the polymer was dissolved in xylene (350 mL) at 130 °C. After a homogeneous solution was obtained, the batch was divided into 3 parts (by weight). To each aliquot, a solution of zinc, calcium or magnesium stearate in xylene (50 mL) was added, respectively (1.3 mmol, 0.008 eq.). The mixtures were stirred for 10 min and precipitated in cold ^{i}PrOH (-30 °C). After filtration, the polymers were washed with acetone and dried in a vacuum drying oven for 3 days.

PE18.18-SO3Mg ^{1}H NMR (500 MHz, $C_2D_2Cl_4$, 323 K) δ [ppm] = 4.45 (dd, $^{3}J_{HH}$ = 10.5, 4.2 Hz, H-6), 4.3 – 3.89 (m, H-4), 3.70 & 3.68 (s, *end groups* E3 & E3'), 3.63 (t, $^{3}J_{HH}$ = 6.7 Hz, *end group* E1), 3.39 (t, $^{3}J_{HH}$ = 6.7 Hz, H-7), 3.26 (dd, $^{3}J_{HH}$ = 17.3, 10.5 Hz, H-5), 3.07 (dd, $^{3}J_{HH}$ = 17.3, 4.2 Hz, H-5), 2.38 (t, $^{3}J_{HH}$ = 6.7 Hz, *stearate* S1 and *end group* E2), 2.30 (t, $^{3}J_{HH}$ = 7.5 Hz, H-1), 1.70 – 1.55 (m, H 2 & H2'), 1.41 – 1.17 (m, H-3), 0.91 (t, , $^{3}J_{HH}$ = 6.8 Hz, *stearate* S2).

PE18.18-SO3Ca ^{1}H NMR (500 MHz, $C_2D_2Cl_4$, 323 K) δ [ppm] = 4.45 (dd, $^{3}J_{HH}$ = 10.5, 4.1 Hz, H-6), 4.33 – 3.88 (m, H-4), 3.70 & 3.68 (s, *end groups* E3 & E3'), 3.63 (t, $^{3}J_{HH}$ = 6.7 Hz, end group E1), 3.39 (t, $^{3}J_{HH}$ = 6.7 Hz, H-7), 3.26 (dd, 3JHH = 17.3, 10.5 Hz, H-5), 3.07 (dd, $^{3}J_{HH}$ = 17.3, 4.1 Hz, H-5), 2.36 (t, $^{3}J_{HH}$ = Hz, *stearate* S1 and *end group* E2), 2.30 (t, $^{3}J_{HH}$ = 7.5 Hz, H-1), 1.69 – 1.57 (m, H2 & H2'), 1.40 – 1.18 (m, H-3), 0.91 (t, $^{3}J_{HH}$ = 6.8 Hz, *stearate* S2).

PE18.18-SO3Zn ^{1}H NMR (500 MHz, $C_2D_2Cl_4$, 323 K) δ [ppm] = 4.45 (dd, $^{3}J_{HH}$ = 10.4, 4.1 Hz, H-6), 4.36 – 3.86 (m, H-4), 3.70 & 3.68 (s, *end groups* E3 & E3'), 3.63 (t, $^{3}J_{HH}$ = 6.7 Hz, *end group* E1), 3.40 (t, $^{3}J_{HH}$ = 6.7 Hz, H-7), 3.26 (dd, $^{3}J_{HH}$ = 17.5, 10.4 Hz, H-5), 3.07 (dd, $^{3}J_{HH}$ = 17.5, 4.1 Hz, H 5), 2.37

(t, $^3J_{HH}$ = 7.6 Hz, *stearate* S1 and *end group* E2), 2.30 (t, $^3J_{HH}$ = 7.5 Hz, H-1), 1.68 – 1.57 (m, H2 & H2'), 1.42 – 1.21 (m, H-3), 0.91 (t, $^3J_{HH}$ = 6.8 Hz, *stearate* S2).

Synthesis of Reference Composites Polyesters PE12.12-$M_{stearate}$ ($M = Mg^{2+}$, Ca^{2+}, Zn^{2+})

For the synthesis of PE12.12-$M_{stearate}$, 1,12-dodecanediol (50.00 g, 247 mmol, 1.00 eq.), 1,12-dodecanedioic acid (56.35 g, 247 mmol, 1.00 eq.) and dimethyl succinate (0.36 g, 2.47 mmol, 0.01 eq.) were weighed into a 1 L round bottom flask equipped with a distillation bridge and a collecting flask. The reaction mixture was degassed, and the collecting flask cooled with liquid nitrogen. To stir the mixture, an elliptical PTFE coated stir bar with a lanthanide magnetic core was used. The reaction mixture was heated to 145 °C and stirred at 350 rpm in a 250 mL sandwich-type aluminum block, so that the flask was heated up to the top. When a homogeneous melt was obtained, the catalyst [$Ti(O^nBu)_4$] (0.25 g, 0.74 mmol, 3 mol%) was added and the collecting flask was connected to a membrane pump. Within 3 hours, the pressure was gradually reduced from 900 mbar to 50 mbar, upon which the viscosity increased significantly. The stirring speed was reduced at the same time, until the stir bar no longer moved. The membrane pump was replaced by an oil pump (5×10^{-3} mbar), which was applied for 36 h, until a sufficiently high melt viscosity was reached. The polymer was dissolved in xylene (200 mL) at 130 °C until a homogeneous solution as obtained. The batch was divided into 3 equally sized parts by weight, and to each part, a solution of zinc, calcium or magnesium stearate in xylene (50 mL) was added (3.7 mmol, 0.015 eq.). The mixtures were stirred for 10 min at 130 °C and precipitated in cold ^{i}PrOH (-30 °C). After filtration, the polymers were washed with acetone and dried in a vacuum drying oven for 3 days.

PE12.12-$Mg_{stearate}$ ^{1}H NMR (500 MHz, $C_2D_2Cl_4$, 323 K) δ [ppm] = 4.06 (t, $^3J_{HH}$ = 6.8 Hz, H-4 & H-4'), 3.71 & 3.67 (s, *end groups* E3 & E3'), 3.63 (t, $^3J_{HH}$ = 6.6 Hz, *end group* E1), 2.63 & 2.62 (s, H-5) 2.36 (t, $^3J_{HH}$ = 7.2 Hz, *stearate* S1 and *end group* E2), 2.30 (t, $^3J_{HH}$ = 7.5 Hz, H-1), 1.68 – 1.58 (m, H2 & H2'), 1.40 – 1.25 (m, H-3), 0.91 (t, $^3J_{HH}$ = 6.8 Hz, *stearate* S2).

PE12.12-$Ca_{stearate}$ ^{1}H NMR (500 MHz, $C_2D_2Cl_4$, 323 K) δ [ppm] = 4.06 (t, $^3J_{HH}$ = 6.8 Hz, H-4 & H-4'), 3.71 & 3.67 (s, *end groups* E3 & E3'), 3.63 (t, $^3J_{HH}$ = 6.6 Hz, *end group* E1), 2.63 & 2.62 (s, H-5) 2.36 (t, $^3J_{HH}$ = 7.2 Hz, *stearate* S1 and *end group* E2), 2.30 (t, $^3J_{HH}$ = 7.5 Hz, H-1), 1.68 – 1.58 (m, H2 & H2'), 1.40 – 1.25 (m, H-3), 0.91 (t, $^3J_{HH}$ = 6.8 Hz, *stearate* S2).

PE12.12-Zn$_{stearate}$ ^{1}H NMR (500 MHz, $C_2D_2Cl_4$, 323 K) δ [ppm] = 4.06 (t, $^3J_{HH}$ = 6.8 Hz, H-4 & H-4'), 3.71 & 3.67 (s, *end groups* E3 & E3'), 3.63 (t, $^3J_{HH}$ = 6.6 Hz, *end group* E1), 2.63 & 2.62 (s, H-5) 2.36 (t, $^3J_{HH}$ = 7.2 Hz, *stearate* S1 and *end group* E2), 2.30 (t, $^3J_{HH}$ = 7.5 Hz, H-1), 1.68 – 1.58 (m, H2 & H2'), 1.40 – 1.25 (m, H-3), 0.91 (t, $^3J_{HH}$ = 6.8 Hz, *stearate* S2).

Processing Conditions

All polymers were processed in a micro-compounder to homogenize the polymer melt and were subsequently injection-moulded into test specimens for tensile testing (ISO 527-2, type 5A; *cf.* section 5.5, Materials and Methods). At least 5 test specimens were prepared for each polymer. The temperature of the micro-compounder (T_{melt}) and of the injection mould (T_{mould}) were set to different values depending on the nature of the polymer. An overview of the processing conditions is listed in Table 5.7. The stirring speed was set to 10 rpm and the mixing time before the first extrusion to homogenize the melt was 10 min in all cases.

Table 5.7 Conditions for processing of the ion-containing polyesters PE12.12 and PE18.18.

	T_{melt} [°C]	T_{mould} [°C]
PE12.12-SO_3H-x	160	55
PE18.18-SO_3H-x	180	60
PE18.18-SO_3M-x	160	55
PE18.18-SO_3M-x	180	60

Film drawing employed a micro-cast film line, with varying speed of the film line to obtain different film thicknesses. A film drawing was possible with all polymers PE12.12-SO3M and PE18.18-SO3M, as well as with the reference polymers PE12.12, PE18.18 and HDPE. For PE12.12-M$_{stearate}$, films were only possible to draw for PE12.12-Mg$_{stearate}$ and PE12.12-Ca$_{stearate}$. The melt viscosity of PE12.12-Zn$_{stearate}$ was too low, and no continuous film could be drawn.

Recycling to monomer

For the recycling to monomer of PE18.18-SO_3H-1.0, a stainless-steel reactor with a glass inlet (total volume of 20 mL) was charged with 200 mg of injection moulded specimen and methanol (8 mL, > 99.8 % purity) as well as a stir bar. The reaction mixture was heated to 150 °C for 6 days and stirred at 300 rpm, upon which a pressure of 12 bar developed. After cooling to room temperature without further stirring, a crystallized solid was obtained. The supernatant was

removed, and methanol (5 mL) was added. The mixture was heated to reflux until a clear solution was obtained and subsequently was cooled to 4 °C. The crystallized solid was centrifuged off, washed with methanol and dried. A 1:0.99 mixture of C_{18}-diol:C_{18}-diester was obtained according to the ^{1}H NMR spectrum (*cf.* appendix, section 5.6.12, Figure 5.71) in 80 % yield.

5.5 Materials and Methods

Sodium dimethyl sulfosuccinate (SMSS) was synthesized according to a reported procedure.[51] Dimethyl sulfosuccinic (HMSS) acid was synthesized from SMSS by ion exchange using Amberlyst IR-120H in water. 1,12-Dodecanedioic acid and 1,12-dodecanediol were obtained from tci. 1,18-Octadecanedioic acid was purchased from Elevance Renewable Sciences. 1,18-Octadecanediol was synthesized according to a previously reported procedure.[39] The catalysts DBTO and [Ti(O^{n}Bu)$_4$] and the ion exchange resin (Amberlyst IR-120H) were purchased from Merck. Xylene (isomeric mixture, ≥99%) was obtained from Carl Roth. *Iso*-propanol and acetone used for the precipitation and washing procedure of the polymers were used in technical grade.

Deuterated NMR solvents were supplied by Eurisotop.

NMR spectra were recorded on a Bruker Avance III HD 400 spectrometer using Bruker TopSpin (version 3.6.2) for data acquisition, or a JEOL ECZ500R spectrometer using JEOL Delta (version 5.3) for data aquisition. ^{1}H NMR signals were referenced to the residual solvent signals. Data evaluation was conducted with MestReNova software by Mestrelab Research SL (version 14.2.0).

Molecular weights of the polymers containing metal counterions (PEx.x-SO_3M with M = Na, Mg, Ca, Zn) were determined by gel permeation chromatography on a SECcurity^2 GPC System from PSS with chloroform as solvent at 35 °C and a flow rate of 1 mL/min, using a PSS SDV linear M column and a refractive index detector. The determination of the molecular weight was performed with a linear calibration against narrow polystyrene standards, obtained from Varian. Analysis was carried out using WinGPC UniChrom software (version 8.30).

For differential scanning calorimetry, a Netsch DSC 204 F1 with a heating rate of 10 K/min was used. All data reported are from the second heating cycles, unless stated otherwise. Three heating/cooling cycles were performed to ensure the reversibility of the curves and the stability of the polymers in the respective temperature window. Data were evaluated using NETZSCH Proteus Thermal Analysis software (version 6.1.0). Thermogravimetric analysis (TGA) was performed on a Netzsch STA 429 F3 Jupiter. All measurements were performed with 80 mL/min flowrate and a heating rate of 10 °C/min. For measurements under air, a synthetic 80:20 mixture of N_2:O_2 was used. Samples were dried in a vacuum drying oven for at least 48 h (5 mbar, 50 °C) prior to measurements.

X-ray scattering measurements were performed with a Bruker D8 Avance X-ray diffractometer with scintillation counter, Bruker D8 Discover. As a Cu-K_α source, a Bruker IμS Diamond was used. As a detector, a Vantec-500 or a Lynxeye XE-T was used. Measured samples were either taken from injection molding to relate the results to the tensile properties, or were cooled in DSC pans from 200 °C to room temperature with a rate of 10 °C/min.

Crystallinities were determined from orthorhombic reflexes (110) and (200) and the amorphous halo in WAXS spectra, with $\chi = [A_c(110) + A_c(200)]/[A_c(110) + A_c(200) + A_a]$; A_c being the area of the respective orthorhombic Bragg reflections and A_a the area of the amorphous halo.[103] As fitting function, a Voigt fit was used.

For tensile testing, polymers were processed in a micro compounder (Xplore MC 5). The melt was filled into a micro-injection-moulding machine (Xplore IM 5.5). The temperature of the cylinder and mould was varied (details can be found in section 5.4). An injection pressure of 16 bar (10 s) and 12 bar (15 s) was applied. Tensile tests were performed on a Zwick /005/1446 Retroline tC II instrument, with a crosshead speed of 5 mm/min (ISO 527-2, type 5A). To determine the Young's modulus, a crosshead speed of 1 mm/min was applied. All samples were stored at room temperature for 24 h before tensile tests were performed. For data evaluation, Zwick Roell testXpert software version 11.0 was used.

To determine the water contact angle, samples were taken from injection moulded specimens and washed with *iso*-propanol to remove impurities from the surface. They were measured after storage in a vacuum drying oven for 3 days (50 °C, 50 mbar). The contact angle of a sessile drop of Milli-Q water was determined with a Krüss DSA25 drop shape analyzer using KRÜSS ADVANCE software for data evaluation (version 1.8.0.4).

Rheologic measurements were taken on an ARES-G2 rheometer (TA instruments) using either 13 mm or 8 mm parallel plates made of Invar. All measurements were taken with an ARES-G2 Forced Convection Oven and flushed with nitrogen during the measurements. Oscillation strain sweeps (γ_0 = 0.1 – 100%) at an angular frequency of 100 rad/s were performed at 140 °C to determine the linear viscoelastic regime, followed by oscillatory frequency sweeps at 150 and 180 °C and a temperature ramp. For the frequency sweeps, a strain amplitude of γ_0 = 10 % was applied. For the temperature ramp, a rate of 10 °C/min was applied from 80 to 180 °C with a strain amplitude of γ_0 = 0.1 %. The master curves for PE18.18-SO_3M derivatives were obtained by shifting G' (storage modulus) and G'' (loss modulus) to 180 °C as a reference

temperature (by making use of the time-temperature superposition principle). For data acquisition and evaluation, TRIOS software (version 5.5.1.5) was used.

Infrared (IR) spectra were measured on a Perkin Elmer 100 FT-IR spectrometer with an attenuated total reflection (ATR) unit and analyzed with the software Perkin Elmer Inc. (version 6.2.0).

For the water uptake study of PE12.12-SO3H and PE18.18-SO3H, injection moulded specimens were immersed in MilliQ water (10 mL). They were weighed on a Sartorius ME36S balance (error: 1 µg). Samples were patted dry, weighed and re-immersed in water between individual measurements. This was repeated until three values were obtained with a deviation of less than 10 µg. A mean value of these three measurements was taken for the data evaluation.

For printing on films, an ink-jet printer Canon Pixma TS705 with ink cartridges IC-Office XXL was used. Only the blue color of the cartridge was used, the other printer cartridges were masked to ensure no leakage of their color and to prevent color mixing. The printing was performed on films which were produced with a micro-cast film line. The thicknesses of the films ranged from 50 to 100 µm. The respective films were attached to a Sellotape line on a sheet of paper before introduction to the printer. The logo of the University of Konstanz was printed on the film in blue color. After printing, the films were dried for 24 hours in a drying cabinet at 50 °C. A microfiber cloth was used to wipe the film with even pressure. Similar pressure was applied on the samples to wipe away the design on the films.

5.5.1 Determination of DP_n and M_n

The degree of polymerization (DP_n) and the number weighted molecular weight (M_n) of the PE12.12-SO_3H-x and PE18.18-SO_3H-x materials were determined by end group analysis from ^{1}H NMR spectra.

A signal of the backbone of the oligomethylene segment (B, multiplet at 4.27 – 3.87 ppm) was integrated and referenced to 100H. The end group signals for the hydroxymethyl group (E1, 2H, triplet at 3.63 ppm), the methyl ester (E3 and E3', 3H, singlet at 3.68 ppm) and the acid end group (E2, 2H, triplet at 2.38 ppm) were integrated. In case of the acid end group, the integral cannot be taken directly due to a strong overlap of the signal with the backbone signal H-1. Therefore, only the most downfield shifted and best isolated line of the triplet was integrated and multiplied by a factor of 4. All end groups are assigned representatively for PE18.18-SO3H-1.0 in Figure 5.16.

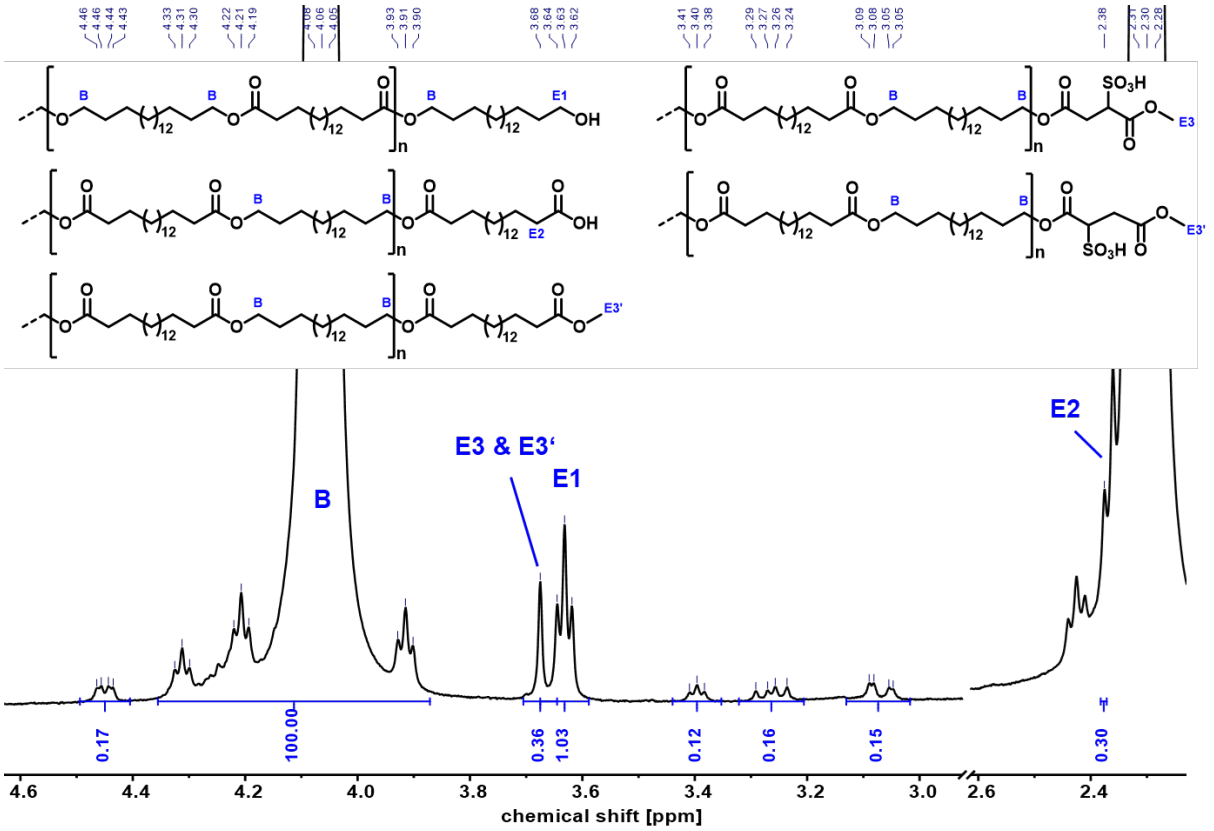

Figure 5.16 Detailed section of ^{1}H NMR spectra (500 MHz, 323 K, $C_2D_2Cl_4$) of PE18.18-SO3H-1.0 with end group assignment for calculation of the DP_n. Note that the repeat unit can also contain sulfosuccinate units instead of C_{18}-diester units.

The DP_n was calculated according to

$$DP_n = \frac{\int Backbone\ (\mathrm{B})}{\frac{\int E1}{2} + \frac{\int E2}{2} + \frac{\int E3\ \&\ E3'}{3}} + 1 = \frac{100}{\frac{\int E_1}{3} + \frac{\int E_2}{2} + \frac{\int E3\ \&\ E3'}{3}} + 1$$

and the number weighted molecular weights (M_n) were calculated from the DP_n and the molecular weight of the repeat unit (M_{rep})

$$M_n = M_{rep} \times \frac{DP_n}{2}$$

Since the molecular weight differences of the two co-polymer repeating units (C_{18}-diol & C_{18}-diester, or C_{18}-diol & sulfosuccinic acid) are small (PE12.12-SO_3H-x: 397 g/mol *vs.* 364 g/mol; PE18.18-SO_3H-x: 551 g/mol *vs.* 449 g/mol) and the amounts of sulfonic acid repeating units are low, the molecular weights M_n were calculated from M_{rep} of the non-ionic PE12.12 or PE18.18 polymer repeating unit, respectively.

The respective integrals and calculated values are listed in Table 5.8.

Table 5.8 Calculation of the DP_n and the M_n of PE12.12-SO_3H-x and PE18.18-SO_3H-x polymers from the end group integrals as obtained from ^1H NMR spectra. The integrals of the end groups are referenced to the backbone signal (B), being fixed to 100H.

	∫CH_2OH (E1)	∫CH_2COOH (E2)	∫$COOCH_3$ (E3 & E3')	DP_n	M_n [kg/mol]
PE12.12	0.46	1.12	0.08	123	24.4
PE12.12-SO3H-1.0	0.79	1.08	0.39	95	17.3
PE18.18	1.13	0.00	1.82	86	23.8
PE18.18-SO3H-0.5	1.02	1.28	0.17	84	23.1
PE18.18-SO3H-0.8	0.84	1.20	0.31	90	24.8
PE18.18-SO3H-1.0	1.03	1.20	0.36	82	22.6

5.5.2 Estimation of the -SO_3H Content

The successful incorporation of HMSS into the polymer was verified by ^1H NMR spectroscopy, and an estimation of the incorporated amount of HMSS was performed. The incorporated amount is defined as the molar percentage of repeat units containing sulfosuccinate in the copolymer. The molar input into the reaction mixture is denoted in the polymer nomenclature (PE12.12-SO_3H-1.0 and PE18.18-SO_3H-x, with x = 0.5, 0.8 and 1.0, respectively). The signal of the oligomethylene backbone segment (H-4 and H-7, multiplet at 4.27-3.87 ppm) was integrated and referenced to 400H. A mean value of the three protons corresponding to the HMSS unit (δ = 4.45 ppm, H-6; δ = 3.26 ppm, H-5; δ = 3.07 ppm, H-5) was calculated.

The results are generally lower than the input amounts (PE12.12-SO3H-1.0: 0.64 mol%, PE18.18-SO3H-0.8: 0.57 mol%, PE18.18-SO3H-1.0: 0.64 mol%), and are conclusive within the expected margin of error. Higher input amounts result in higher incorporated amounts, and the signals deriving from the sulfosuccinate units can be identified in all polymer spectra.

Note that for the lowest amount of HMSS input (PE18.18-SO3H-0.5), the estimation of the sulfonic acid content was impeded by the low signal-to-noise ratio.

5.5.3 Simulation of the Sulfonate Distribution

To estimate the amount of sulfonate units per polymer chains, a statistical simulation approach was used as previously established by Wu et al.[151], and applied by Odenwald et al.[152] to acrylate containing vitrimers. The same calculation method and script as described by Odenwald et al. was used herein.

A Schulz-Flory distribution is assumed in these calculations. Note that for simplicity, a Stirling approximation for large factorials was implemented to limit the amount of numerical calculations.

The degree of polymerization and the molar amount of sulfosucccinic acid employed in the synthesis of the PE18.18 SO3H-x polymers was considered. First, a fully statistical incorporation of the sulfosuccinic acid within the polymer chains without any end group enrichment was assumed.

In case of PE18.18-SO_3H-0.8, ~ 62 % of the polymer chains are unfunctionalized. As this material is the basis for the PE18.18-SO3M materials, an alternative simulation under consideration of the end group enrichment of the sulfosuccinate unit was performed. The degree of enrichment was calculated from the evolving methylene signal forming upon the reaction of sulfosuccinate with C_{18}-diol (triplet at 3.40 ppm, H-7).

Note that a full transesterification is assumed for the following calculations, meaning that the methyl ester end groups detected in the ^{1}H NMR spectra are placed to 99.2 % at the C_{18}-dioate and 0.8 % are placed at the sulfosuccinate unit. This assumption supported by the TOCSY results discussed in section 5.2.1, Results and Discussion.

A detailed analysis of the ester groups from ^{1}H NMR spectra is required (see Figure 5.17). The successful esterification of sulfosuccinate with C_{18}-diol is visible from the signal H-7 (3.40 ppm). A full incorporation into the chain would result in a 2-fold integral of H-7 compared to H-5. From the ratio I(H-7)/(2*I(H-5)), the amount of esterification of one end of the sulfosuccinate was calculated. A successful esterification of the other end results in a signal (H-7') that overlaps with the backbone signal (B). A full incorporation is assumed, as this side is much more reactive since the sulfonic acid group is placed in β-position to the reactive ester.

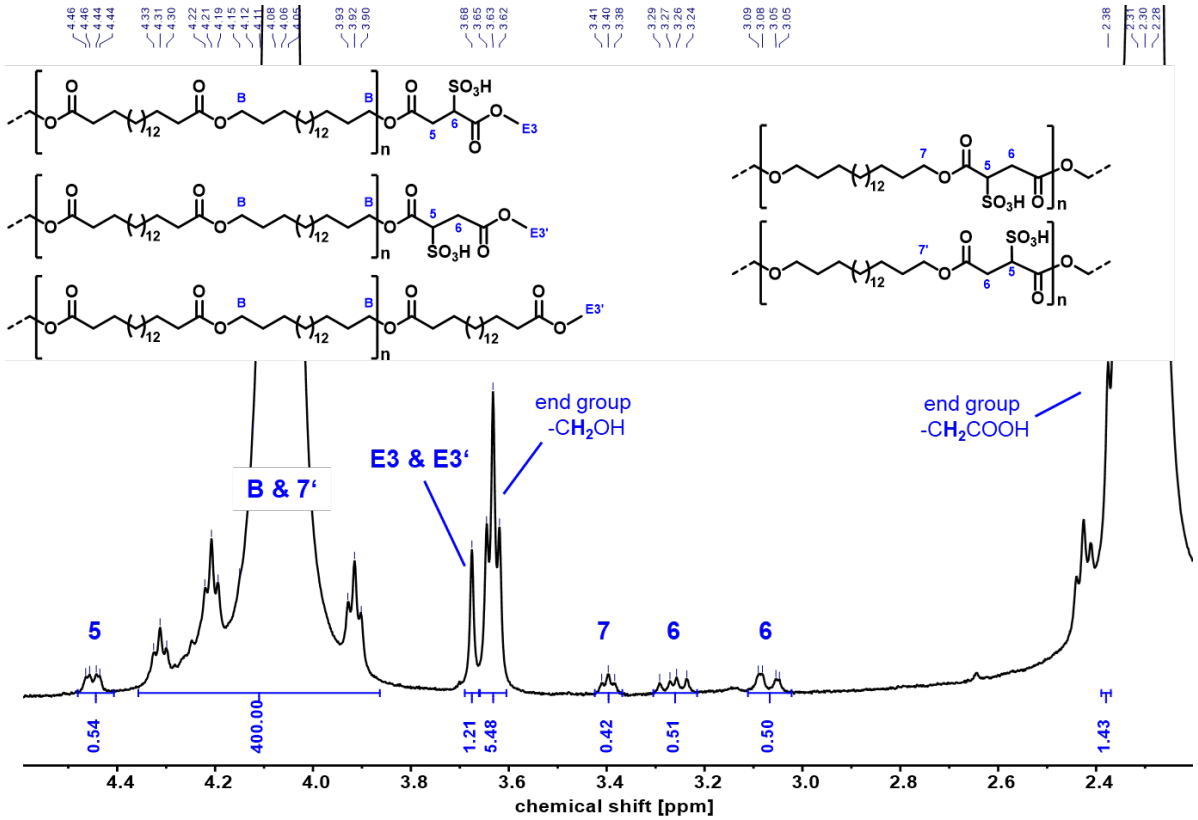

Figure 5.17 ^{1}H NMR spectrum (500 MHz, 323 K, $C_2D_2Cl_4$) of PE18.18-SO3H-0.8 with assignment of the end groups and the signals deriving from the sulfosuccinate unit.

From these incorporations (accounting for a total of 71% incorporation of the sulfosuccinate ester groups), and the total amounts of acid and ester end groups, the probabilities to obtain a sulfonate ester end group was calculated. A value of 6.7 % of the ester and acid end groups were found to derive from the sulfosuccinate. Upon consideration of the probability to find an acid or ester end group rather than an alcohol end group, it was found that 3.7 % of the total amount of end groups are sulfosuccinate end groups.

From this result, the probabilities of zero, one or two sulfosuccinate end groups were calculated according to

$$P_0 = (1\text{-}0.037) \times (1\text{-}0.037)$$

$$P_1 = 2 \times 0.037 \times (1\text{-}0.037)$$

$$P_2 = 0.037 \times 0.037$$

These values were used to calculate the end group enrichment according to the method used by Odenwald et al., the results are shown graphically in Figure 5.18. The probability (p) depending on the number of repeating units (N) and the amount of sulfosuccinate units found in a polymer chain (f).

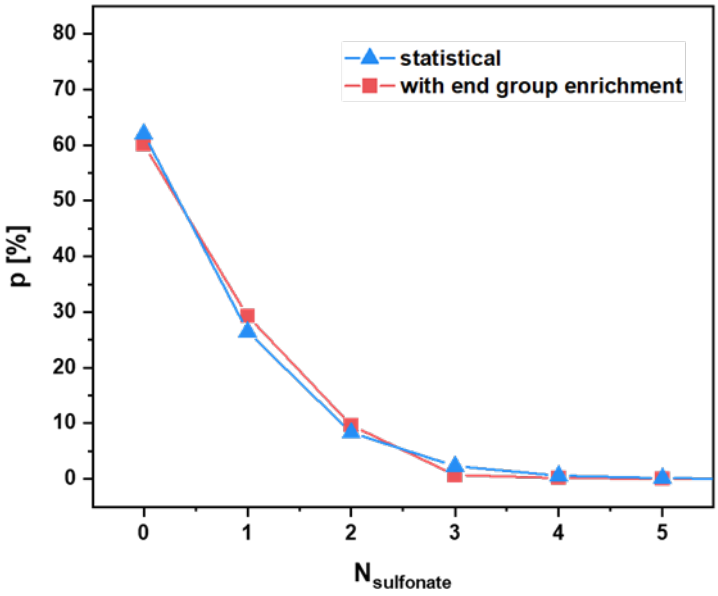

Figure 5.18 Probability of N sulfonate groups per polymer chain with and without consideration of end group enrichment.

5.6 Appendix

5.6.1 GPC traces

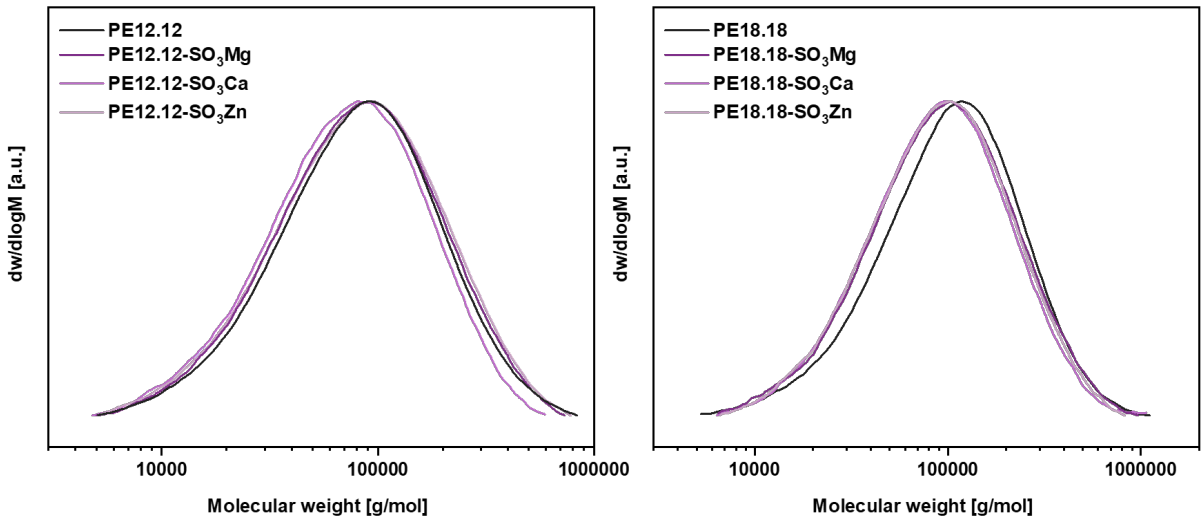

Figure 5.19 GPC traces of PE12.12-SO3M (left) and PE18.18-SO3M (right) and their reference polymers PE12.12 and PE18.18, respectively. Linear calibration against PS standards was applied (chloroform, 35 °C).

Table 5.9 Number average molecular weights (M_n) and polydispersity indexes (Đ) as determined by GPC analysis.

	M_n [kg/mol]	Đ		M_n [kg/mol]	Đ
PE12.12	53	2.2	PE18.18	68	2.1
PE12.12-SO3Mg	52	2.1	PE18.18-SO3Mg	61	2.1
PE12.12-SO3Ca	48	2.0	PE18.18-SO3Ca	61	2.2
PE12.12-SO3Zn	52	2.2	PE18.18-SO3Zn	61	2.1

GPC measurements were performed in chloroform at 35 °C, refractive index detection. Linear calibration against polystyrene applied.

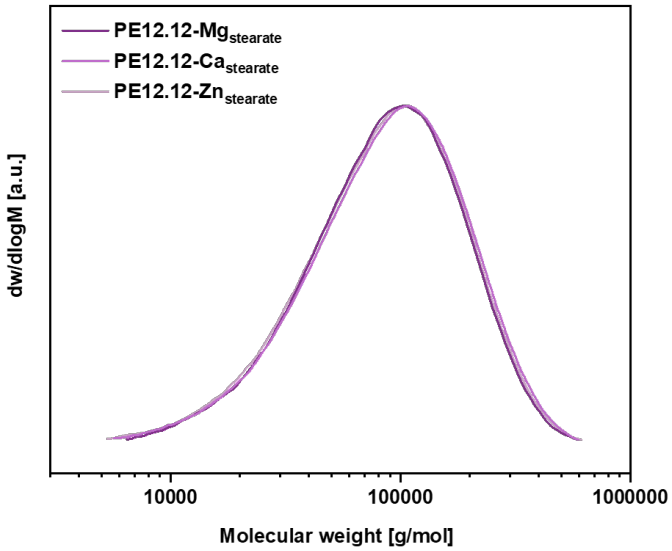

Figure 5.20 GPC traces of PE12.12-$M_{stearate}$. Linear calibration against PS standards was applied (chloroform, 35 °C).

Table 5.10 Number average molecular weights (M_n) and polydispersity indexes (Đ) as determined by GPC analysis.

	M_n [kg/mol]	Đ
PE12.12-$Mg_{stearate}$	60	1.8
PE12.12-$Ca_{stearate}$	60	1.9
PE12.12-$Zn_{stearate}$	58	1.9

GPC measurements were performed in chloroform at 35 °C, refractive index detection. Linear calibration against polystyrene applied.

5.6.2 ATR-IR Spectra

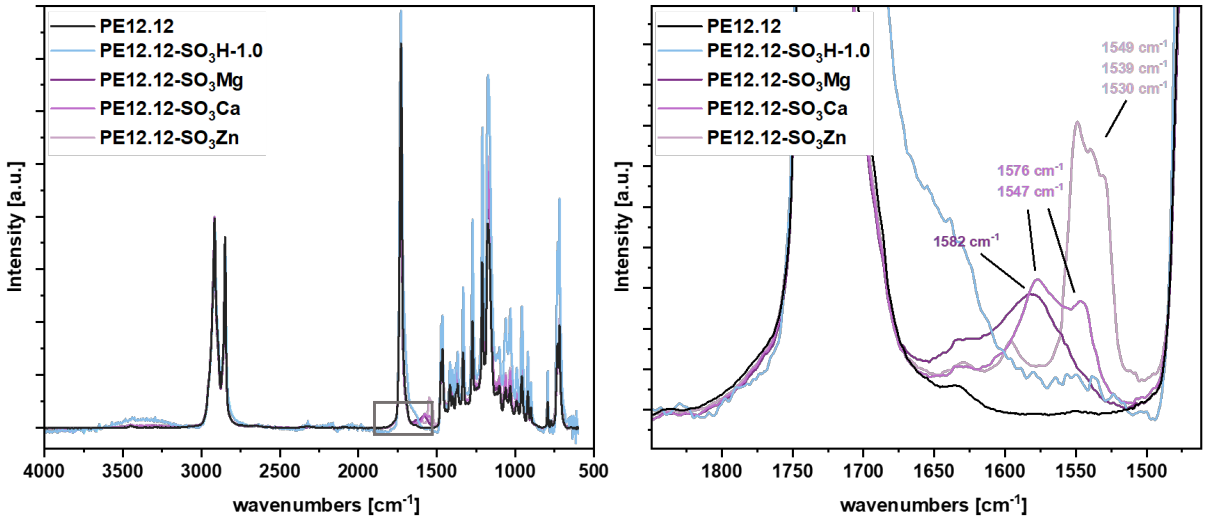

Figure 5.21 ATR-IR spectra of PE12.12, PE12.12-SO3H-1.0 and PE12.12-SO3M. Left graph shows full range; right graph shows the grey marked carbonyl region.

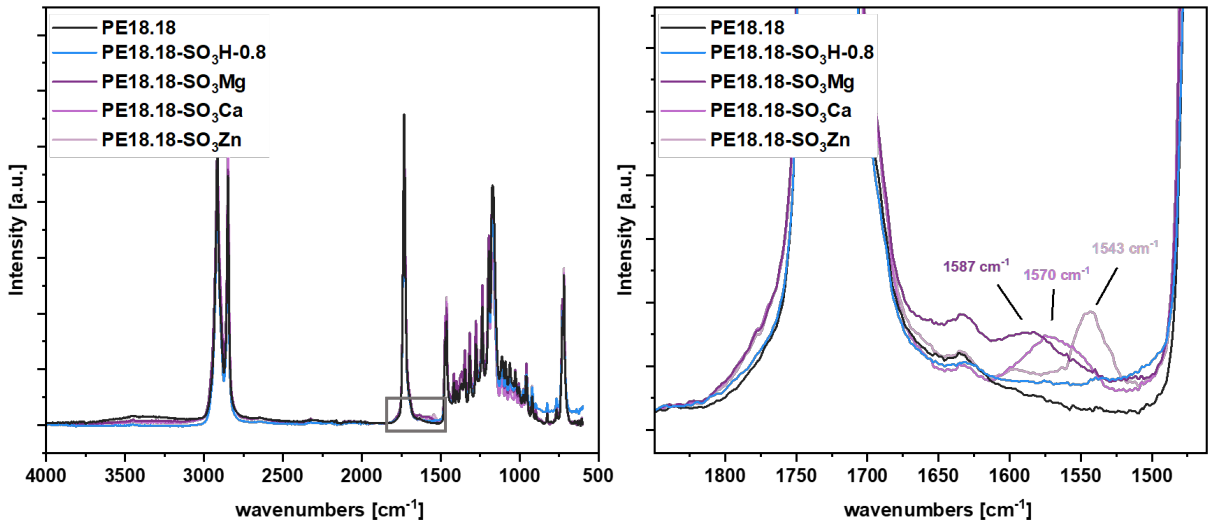

Figure 5.22 ATR-IR spectra of PE18.18, PE18.18-SO3H-0.8 and PE18.18-SO3M. Left graph shows full range; right graph shows the grey marked carbonyl region.

5.6.3 DSC and TGA Thermograms

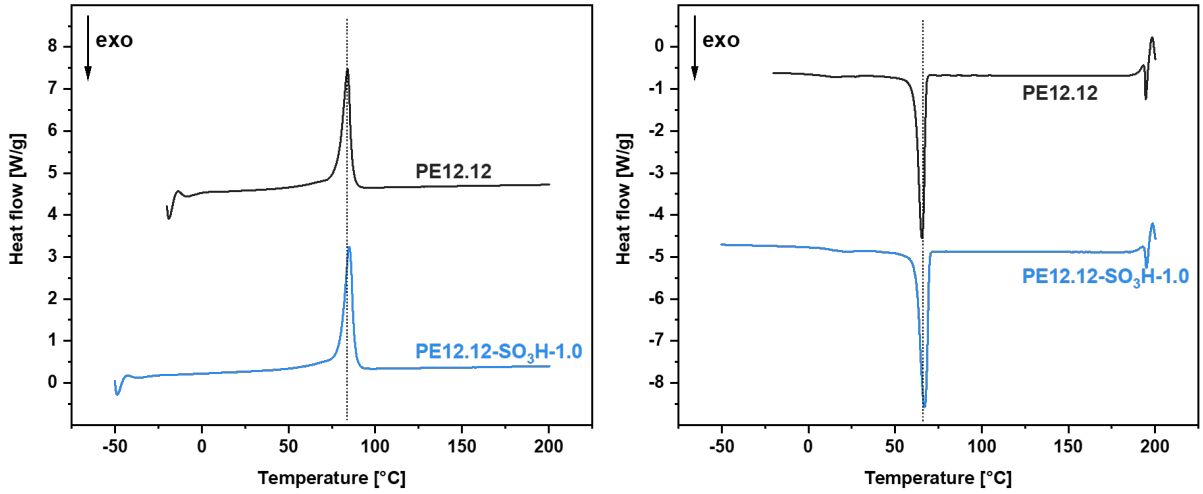

Figure 5.23 DSC thermograms of PE12.12 and PE12.12-SO3H-1.0 upon heating (left) and cooling (right). Data from the second cycle with a heating/cooling rate of 10 °C/min are displayed. Data was shifted vertically for clarity.

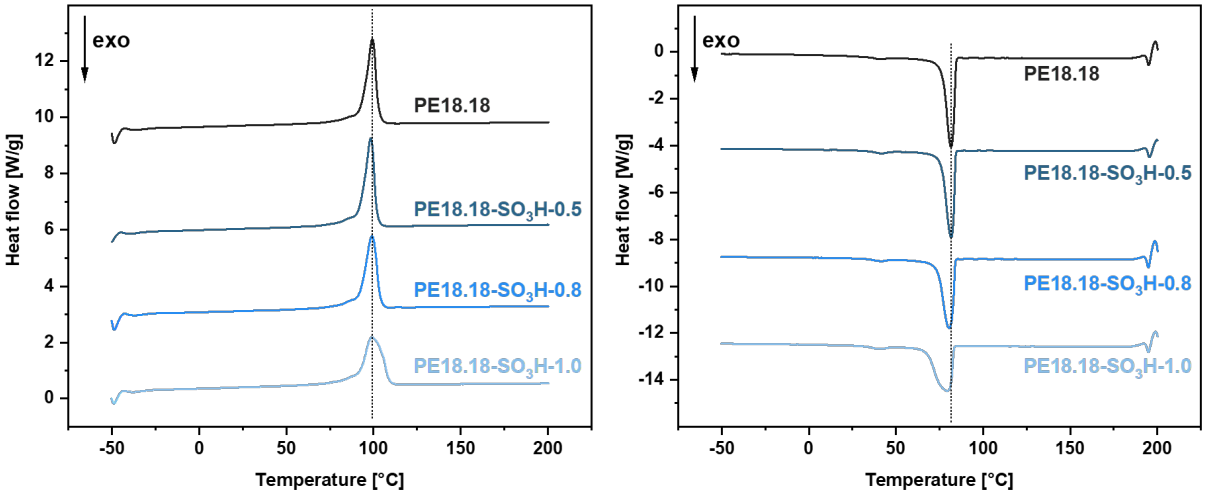

Figure 5.24 DSC thermograms of PE18.18 and PE18.18-SO3H upon heating (left) and cooling (right). Data from the second cycle with a heating/cooling rate of 10 °C/min are displayed. Data was shifted vertically for clarity.

Table 5.11 Thermal properties of PE12.12-SO3H and PE18.18-SO3H derivatives as obtained from DSC measurements. Peak melting temperatures (T_m), enthalpies of fusion (ΔH_m), peak crystallization temperatures (T_c) and enthalpies of crystallization (ΔH_c) are listed. Data were taken from the second heating/cooling cycle (10 K/min heating/cooling rate).

	T_m [°C]	ΔH_m [J/g]	T_c [°C]	ΔH_c [J/g]
PE12.12	84.9	136	66.2	-114
PE12.12-SO3H-1.0	85.0	136	66.9	-126
PE18.18	99.4	145	81.6	-131
PE18.18-SO3H-0.5	98.4	151	81.2	-124
PE18.18-SO3H-0.8	99.1	139	80.4	-124
PE18.18-SO3H-1.0	99.1	142	79.5	-127

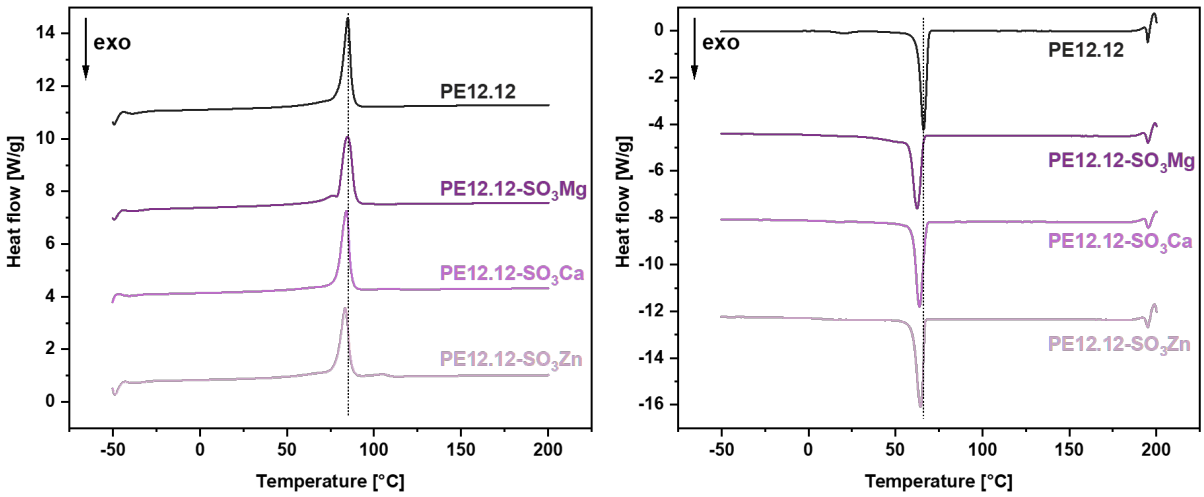

Figure 5.25 DSC thermograms of PE12.12 and PE12.12-SO3M upon heating (left) and cooling (right). Data from the second cycle with a heating/cooling rate of 10 °C/min are displayed. Data was shifted vertically for clarity.

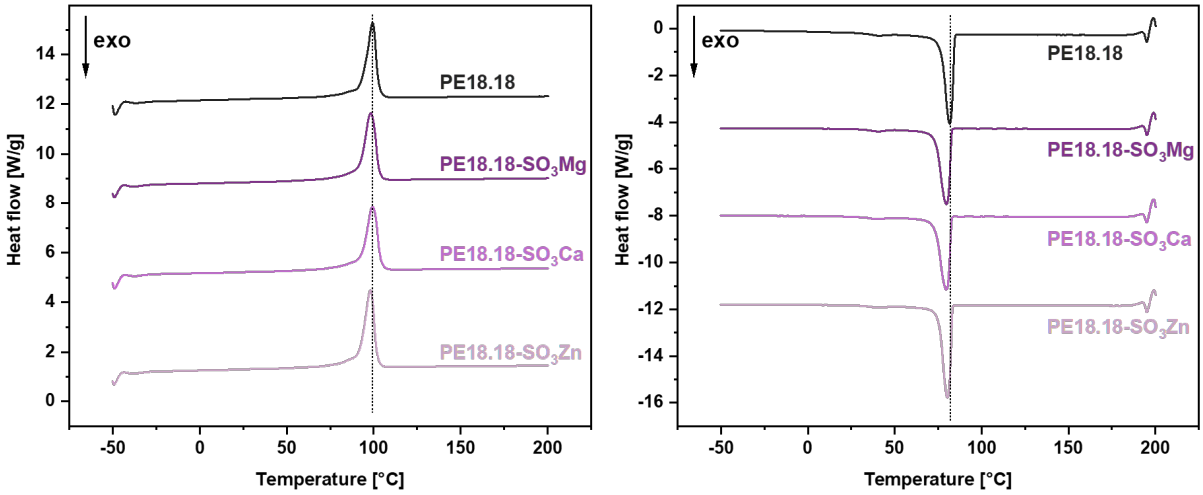

Figure 5.26 DSC thermograms of PE18.18 and PE18.18-SO3M upon heating (left) and cooling (right). Data from the second cycle with a heating/cooling rate of 10 °C/min are displayed. Data was shifted vertically for clarity.

Table 5.12 Thermal properties of PE12.12-SO3M and PE18.18-SO3M derivatives as obtained from DSC measurements. Peak melting temperatures (T_m), enthalpies of fusion (ΔH_m), peak crystallization temperatures (T_c) and enthalpies of crystallization (ΔH_c) are listed. Data were taken from the second heating/cooling cycle (10 K/min heating/cooling rate).

	T_m [°C]	ΔH_m [J/g]	T_c [°C]	ΔH_c [J/g]
PE12.12	84.9	136	66.2	-114
PE12.12-SO3Mg	84.8	134	62.4	-115
PE12.12-SO3Ca	84.1	122	63.8	-113
PE12.12-SO3Zn	83.5	111	64.5	-104
PE18.18	99.4	145	81.6	-131
PE18.18-SO3Mg	98.3	151	79.6	-121
PE18.18-SO3Ca	99.4	142	79.9	-116
PE18.18-SO3Zn	98.1	151	80.3	-122

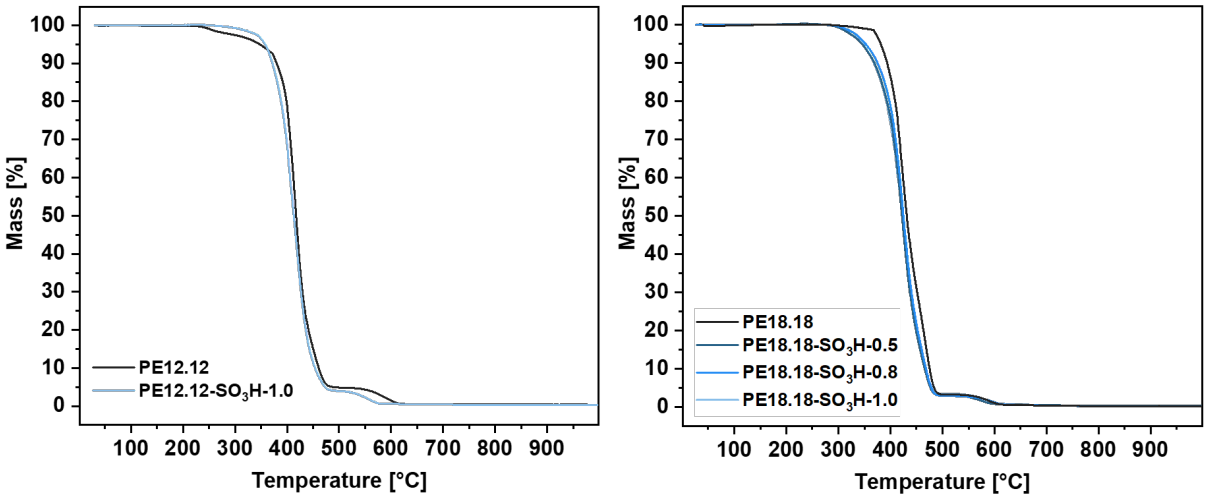

Figure 5.27 TGA traces of PE12.12-SO3H-1.0 (left) and PE18.18-SO_3H-x (right) as well as their non-ionic parent polyesters (PE12.12 and PE18.18, respectively) under air, measured from 30 to 1000 °C with a heating rate of 10 °C/min.

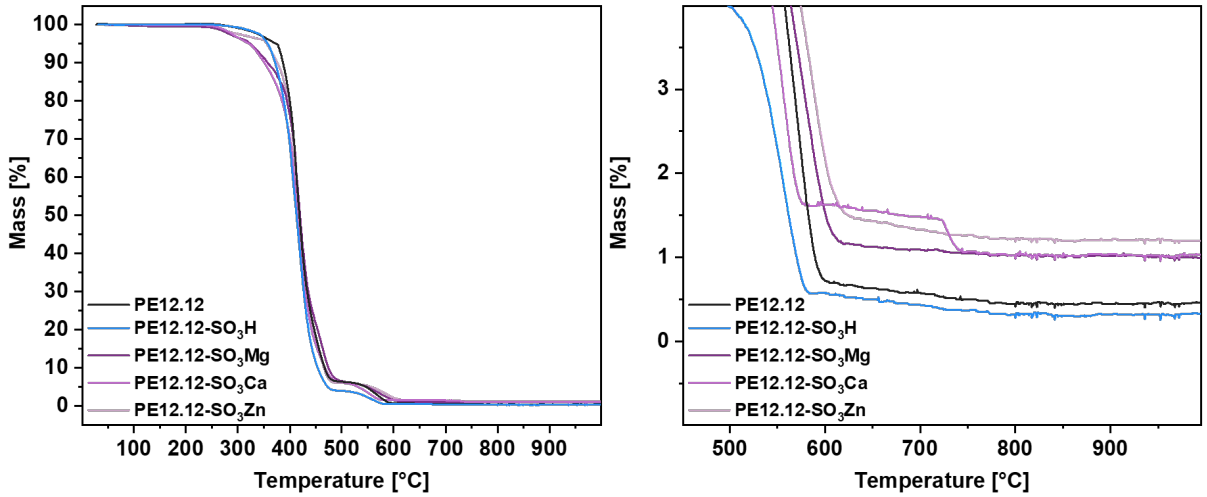

Figure 5.28 TGA traces of PE12.12, PE12.12-SO3H-1.0 and PE12.12-SO3M (M = Mg, Ca, Zn) under air, measured from 30 to 1000 °C with a heating rate of 10 °C/min. Left: full temperature range; right: detailed view on residual masses.

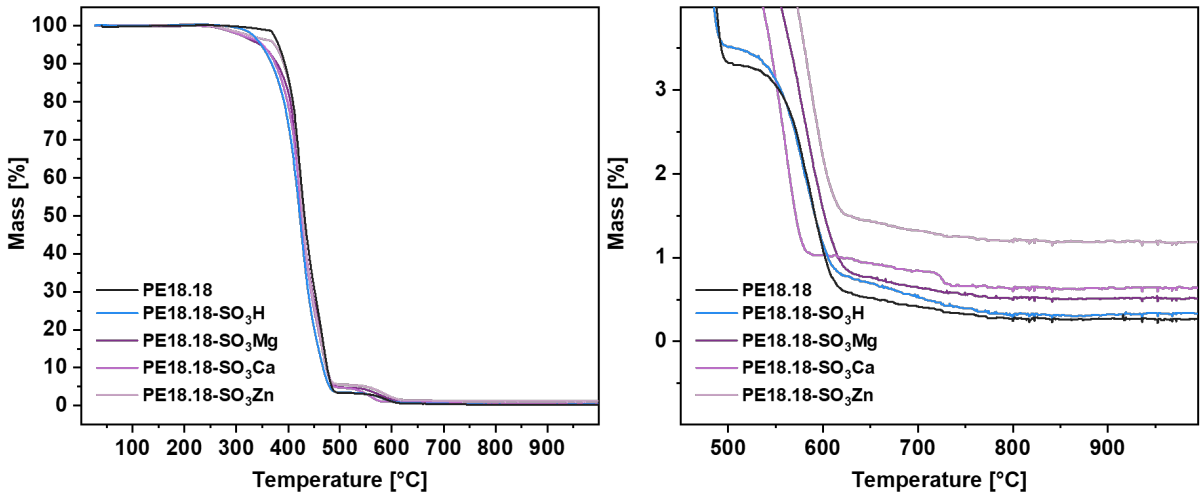

Figure 5.29 TGA traces of PE18.18, PE18.18-SO3H-0.8 and PE18.18-SO3M (M = Mg, Ca, Zn) under air, measured from 30 to 1000 °C with a heating rate of 10 °C/min. Left: full temperature range; right: detailed view on residual masses.

5.6.4 WAXS Measurements

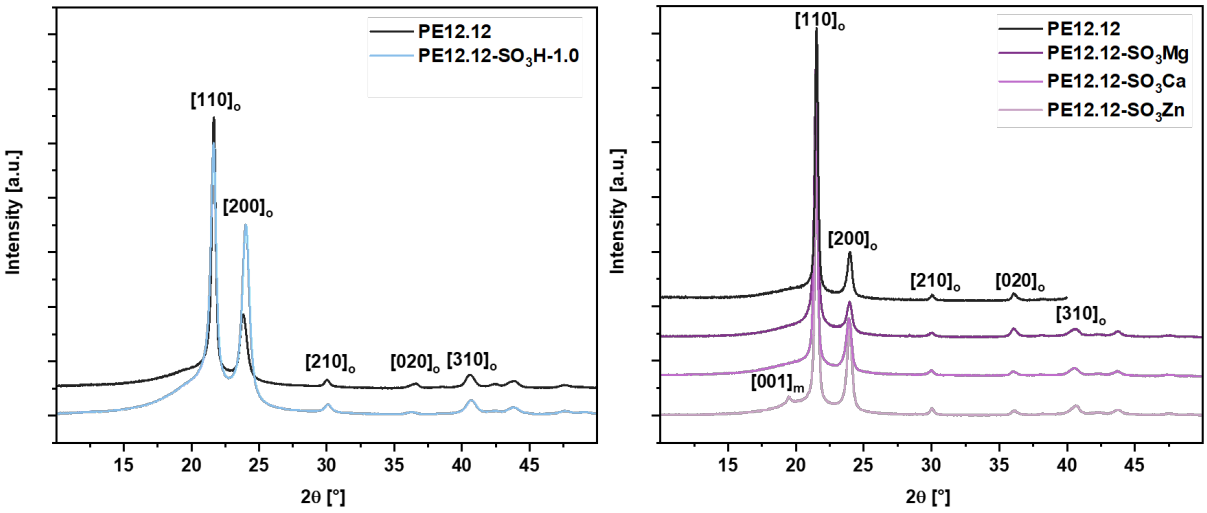

Figure 5.30 WAXS traces of PE12.12 and PE12.12-SO3H-1.0 (left) and PE12.12-SO3M (right). Reflexes corresponding to the unit cell of polyethylene are labeled, index o abbreviates orthorhombic, index m abbreviates monoclinic. Data was shifted vertically for clarity.

5.6.5 Rheological Measurements

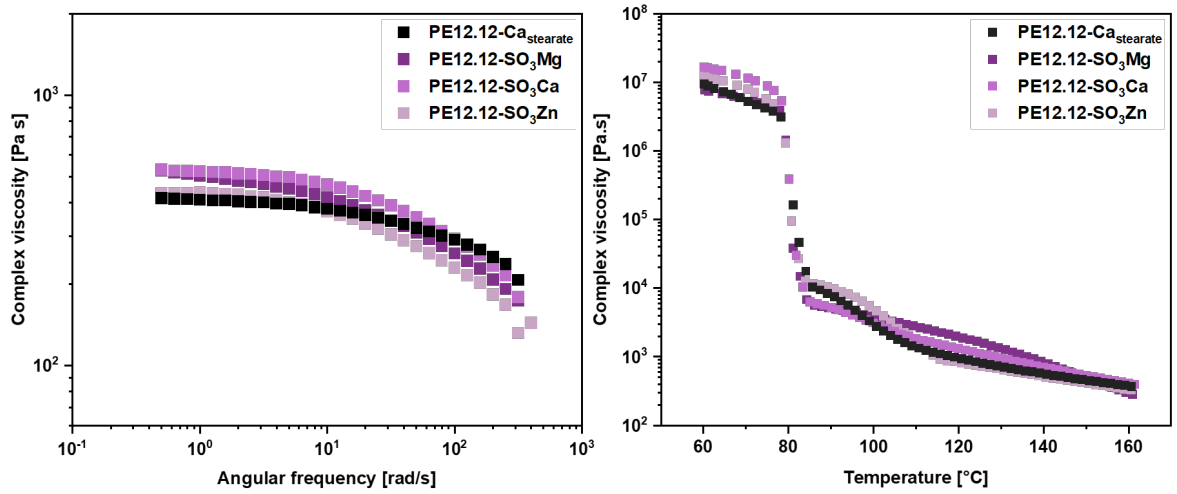

Figure 5.31 Left: Absolute complex viscosity as a function of the angular frequency of PE2.12-Ca$_{stearate}$ and PE12.12-SO3M at 150 °C. Right: Temperature sweep of PE12.12-Ca$_{stearate}$ and PE12.12-SO3M (strain 0.1 %, angular frequency 6.28 rad/s, heating rate 10 °C/min).

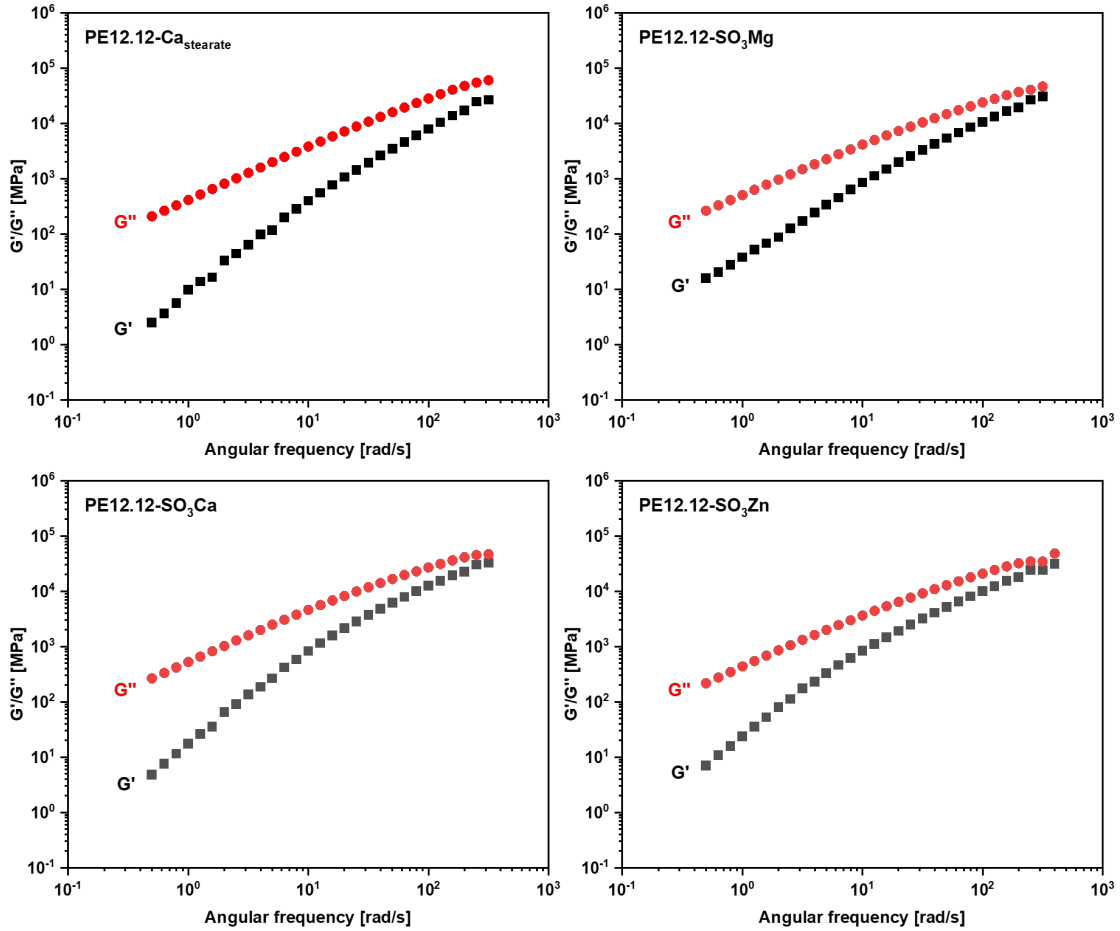

Figure 5.32 Frequency sweep raw data on PE12.12-Ca$_{stearate}$ and PE12.12-SO$_3$M (150 °C, strain amplitude: 10 %). Storage (G') and loss modulus (G'') as a function of angular frequency are displayed.

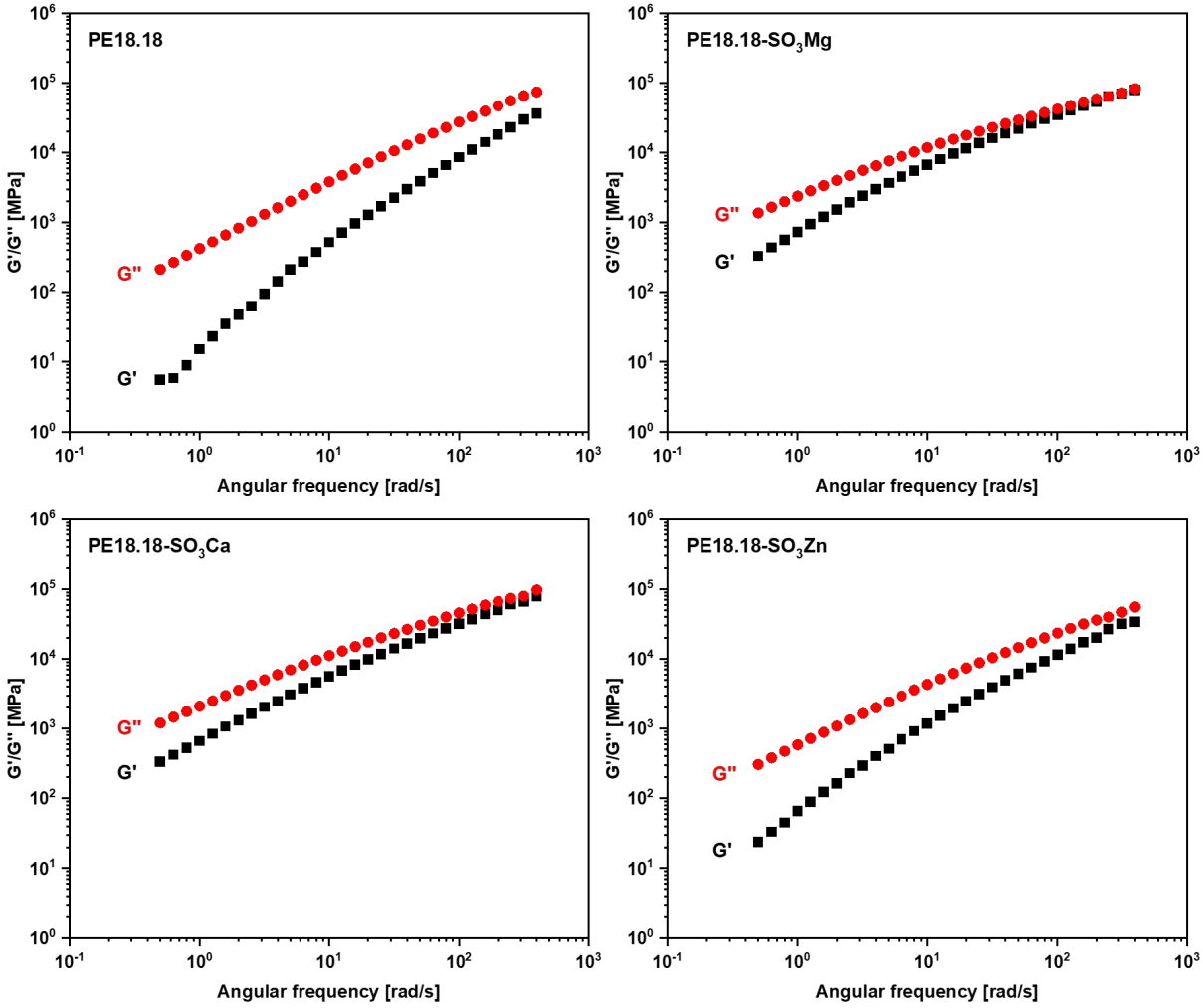

Figure 5.33 Frequency sweep raw data on PE18.18 and PE18.18-SO_3M (180 °C, strain amplitude: 10 %). Storage (G') and loss modulus (G'') as a function of angular frequency are displayed.

5.6.6 Tensile Testing Results

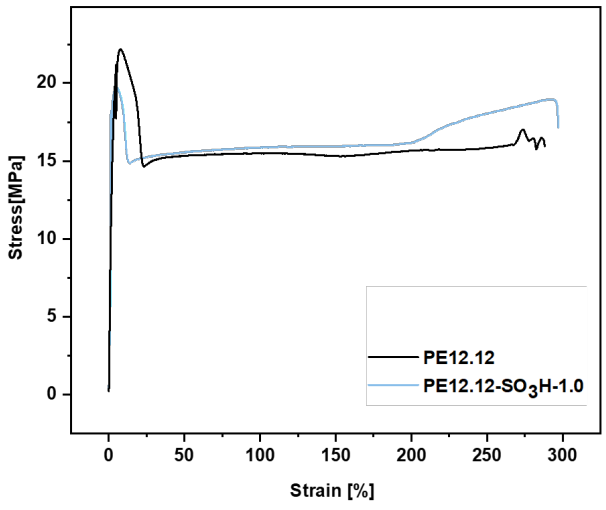

Figure 5.34 Stress-strain curves of PE12.12 and PE12.12-SO3H-1.0.

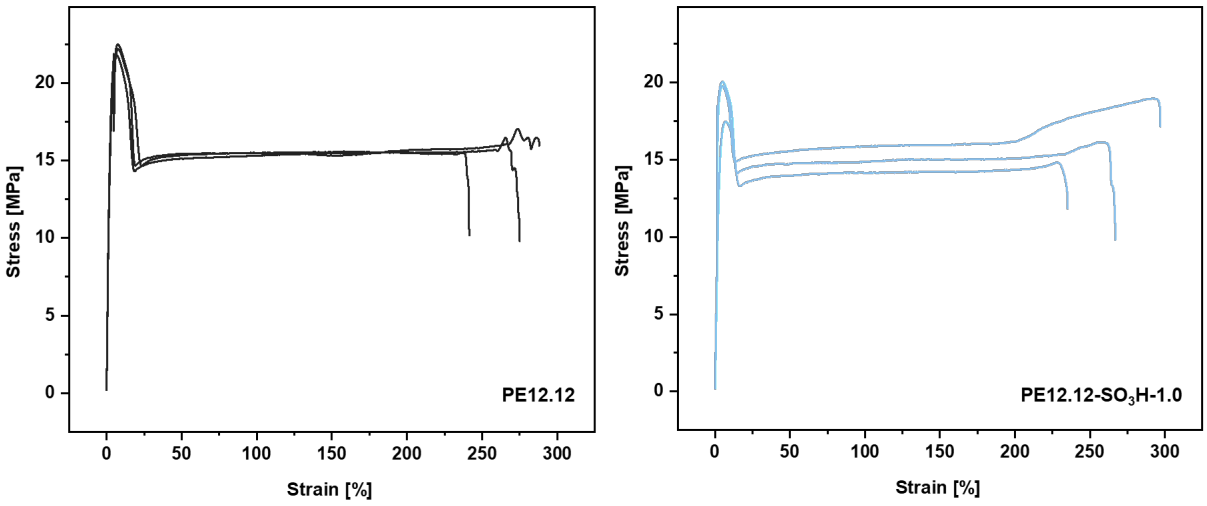

Figure 5.35 Stress-strain curves of PE12.12 and PE12.12-SO3H-1.0. For each polymer, three representative curves are shown to demonstrate reproducibility.

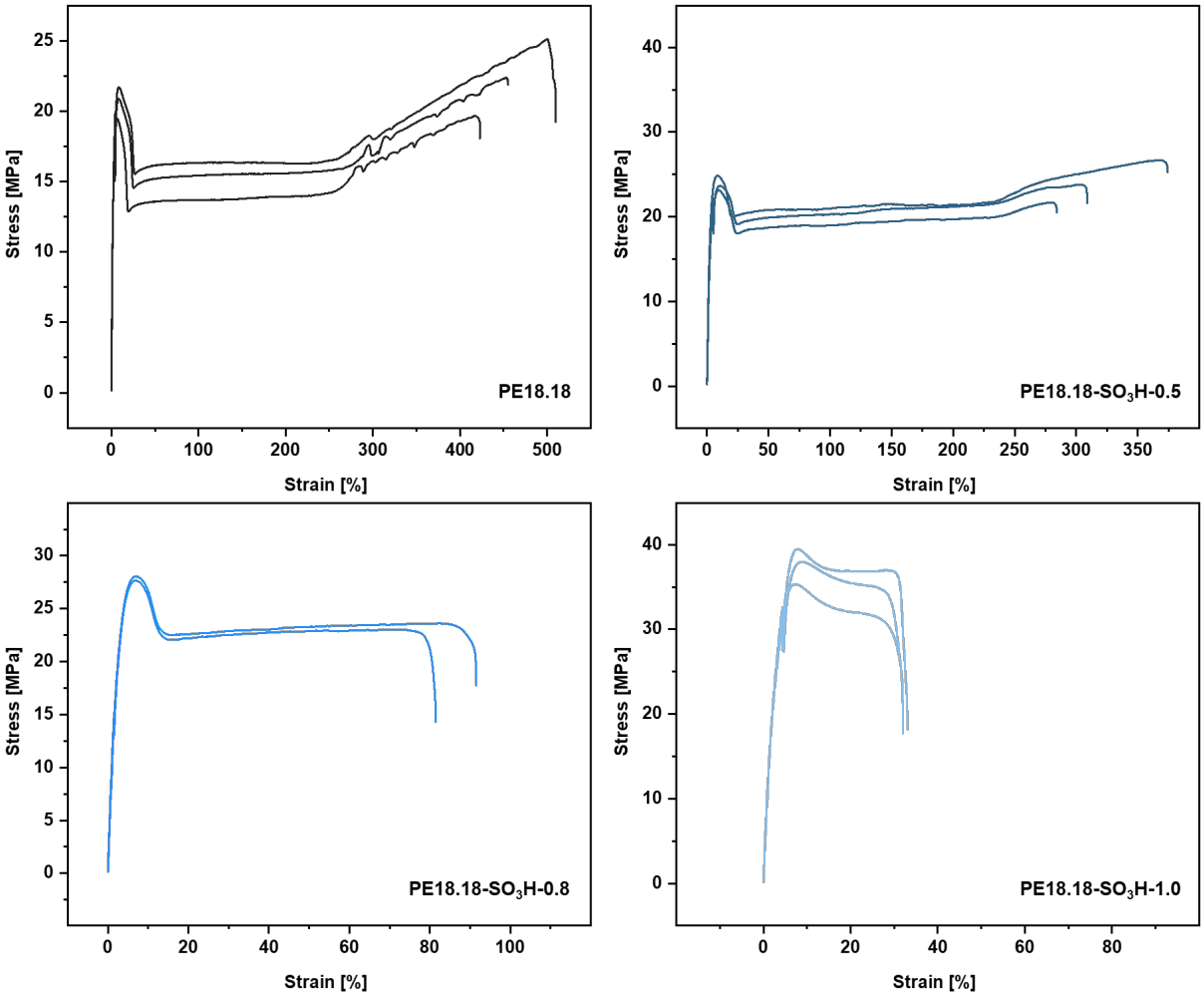

Figure 5.36 Stress-strain curves of PE18.18 and polymers PE18.18-SO3H. For each polymer, three representative curves are shown to demonstrate reproducibility (only two curves in case of PE18.18-SO3H-0.8 are shown).

Table 5.13 Tensile testing results of PE12.12-SO3H and PE18.18-SO3H.

	ε_{tb} [a] [%]	U_T [b] [J/m³]	E_t [c] [MPa]	σ_y [d] [MPa]
PE12.12	270 ± 20	4300 ± 330	860 ± 30	22.2 ± 1.1
PE12.12- SO3H-1.0	270 ± 25	4100 ± 640	595 ± 25	19.7 ± 1.0
PE18.18	490 ± 30	8700 ± 630	840 ± 10	21.3 ± 0.4
PE18.18- SO3H-0.5	330 ± 40	6900 ± 1200	940 ± 30	23.9 ± 0.7
PE18.18- SO3H-0.8	90 ± 5	2000 ± 140	1100 ± 35	27.8 ± 0.2
PE18.18- SO3H-1.0	40 ± 3	1000 ± 40	1200 ± 40	35.4 ± 2.0

a) elongation at break, b) toughness, c) Young's modulus, d) stress at yield point.

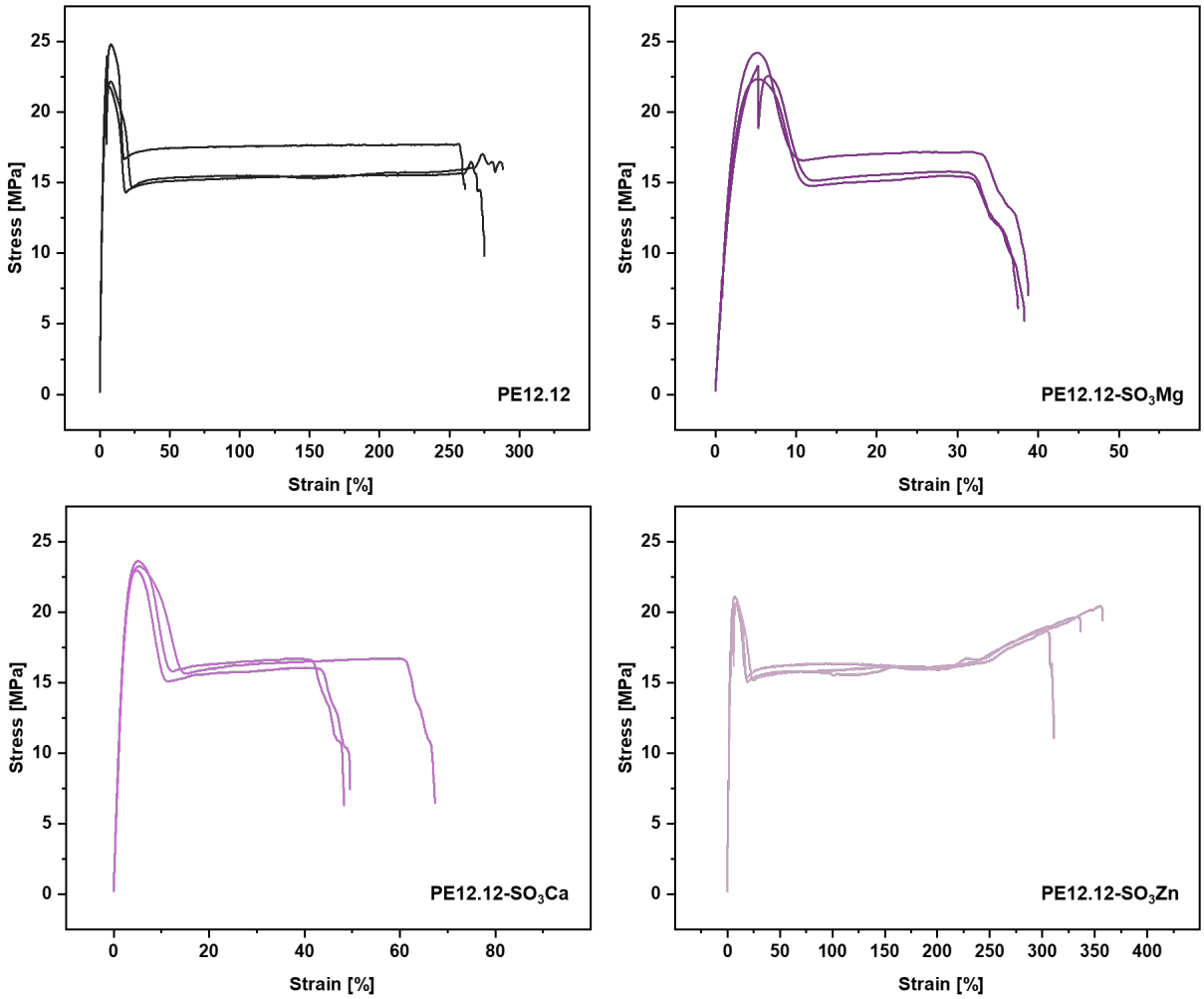

Figure 5.37 Stress-strain curves of PE12.12 and polymers PE12.12-SO3M. For each polymer, three representative curves are shown to demonstrate reproducibility.

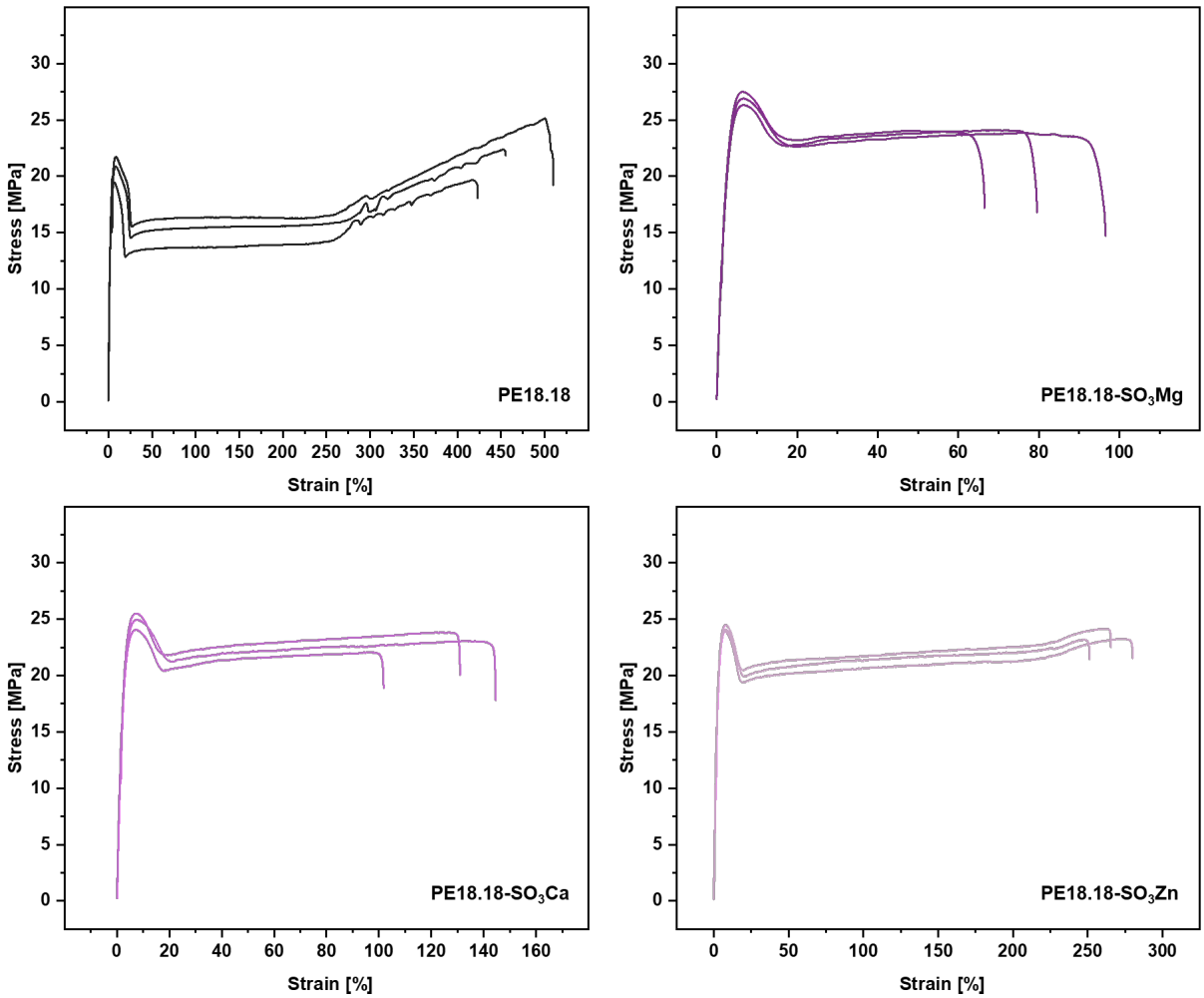

Figure 5.38 Stress-strain curves of PE18.18 and polymers PE18.18-SO3M. For each polymer, three representative curves are shown to demonstrate reproducibility.

Table 5.14 Tensile testing results of PE12.12-SO3M and PE18.18-SO3M.

	ε_{tb} [a] [%]	U_T [b] [J/m³]	E_t [c] [MPa]	σ_y [d] [MPa]
PE12.12	270 ± 20	4300 ± 330	860 ± 30	22.2 ± 1.1
PE12.12-SO3Mg	40 ± 5	610 ± 30	900 ± 40	23.3 ± 0.8
PE12.12-SO3Ca	60 ± 10	1000 ± 100	1020 ± 40	24.0 ± 0.9
PE12.12-SO3Zn	340 ± 20	5600 ± 410	750 ± 20	20.6 ± 0.4
PE18.18	490 ± 30	8700 ± 630	840 ± 10	21.3 ± 0.4
PE18.18-SO3Mg	80 ± 10	1900 ± 270	1010 ± 20	26.9 ± 0.5
PE18.18-SO3Ca	120 ± 20	2800 ± 450	950 ± 50	24.8 ± 0.6
PE18.18-SO3Zn	270 ± 10	5700 ± 230	930 ± 20	26.8 ± 0.2

a) elongation at break, b) toughness, c) Young's modulus, d) stress at yield point.

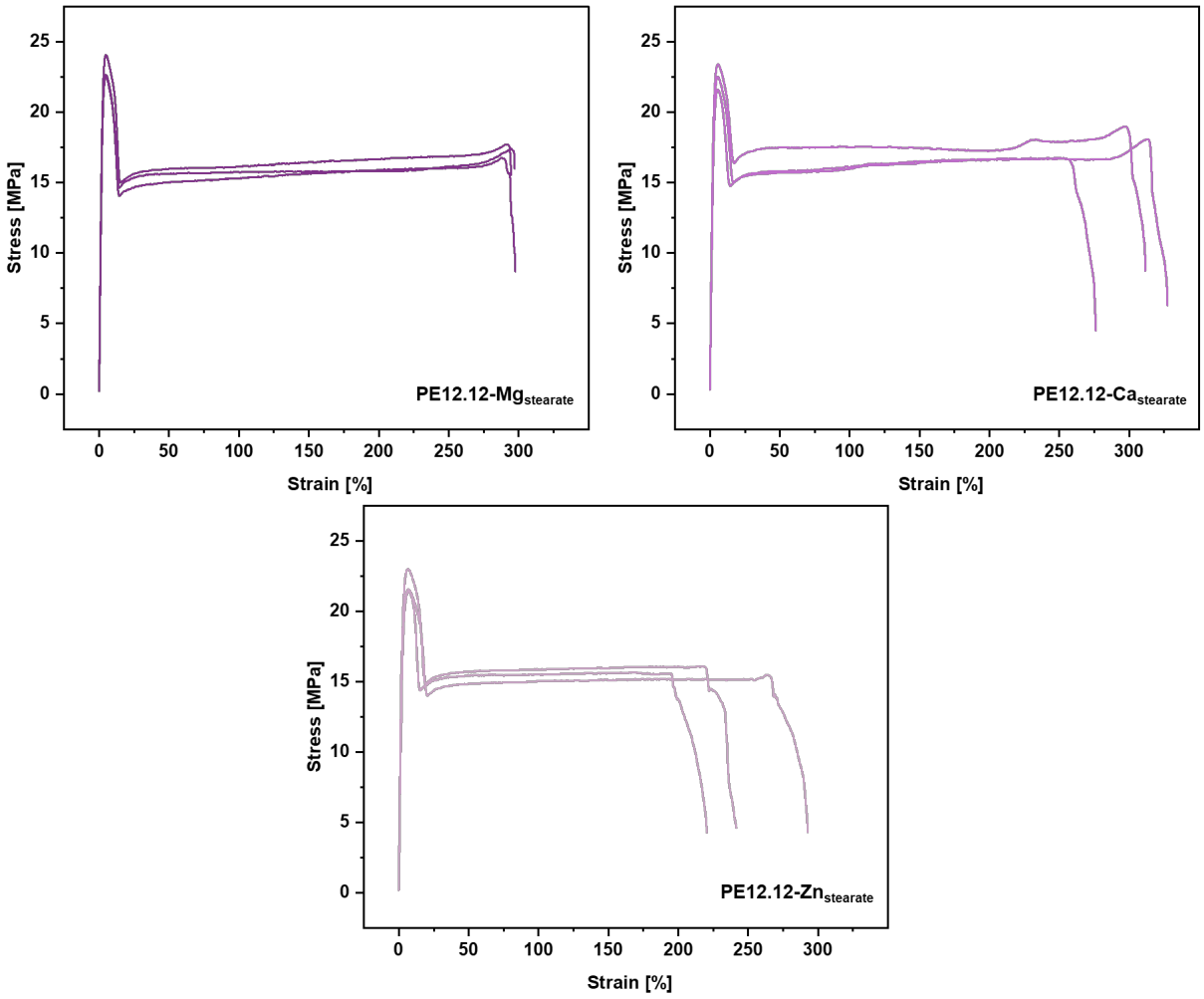

Figure 5.39 Stress-strain curves of PE12.12-M$_{stearate}$. For each polymer, three representative curves are shown to demonstrate reproducibility.

Table 5.15 Tensile testing results of PE12.12-M$_{stearate}$.

	ε_{tb} [a] [%]	U_T [b] [J/m^3]	E_t [c] [MPa]	σ_y [d] [MPa]
PE12.12-Mg$_{stearate}$	290 ± 10	4800 ± 90	960 ± 40	23.7 ± 0.8
PE12.12-Ca$_{stearate}$	310 ± 20	5100 ± 450	860 ± 40	22.5 ±0.7
PE12.12-Zn$_{stearate}$	250 ± 30	3800 ± 420	820 ± 70	21.9 ± 0.8

a) elongation at break, b) toughness, c) Young's modulus, d) stress at yield point.

5.6.7 Water Uptake Study

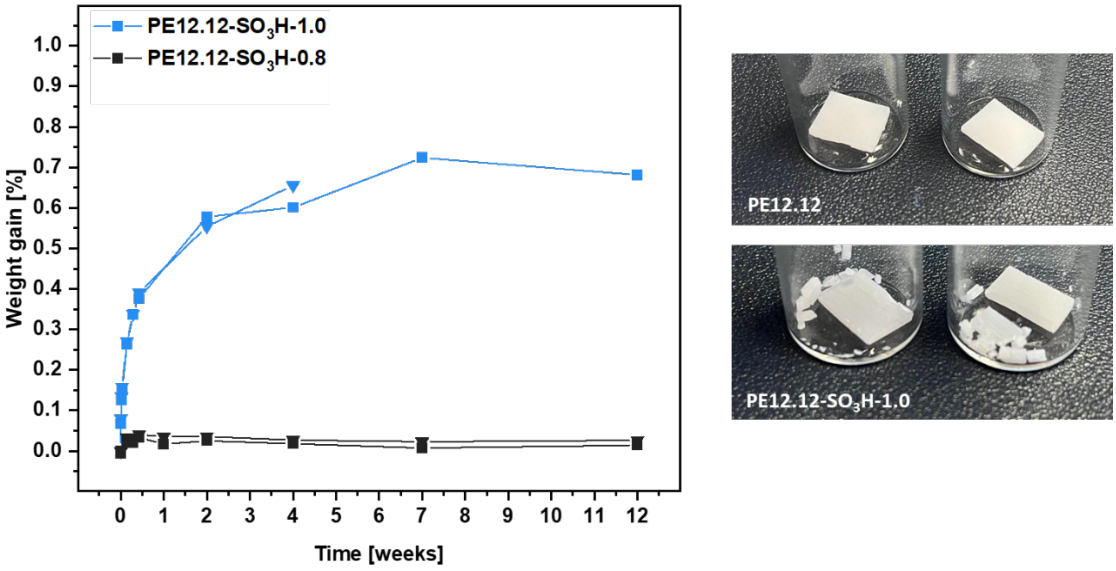

Figure 5.40 Left: Weight gain of PE12.12 and PE12.12-SO3H-1.0 after storage in water for 12 weeks. Duplicates were investigated. In case of PE12.12-SO3H-1.0, one of the samples embrittled significantly after 4 weeks and could not further be weighed but was incubated further. Right: Images of dried samples after 12 weeks.

5.6.8 Water Contact Angle Measurements

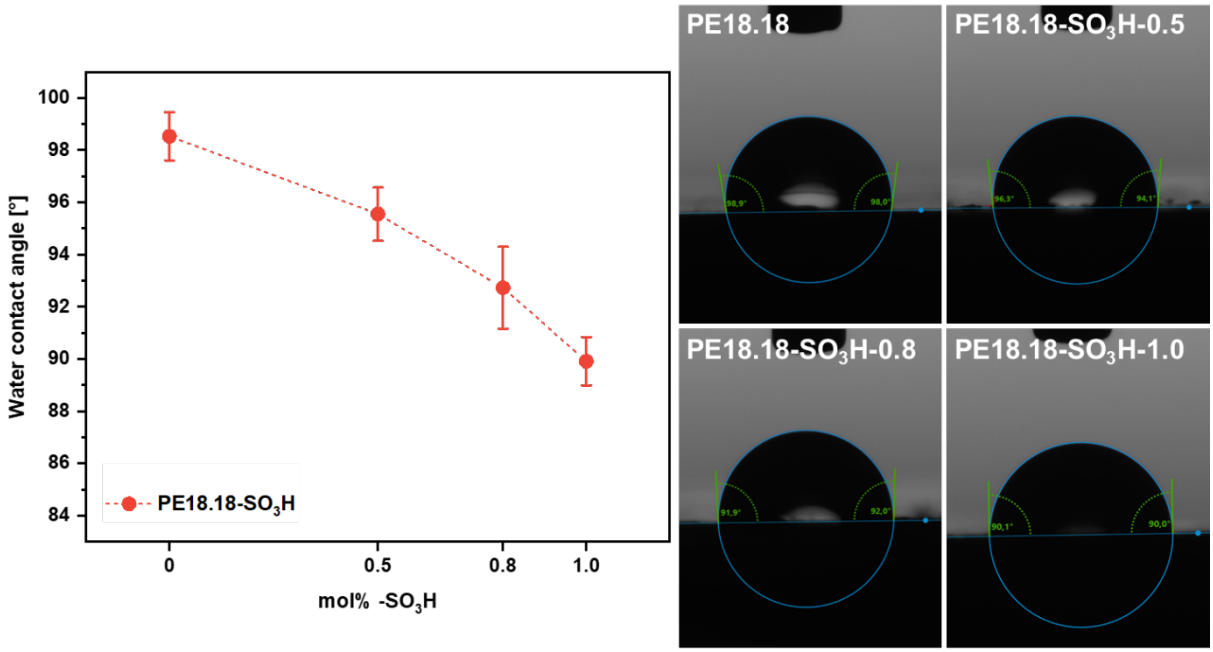

Figure 5.41 Water contact angle of PE18.18-SO3H as well as the non-ionic reference polyester PE18.18. Error bars represent standard deviations calculated from three different droplets (six angles). Samples were surface cleaned with ^{i}PrOH and dried for 48 h prior to the measurements. Images show representative measurements of each polymer.

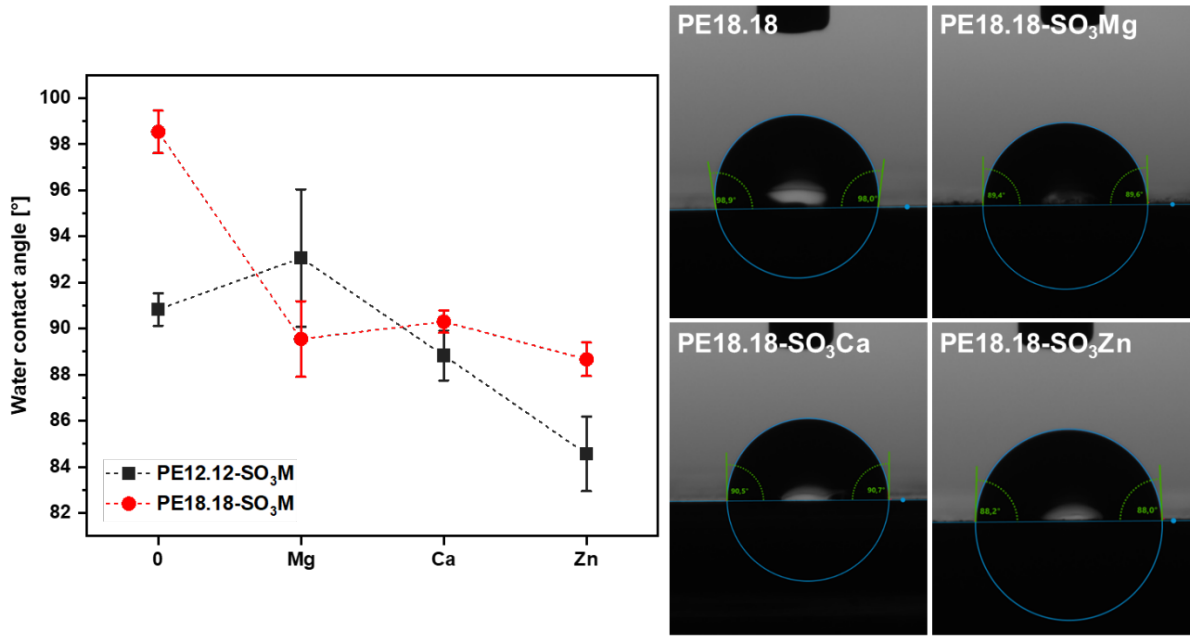

Figure 5.42 Water contact angle of PE12.12-SO3M and PE18.18-SO3M as well as their non-ionic reference polyesters, PE12.12 and PE18.18. Error bars represent standard deviations calculated from three different droplets (six angles). Samples were surface cleaned with ^{i}PrOH and dried for 48 h prior to the measurements. Images show representative measurements of each polymer.

5.6.9 ^{1}H NMR Spectra of Polymers PEx.x-SO3H

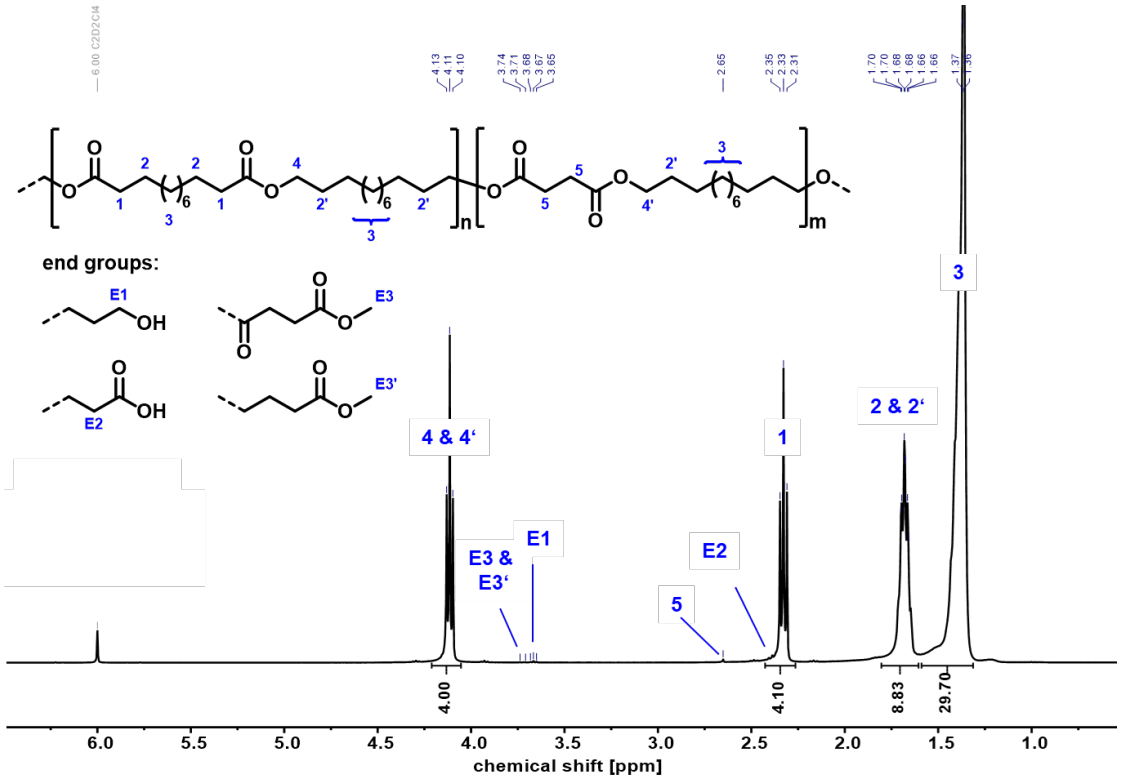

Figure 5.43 Full ^{1}H NMR spectrum (400 MHz, 383 K, $C_2D_2Cl_4$) of **PE12.12.**

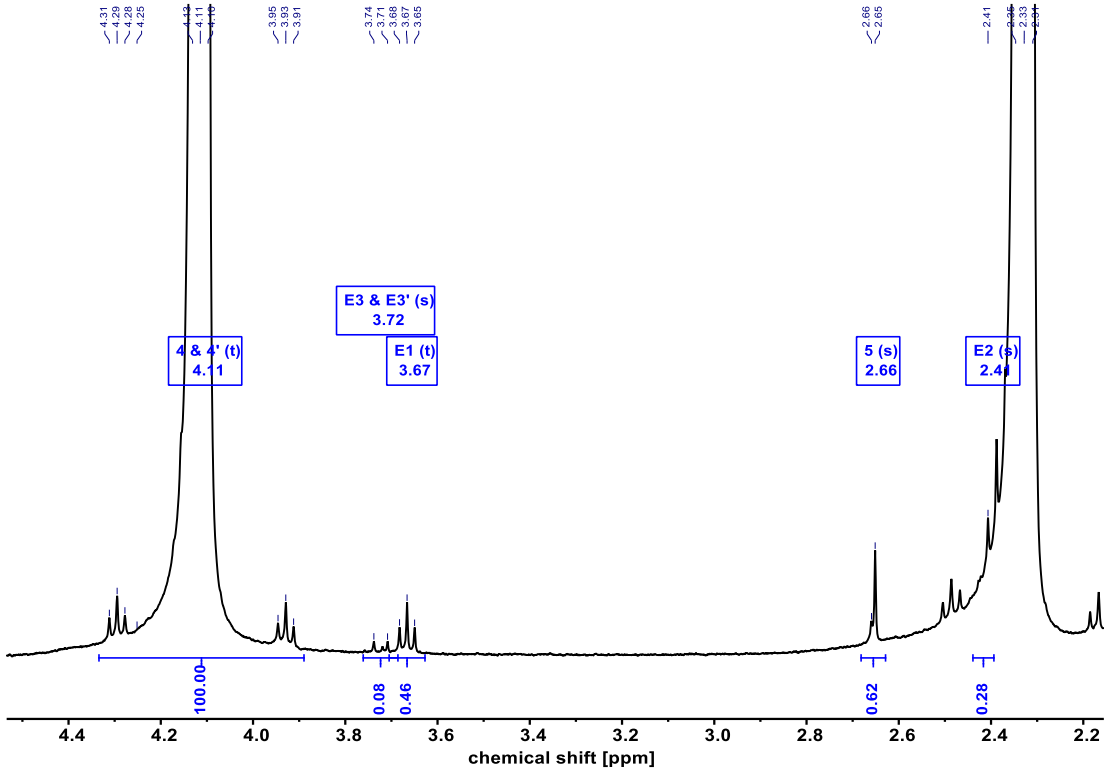

Figure 5.44 Detailed section of ^{1}H NMR spectrum (500 MHz, 383 K, $C_2D_2Cl_4$) of **PE12.12** with integrals of end groups and of the succinate unit. Assignment of signals according to Figure 5.43.

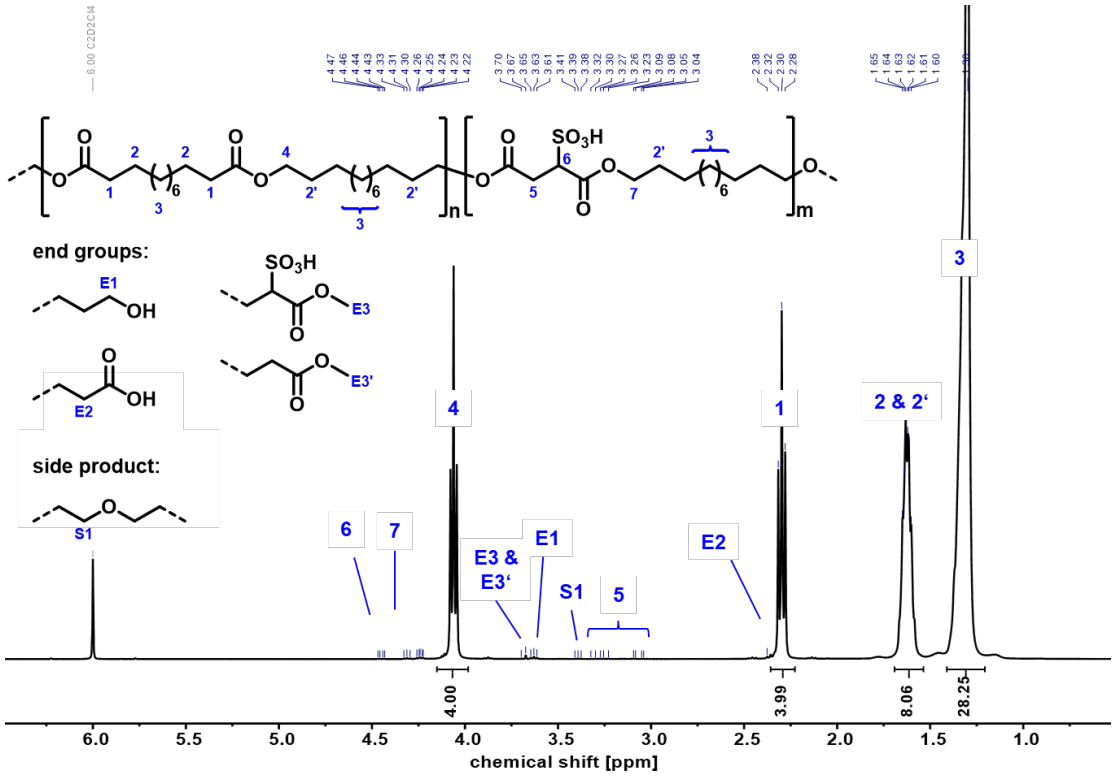

Figure 5.45 Full ^{1}H NMR spectrum (400 MHz, 323 K, $C_2D_2Cl_4$) of **PE12.12-SO3H-1.0**. Note that protons **5** located next to the sulfonic acid group are diastereotopic and that the -SO3H group can be oriented either as shown, or the repeat unit can be oppositely arranged.

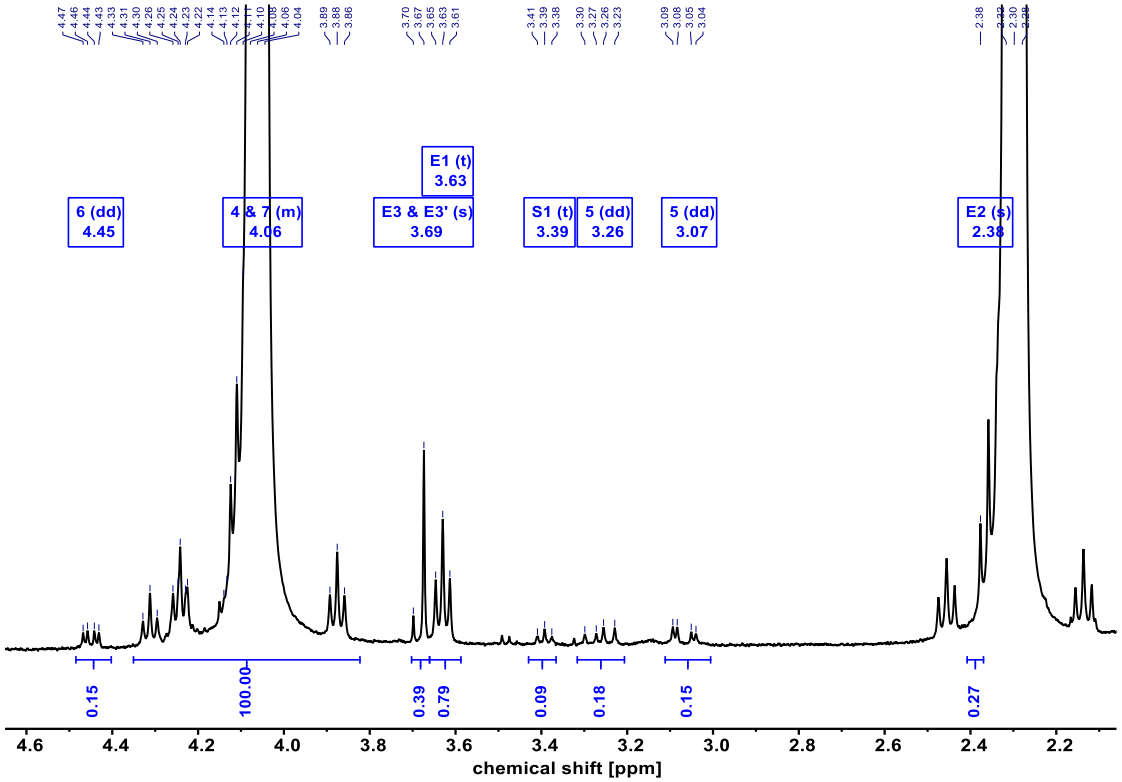

Figure 5.46 Detailed section of ^{1}H NMR spectrum (500 MHz, 323 K, $C_2D_2Cl_4$) of **PE12.12-SO3H-1.0** with integrals of end groups as well as protons located close to the -SO3H group. Assignment of signals according to Figure 5.45.

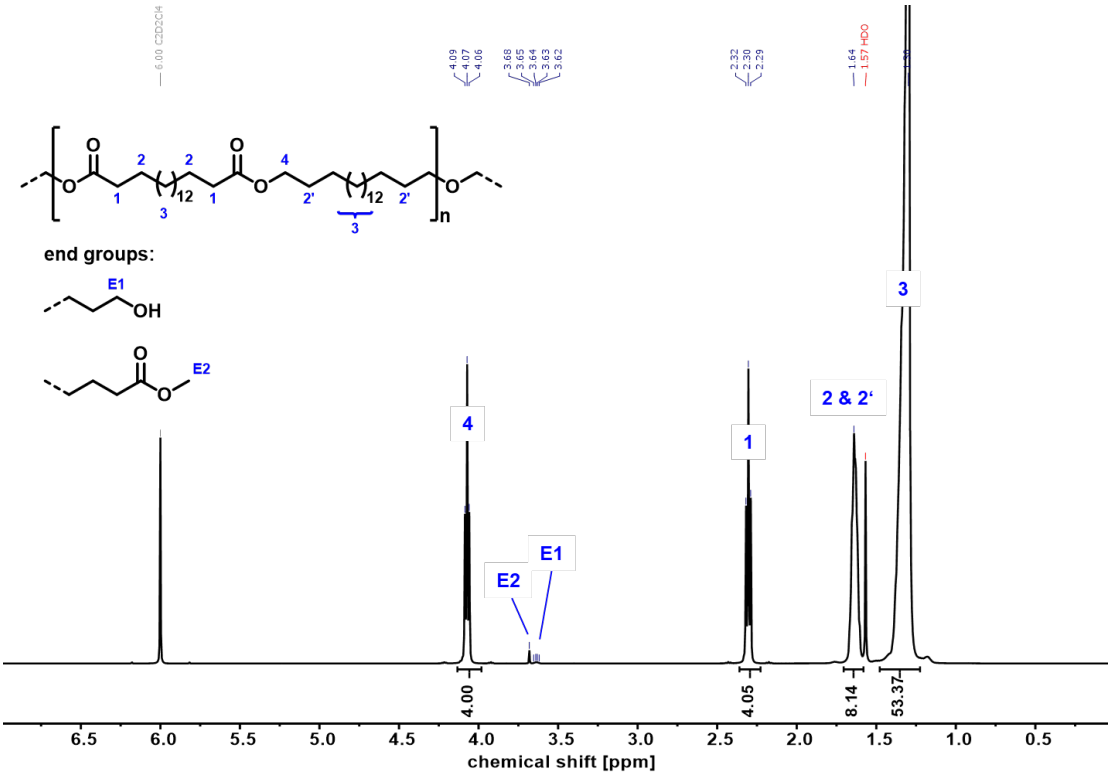

Figure 5.47 Full ^{1}H NMR spectrum (500 MHz, 323 K, $C_2D_2Cl_4$) of **PE18.18**.

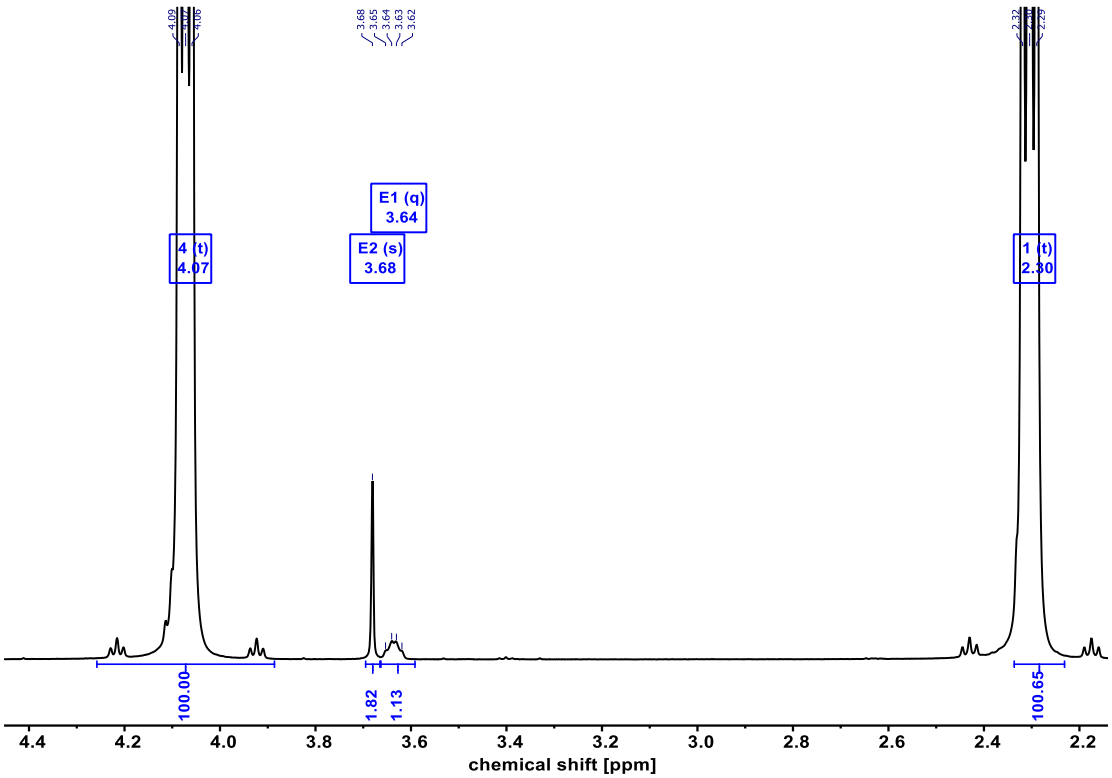

Figure 5.48 Detailed section of ^{1}H NMR spectrum (500 MHz, 323 K, $C_2D_2Cl_4$) of **PE18.18** with integrals of end groups. Assignment of signals according to Figure 5.47.

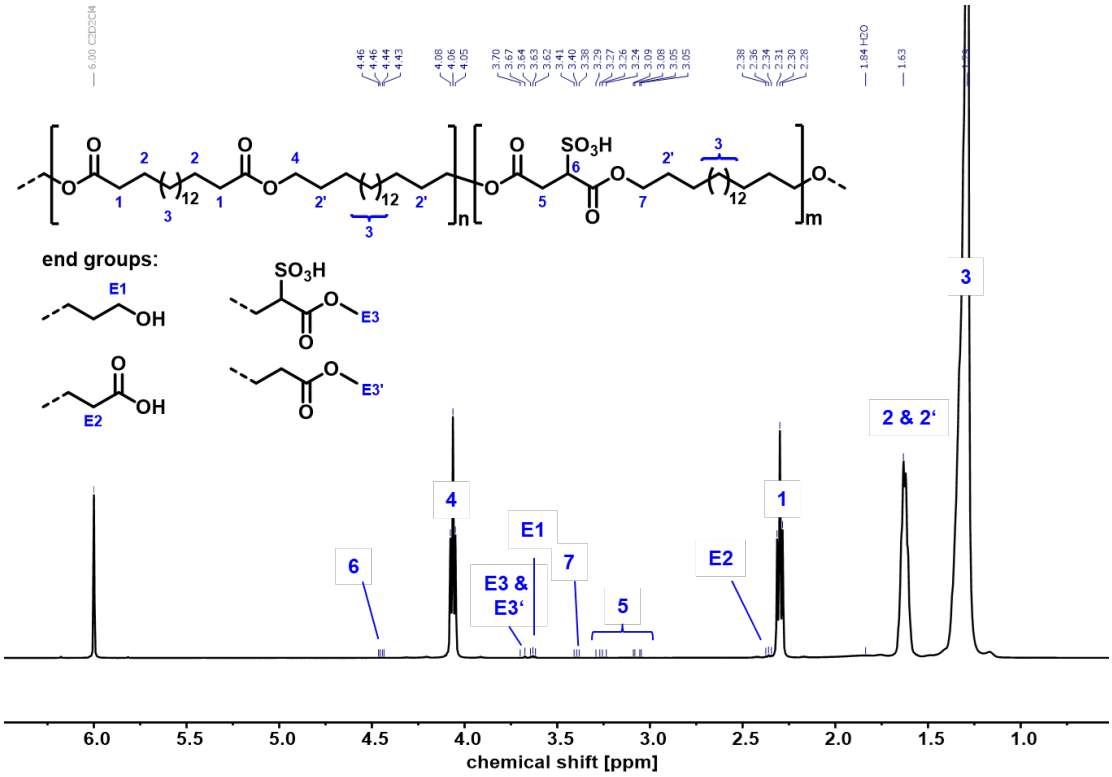

Figure 5.49 Full ^{1}H NMR spectrum (500 MHz, 323 K, $C_2D_2Cl_4$) of PE18.18-SO3H-0.8. Note that protons 5 located next to the sulfonic acid group are diastereotopic and that the -SO3H group can be oriented either as shown, or the repeat unit can be oppositely arranged.

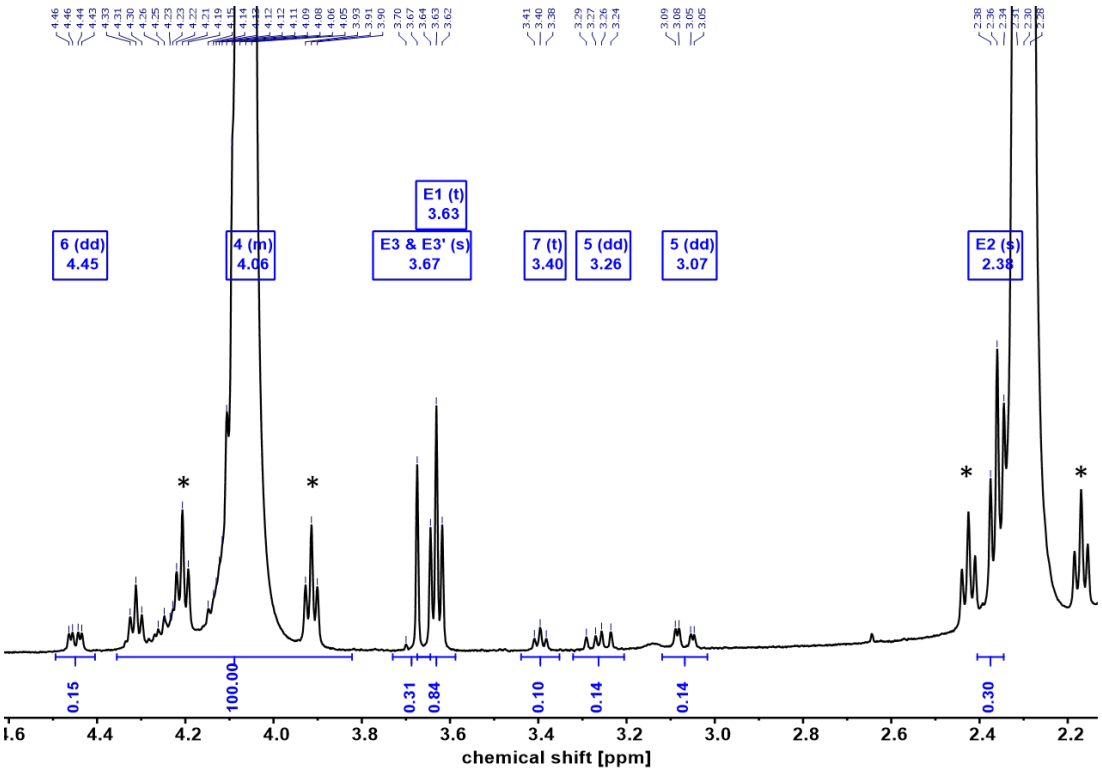

Figure 5.50 Detailed section of ^{1}H NMR spectrum (500 MHz, 323 K, $C_2D_2Cl_4$) of PE18.18-SO3H-0.8 with integrals of end groups as well as protons located close to the -SO3H group (* = ^{13}C-coupled satellites). Assignment of signals according to Figure 5.49.

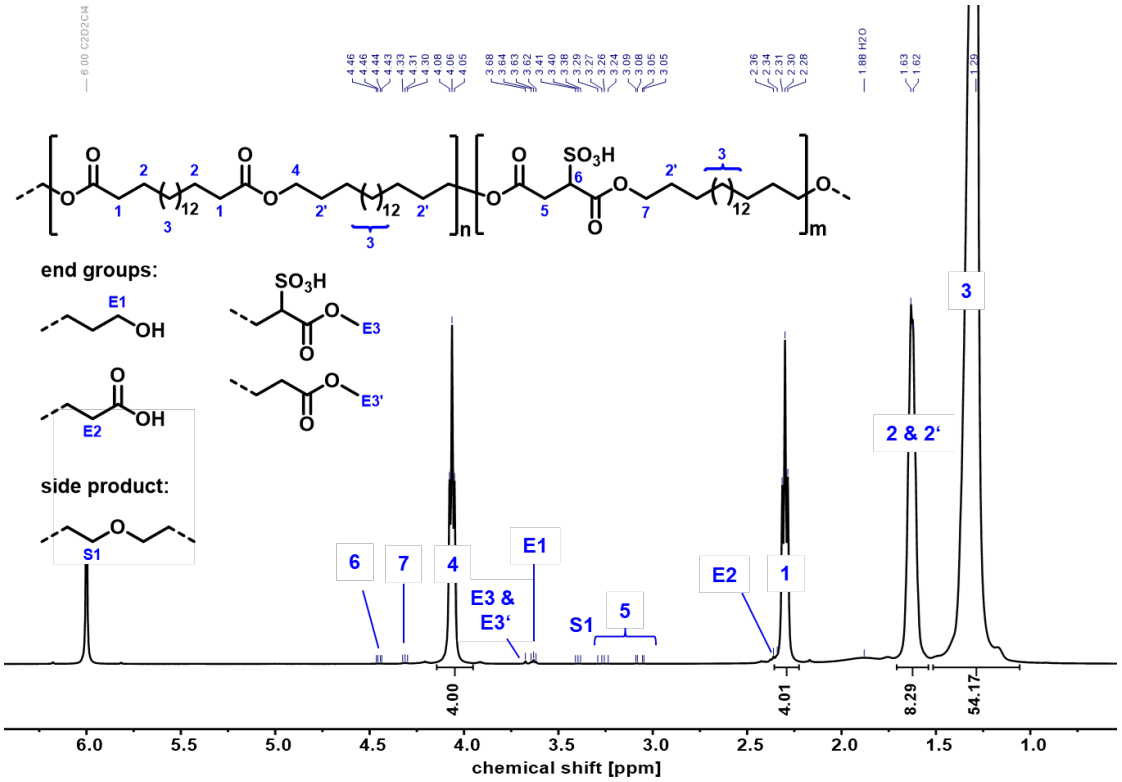

Figure 5.51 Full ^{1}H NMR spectrum (500 MHz, 323 K, $C_2D_2Cl_4$) of **PE18.18-SO3H-1.0**. Note that protons **5** located next to the sulfonic acid group are diastereotopic and that the -SO3H group can be oriented either as shown, or the repeat unit can be oppositely arranged.

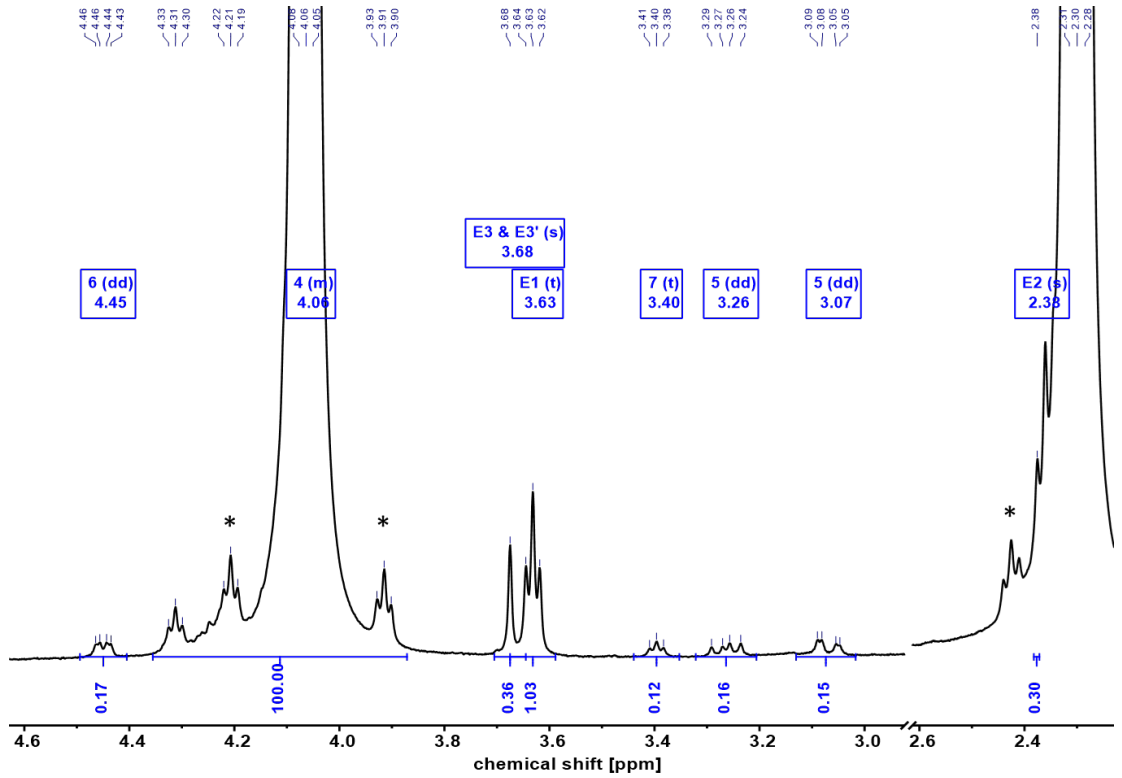

Figure 5.52 Detailed section of ^{1}H NMR spectrum (500 MHz, 323 K, $C_2D_2Cl_4$) of **PE18.18-SO3H-1.0** with integrals of end groups as well as protons located close to the -SO3H group (* = ^{13}C-coupled satellites). Assignment of signals according to Figure 5.51.

5.6.10 ^{1}H NMR Spectra of Polymers PEx.x-SO3M

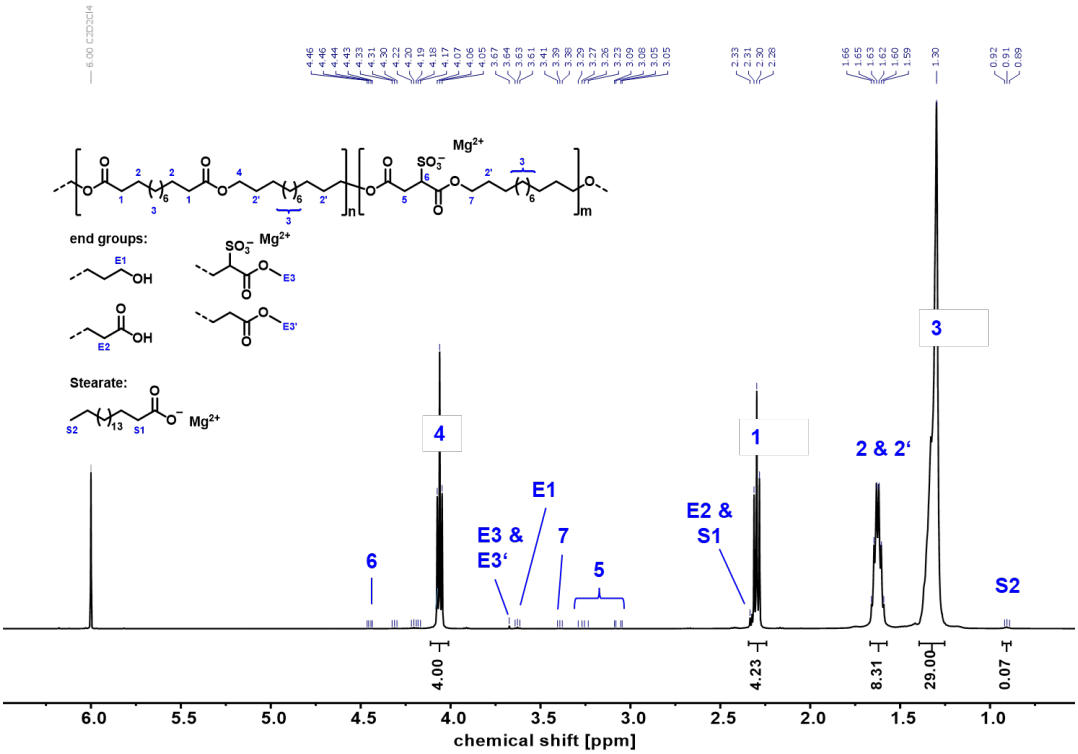

Figure 5.53 Full ^{1}H NMR spectrum (500 MHz, 323 K, $C_2D_2Cl_4$) of **PE12.12-SO$_3$Mg**. Note that protons 5 located next to the sulfonate group are diastereotopic and that the sulfonate group can be oriented either as shown, or the repeat unit can be oppositely arranged.

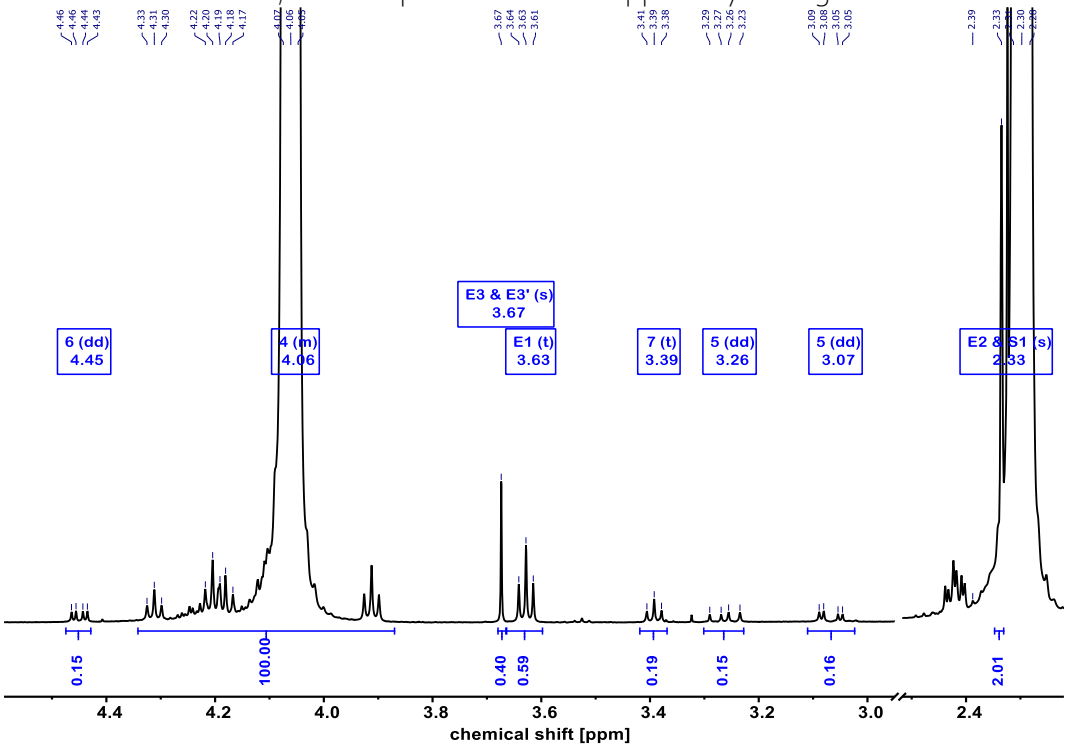

Figure 5.54 Detailed section of ^{1}H NMR spectrum (500 MHz, 323 K, $C_2D_2Cl_4$) of **PE12.12-SO$_3$Mg** with integrals of end groups as well as protons located close to the sulfonate group. Assignment of signals according to Figure 5.53.

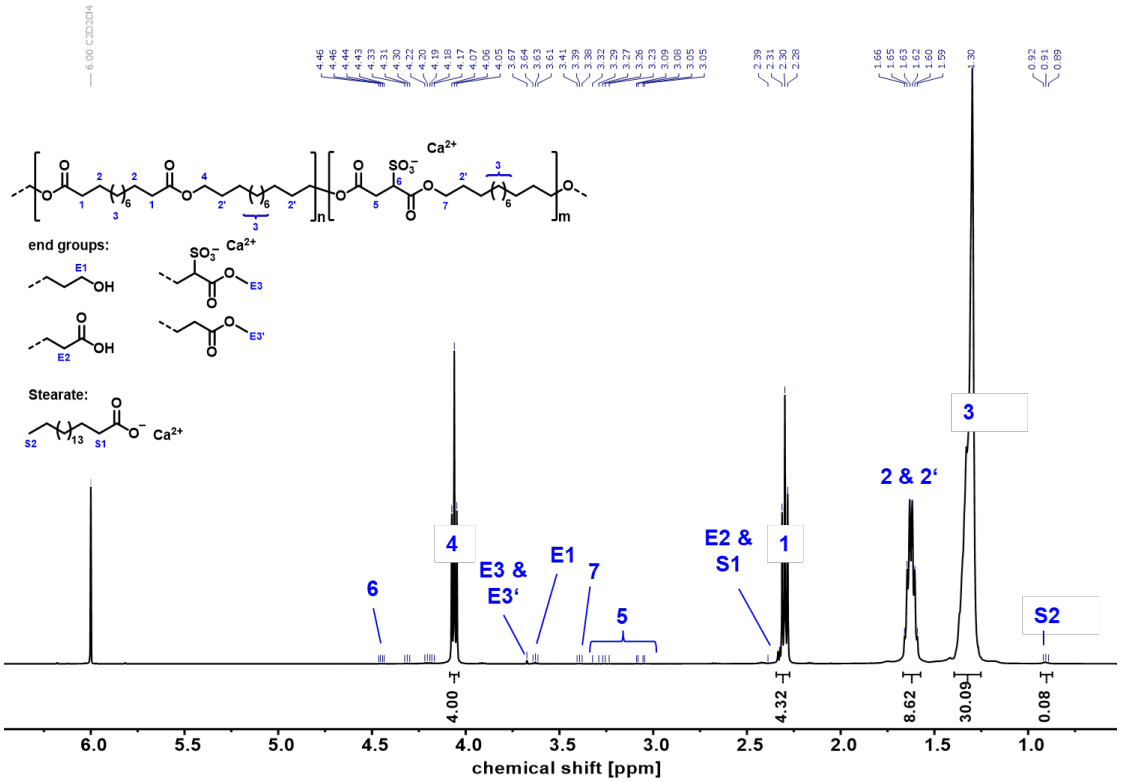

Figure 5.55 Full ^{1}H NMR spectrum (500 MHz, 323 K, $C_2D_2Cl_4$) of **PE12.12-SO$_3$Ca**. Note that protons 5 located next to the sulfonate group are diastereotopic and that the sulfonate group can be oriented either as shown, or the repeat unit can be oppositely arranged.

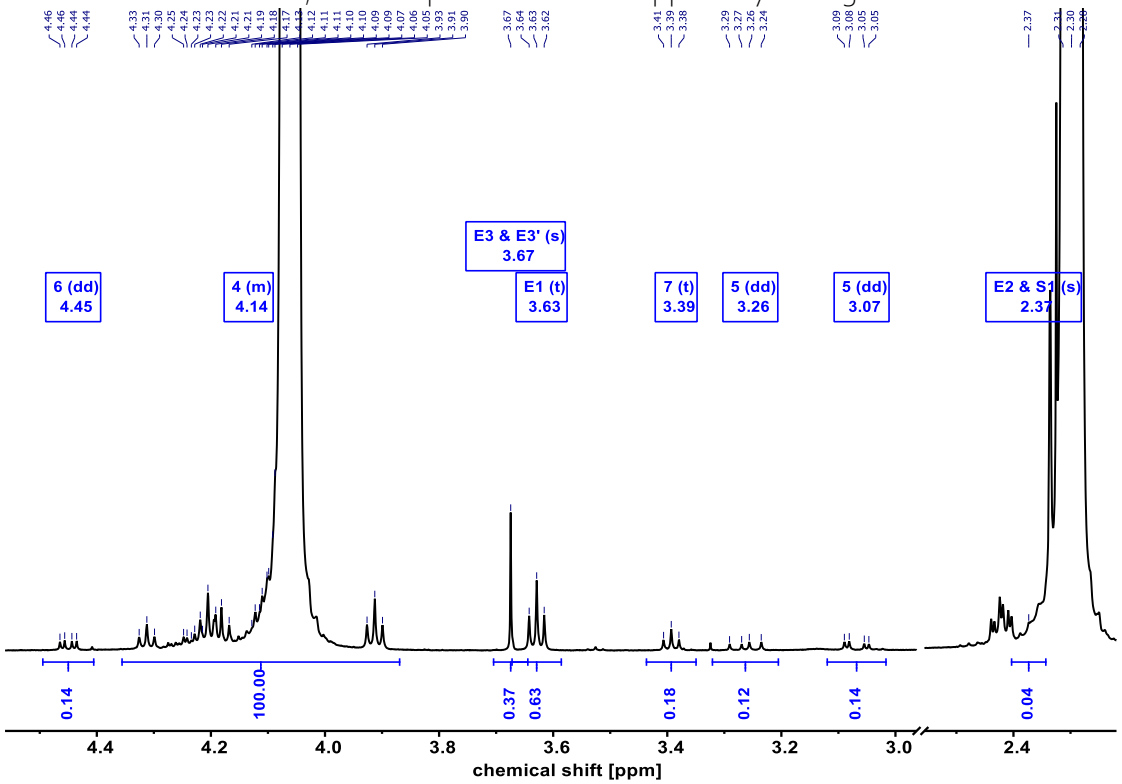

Figure 5.56 Detailed section of ^{1}H NMR spectrum (500 MHz, 323 K, $C_2D_2Cl_4$) of **PE12.12-SO$_3$Ca** with integrals of end groups as well as protons located close to the sulfonate group. Assignment of signals according to Figure 5.55.

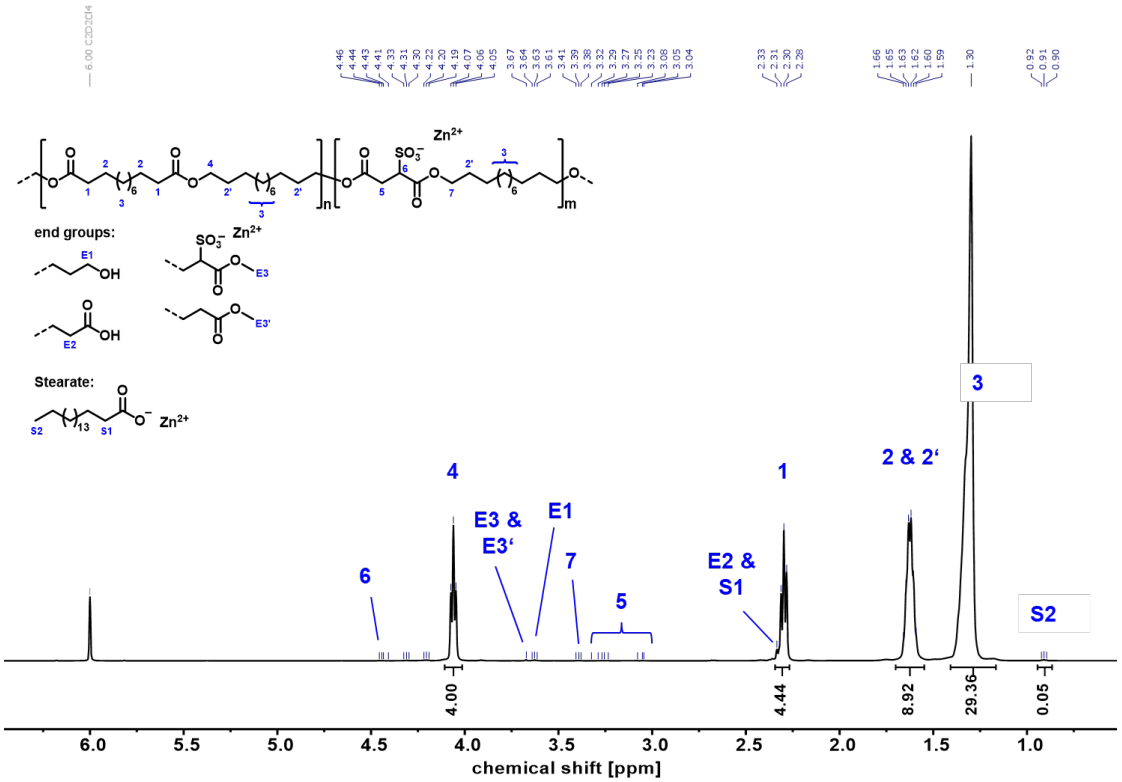

Figure 5.57 Full ^{1}H NMR spectrum (500 MHz, 323 K, $C_2D_2Cl_4$) of **PE12.12-SO$_3$Zn**. Note that protons 5 located next to the sulfonate group are diastereotopic and that the sulfonate group can be oriented either as shown, or the repeat unit can be oppositely arranged.

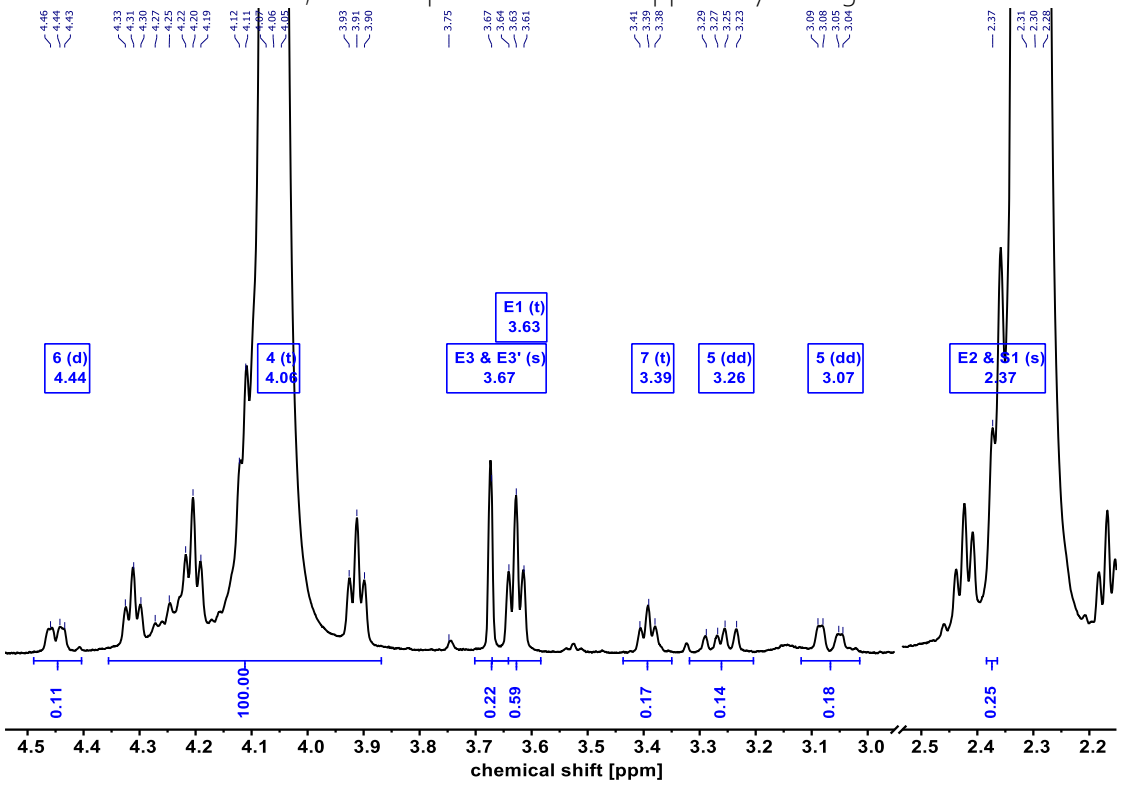

Figure 5.58 Detailed section of ^{1}H NMR spectrum (500 MHz, 323 K, $C_2D_2Cl_4$) of **PE12.12-SO$_3$Zn** with integrals of end groups as well as protons located close to the sulfonate group. Assignment of signals according to Figure 5.57.

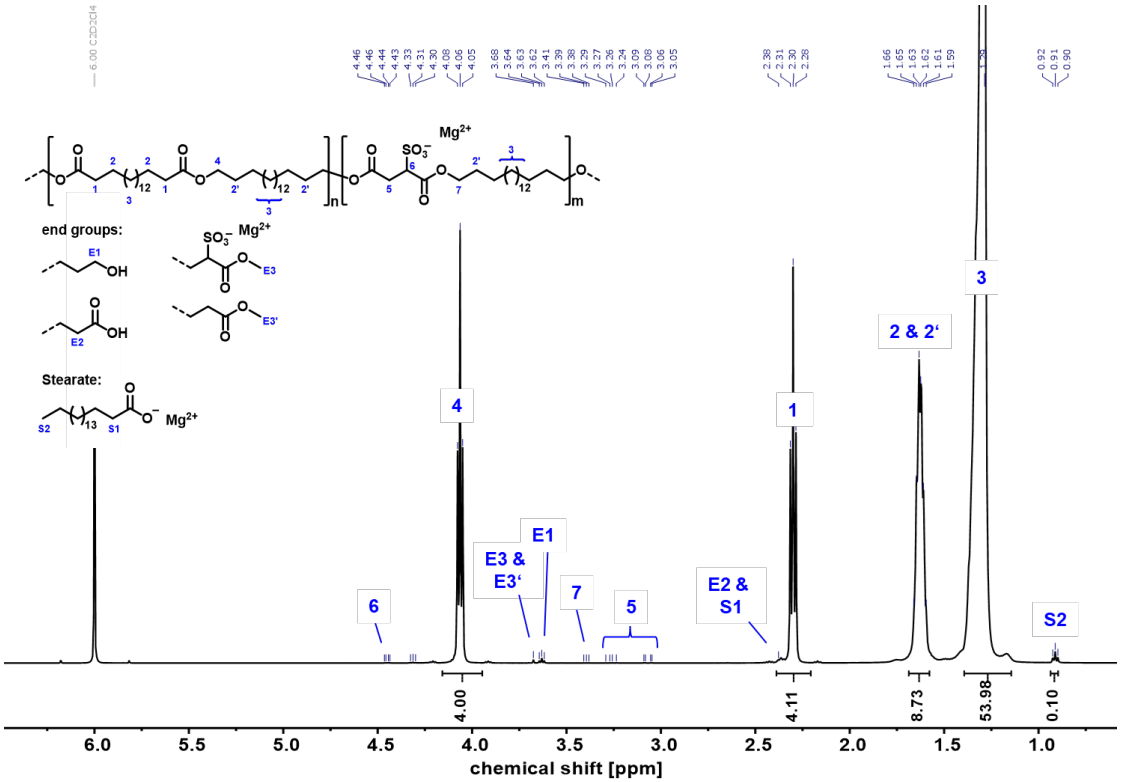

Figure 5.59 Full ^{1}H NMR spectrum (500 MHz, 323 K, $C_2D_2Cl_4$) of **PE18.18-SO$_3$Mg.** Note that protons 5 located next to the sulfonate group are diastereotopic and that the sulfonate group can be oriented either as shown, or the repeat unit can be oppositely arranged.

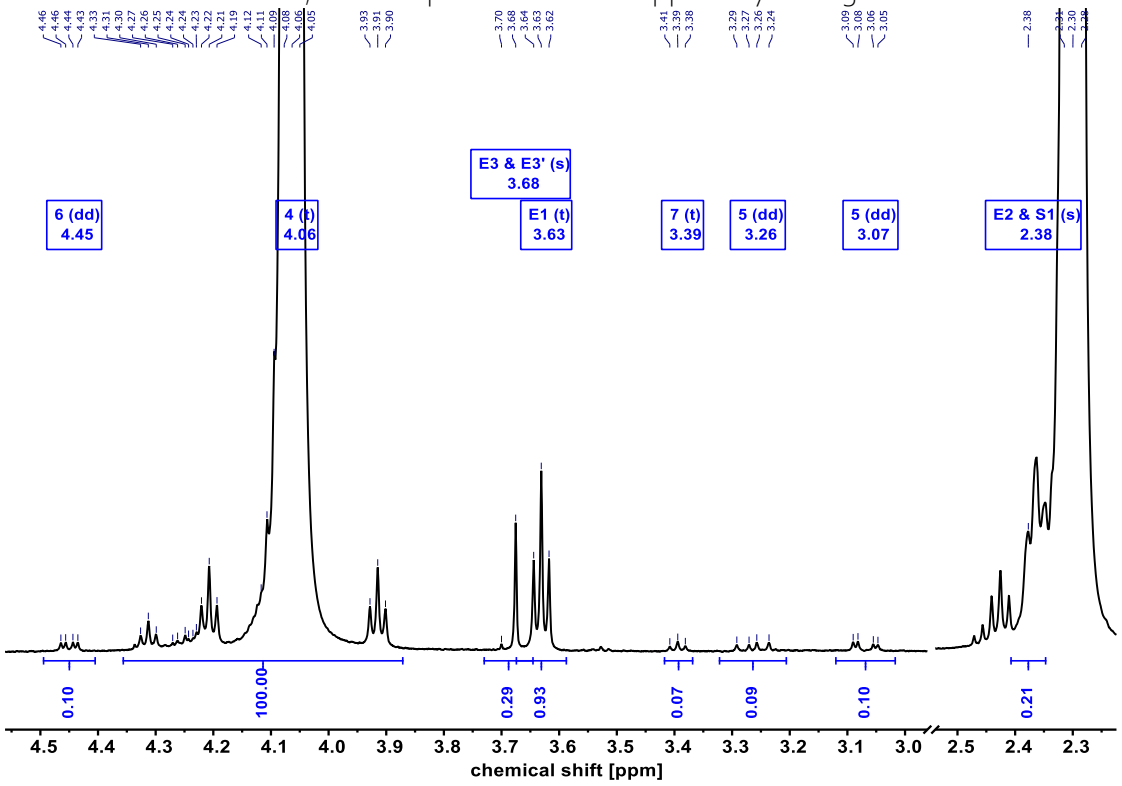

Figure 5.60 Detailed section of ^{1}H NMR spectrum (500 MHz, 323 K, $C_2D_2Cl_4$) of **PE18.18-SO$_3$Mg** with integrals of end groups as well as protons located close to the sulfonate group. Assignment of signals according to Figure 5.59.

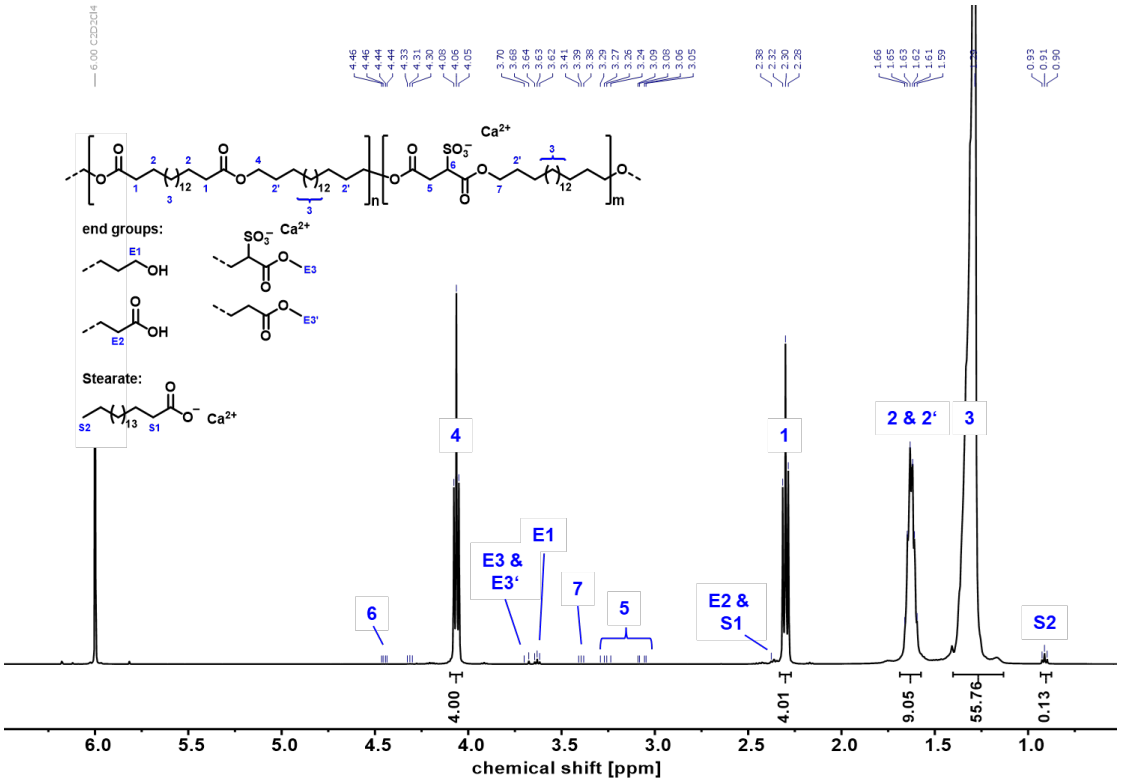

Figure 5.61 Full ^{1}H NMR spectrum (500 MHz, 323 K, $C_2D_2Cl_4$) of **PE18.18-SO$_3$Ca**. Note that protons 5 located next to the sulfonate group are diastereotopic and that the sulfonate group can be oriented either as shown, or the repeat unit can be oppositely arranged.

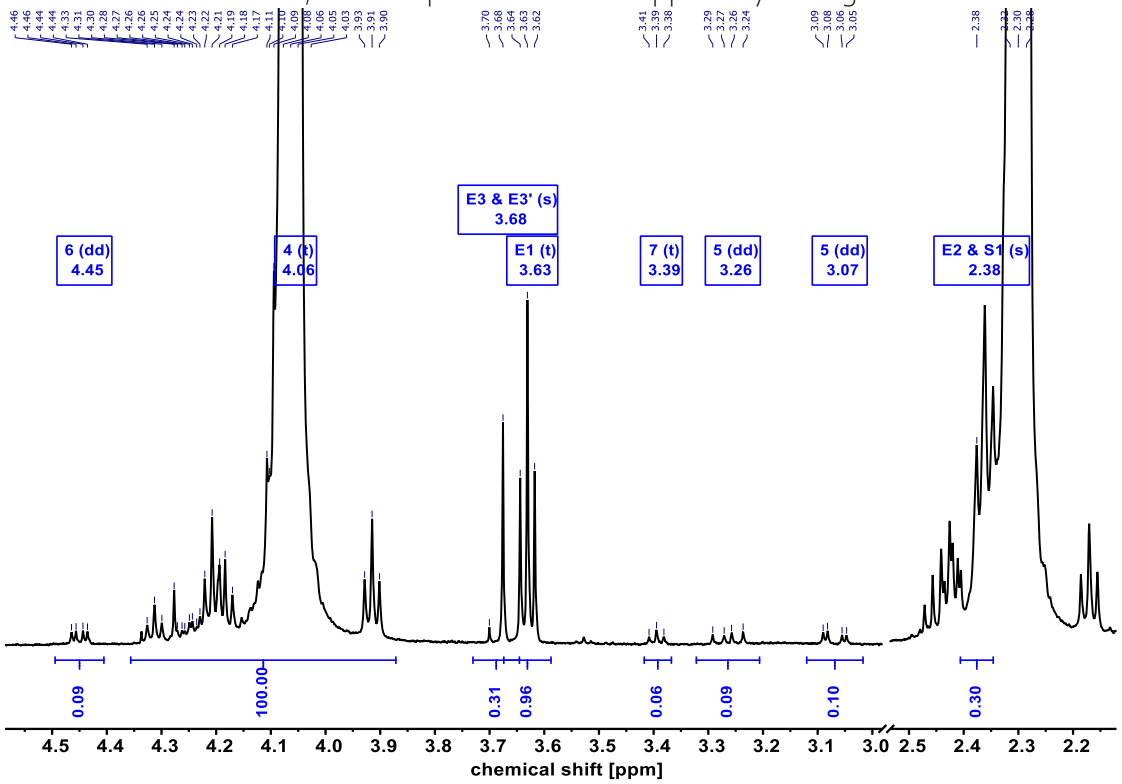

Figure 5.62 Detailed section of ^{1}H NMR spectrum (500 MHz, 323 K, $C_2D_2Cl_4$) of **PE18.18-SO$_3$Ca** with integrals of end groups as well as protons located close to the sulfonate group. Assignment of signals according to Figure 5.61.

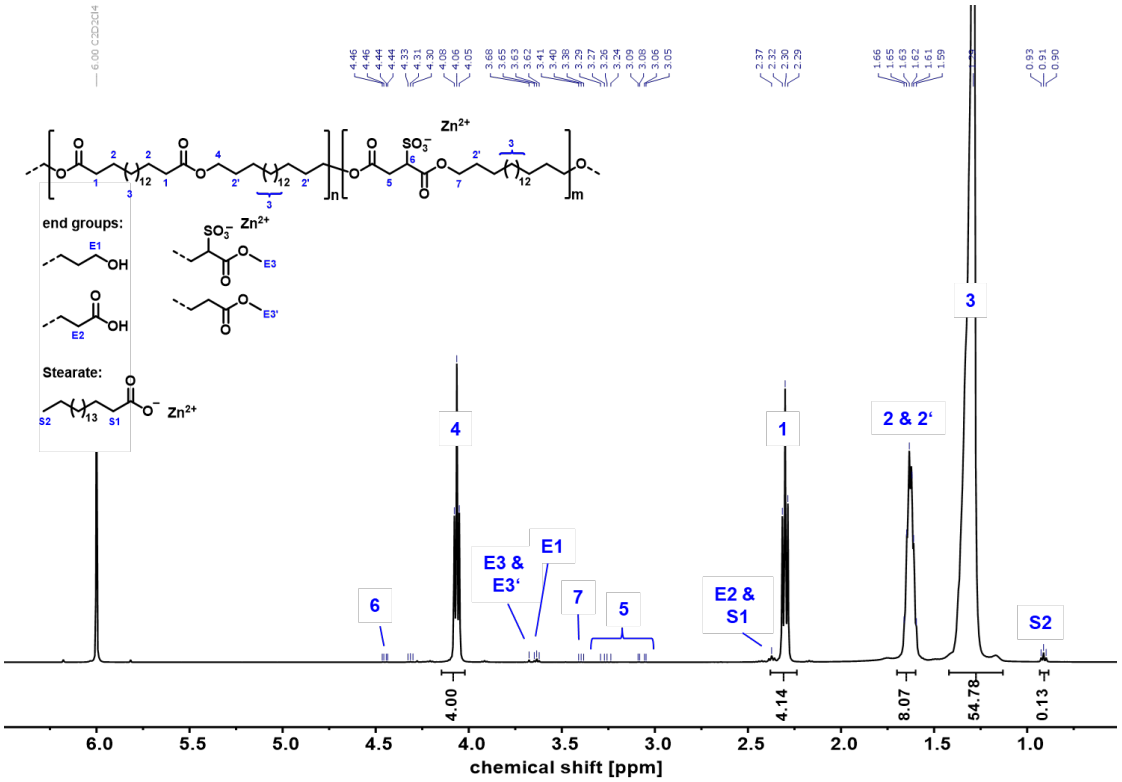

Figure 5.63 Full ^{1}H NMR spectrum (500 MHz, 323 K, $C_2D_2Cl_4$) of **PE18.18-SO$_3$Zn**. Note that protons 5 located next to the sulfonate group are diastereotopic and that the sulfonate group can be oriented either as shown, or the repeat unit can be oppositely arranged.

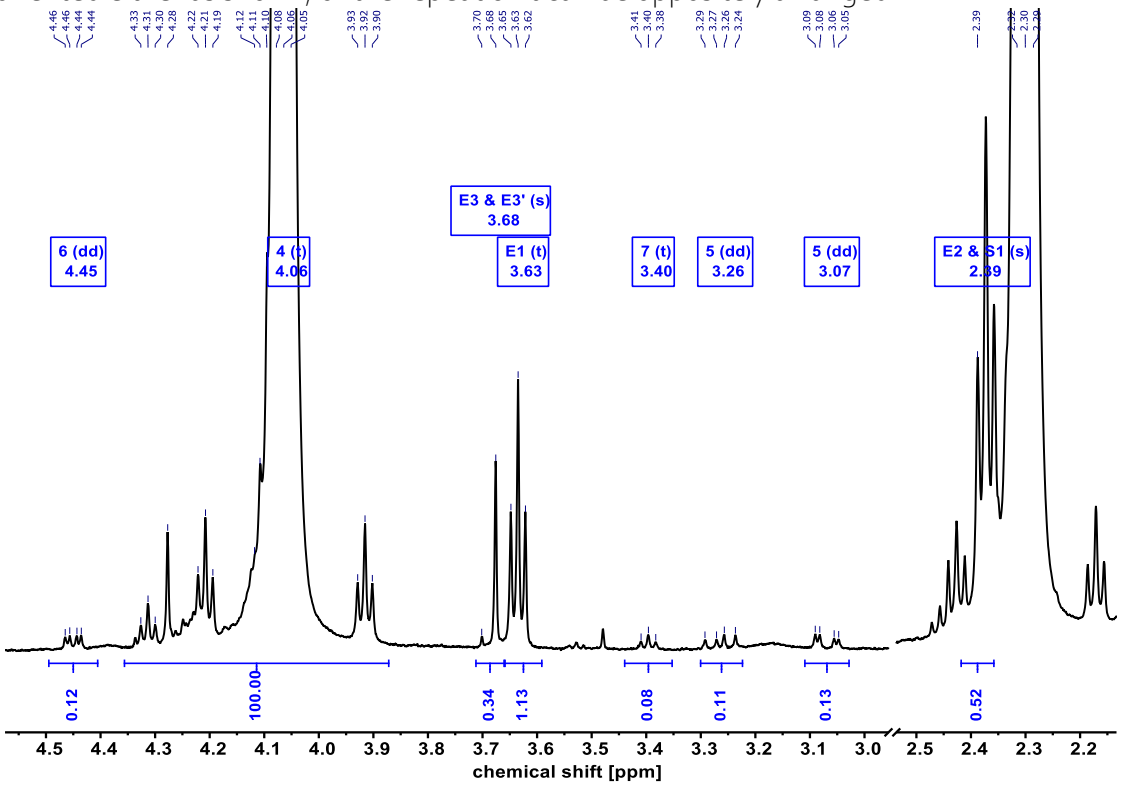

Figure 5.64 Detailed section of ^{1}H NMR spectrum (500 MHz, 323 K, $C_2D_2Cl_4$) of **PE18.18-SO$_3$Zn** with integrals of end groups as well as protons located close to the sulfonate group. Assignment of signals according to Figure 5.63.

5.6.11 ^{1}H NMR Spectra of PE12.12-M$_{stearate}$

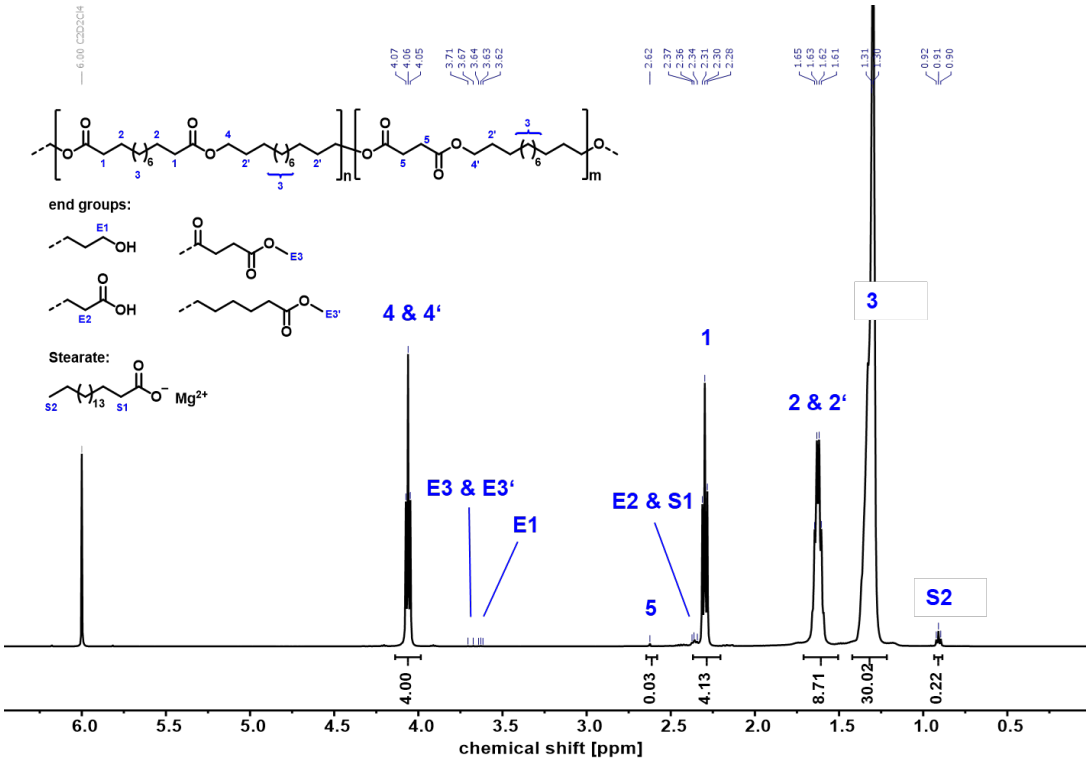

Figure 5.65 Full ^{1}H NMR spectrum (500 MHz, 323 K, $C_2D_2Cl_4$) of **PE12.12-Mg$_{stearate}$**.

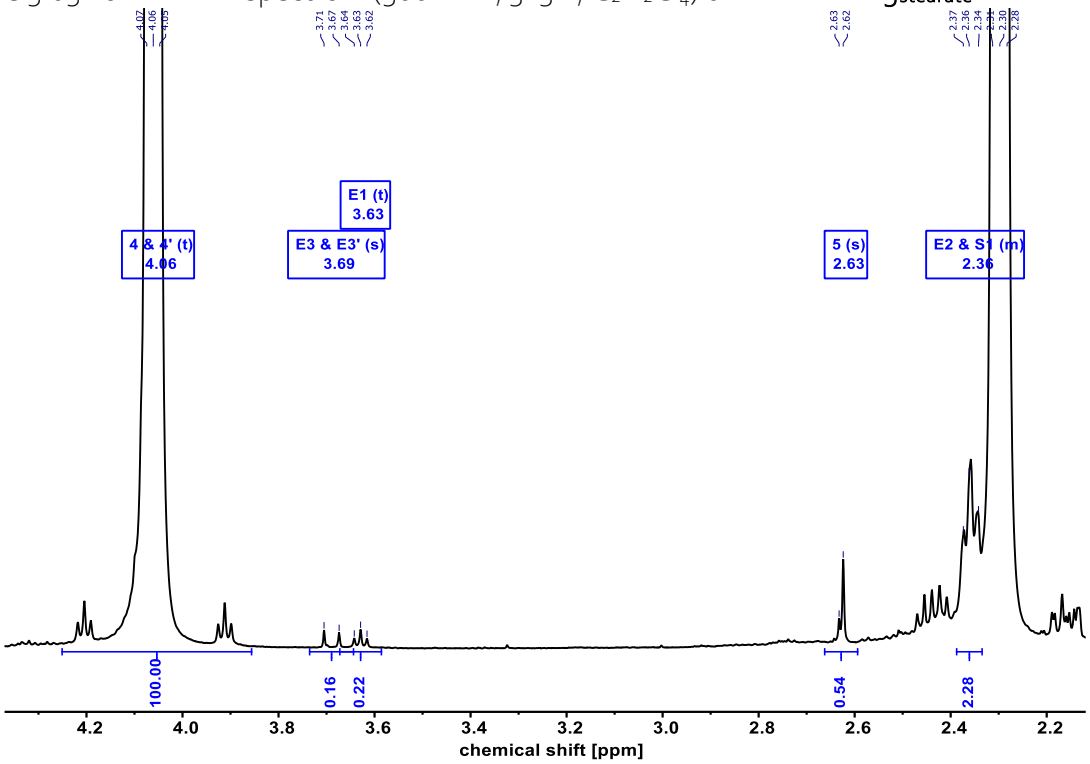

Figure 5.66 Detailed section of ^{1}H NMR spectrum (500 MHz, 323 K, $C_2D_2Cl_4$) of **PE12.12-Mg$_{stearate}$** with integrals of end groups, the succinate unit and excess stearate. Assignment of signals according to Figure 5.65.

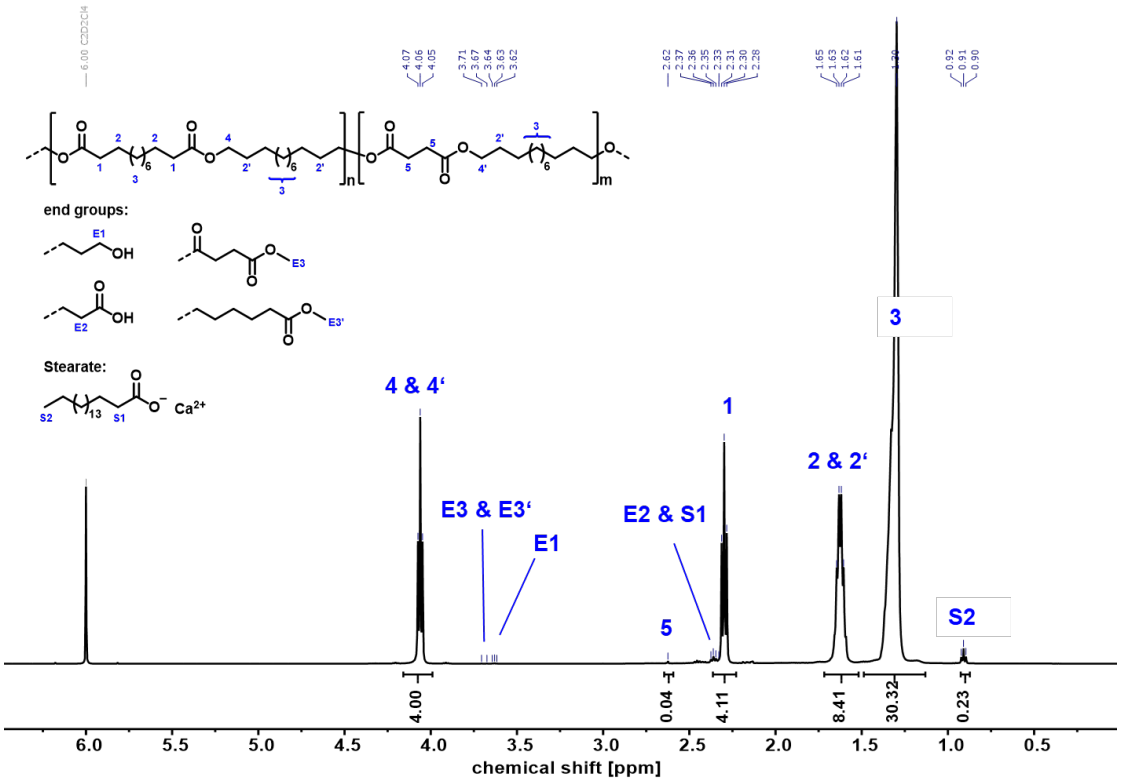

Figure 5.67 Full ^{1}H NMR spectrum (500 MHz, 323 K, $C_2D_2Cl_4$) of **PE12.12-Ca$_{stearate}$**.

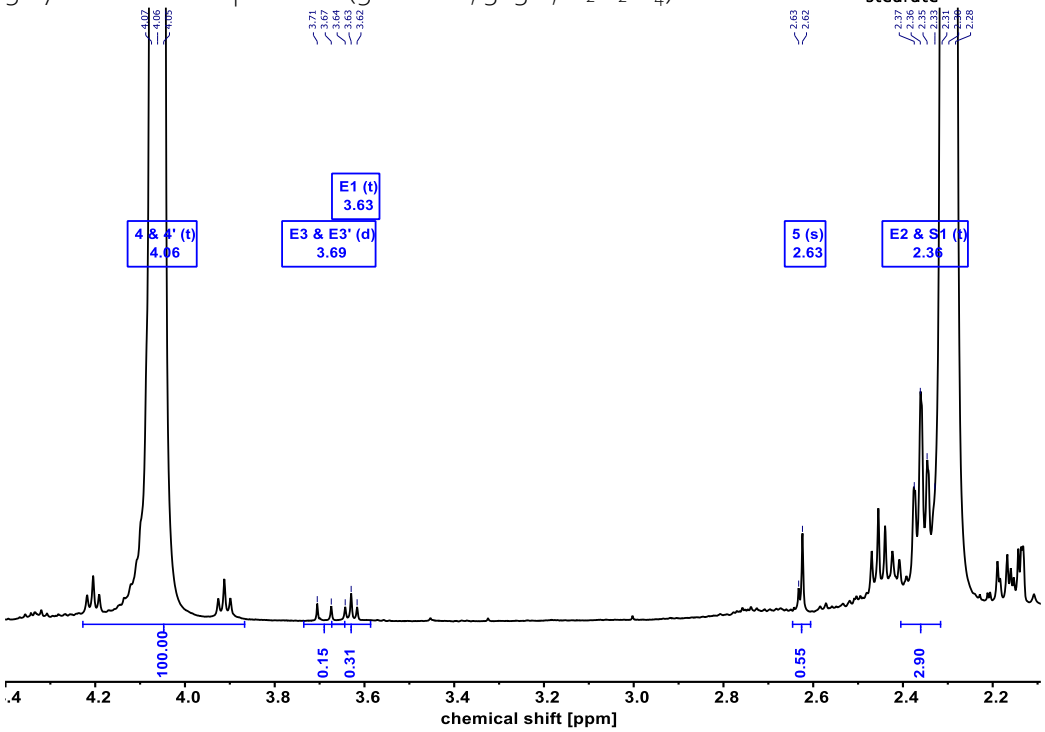

Figure 5.68 Detailed section of ^{1}H NMR spectrum (500 MHz, 323 K, $C_2D_2Cl_4$) of **PE12.12-Ca$_{stearate}$** with integrals of end groups, the succinate unit and excess stearate. Assignment of signals according to Figure 5.67.

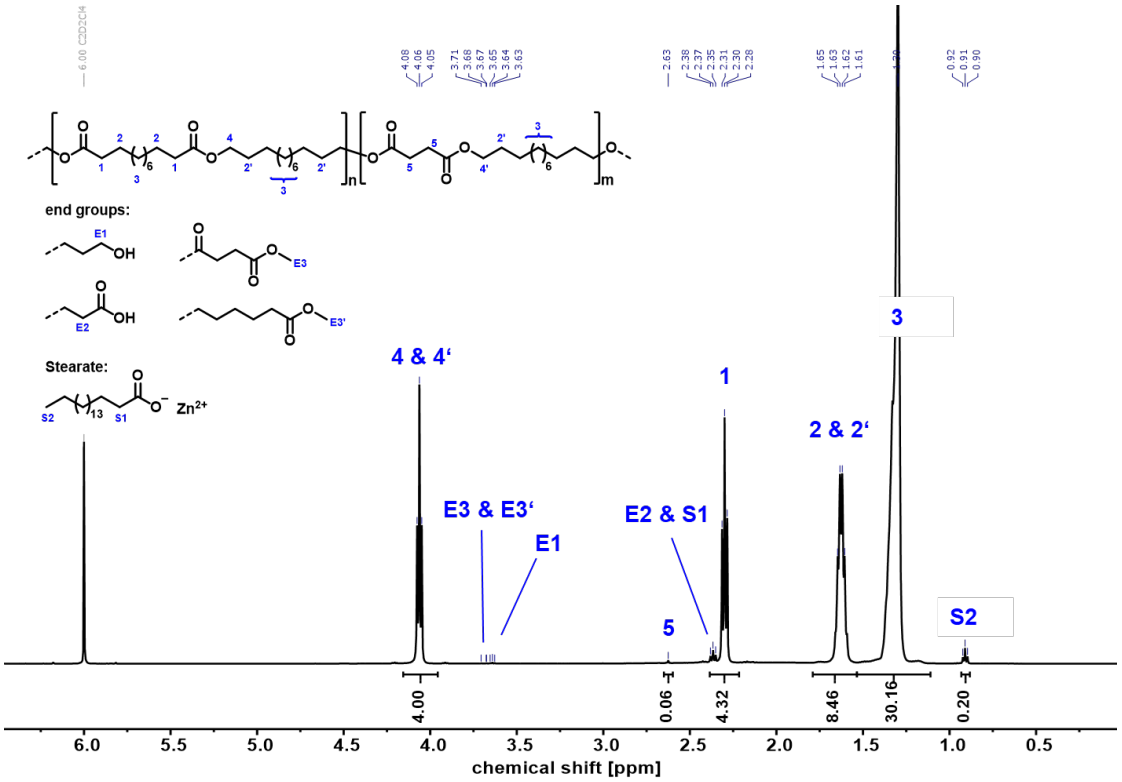

Figure 5.69 Full ^{1}H NMR spectrum (500 MHz, 323 K, $C_2D_2Cl_4$) of **PE12.12-Zn$_{stearate}$**.

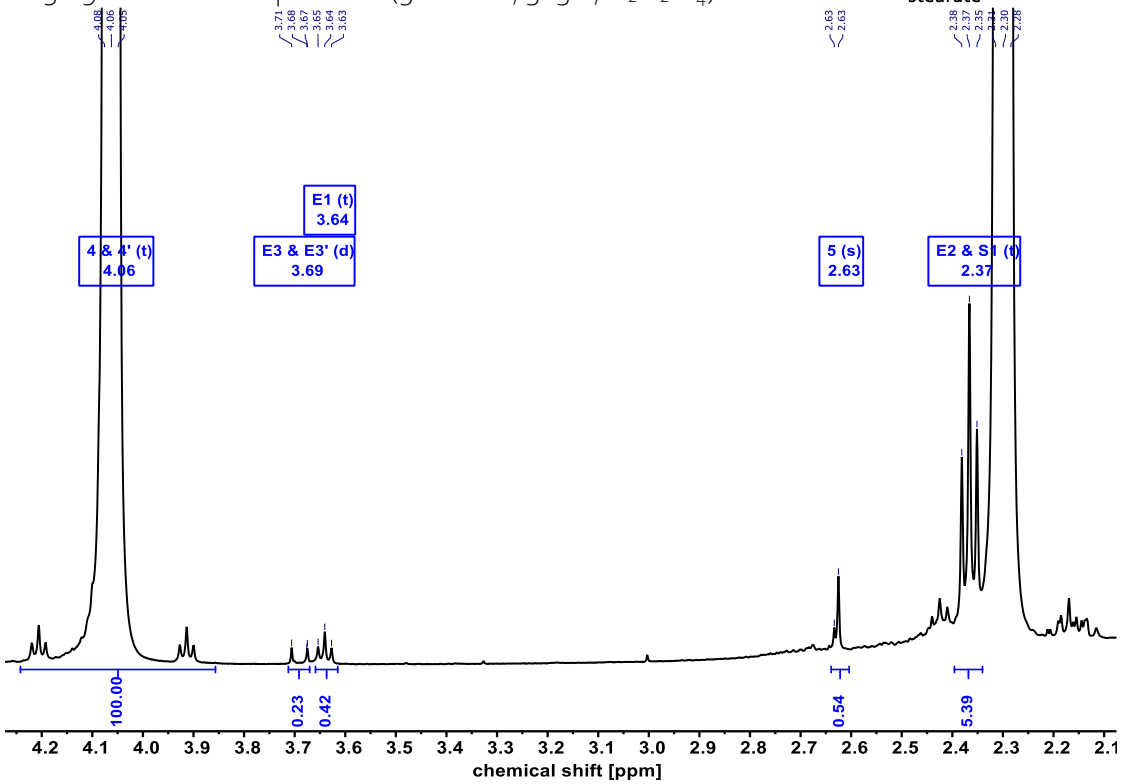

Figure 5.70 Detailed section of ^{1}H NMR spectrum (500 MHz, 323 K, $C_2D_2Cl_4$) of **PE12.12-Zn$_{stearate}$** with integrals of end groups, the succinate unit and excess stearate. Assignment of signals according to Figure 5.69.

5.6.12 ^{1}H NMR Spectrum of Recycling to Monomer

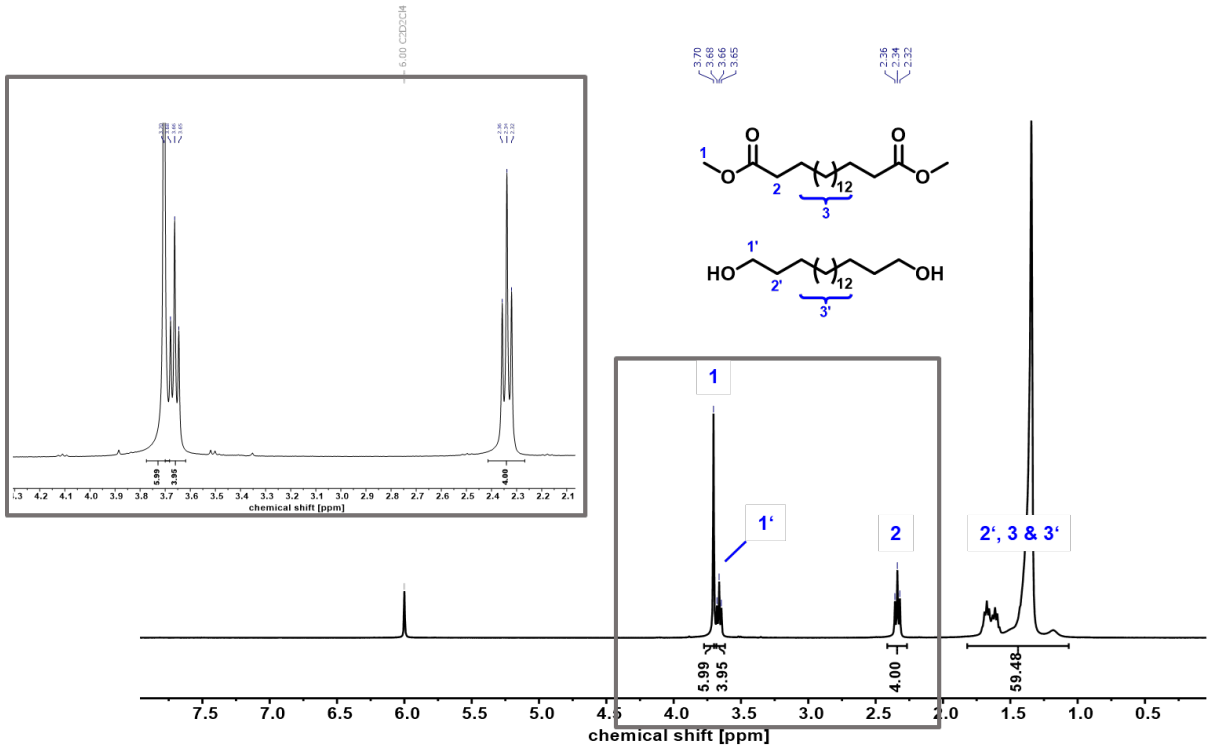

Figure 5.71 ^{1}H NMR spectrum (400 MHz, 383 K, $C_2D_2Cl_4$) monomer regenerated from PE18.18-SO3H-1.0. The product mixture contains C_{18}-diol and C_{18}-diester in a ratio of 1:0.99 as calculated from the ratio of signal 1' (triplet, 2.66 ppm) and 2 (triplet at 3.34 ppm). Inset shows grey marked region in closer detail and highlights the purity of the monomer mixture.

6 Conclusive Summary

It is undisputed that the microstructure of polymers is decisive for the crystallinity, the crystal structure, as well as other effects that can occur depending on the material. In the case of polymers with ionic groups, such additional influences are in particular the occurrence and structure of ionic aggregates. Ion-containing materials represent an important class of materials due to their specific properties that can only be achieved by the introduction of ionic groups covalently attached to the polymer backbones. Polymers with a precise chain length or spacing between functional groups allow predictable and fine tuning of structure-property relationships. To date, few such precisely defined polymers exist, and they usually require lengthy multistep syntheses on a laboratory scale, making them unfeasible for industrial applications. In contrast, polymers with ionic groups and uncontrolled morphology, such as Nafion or Surlyn as random copolymers, can be easily and inexpensively prepared on a large scale, but a deeper understanding of their structure-property relationship is lacking, and a control thereof remains elusive. In the present work, these issues have been addressed in different approaches, both in polymer electrolytes focusing on ion transport and by introducing very low ionic contents on fully recyclable polyethylene-like polyesters, thus tuning the material properties of the underlying polymers.

Polymers bearing phosphonic acid groups have been proposed as anhydrous proton-conducting membranes at elevated operating temperatures for applications in fuel cells. However, the synthesis of phosphonated polymers and the control over the nanostructure of such polymers is challenging. Here, a straight-forward synthesis of phosphonic acid-terminated, long-chain aliphatic materials with precisely 26 and 48 carbon atoms was developed from renewable resources ($C_{26}PA_2$ and $C_{48}PA_2$). These materials combine the structuring ability of monodisperse polyethylenes with the ability of phosphonic acid groups to form strong hydrogen-bonding networks. Undesired anhydride formation was found to not occur, so that charge carrier loss by a condensation reaction is avoided even at elevated temperatures. Below the melting temperature, both materials exhibit a crystalline polyethylene backbone and a layered

morphology with planar phosphonic acid aggregates separated by 29 and 55 Å for $C_{26}PA_2$ and $C_{48}PA_2$, respectively (see Figure 6.1). Above the melting temperature, the amorphous polyethylene segments coexist with the layered aggregates. This phenomenon is especially pronounced for the $C_{26}PA_2$ and is identified as a thermotropic smectic liquid crystalline phase. Under these conditions, an extraordinarily high correlation length (940 Å) along the layer normal is observed, demonstrating the strength of the hydrogen bond network formed by the phosphonic acid groups. The proton conductivity in both materials in the absence of water reaches 10^{-4} S/cm at 150 °C. These new precise phosphonic acid–based materials illustrate the importance of controlling the chemistry to form self-assembled nanoscale aggregates that facilitate rapid proton conductivity.

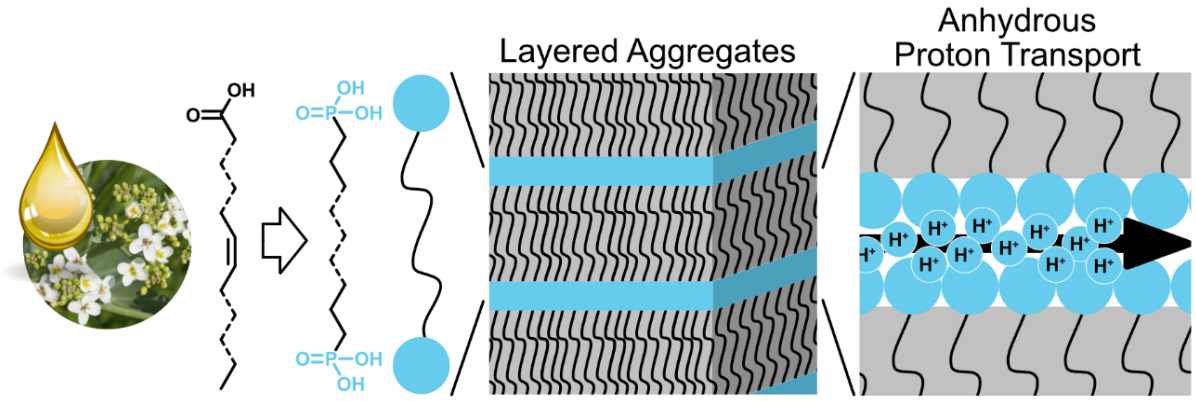

Figure 6.1 Schematic representation of the synthesis of phosphonic acid-terminated precise polyethylene-like materials from plant oils, their layered bulk structure below and above the melting temperature and the anhydrous proton transport within the layered aggregates.

The transport properties in precisely functionalized ion-containing materials is of interest regarding the development of single-ion conducting polymer electrolytes. The controlled positioning of the ionic groups results in a nanoscale morphology, that in turn controls the ion conductivity. This was studied for the case of precisely sulfonated polyester materials, accessed *via* step-growth polycondensation from a short-chain ionic, sulfonated block (dimethyl sulfosuccinate) and a long-chain, hydrophobic polyethylene-spacer with precisely 10, 12 or 18 methylene units. An investigation of the morphology and conductivity was performed in the group of Prof. Dr. K. I. Winey. At room temperature, these polymers exhibit layered ionic aggregates, which transition into hexagonal or double gyroid morphologies upon heating. Along with previously reported sulfonated polyesters with a higher length of the polyethylene spacer, a phase diagram was developed that reveals the dependence of the ionic aggregate morphology on the polar volume fraction f_{polar} and the temperature (see Figure 6.2). The desired bicontinuous

gyroid morphology was found at $0.27 < f_{polar} < 0.41$, which is a broad range compared to previously reported diblock copolymers. The found correlation of the ion transport with the ionic aggregate morphology shows the bicontinuous gyroid morphology is superior to the one-dimensional hexagonal and the two-dimensional layered morphologies. With these results at hand, guidelines for the development of single-ion conducting polymers exhibiting bicontinuous morphology structures are established, to rationalize the design of materials with effective ion transport.

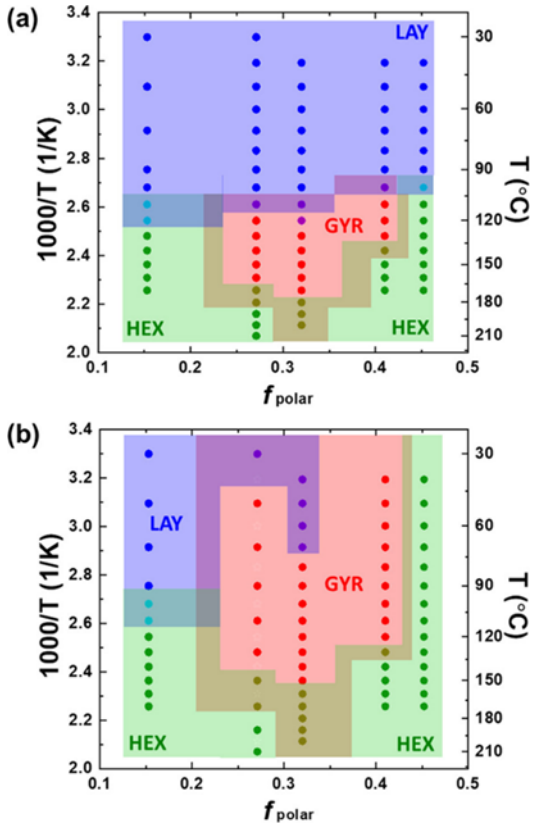

Figure 6.2 Morphology maps of polyestersulfonates bearing sodium counterions upon heating (a) and cooling (b). Ionic aggregate morphologies are denoted as LAY (layered), GYR (gyroid) and HEX (hexagonal).

Since the double gyroid morphology forms only when the polyethylene backbone is melted, an expansion of the gyroid regime to lower temperatures – ideally room temperature – could potentially be achieved by disrupting the crystalline order in the polyethylene backbone. To this end, branched repeat units that disturb crystallization are introduced by replacing a part of the linear long-chain diol by a so called fatty acid dimer diol (commercially available Pripol). Since the introduction of this monomer (C_{36}) reduces the polar volume fraction, a close analysis of f_{polar} depending on the molar amount of Pripol included and the length of the linear diol spacer was

conducted (see Figure 6.3). Different combinations of Pripol and lengths of the diol spacer were tested experimentally and a strong influence of the branched Pripol on the morphology was found. For example, the crystallinity in the polyethylene backbone was successfully hindered with 20 % Pripol in combination with C_{12}-diol as well as C_{18}-diol, yet a hexagonal morphology was found at room temperature for C_{18}-containing polymers and undefined layers were found for C_{12}-containing polymers. This shows the strong influence of Pripol not only on f_{polar} but also on the overall ordering in the materials.

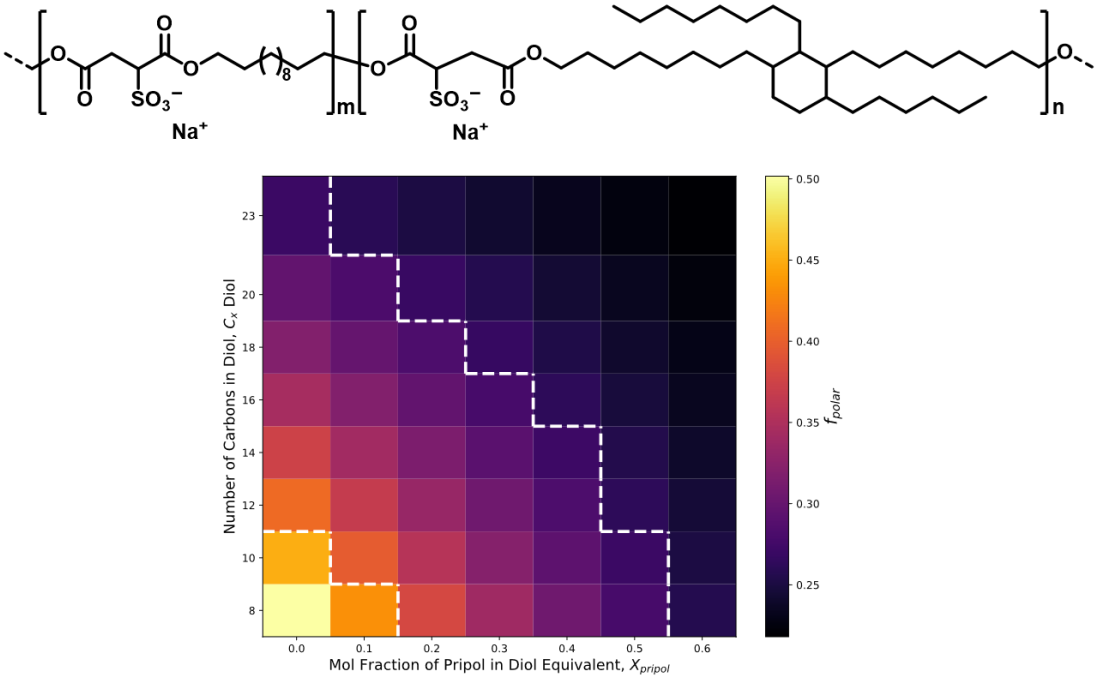

Figure 6.3 Top: structure of polyestersulfonates with branched repeat units, shown for sodium as counterion. Bottom: Calculated f_{polar} with respect to the amount of Pripol and the length of the diol spacer. Dashed lines show the different predicted morphologies, where $f_{polar} > 0.41$ leads to hexagonal morphologies, $f_{polar} < 0.27$ leads to layered aggregates, and $0.27 < f_{polar} < 0.41$ represents the expected gyroid region.

The introduced ionic interactions in these materials influence the material properties to a large extent. The non-ionic derivatives, polyesters from 1,18-octadecanediol and 1,18-octadecanedioic acid (PE18.18) exhibit properties comparable to HDPE with similar elasticity and ductility.[38] The polyestersulfonates, however, are salt-like, brittle materials due to the high ionic contents and, consequently, strong Coulombic interactions. Controlling these strong interactions is difficult but necessary, since they significantly influence the material properties (e.g. mechanical or thermal properties). Within this work, it was possible to introduce very low amounts of sulfonate groups into the HDPE-like polyester (PE18.18). This approach allowed for a

significant influence of the processing and materials properties despite the relatively low amounts of ionic groups (0.5 – 1.0 mol-%). The stiffness and ductility are influenced, and water uptake and hydrolytic degradation of the polyesters is promoted by the sulfonate units. This is noteworthy regarding the otherwise hydrophobic and hydrolytically stable non-ionic analogue (PE12.12 or PE18.18). The melt viscosity is substantially increased upon the introduction of bivalent counterions to the in-chain sulfonate groups, making these materials especially interesting for processing methods that require high melt stability (e.g. film blowing). The increased surface energy of the ion-containing polyesters is additionally reflected in a higher adhesion of inks. Regarding the recyclability, these materials can be fully depolymerized to reobtain the long-chain aliphatic monomers owing to the solvolytically cleavable in-chain ester groups.

In summary, this work provides guidelines for the generation and investigation of precise ion-containing polymers for applications such as proton exchange membranes in fuel cells or solid polymer electrolytes. The advantages were shown to include their controlled morphology of both, the non-ionic spacers and the ionic aggregates. A random clustering of the ionic aggregates, which is a major issue and disadvantage of classical polymer electrolytes, can be hindered by following this approach. A deeper understanding of the appearance of such desirable morphologies in polymer electrolytes is gained from these investigations.

A straight-forward synthetic approach was extended to ion-containing materials with low amounts of ionic groups, giving rise to recyclable and degradable ion-containing polymers with HDPE-like properties. Despite their low concentration, the ionic groups and their counterions have a profound impact on the melt rheology and on the surface properties of the materials. An object of future interest could be the impact of low concentrations of ionic groups on the degradability of HDPE-like materials, as well as ionomers with higher concentrations of ionic groups as intermediates to these materials and the polymer electrolytes discussed in this work.

7 References

1. Strobl, G. R., *The Physics of Polymers: Concepts for Understanding Their Structures and Behavior*, Springer Berlin Heidelberg, **2007**.

2. Zhang, L.; Brostowitz, N. R.; Cavicchi, K. A.; Weiss, R. A., Perspective: Ionomer Research and Applications. *Macromolecular Reaction Engineering* **2014,** *8* (2), 81-99.

3. *Ionomers*, Tant, M. R.; Mauritz, K. A.; Wilkes, G. L., Eds. Springer Netherlands, Dordrecht, **1997**.

4. Press release. NobelPrize.org. **https://www.nobelprize.org/prizes/chemistry/2019/press-release/** (accessed 16th Jan 2023).

5. Künkel, A.; Becker, J.; Börger, L.; Hamprecht, J.; Koltzenburg, S.; Loos, R.; Schick, M. B.; Schlegel, K.; Sinkel, C.; Skupin, G.; Yamamoto, M., Polymers, Biodegradable. In *Ullmann's Encyclopedia of Industrial Chemistry*, **2016**; 1-29.

6. Elias, H. G., Specialty Plastics. *Ullmann's Encyclopedia of Industrial Chemistry* **2000**.

7. Jérôme, R.; Mazurek, M., Synthesis and characterization of molecular structure. In *Ionomers: Synthesis, structure, properties and applications*, Tant, M. R.; Mauritz, K. A.; Wilkes, G. L., Eds. Springer Netherlands: Dordrecht, **1997**; 3-40.

8. Rees, R. W. US Patent 3264272, Ionic Hydrocarbon Polymers. 1966.

9. Middleton, L. R.; Winey, K. I., Nanoscale Aggregation in Acid- and Ion-Containing Polymers. *Annual Review of Chemical and Biomolecular Engineering* **2017,** *8* (1), 499-523.

10. Eisenberg, A.; Hird, B.; Moore, R. B., A new multiplet-cluster model for the morphology of random ionomers. *Macromolecules* **1990,** *23* (18), 4098-4107.

11. Bose, R. K.; Hohlbein, N.; Garcia, S. J.; Schmidt, A. M.; van der Zwaag, S., Connecting supramolecular bond lifetime and network mobility for scratch healing in poly(butyl acrylate) ionomers containing sodium, zinc and cobalt. *Physical Chemistry Chemical Physics* **2015,** *17* (3), 1697-1704.

12. Longworth, R.; Vaughan, D. J., Physical Structure of Ionomers. *Nature* **1968,** *218* (5136), 85-87.

13. Eisenberg, A.; Kim, J.-S., *Introduction to Ionomers*, Wiley, New York, **1998**.

14. Seitz, M. E.; Chan, C. D.; Opper, K. L.; Baughman, T. W.; Wagener, K. B.; Winey, K. I., Nanoscale Morphology in Precisely Sequenced Poly(ethylene-co-acrylic acid) Zinc Ionomers. *Journal of the American Chemical Society* **2010,** *132* (23), 8165-8174.

15. Middleton, L. R.; Szewczyk, S.; Azoulay, J.; Murtagh, D.; Rojas, G.; Wagener, K. B.; Cordaro, J.; Winey, K. I., Hierarchical Acrylic Acid Aggregate Morphologies Produce Strain-Hardening in Precise Polyethylene-Based Copolymers. *Macromolecules* **2015,** *48* (11), 3713-3724.

16. Buitrago, C. F.; Jenkins, J. E.; Opper, K. L.; Aitken, B. S.; Wagener, K. B.; Alam, T. M.; Winey, K. I., Room Temperature Morphologies of Precise Acid- and Ion-Containing Polyethylenes. *Macromolecules* **2013,** *46* (22), 9003-9012.

17. Baughman, T. W.; Chan, C. D.; Winey, K. I.; Wagener, K. B., Synthesis and Morphology of Well-Defined Poly(ethylene-co-acrylic acid) Copolymers. *Macromolecules* **2007,** *40* (18), 6564-6571.

18. Trigg, E. B.; Stevens, M. J.; Winey, K. I., Chain Folding Produces a Multilayered Morphology in a Precise Polymer: Simulations and Experiments. *Journal of the American Chemical Society* **2017,** *139* (10), 3747-3755.

19. Scogna, R. C.; Register, R. A., Yielding in ethylene/methacrylic acid ionomers. *Polymer* **2009,** *50* (2), 585-590.

20. Han, S.-I.; Yoo, Y.; Kim, D. K.; Im, S. S., Biodegradable Aliphatic Polyester Ionomers. *Macromolecular Bioscience* **2004,** *4* (3), 199-207.

21. Hwang, S. Y.; Jin, X. Y.; Yoo, E. S.; Im, S. S., Synthesis, physical properties and enzymatic degradation of poly (oxyethylene-b-butylene succinate) ionomers. *Polymer* **2011,** *52* (13), 2784-2791.

22. Lv, L.; Wu, F.; Chen, S.-C.; Wang, Y.-Z.; Zeng, J.-B., Properties regulation of poly(butylene succinate) ionomers through their ionic group distribution. *Polymer* **2015,** *66*, 148-159.

23. Wu, S.; Zheng, L.; Li, C.; Huo, S.; Xiao, Y.; Guan, G.; Zhu, W., A facile and versatile strategy to efficiently synthesize sulfonated poly(butylene succinate), self-assembly behavior and biocompatibility. *Polymer Chemistry* **2015,** *6* (9), 1495-1501.

24. Lee, H. J.; Cho, W. Y.; Lee, H. C.; Seo, Y. H.; Baek, J. W.; Lee, P. C.; Lee, B. Y., Rapid Biodegradable Ionic Aggregates of Polyesters Constructed with Fertilizer Ingredients. *Journal of the American Chemical Society* **2022,** *144* (35), 15911–15915.

25. Huang, F.; Wu, L.; Li, B.-G., Sulfonated biodegradable PBAT copolyesters with improved gas barrier properties and excellent water dispersibility: From synthesis to structure-property. *Polymer Degradation and Stability* **2020,** *182*, 109391.

26. Tasdelen, M. A.; Kahveci, M. U.; Yagci, Y., Telechelic polymers by living and controlled/living polymerization methods. *Progress in Polymer Science* **2011,** *36* (4), 455-567.

27. Jian, Z.; Falivene, L.; Boffa, G.; Sánchez, S. O.; Caporaso, L.; Grassi, A.; Mecking, S., Direct Synthesis of Telechelic Polyethylene by Selective Insertion Polymerization. *Angewandte Chemie International Edition* **2016,** *55* (46), 14378-14383.

28. Yan, L.; Häußler, M.; Bauer, J.; Mecking, S.; Winey, K. I., Monodisperse and Telechelic Polyethylenes Form Extended Chain Crystals with Ionic Layers. *Macromolecules* **2019,** *52* (13), 4949-4956.

29. Paren, B. A.; Häußler, M.; Rathenow, P.; Mecking, S.; Winey, K. I., Decoupled Cation Transport within Layered Assemblies in Sulfonated and Crystalline Telechelic Polyethylenes. *Macromolecules* **2022,** *55* (7), 2813-2820.

30. Witt, T.; Häußler, M.; Kulpa, S.; Mecking, S., Chain Multiplication of Fatty Acids to Precise Telechelic Polyethylene. *Angewandte Chemie International Edition* **2017,** *56* (26), 7589-7594.

31. Jiménez-Rodriguez, C.; Eastham, G. R.; Cole-Hamilton, D. J., Dicarboxylic acid esters from the carbonylation of unsaturated esters under mild conditions. *Inorganic Chemistry Communications* **2005,** *8* (10), 878-881.

32. Pugh, R. I.; Drent, E.; Pringle, P. G., Tandem isomerisation–carbonylation catalysis: highly active palladium(ii) catalysts for the selective methoxycarbonylation of internal alkenes to linear esters. *Chemical Communications* **2001,** (16), 1476-1477.

33. Stempfle, F.; Quinzler, D.; Heckler, I.; Mecking, S., Long-Chain Linear C19 and C23 Monomers and Polycondensates from Unsaturated Fatty Acid Esters. *Macromolecules* **2011,** *44* (11), 4159-4166.

34. Quinzler, D.; Mecking, S., Linear Semicrystalline Polyesters from Fatty Acids by Complete Feedstock Molecule Utilization. *Angewandte Chemie International Edition* **2010,** *49* (25), 4306-4308.

35. Biermann, U.; Bornscheuer, U.; Meier, M. A. R.; Metzger, J. O.; Schäfer, H. J., Oils and Fats as Renewable Raw Materials in Chemistry. *Angewandte Chemie International Edition* **2011,** *50* (17), 3854-3871.

36. Eck, M.; Schwab, S. T.; Nelson, T. F.; Wurst, K.; Iberl, S.; Schleheck, D.; Link, C.; Battagliarin, G.; Mecking, S., Biodegradable High-Density Polyethylene-like Material. *Angewandte Chemie International Edition* **2022,** *n/a* (n/a), e202213438.

37. Mecking, S., Polyethylene-like materials from plant oils. *Philosophical Transactions of the Royal Society A: Mathematical, Physical and Engineering Sciences* **2020,** *378* (2176), 20190266.

38. Häußler, M.; Eck, M.; Rothauer, D.; Mecking, S., Closed-loop recycling of polyethylene-like materials. *Nature* **2021,** *590* (7846), 423-427.

39. Ortmann, P.; Heckler, I.; Mecking, S., Physical properties and hydrolytic degradability of polyethylene-like polyacetals and polycarbonates. *Green Chemistry* **2014,** *16* (4), 1816-1827.

40. Busch, H.; Schiebel, E.; Sickinger, A.; Mecking, S., Ultralong-Chain-Spaced Crystalline Poly(H-phosphonate)s and Poly(phenylphosphonate)s. *Macromolecules* **2017,** *50* (20), 7901-7910.

41. Stempfle, F.; Ortmann, P.; Mecking, S., Which Polyesters Can Mimic Polyethylene? *Macromolecular Rapid Communications* **2013,** *34* (1), 47-50.

42. Winter, M.; Brodd, R. J., What Are Batteries, Fuel Cells, and Supercapacitors? *Chemical Reviews* **2004,** *104* (10), 4245-4270.

43. Li, M.; Lu, J.; Chen, Z.; Amine, K., 30 Years of Lithium-Ion Batteries. *Advanced Materials* **2018,** *30* (33), 1800561.

44. Hallinan, D. T.; Balsara, N. P., Polymer Electrolytes. *Annual Review of Materials Research* **2013,** *43* (1), 503-525.

45. Zhang, H.; Shen, P. K., Recent Development of Polymer Electrolyte Membranes for Fuel Cells. *Chemical Reviews* **2012,** *112* (5), 2780-2832.

46. Quartarone, E.; Mustarelli, P., Electrolytes for solid-state lithium rechargeable batteries: recent advances and perspectives. *Chemical Society Reviews* **2011,** *40* (5), 2525-2540.

47. Manthiram, A.; Yu, X.; Wang, S., Lithium battery chemistries enabled by solid-state electrolytes. *Nature Reviews Materials* **2017,** *2* (4), 16103.

48. Fenton, D. E.; Parker, J. M.; Wright, P. V., Complexes of alkali metal ions with poly(ethylene oxide). *Polymer* **1973,** *14*, 589.

49. Strauss, E.; Menkin, S.; Golodnitsky, D., On the way to high-conductivity single lithium-ion conductors. *Journal of Solid State Electrochemistry* **2017,** *21* (7), 1879-1905.

50. Zhang, H.; Li, C.; Piszcz, M.; Coya, E.; Rojo, T.; Rodriguez-Martinez, L. M.; Armand, M.; Zhou, Z., Single lithium-ion conducting solid polymer electrolytes: advances and perspectives. *Chemical Society Reviews* **2017,** *46* (3), 797-815.

51. Rank, C.; Yan, L.; Mecking, S.; Winey, K. I., Periodic Polyethylene Sulfonates from Polyesterification: Bulk and Nanoparticle Morphologies and Ionic Conductivities. *Macromolecules* **2019,** *52* (21), 8466-8475.

52. Trigg, E. B.; Middleton, L. R.; Moed, D. E.; Winey, K. I., Transverse Orientation of Acid Layers in the Crystallites of a Precise Polymer. *Macromolecules* **2017,** *50* (22), 8988-8995.

53. Trigg, E. B.; Gaines, T. W.; Maréchal, M.; Moed, D. E.; Rannou, P.; Wagener, K. B.; Stevens, M. J.; Winey, K. I., Self-assembled highly ordered acid layers in precisely sulfonated polyethylene produce efficient proton transport. *Nature Materials* **2018,** *17* (8), 725-731.

54. Abbott, L. J.; Buss, H. G.; Thelen, J. L.; McCloskey, B. D.; Lawson, J. W., Polyanion Electrolytes with Well-Ordered Ionic Layers in Simulations and Experiment. *Macromolecules* **2019**.

55. Ichikawa, T.; Yoshio, M.; Hamasaki, A.; Mukai, T.; Ohno, H.; Kato, T., Self-Organization of Room-Temperature Ionic Liquids Exhibiting Liquid-Crystalline Bicontinuous Cubic Phases: Formation of Nano-Ion Channel Networks. *Journal of the American Chemical Society* **2007,** *129* (35), 10662-10663.

56. Yan, L.; Rank, C.; Mecking, S.; Winey, K. I., Gyroid and Other Ordered Morphologies in Single-Ion Conducting Polymers and Their Impact on Ion Conductivity. *Journal of the American Chemical Society* **2020,** *142* (2), 857-866.

57. Mauritz, K. A.; Moore, R. B., State of Understanding of Nafion. *Chemical Reviews* **2004,** *104* (10), 4535-4586.

58. Kusoglu, A.; Weber, A. Z., New Insights into Perfluorinated Sulfonic-Acid Ionomers. *Chemical Reviews* **2017,** *117* (3), 987-1104.

59. Peighambardoust, S. J.; Rowshanzamir, S.; Amjadi, M., Review of the proton exchange membranes for fuel cell applications. *International Journal of Hydrogen Energy* **2010,** *35* (17), 9349-9384.

60. Kreuer, K.-D., Ion Conducting Membranes for Fuel Cells and other Electrochemical Devices. *Chemistry of Materials* **2014,** *26* (1), 361-380.

61. Gierke, T. D.; Munn, G. E.; Wilson, F. C., The morphology in nafion perfluorinated membrane products, as determined by wide- and small-angle x-ray studies. *Journal of Polymer Science: Polymer Physics Edition* **1981,** *19* (11), 1687-1704.

62. Trigg, E. B.; Winey, K. I., Nanoscale layers in polymers to promote ion transport. *Molecular Systems Design & Engineering* **2019,** *4* (2), 252-262.

63. Cheng, S.; Smith, D. M.; Li, C. Y., How Does Nanoscale Crystalline Structure Affect Ion Transport in Solid Polymer Electrolytes? *Macromolecules* **2014,** *47* (12), 3978-3986.

64. Alberti, G.; Casciola, M.; Massinelli, L.; Bauer, B., Polymeric proton conducting membranes for medium temperature fuel cells (110–160°C). *Journal of Membrane Science* **2001,** *185* (1), 73-81.

65. Chandan, A.; Hattenberger, M.; El-kharouf, A.; Du, S.; Dhir, A.; Self, V.; Pollet, B. G.; Ingram, A.; Bujalski, W., High temperature (HT) polymer electrolyte membrane fuel cells (PEMFC) – A review. *Journal of Power Sources* **2013,** *231*, 264-278.

66. Devanathan, R., Recent developments in proton exchange membranes for fuel cells. *Energy & Environmental Science* **2008,** *1* (1), 101-119.

67. Zawodzinski, T. A., Water Uptake by and Transport Through Nafion® 117 Membranes. *Journal of The Electrochemical Society* **1993,** *140* (4), 1041.

68. Rosli, R. E.; Sulong, A. B.; Daud, W. R. W.; Zulkifley, M. A.; Husaini, T.; Rosli, M. I.; Majlan, E. H.; Haque, M. A., A review of high-temperature proton exchange membrane fuel cell (HT-PEMFC) system. *International Journal of Hydrogen Energy* **2017,** *42* (14), 9293-9314.

69. Araya, S. S.; Zhou, F.; Liso, V.; Sahlin, S. L.; Vang, J. R.; Thomas, S.; Gao, X.; Jeppesen, C.; Kær, S. K., A comprehensive review of PBI-based high temperature PEM fuel cells. *International Journal of Hydrogen Energy* **2016,** *41* (46), 21310-21344.

70. Miyatake, K.; Hay, A. S., New poly(arylene ether)s with pendant phosphonic acid groups. *Journal of Polymer Science Part A: Polymer Chemistry* **2001,** *39* (21), 3770-3779.

71. Schuster, M.; Kreuer, K.-D.; Steininger, H.; Maier, J., Proton conductivity and diffusion study of molten phosphonic acid H_3PO_3. *Solid State Ionics* **2008,** *179* (15), 523-528.

72. Jung, H. Y.; Kim, S. Y.; Kim, O.; Park, M. J., Effect of the Protogenic Group on the Phase Behavior and Ion Transport Properties of Acid-Bearing Block Copolymers. *Macromolecules* **2015,** *48* (17), 6142-6152.

73. Paddison, S. J.; Kreuer, K.-D.; Maier, J., About the choice of the protogenic group in polymer electrolyte membranes: Ab initio modelling of sulfonic acid, phosphonic acid, and imidazole functionalized alkanes. *Physical Chemistry Chemical Physics* **2006,** *8* (39), 4530-4542.

74. Meng, Y. Z.; Tjong, S. C.; Hay, A. S.; Wang, S. J., Proton-exchange membrane electrolytes derived from phosphonic acid containing poly(arylene ether)s. *European Polymer Journal* **2003,** *39* (3), 627-631.

75. Steininger, H.; Schuster, M.; Kreuer, K. D.; Kaltbeitzel, A.; Bingöl, B.; Meyer, W. H.; Schauff, S.; Brunklaus, G.; Maier, J.; Spiess, H. W., Intermediate temperature proton conductors for PEM fuel cells based on phosphonic acid as protogenic group: A progress report. *Physical Chemistry Chemical Physics* **2007,** *9* (15), 1764-1773.

76. Jang, S.; Kim, S. Y.; Jung, H. Y.; Park, M. J., Phosphonated Polymers with Fine-Tuned Ion Clustering Behavior: Toward Efficient Proton Conductors. *Macromolecules* **2018,** *51* (3), 1120-1128.

77. Frischknecht, A. L.; Paren, B. A.; Middleton, L. R.; Koski, J. P.; Tarver, J. D.; Tyagi, M.; Soles, C. L.; Winey, K. I., Chain and Ion Dynamics in Precise Polyethylene Ionomers. *Macromolecules* **2019,** *52* (20), 7939-7950.

78. Paren, B. A.; Thurston, B. A.; Neary, W. J.; Kendrick, A.; Kennemur, J. G.; Stevens, M. J.; Frischknecht, A. L.; Winey, K. I., Percolated Ionic Aggregate Morphologies and Decoupled Ion Transport in Precise Sulfonated Polymers Synthesized by Ring-Opening Metathesis Polymerization. *Macromolecules* **2020,** *53* (20), 8960-8973.

79. Paren, B. A.; Thurston, B. A.; Kanthawar, A.; Neary, W. J.; Kendrick, A.; Maréchal, M.; Kennemur, J. G.; Stevens, M. J.; Frischknecht, A. L.; Winey, K. I., Fluorine-Free Precise Polymer Electrolyte for Efficient Proton Transport: Experiments and Simulations. *Chemistry of Materials* **2021,** *33* (15), 6041-6051.

80. Atanasov, V.; Oleynikov, A.; Xia, J.; Lyonnard, S.; Kerres, J., Phosphonic acid functionalized poly(pentafluorostyrene) as polyelectrolyte membrane for fuel cell application. *Journal of Power Sources* **2017,** *343*, 364-372.

81. Parvole, J.; Jannasch, P., Polysulfones Grafted with Poly(vinylphosphonic acid) for Highly Proton Conducting Fuel Cell Membranes in the Hydrated and Nominally Dry State. *Macromolecules* **2008,** *41* (11), 3893-3903.

82. Subianto, S.; Choudhury, N. R.; Dutta, N. K., Palladium-catalyzed phosphonation of SEBS block copolymer. *Journal of Polymer Science Part A: Polymer Chemistry* **2008,** *46* (16), 5431-5441.

83. Opper, K. L.; Markova, D.; Klapper, M.; Müllen, K.; Wagener, K. B., Precision Phosphonic Acid Functionalized Polyolefin Architectures. *Macromolecules* **2010,** *43* (8), 3690-3698.

84. Buitrago, C. F.; Alam, T. M.; Opper, K. L.; Aitken, B. S.; Wagener, K. B.; Winey, K. I., Morphological Trends in Precise Acid- and Ion-Containing Polyethylenes at Elevated Temperature. *Macromolecules* **2013,** *46* (22), 8995-9002.

85. Martínez-Felipe, A., Liquid crystal polymers and ionomers for membrane applications. *Liquid Crystals* **2011,** *38* (11-12), 1607-1626.

86. Kato, T.; Mizoshita, N.; Kishimoto, K., Functional Liquid-Crystalline Assemblies: Self-Organized Soft Materials. *Angewandte Chemie International Edition* **2006,** *45* (1), 38-68.

87. Kato, T.; Yoshio, M.; Ichikawa, T.; Soberats, B.; Ohno, H.; Funahashi, M., Transport of ions and electrons in nanostructured liquid crystals. *Nature Reviews Materials* **2017,** *2* (4), 17001.

88. Liang, T.; Tan, S.; Cao, S.; Wu, Y., Synthesis and characterization of proton conductive liquid crystals bearing phosphonic acid moieties. *Journal of Molecular Structure* **2017,** *1150*, 574-579.

89. Noonan, K. J. T.; Hugar, K. M.; Kostalik, H. A.; Lobkovsky, E. B.; Abruña, H. D.; Coates, G. W., Phosphonium-Functionalized Polyethylene: A New Class of Base-Stable Alkaline Anion Exchange Membranes. *Journal of the American Chemical Society* **2012,** *134* (44), 18161-18164.

90. Buggy, N. C.; Du, Y.; Kuo, M.-C.; Ahrens, K. A.; Wilkinson, J. S.; Seifert, S.; Coughlin, E. B.; Herring, A. M., A Polyethylene-Based Triblock Copolymer Anion Exchange Membrane with High Conductivity and Practical Mechanical Properties. *ACS Applied Polymer Materials* **2020,** *2* (3), 1294-1303.

91. Zhu, L.; Yu, X.; Peng, X.; Zimudzi, T. J.; Saikia, N.; Kwasny, M. T.; Song, S.; Kushner, D. I.; Fu, Z.; Tew, G. N.; Mustain, W. E.; Yandrasits, M. A.; Hickner, M. A., Poly(olefin)-Based Anion Exchange Membranes Prepared Using Ziegler–Natta Polymerization. *Macromolecules* **2019,** *52* (11), 4030-4041.

92. Khurana, R.; Schaefer, J. L.; Archer, L. A.; Coates, G. W., Suppression of Lithium Dendrite Growth Using Cross-Linked Polyethylene/Poly(ethylene oxide) Electrolytes: A New Approach for Practical Lithium-Metal Polymer Batteries. *Journal of the American Chemical Society* **2014,** *136* (20), 7395-7402.

93. Nzahou Ottou, W.; Norsic, S.; Belaid, I.; Boisson, C.; D'Agosto, F., Amino End-Functionalized Polyethylenes and Corresponding Telechelics by Coordinative Chain Transfer Polymerization. *Macromolecules* **2017,** *50* (21), 8372-8377.

94. Norsic, S.; Thomas, C.; D'Agosto, F.; Boisson, C., Divinyl-End-Functionalized Polyethylenes: Ready Access to a Range of Telechelic Polyethylenes through Thiol–Ene Reactions. *Angewandte Chemie International Edition* **2015,** *54* (15), 4631-4635.

95. Rank, C.; Häußler, M.; Rathenow, P.; King, M.; Globisch, C.; Peter, C.; Mecking, S., Anisotropic Extended-Chain Polymer Nanocrystals. *Macromolecules* **2019,** *52* (16), 6142-6148.

96. Ngo, H. L.; Jones, K.; Foglia, T. A., Metathesis of unsaturated fatty acids: Synthesis of long-chain unsaturated-α,ω-dicarboxylic acids. *Journal of the American Oil Chemists' Society* **2006,** *83* (7), 629-634.

97. Häußler, M., PhD Thesis, Universität Konstanz, **2020**. Polyethylene-Like Building Blocks from Plant Oils for Recyclable Polymers, Nanocrystals and Ion-Conductive Materials.

98. Fiedler, T.; Barbasiewicz, M.; Stollenz, M.; Gladysz, J. A., Non-metal-templated approaches to bis(borane) derivatives of macrocyclic dibridgehead diphosphines via alkene metathesis. *Beilstein J Org Chem* **2018,** *14*, 2354-2365.

99. McKenna, C. E.; Higa, M. T.; Cheung, N. H.; McKenna, M.-C., The facile dealkylation of phosphonic acid dialkyl esters by bromotrimethylsilane. *Tetrahedron Letters* **1977,** *18* (2), 155-158.

100. Atanasov, V.; Lee, A. S.; Park, E. J.; Maurya, S.; Baca, E. D.; Fujimoto, C.; Hibbs, M.; Matanovic, I.; Kerres, J.; Kim, Y. S., Synergistically integrated phosphonated poly(pentafluorostyrene) for fuel cells. *Nature Materials* **2020,** *20*, 370-377.

101. Schuster, M.; Rager, T.; Noda, A.; Kreuer, K. D.; Maier, J., About the Choice of the Protogenic Group in PEM Separator Materials for Intermediate Temperature, Low Humidity Operation: A Critical Comparison of Sulfonic Acid, Phosphonic Acid and Imidazole Functionalized Model Compounds. *Fuel Cells* **2005,** *5* (3), 355-365.

102. Staiger, A.; Paren, B. A.; Zunker, R.; Hoang, S.; Häußler, M.; Winey, K. I.; Mecking, S., Anhydrous Proton Transport within Phosphonic Acid Layers in Monodisperse Telechelic Polyethylenes. *Journal of the American Chemical Society* **2021,** *143* (40), 16725-16733.

103. Russell, K. E.; Hunter, B. K.; Heyding, R. D., Monoclinic polyethylene revisited. *Polymer* **1997,** *38* (6), 1409-1414.

104. Dierking, I., *Textures of liquid crystals*, John Wiley & Sons, **2003;** p 33-41.

105. Kumar, K. R. S.; Gupta, M.; Sakamoto, T.; Kato, T., Thermotropic Columnar Liquid Crystals Based on Wedge-Shaped Phenylphosphonic Acids. *Bulletin of the Chemical Society of Japan* **2019,** *92* (9), 1450-1452.

106. Tan, S.; Wang, C.; Wu, Y., Anisotropic assembly of a side chain liquid crystal polymer containing sulfoalkoxy groups for anhydrous proton conduction. *Journal of Materials Chemistry A* **2013,** *1* (4), 1022-1025.

107. Yang, X.; Tan, S.; Liang, T.; Wei, B.; Wu, Y., A unidomain membrane prepared from liquid-crystalline poly(pyridinium 4-styrene sulfonate) for anhydrous proton conduction. *Journal of Membrane Science* **2017,** *523*, 355-360.

108. Ueda, S.; Kagimoto, J.; Ichikawa, T.; Kato, T.; Ohno, H., Anisotropic Proton-Conductive Materials Formed by the Self-Organization of Phosphonium-Type Zwitterions. *Advanced Materials* **2011,** *23* (27), 3071-3074.

109. Mindemark, J.; Lacey, M. J.; Bowden, T.; Brandell, D., Beyond PEO—Alternative host materials for Li+-conducting solid polymer electrolytes. *Progress in Polymer Science* **2018,** *81*, 114-143.

110. Kang, S.; Park, M. J., 100th Anniversary of Macromolecular Science Viewpoint: Block Copolymers with Tethered Acid Groups: Challenges and Opportunities. *ACS Macro Letters* **2020,** *9* (11), 1527-1541.

111. Park, M. J., Confinement-entitled morphology and ion transport in ion-containing polymers. *Molecular Systems Design & Engineering* **2019,** *4* (2), 239-251.

112. Zhai, C.; Zhou, H.; Gao, T.; Zhao, L.; Lin, S., Electrostatically Tuned Microdomain Morphology and Phase-Dependent Ion Transport Anisotropy in Single-Ion Conducting Block Copolyelectrolytes. *Macromolecules* **2018,** *51* (12), 4471-4483.

113. Shen, K.-H.; Brown, J. R.; Hall, L. M., Diffusion in Lamellae, Cylinders, and Double Gyroid Block Copolymer Nanostructures. *ACS Macro Letters* **2018,** *7* (9), 1092-1098.

114. Middleton, L. R.; Trigg, E. B.; Yan, L.; Winey, K. I., Deformation-induced morphology evolution of precise polyethylene ionomers. *Polymer* **2018,** *144*, 184-191.

115. Cho, B.-K.; Jain, A.; Gruner, S. M.; Wiesner, U., Mesophase Structure-Mechanical and Ionic Transport Correlations in Extended Amphiphilic Dendrons. *Science* **2004,** *305* (5690), 1598-1601.

116. Jo, G.; Ahn, H.; Park, M. J., Simple Route for Tuning the Morphology and Conductivity of Polymer Electrolytes: One End Functional Group is Enough. *ACS Macro Letters* **2013,** *2* (11), 990-995.

117. Dair, B. J.; Honeker, C. C.; Alward, D. B.; Avgeropoulos, A.; Hadjichristidis, N.; Fetters, L. J.; Capel, M.; Thomas, E. L., Mechanical Properties and Deformation Behavior of the Double Gyroid Phase in Unoriented Thermoplastic Elastomers. *Macromolecules* **1999,** *32* (24), 8145-8152.

118. Avgeropoulos, A.; Dair, B. J.; Hadjichristidis, N.; Thomas, E. L., Tricontinuous Double Gyroid Cubic Phase in Triblock Copolymers of the ABA Type. *Macromolecules* **1997,** *30* (19), 5634-5642.

119. Park, J., PhD Thesis, University of Pennsylvania, **2022**. Morphologies, Phase Behavior, And Applications Of Precise Ion-Containing Multiblock Copolymers.

120. Park, J.; Staiger, A.; Mecking, S.; Winey, K. I., Structure–Property Relationships in Single-Ion Conducting Multiblock Copolymers: A Phase Diagram and Ionic Conductivities. *Macromolecules* **2021,** *54* (9), 4269-4279.

121. Park, J.; Staiger, A.; Mecking, S.; Winey, K. I., Sub-3-Nanometer Domain Spacings of Ultrahigh-χ Multiblock Copolymers with Pendant Ionic Groups. *ACS Nano* **2021,** *15* (10), 16738-16747.

122. Park, J.; Staiger, A.; Mecking, S.; Winey, K. I., Ordered Nanostructures in Thin Films of Precise Ion-Containing Multiblock Copolymers. *ACS Central Science* **2022,** *8* (3), 388-393.

123. Park, J.; Staiger, A.; Mecking, S.; Winey, K. I., Enhanced Li-Ion Transport through Selectively Solvated Ionic Layers of Single-Ion Conducting Multiblock Copolymers. *ACS Macro Letters* **2022**, 1008-1013.

124. Tsubakihara, S.; Nakamura, A.; Yasuniwa, M., Hexagonal Phase of Polyethylene Fibers under High Pressure. *Polymer Journal* **1991,** *23* (11), 1317-1324.

125. Bates, F. S.; Fredrickson, G. H., Block copolymers-designer soft materials. *Physics Today* **1999,** *52* (2), 32-38.

126. Srilakshmi, G. V.; Chaudhuri, A., "Snap-Shooting" the Interface of AOT Reverse Micelles: Use of Chemical Trapping. *Chemistry – A European Journal* **2000,** *6* (15), 2847-2853.

127. Lu, X.; You, W.; Peltier, C. R.; Coates, G. W.; Abruña, H. D., Influence of Ion-Exchange Capacity on the Solubility, Mechanical Properties, and Mass Transport of Anion-Exchange Ionomers for Alkaline Fuel Cells. *ACS Applied Energy Materials* **2023,** *6* (2), 876-884.

128. Yi, N.; Chen, T. T. D.; Unruangsri, J.; Zhu, Y.; Williams, C. K., Orthogonal functionalization of alternating polyesters: selective patterning of (AB)n sequences. *Chemical Science* **2019,** *10* (43), 9974-9980.

129. Tant, M. R.; Wilkes, G. L., Structure and properties of hydrocarbon-based ionomers. In *Ionomers: Synthesis, structure, properties and applications*, Tant, M. R.; Mauritz, K. A.; Wilkes, G. L., Eds. Springer Netherlands: Dordrecht, **1997**; 261-285.

130. Longworth, R.; Nagel, H., Packaging. In *Ionomers: Synthesis, structure, properties and applications*, Tant, M. R.; Mauritz, K. A.; Wilkes, G. L., Eds. Springer Netherlands: Dordrecht, **1997**; 261-285.

131. Hong, M.; Chen, E. Y. X., Chemically recyclable polymers: a circular economy approach to sustainability. *Green Chemistry* **2017,** *19* (16), 3692-3706.

132. Johnston, P.; Adhikari, R., Synthesis, properties and applications of degradable ionomers. *European Polymer Journal* **2017,** *95*, 138-160.

133. Atthoff, B.; Nederberg, F.; Hilborn, J.; Bowden, T., Biodegradable Ionomers. *Macromolecules* **2006,** *39* (11), 3907-3913.

134. Atthoff, B.; Nederberg, F.; Söderberg, L.; Hilborn, J.; Bowden, T., Synthetic Biodegradable Ionomers that Engulf, Store, and Deliver Intact Proteins. *Biomacromolecules* **2006,** *7* (8), 2401-2406.

135. Nederberg, F.; Watanabe, J.; Ishihara, K.; Hilborn, J.; Bowden, T., Biocompatible and biodegradable phosphorylcholine ionomers with reduced protein adsorption and cell adhesion. *Journal of Biomaterials Science, Polymer Edition* **2006,** *17* (6), 605-614.

136. Daemi, H.; Barikani, M.; Barmar, M., A simple approach for morphology tailoring of alginate particles by manipulation ionic nature of polyurethanes. *International Journal of Biological Macromolecules* **2014,** *66*, 212-220.

137. Nakayama, Y.; Inaba, T.; Toda, Y.; Tanaka, R.; Cai, Z.; Shiono, T.; Shirahama, H.; Tsutsumi, C., Synthesis and properties of cationic ionomers from poly(ester-urethane)s based on polylactide. *Journal of Polymer Science Part A: Polymer Chemistry* **2013,** *51* (20), 4423-4428.

138. Bullermann, J.; Spohnholz, R.; Friebel, S.; Salthammer, T., Synthesis and characterization of polyurethane ionomers with trimellitic anhydride and dimethylol propionic acid for waterborne self-emulsifying dispersions. *Journal of Polymer Science Part A: Polymer Chemistry* **2014,** *52* (5), 680-690.

139. Wan, A. C. A.; Mao, H.-Q.; Wang, S.; Phua, S. H.; Lee, G. P.; Pan, J.; Lu, S.; Wang, J.; Leong, K. W., Poly(phosphoester) ionomers as tissue-engineering scaffolds. *Journal of Biomedical Materials Research Part B: Applied Biomaterials* **2004,** *70B* (1), 91-102.

140. Rafiqah, S. A.; Khalina, A.; Harmaen, A. S.; Tawakkal, I. A.; Zaman, K.; Asim, M.; Nurrazi, M. N.; Lee, C. H., A Review on Properties and Application of Bio-Based Poly(Butylene Succinate). *Polymers* **2021,** *13* (9), 1436.

141. Jian, J.; Xiangbin, Z.; Xianbo, H., An overview on synthesis, properties and applications of poly(butylene-adipate-co-terephthalate)–PBAT. *Advanced Industrial and Engineering Polymer Research* **2020,** *3* (1), 19-26.

142. Zhan, S.; Wang, X.; Sun, J., Rediscovering Surlyn: A Supramolecular Thermoset Capable of Healing and Recycling. *Macromolecular Rapid Communications* **2020,** *41* (24), 2000097.

143. Eck, M., unpublished results (ongoing PhD thesis). Universität Konstanz: 2023.

144. Hahladakis, J. N.; Velis, C. A.; Weber, R.; Iacovidou, E.; Purnell, P., An overview of chemical additives present in plastics: Migration, release, fate and environmental impact during their use, disposal and recycling. *J Hazard Mater* **2018,** *344*, 179-199.

145. Makowski, H.; Lundberg, R.; Westerman, L.; Bock, J., Synthesis and properties of sulfonated EPDM. ACS Publications: **1980**.

146. Bautista, M.; De Ilarduya, A. M.; Alla, A.; Muñoz-Guerra, S., Poly(butylene succinate) Ionomers with Enhanced Hydrodegradability. *Polymers* **2015,** *7* (7), 1232-1247.

147. Pearson, R. G., *Hard and soft acids and bases.*, Pearson, R. G., Ed. Dowden, Hutchinson & Ross, Stroudsburg, **1973**.

148. Han, S.-I.; Kang, S.-W.; Kim, B.-S.; Im, S. S., A Novel Polymeric Ionomer as a Potential Biomaterial: Crystallization Behavior, Degradation, and In-Vitro Cellular Interactions. *Advanced Functional Materials* **2005,** *15* (3), 367-374.

149. *Canon Ink Tank CLI-551 Y.* ICW 0602 R - 02 EU EN. Canon 2016. Safety Data Sheet.

150. Novák, I.; Popelka, A.; Špitalský, Z.; Krupa, I.; Tavman, S., Polyolefin in Packaging and Food Industry. In *Polyolefin Compounds and Materials: Fundamentals and Industrial Applications*, Al-Ali AlMa'adeed, M.; Krupa, I., Eds. Springer International Publishing: Cham, **2016**; 181-199.

151. Wu, S.; Yang, H.; Huang, S.; Chen, Q., Relationship between Reaction Kinetics and Chain Dynamics of Vitrimers Based on Dioxaborolane Metathesis. *Macromolecules* **2020,** *53* (4), 1180-1190.

152. Odenwald, L.; Wimmer, F. P.; Mast, N. K.; Schußmann, M. G.; Wilhelm, M.; Mecking, S., Molecularly Defined Polyolefin Vitrimers from Catalytic Insertion Polymerization. *Journal of the American Chemical Society* **2022,** *144* (29), 13226-13233.